CREEP BUCKLING WITH LATERAL CONSTRAINT

BY

Neville Hannan Freed, M.Sc.(Eng) (RAND)

SEPTEMBER 1965

Thesis presented for the degree of
Doctor of Philosophy
in the
University of London

Abstract

The title problem arises from the use of stacked fuel elements in the first generation Calder Hall type of power station.

Previous theoretical work on symmetrical bowing, based on the tangent rate modulus approach, is extended to cover all phases of creep and elastic deformation, for both symmetric and asymmetric bowing. It is shown that a generalised solution can be derived, valid for an arbitrary range of material properties. For 'Magnox' at 295°C, the theoretical significance of elastic deformation in this problem is found to be small.

In an experiment on a rectangular specimen, during which the deformation remained two dimensional, good agreement with the theory could be obtained. An experimental study of the restrained bowing of axisymmetric sections, typical of reactor fuel elements, revealed however that it is not possible to maintain two dimensional deformation, as assumed in the theory. A rigorous treatment of the three dimensional problem was not found to be practical, but a resolution of the measured deflections into major and minor planes enabled some reasonably good correlations to be made with the theory.

Notation

A	Cross-sectional area
A'	Constant = $4EI/PL^2$
$[A]$	Matrix
a, a_1, a_2	Distance to points of contact
B	Constant = $\dfrac{P/P_E}{(1 - P/P_E)\ \ln 2}$
$[B]$	Column vector
b, b_1, b_2	Amplitude of sine wave
$\underset{\sim}{b}$	Deflection vector
C	Constant = $\dfrac{4}{\pi^2(1 - P/P_E)\ \ln 2}$
C_1, C_2, C_3	Creep coefficient constants
c	Dimensionless deflection variable = y/q
D	Constant = $\dfrac{}{\pi^2(1 - P/P_E)\ \ln 2}$
D'	Constant = $\dfrac{4}{\pi^2\ \ln 2}$
d	Diameter
E	Youngs modulus
$\dot{E}$	Tangent rate modulus = $(\partial\sigma/\partial\dot{\varepsilon})_{\sigma_0}$
$E(\partial u/\partial v)$	Finite difference operator - see section 10.6.5
e_1, e_2, e_3	Coefficients of operator E
e, $\dot{e}$	Total strain, total strain rate
$F(\mathfrak{S})$	Finite difference operator - see section 10.6.6
F_M, F_N	Major and minor plane wall forces
f_1, f_2, f_3	Coefficients of finite difference operator F
$G\ (\partial u/\partial v)$	Finite difference operator - see section 10.6.1
g_1, g_2, g_3	Coefficients of operator G
$H\ (\partial u/\partial v)$	Finite difference operator - see section 10.6.4
h	Flange separation

h_1, h_2, h_3	Coefficients of operator H
I	Moment of inertia
J	Integer locating mesh point
K, $\dot{K}$	Curvature, rate of change of curvature
K_i	Constants in Graham-Walles formulae
k_{1-3}	Constants
L	Length
M, $\dot{M}$	Bending moment, rate of change of moment. Also, number of meshes in numerical analysis
m	Integer locating position in space mesh
n, n_1, n_2, n_3	stress exponents in creep law
0	Integer locating mesh point
o	Subscript referring to neutral axis
P	End load
P_E	Euler buckling load
Q	Constant
q	Eccentricity of load
R, $\dot{R}$	Total wall force, rate of change of force
R', R'', R_3, R_4	Reactions at supports from lateral loads
R_1, R_2	Wall forces
r, r_1, r_2	Dimensionless distances to points of contact
$\underset{\sim}{r}$	Deflection increment
s	Dimensionless independent space variable
T	Temperature
t, t_D	Time (hours), doubling time
u	Dimensionless dependent deflection variable
v	'Solution' time
v_c	'Solution' time, considering creep only
$v_{ce.}$	'Solution' time, including creep and elasticity
W, $\dot{W}$	Half the total force (= R/2) for symmetrical cases, rate of change of force
w	Dummy integration variable
X	Dimensionless force = $WL/2P\delta$ = $RL/4P\delta$ in symmetrical cases

x	Distance from origin
Y, Y_1, Y_2	Dimensionless force = $RL/P\delta$, $R_1L/P\delta$, $R_2L/P\delta$ for asymmetric cases
y, $\dot{y}$	Deflection, rate of change of deflection. Also distance from neutral axis.
Z	Lateral force from eccentricity
z	Distance from neutral axis
α	Function in Graham-Walles equation. Also, an included angle in deflection measurement
β, γ	Functions in Graham-Walles equation
$\gamma(u)$	Finite difference operator - section 10.6.8
δ	Also angle associated with current deflection b Radial clearance between channel and undeformed specimen
δs, δx	Increment in space variable
δt, δv	Increments in time, solution time
$\varepsilon, \dot{\varepsilon}$	Creep strain, creep strain rate
η	Finite difference operator - section 10.6.9
$\eta_{1, 2, 3}$	Coefficients of operator
θ	Angle associated with deflection increment r
$\sigma, \dot{\sigma}$	Stress, stress rate
μ	Coefficient of friction
φ	Finite difference operator - section 10.6.7 Also, angle associated with initial deflection vector v_o
$\varphi_{1, 2, 3}$	Coefficients of operator

TABLE OF CONTENTS

	Page
Abstract	1
Notation	2
1.0 Introduction	11
1.1 Origin of the problem	11
1.2 Brief review of previous work	12
1.2.1 Theoretical work	12
1.2.2 Experimental work	13
1.3 Brief purpose of the present study	13
1.3.1 Proposed theoretical work	13
1.3.1.1 Symmetric bowing	13
1.3.1.2 Asymmetric bowing	13
1.3.1.3 Extension of the tangent modulus theory	13
1.3.2 Proposed experimental work	14
1.3.2.1 Assessment of the tangent modulus theory	14
1.3.2.2 Restrained bowing experiments	14
1.4 Main conclusions arising from the project	15
1.4.1 Accuracy of the tangent modulus theory	15
1.4.2 Symmetric restrained bowing	15
1.4.3 Asymmetric restrained bowing	15
2.0 Review of the literature on creep buckling	16
2.1 Perfect columns	16
2.1.1 Shanley, Gerard	16
2.1.2 Rabotnov-Shesterikov	17
2.1.3 Conclusions	18
2.2 Geometric instability	19
2.2.1 Pian, Hult	19
2.2.2 Gjelsvik and Bodner	19
2.2.3 Conclusions	20
2.3 Imperfect columns	20
2.3.1 Marin, Shanley, Higgins.	20

	Page
2.3.2 Libove, Hilton, Kempner	21
2.3.3 Hoff, Hult, Carlson	21
2.3.4 Johnson, Lin, Mendelson	23
2.3.5 Sanders et al, Schlechte	24
2.3.6 Hu, Sidebottom, Bleich	24
2.3.7 Alexander, Blackburn	25
2.3.8 Conclusions	26
2.4 Restrained bowing	27
2.4.1 Young	27
2.4.2 Blackburn and Percy	28
2.4.3 Fudge, Haigh	28
2.4.4 Blackburn	29
2.4.5 English Electric experiments	29
2.4.6 Conclusions	30
3.0 Detailed object of investigation	31
3.1 Theoretical work	31
3.1.1 Extension of the tangent modulus theory	31
3.1.2 Modification of existing symmetric solutions to include elasticity and primary creep	31
3.1.3 Derivation of the equations for asymmetric bowing	31
3.2 Experimental work	32
3.2.1 Verification of the E modulus	32
3.2.2 Restrained bowing	32
4.0 Derivation of equations	33
4.1 Incorporating elastic strains in Alexander's equations	33
4.2 Symmetric restrained bowing	35
4.2.1 Creep only	36
4.2.1.1 Introduction of dimensionless variables	38
4.2.1.2 Splitting of point contact	39

	Page
4.2.1.3 Rate of splitting finite	42
4.2.1.4 Rate of splitting infinite	42
4.2.1.5 Flattening phase	43
4.2.2 Creep and elasticity	44
4.2.2.1 Dimensionless equations	45
4.2.2.2 Splitting of point contact	47
4.2.2.3 Flattening phase	47
4.3 Asymmetric restrained bowing	48
4.3.1 First phase of deformation	48
4.3.2 Second phase	50
4.4 Miscellaneous equations	52
4.4.1 Free bowing	52
4.4.1.1 Doubling times	52
4.4.1.2 Non sinusoidal shapes	53
4.4.2 Effect of eccentricity	53
4.4.3 Initial elastic deflections	54
5.0 Numerical analysis	55
5.1 Restrained bowing equations	55
5.1.1 Symmetric equations, creep only	55
5.1.1.1 Flattening phase	55
5.1.1.2 Splitting of point contact	59
5.1.1.3 Final phase of deformation	60
5.1.2 Symmetric equations, including elasticity	62
5.1.2.1 Flattening phase	62
5.1.2.2 Splitting of point contact	63
5.1.2.3 Final phase of deformation	63
5.1.3 Asymmetric equations, including creep and elastic deformation	64
5.1.3.1 First phase of deformation	64
5.1.3.2 Final phase of deformation	66
5.1.3.3 Improvement of solution	67
5.2 Free bowing	68

	Page
5.3 Effect of eccentricity	69
5.4 Elastic deflections	69
6.0 Description of apparatus and experiments	70
6.1 Conventional creep buckling experiments	70
6.1.1 Apparatus	70
6.1.1.1 Buckling furnaces	70
6.1.1.2 Tensile creep	71
6.1.2 Description of experiments	72
6.1.2.1 Buckling experiments	72
6.1.2.2 Tensile creep experiments	73
6.1.2.3 Eccentricity experiments	73
6.1.2.4 Hot elastic properties	74
6.2 Restrained bowing experiments	74
6.2.1 Apparatus	75
6.2.1.1 The measuring system	75
6.2.1.2 The restraining channel and force measuring systems	77
6.2.1.3 Detection of first contact with the channel	78
6.2.2 Calibration of the apparatus	78
6.2.3 Description of experiments	80
6.2.3.1 Round specimens	80
6.2.3.2 Rectangular specimens	81
7.0 Analysis of experimental results and processing of data	82
7.1 Free bowing and tensile experiments	82
7.1.2 Reduction of bowing data	83
7.1.3 Reduction of tensile data	85
7.2 Analysis of computations on eccentricity equations	86
7.3 Restrained bowing	88
7.3.1 Round specimens	88
7.3.2 Rectangular specimens	90

	Page
7.3.3 Consistency correlations	90
7.3.4 Lead bowing experiments	91
8.0 Discussion	92
8.1 Accuracy of the tangent modulus method	92
8.1.1 Reliability of the Graham-Walles method	92
8.1.2 Comparison between buckling and tensile data	93
8.1.3 Time to contact channel	94
8.1.4 Conclusions	94
8.2 Symmetric restrained bowing	95
8.2.1 Computations on analytical shapes	95
8.2.1.1 General results	95
8.2.1.2 Significance of primary creep	96
8.2.1.3 Effect of elastic deformation	96
8.2.2 Correlations with experiment	97
8.2.2.1 Rectangular specimens	97
8.2.2.2 Lead bar experiment	97
8.2.3 Conclusions	98
8.3 Asymmetric restrained bowing	98
8.3.1 Computations on asymmetric shapes	98
8.3.2 Experimental work	99
8.3.2.1 Correlations with theory	99
8.3.2.2 Effect of minor bowing	100
8.3.2.3 Measured wall forces	101
8.3.2.4 Consistency correlations	102
8.3.3 Conclusions	102
9.0 Conclusions and sugges tions for further work	104
9.1 Results of present study	104
9.2 Suggestions for further work	105
Acknowledgements	106
10.0 Appendices	107
10.1 Bibliography	107

	Page
10.2 Relation between the $\dot{E}$ method and the equivalent H-section	113
10.3 On the independence of 2-plane bowing	115
10.3.1 General equations	115
10.3.2 Implications of the $\dot{E}$ method	116
10.3.3 Bowing in a circular channel	117
10.4 Relation between solution time and real time	119
10.5 Derivation of equations for dr/dv	120
10.5.1 Symmetrical creep only	120
10.5.2 Symmetrical creep and elasticity	121
10.6 Specification of finite difference operators	124
10.6.1 G - $(\partial^3 u/\partial s^2 \partial v)_{s=1}$	124
10.6.2 $(\partial^3 u/\partial s^3)_{s=1}$	124
10.6.3 $(\partial^4 u/\partial s^4)_{s=1}$	124
10.6.4 H - $(\partial^3 u/\partial s^2 \partial v)_{s=r}$	124
10.6.5 E - $(\partial^2 u/\partial s \partial v)_{s=r}$	125
10.6.6 F - $(\partial^2 u/\partial s^2)_{s=r}$	125
10.6.7 φ - $(\partial^2 u/\partial s \partial v)_{s=r}$	125
10.6.8 γ - $(\partial^2 u/\partial s^2)_{s=r}$	126
10.6.9 η - $(\partial^2 u/\partial s \partial v)_{s=r}$	127
10.7 Temperature dependence of creep rate	128
10.7.1 Tensile data	128
10.7.2 Bowing data	128
Tables	129
Figures	133
Symbols used in restrained bowing data	153

1.0 Introduction

1.1 Origin of the problem

The phenomenon of creep buckling was first discussed in the literature over 20 years ago (84)+, and has been the subject of continued interest ever since[x]. The title problem however, is of more recent origin as it has arisen from the use of the self-supporting, stacked fuel element in first generation 'Magnox' type nuclear power stations.

In this design, the fuel elements are stacked inside a graphite channel, and ambient conditions in the reactor are such as to cause both thermal- and irradiation-creep deformation (76). The clearance between the outermost projections on the fuel element (i.e. the guide-vanes or braces) and the channel is of the order of 1/10th of the diameter of the solid portion of the element (90); thus under the weight of the elements above and in the presence of unavoidable manufacturing tolerances, conventional creep bowing takes place until contact is established between the guide vanes and the channel. This phase of bowing, for the most highly rated element, will occupy only 10 per cent of the design life (90). During the remaining period therefore, bowing is restrained by the channel, and the resulting forces and displacements must be assessed: excessive distortion of the element leads to difficulties in discharging, and the guide-vanes must be known to be capable of withstanding the lateral forces generated.

The uncertainties associated with this deformation led the designers of some of the earlier reactors (Berkeley and Hunterston) to adopt independent vertical support for each element (86), but the Calder Hall, Bradwell, Hinkley Point and Trawsfyndd stations all use stacked elements.

+ Numbers in brackets designate reference in the bibiliography, section 10.1.

[x] A detailed review of the literature appears in section 2.

The present work was initiated therefore by the need of reactor designers for more information on this problem.

1.2 Brief review of previous work

1.2.1 Theoretical Work

The earliest treatment of the restrained bowing problem to appear in the literature was that of Young (90) in 1959. Using the "tangent modulus" method of Alexander (1), (described in section 2.3.7) a numerical solution was obtained for secondary creep only, assuming the element to be symmetric and cylindrical. A rigorous consideration of the moving boundary[+] was not undertaken, and this analysis must therefore be considered to be only approximate. A more detailed solution was presented by Blackburn and Percy in 1963 (8), which considered both cylindrical elements and elements having point restraints: these simulate contact with the braces. The incorporation of these restraints simplifies the theoretical treatment considerably, as it avoids the need to consider the moving boundary. Various symmetric initial shapes were considered, and an elegant treatment of the moving boundary was given. Equations equivalent to the tangent modulus method were used, but this analysis neglected primary creep and elastic deformation.

Three further reports, originating at the English Electric Co., appeared during 1963. The first two, by Fudge (22) and Haigh (29), were concerned with the secondary creep deformation of an element having point restraints and bowing in a single plane; the third, by Fudge and Haigh (23), considered the possibility of bowing in two planes with point restraints. This had the implicit assumption that it was possible to treat the two planes separately, as there was no continuous interdependence of the boundary conditions in the two planes (see section 10.3).

In a recent and as yet unpublished extension of his previous work, Blackburn (9) analysed the behaviour of some continuously restrained

[+] The point of contact between the element and the wall moves during the deformation.

asymmetric shapes, and also considered the effect of small asymmetric perturbations on various symmetric initial shapes. This paper also discussed the behaviour of the element when the ends are allowed to tilt across the channel.

1.2.2 Experimental Work

It appeared that no serious attempt had been made to support any of the theoretical work quoted above. Some experiments on lead bars were initiated at English Electric Co. Ltd. to verify the work of Young (90), but only one appears to have been performed. Unfortunately this was not written up, but the results of this experiment are discussed in section 7.3.4.

1.3 Brief purpose of the present study

1.3.1 Proposed theoretical work

When this project was initiated, the existing theoretical solutions (90) were not considered adequate. However the analysis of Blackburn and Percy (8) appeared during the course of the present work, and with suitable modifications it seemed capable of extension to take account of other factors more representative of actual conditions.

1.3.1.1 Symmetric bowing

The solution of Blackburn and Percy was for secondary creep only. It appeared necessary therefore to assess the possible significance of primary creep and elastic deformation.

1.3.1.2 Asymmetric bowing

It was soon apparent that the symmetric column is only an idealisation of shapes occurring in practice. As the behaviour of asymmetric columns is substantially different from the symmetric shapes, a theory was required for the solution of the asymmetric column.

1.3.1.3 Extension of the tangent modulus theory

The equations derived by Alexander (1) did not include elastic deformation. In a later paper, by Webster and Alexander (95), elastic deflections were incorporated for the special case of free bowing.

These equations are not applicable to any other stress system: it was therefore necessary to derive equations on assumptions analagous to those of Alexander (1), but satisfying the requirement that the total strain distribution be linear. This effectively incorporates elastic deformation.

1.3.2 Proposed experimental work

As discussed previously, there was almost no experimental evidence which could enable the analyses of Young (90) or Blackburn (8) to be used with any confidence. In addition, it appeared that the basis of the above theories, viz. the tangent modulus assumption, was not well supported by experiment. These considerations led to the formulation of the programme below.

1.3.2.1 Assessment of the tangent modulus theory

An experimental verification of this theory had been attempted by Webster and Alexander (95); the effectiveness of this work was limited however by considerable scatter in the tensile data, although the results were consistent with the theory.

To obtain a more precise indication of the errors likely to be inherent in the use of the above theory, a series of experiments were designed using 'Magnox' AL80 at 295°C. In addition to correlating the buckling data with measured tensile data (essentially a repetition of the above work but using partially redesigned equipment), it was proposed to perform tests on different diameters of specimens, and attempt a further assessment of the theory in this way.

1.3.2.2 Restrained bowing experiments

The need for a systematic experimental study of the restrained bowing problem was indicated above. Although the reactor fuel element experiences a combination of point restraint and continuous restraint, the former is a special case of the latter; it was therefore decided to restrict the study to the more general case of continuous restraint.

Experiments were planned using two different specimen diameters and a fixed channel clearance, over a range of Euler loading ratios,[x]

[x] P/P_E.

representative of reactor practice. The resulting deflections and wall forces were to be compared with those predicted theoretically from a computation based on measured tensile data.

1.4 Main conclusions arising from the project

1.4.1 Accuracy of the tangent modulus theory

The experiments showed that the time to achieve a given deflection during free bowing could be predicted to an accuracy of 20 per cent, provided that the secondary creep phase of the buckling was well established. Errors during the primary creep phase could be very much larger, but may be due to differences in compressive and tensile creep.

1.4.2 Symmetric restrained bowing

The importance of elastic deformation at the test temperature was found to be small; the significance of primary creep would depend on the design life, and would only be appreciable in the early stages.

As described below, it was not possible to apply symmetric two dimensional theory to the main body of experiments. However, one experiment was performed on a rectangular specimen in which the deformation remained symmetrical, and good agreement was obtained with the theory.

1.4.3 Assymetric restrained bowing

The experiments on axisymmetric specimens showed that it was impossible to maintain two dimensional deformation. The resulting third dimensional component made the direct application of the theory impossible, but by correlations between the tests it was concluded that the theory was valid.

A rigorous solution for the 3-dimensional continuously restrained bowing problem was not found to be practical; it was also found that the use of predictions from two dimensional theory gave results which were too conservative to be of value.

In a reactor, however, the point restraints resulting from contact with the braces renders the problem more tractable, and it is concluded that the theory can be used with some confidence in these cases.

2.0 Review of the literature on creep buckling

The deformation in the problem can be conveniently divided into two phases. The first, a conventional creep buckling process, is concerned with the bowing of the element from its initial nearly straight form until contact is made with the channel. The second phase, progressive deformation against the channel, would terminate either when contact is made with the opposite surface (due to reverse bow), or if geometric instability develops and the element springs away from the wall.

A very considerable volume of work on creep buckling in general has appeared in the past 15 years, most of it originating in the aerospace industries. Some of the problems treated, e.g. the classically straight column and the snap buckling phenomenon, are found to be of indirect interest only: these are therefore discussed only briefly. However, much of the work on imperfect columns, and on more generalised methods of creep strain analysis, is applicable to the title problem and will be considered in some detail. The references cited in section 1.2, being directly relevant, are also reviewed here.

Finally conclusions are drawn as to what appeared to be the most tractable theoretical approach, and what experimental work would be required.

2.1 Perfect Columns

In the case of perfect columns, a bifurcation of equilibrium occurs at the critical time due to a reduction in stiffness by creep. This is followed by a gradual deviation from the straight shape and eventual collapse.

2.1.1 Shanley, Gerard[+]

One of the earliest analyses is that of Shanley (82). He identified a time at which the tangent modulus slope of the isochronous stress strain curves at the mean stress was reduced such that $P_E^* = P$, where P_E^* is the Euler buckling load based on the reduced modulus.

[+] The development of these sections is chronological as far as possible. The sub-headings refer to the more important papers only.

It was not claimed however, that the column would collapse at this time: it merely represented the onset of continuous bending and was intended to be indicative of trends likely to be observed. This arises from the fact that the isochronous curves are derived for constant stress, while in the column the stress varies with time.

Carlson (14) and his co-workers however were able to show that the tangent modulus load was not necessarily conservative, as incicated by Shanley. It is in fact an approximation to a conservative estimate: the approximation however, may or may not be conservative. This was verified experimentally.

Another theory of perfect column behaviour was proposed by Gerard (24), who postulated that the column would fail when the total strain had become equal to the Euler strain. This followed from the reduction of the short time critical stress for plastic buckling, as calculated from the total secant modulus. Comparison with the experiments of Mathauser and Brooks (63) showed that the theory was qualitatively correct only, and very poor agreement was obtained.

2.1.2 Rabotnov-Shesterikov

The most rigorous theory of perfect columns is undoubtedly the classical stability analysis of Rabotnov and Shesterikov (75). An equation of state was assumed, and small excursions from the undisturbed state were analysed. The analysis showed that a small disturbance applied at time t would be attenuated if $t < t_{cr}$ and would be amplified if $t \geqslant t_{cr}$. This mechanism has been clarified by Hoff (41). In a comprehensive survey of the literature[+], Hoff (40) showed that the theory of Shanley predicted lifetimes considerably longer than that of Rabotnov-Shesterikov. Hoff also showed that Gerard's conjecture was not valid for a general material creep law. An interesting comparison of the three theories mentioned above was given by Jahsman and Field (46). This was obtained by comparing the theoretical predictions of

[+] Other surveys may be found in Finnie and Heller (20), Bodner (11).

creep buckling times with experiments by Mathauser and Brooks (63), Carlsen and Manning (14) and Patel et al (69): the results given in these references were extrapolated to zero initial deviation. The method is of course only approximate, but demonstrated clearly that the theories were extremely conservative.

Better agreement with the Rabotnov-Shesterikov theory might have been expected, and this prompted Jahsman and Field in a further paper (47) to adjust the theory for the temporary halt in creep during unloading on the convex surface. An improvement in the agreement was noted, but the theory still remained conservative. This was assumed to be due to the fact that Rabotnov-Shesterikov theory predicts the onset of instability only: considerable time may elapse between this and actual collapse.

A further comparison of the various perfect-column theories was given by Gerard and Papirno (25), based on the experiments of Carlson et al (14, 15) and Papirno and Gerard (67). The Rabotnov-Shesterikov equation was in this case replaced by total strain equations. This showed that by normalising the theoretical creep buckling stresses, with respect to the short time buckling stresses, the scatter in the data was considerably reduced; this was the basis of Gerard's secant modulus mentioned earlier. Further, the results confirmed that the Rabotnov-Shesterikov theory provided a reliable lower bound to the critical time, whilst the secant modulus theory and isochronous reduced modulus theory form upper bounds.

2.1.3 Conclusions

It appears then that the rigorous dynamic analysis of Rabotnov-Shesterikov provides a reliable lower bound for column collapse times. There is insufficient evidence however, to believe that the upper bounds mentioned above are universally correct. The perfect column approach has the advantage of not requiring specification of the initial imperfection or an explicit creep law, but unfortunately the lower bounds available are often so conservative as to represent inefficient utilisation of the material. It was therefore concluded

that a more realistic approach would be desirable for the present problem, taking account of the initial imperfection.

2.2 Geometric Instability

In this mode of creep deformation, a reduction in stiffness occurs from creep induced geometrical changes: this is usually followed by a jump in deflection. Well known structures that are subject to snap buckling (also known as oil canning) are shallow spherical caps and shallow arches. It was believed initially that in the present problem snap buckling could occur after the element had been in contact with the channel for some time, and that it would suddenly leave the channel after sufficient reverse bow had developed. Accordingly the possibilities of this approach were investigated.

2.2.1 Pian, Hult

The earliest analysis of this type of problem appears to be that of Pian (72). A variational theorem (80) was used to calculate the deflection-time characteristics of a laterally loaded, sinusoidal beam. It was observed that the deflection became multiply valued at a certain time. This was assumed to be the critical time for snap buckling. The analysis was extended in a later paper (73) to include an antisymmetrical mode.

Hult (45) showed that the sudden jump in deflection in this type of problem was due to the presence of simultaneous elastic and plastic deformation. The deflection-time relations for the problems treated were based on previously derived (44) moment-curvature relationships for linear viscoelastic bars; the critical time was defined as the instant at which the deflection rates became infinite.

2.2.2 Gjelsvik and Bodner

In an investigation of the use of an energy criterion for snap creep buckling in clamped arches, Gjelsvik and Bodner (26) have analysed a simple statically determinate model: they showed that the forces in the elastically deforming model at the critical load, were the same as those required for creep snap buckling of the model.

2.2.3 Conclusions

It was concluded from the foregoing references that any attempt to estimate the instant of geometric instability would have to be preceded by a complete deflection-time analysis of the structure. It would then be conceivably possibly to use the multiple deflection approach of Pian (72), or the energy criterion of Gjelsvik to predict the occurence of a jump in deflection.

2.3 Imperfect Columns

The literature surveys described in the preceding sections both enforced the view that a detailed deflection history of the specimen would be required for both phases of the deformation. This is most easily obtained by imperfect column analysis, which consists in essence of establishing moment-curvature rate relationships, which when integrated give deflection-time data.

2.3.1 Marin, Shanley, Higgins

For the case of linear viscoelasticity, the analysis is comparatively simple, and some of the earliest papers use this idealisation. Marin (61) assumed a non linear secondary creep law but considered only bending stresses.

A more realistic treatment was given by Shanley (82), utilising the isochronous stress strain curves. An important feature of his analysis was the introduction of an idealised two flange model; this was used to trace the stress-strain-time paths of the flanges on the diagram, according to a strain hardening law. The changes in strain were then related to increments in deflection. The method is essentially graphical, and did not therefore seem well suited to extensive computation or generalisation to more complex stress systems.

Higgins (33) presented a more rigorous theory, in which the actual stress distribution across the section was calculated. The analysis takes account of the fact that the neutral axis does not necessarily coincide with the centroidal axis, and traces the strain history of a finite number of fibres across the section. The computation is necessarily lengthy, as repeated integrations over the section are required.

Some comparison with experiment is given, but the results are very disappointing.

2.3.2 Libove, Hilton, Kempner

The two flange model was further developed by Libove (56), using the law

$$\dot{e} = \frac{\dot{\sigma}}{E} + \dot{\epsilon}(\sigma, \epsilon)$$

where $\dot{\epsilon}$ is a creep rate function. The column was assumed to remain sinusoidal, and a lengthy numerical solution by one-point collocation was obtained. No experimental confirmation was offered. In a further paper (57) the analysis was extended to rectangular sections, the solution being reduced to an integral equation which was solved by a computer. For shapes other than sinusoidal, a solution by some averaging process would be required, entailing considerably more computation.

An elastic-viscoelastic analogy was used by Hilton (35) to develop equations for viscoelastic columns in terms of an infinite series. The results are not believed to be of more general interest.

A similar solution for linear viscoelastic columns was given by Kempner and Pohle (50). The concepts were later extended (51) to more general linear viscoelastic beams and columns; the analysis for columns was based on a sinusoidal shape. In other papers (52, 53) the work was extended to nonlinear viscoelastic deformation of idealised H-section columns.

2.3.3 Hoff, Hult, Carlson

Using the same idealised column, Hoff (36) developed simple approximate equations for a secondary creep law relating column displacement to time. This method is based on the equivalence of elastic bending stiffness of the model to that of the real section, and the resulting equations are of course capable of generalisation to other stress systems. The effect of primary creep in these equations was investigated by Odqvist (61) and the additional effect of elasticity was studied by Hult (43). A further development of this analysis by Hoff (37) included both elastic and inelastic strains, primary and secondary creep for certain values of the exponent. The same equations were used by Patel (68) to obtain a solution for general values of the

the exponent in the secondary creep law. More generality was achieved by Hult (42) in extending existing solutions to H-sections with unequal flange areas, the most general statically determinate section. Some justification for the assumption of a sine wave shape in all the preceding analyses was given by Patel and Kempner (70). More recently, the effect of recovery has been included quantitatively in the equations by Hedner (32). The effect is to accelerate the bowing.

An analytical investigation of the validity of the equivalent H-section method was made by Carlson (16). He showed that for the moment curvature relationships to remain equivalent, the effective flange separation of the H-section must decrease. The calculation of the actual value of the separation can only be performed iteratively and this was not incorporated in the deflection-time equation. Carlson also attempted to incorporate the effect of recovery in the equations, through the assumption that the creep and recovery rate on the convex flange were equal and opposite. Good agreement with theoretical collapse times were obtained through the use of the relatively simple H-section equations.

A graphical method for use in connection with the incremental form of Hoff's equations was given by Chapman et al (17), and other examples of application of the theory are given by Lempriere (55).

Another application of the H-section equations has been shown by Stowell and Wah (87), applying a hyperbolic sinh creep law. Non dimensional parameters were derived, to compare the theoretical collapse time with the experiments of Mathauser and Brooks (63). The agreement was however very poor.

Calladine (12) attempted to analyse the factors causing real columns to behave differently from the equivalent H-section, and also to derive an empirical relationship for comparing the merits of various cross sectional shapes. It was shown that the fourth moment of inertia seemed to be a relevant parameter, and equations were given relating a lifetime parameter to the shape and creep exponent.

2.3.4 Johnson, Lin, Mendelson et al

Johnson et al (48) considered eccentrically loaded rectangular columns, making the simplifying assumption that the distributions of both creep and elastic strains were linear; this is in contrast with most of the preceding work which had been based on a linear total strain distribution. They also assumed a "time hardening" creep law and were able to obtain excellent agreement with theory. The computations were based on tensile creep data, and seem to show that the interchange of data in this way does not have a material effect on the results. Some investigators - Carlson et al (14, 15, 77) report little difference between tensile and compressive creep behaviour in their experiments, whilst others (78, 79) have found that the difference may be considerable. It seems therefore that this should be investigated for each specific application.

A very useful method of creep stress analysis was developed in a paper by Lin (58). Simple incremental equations relating external moment to the elastic and creep relaxation moments were presented, which have to be satisfied at each section along the length of the column. No iteration is involved and the method is considerably shorter than the equally rigorous method of Higgins (33) noted previously; it is not necessary to make any assumption regarding the deflected shape. The calculation provides a picture of the stress distribution at each instant, and could easily be extended to stress systems other than simple column buckling. In a further paper Lin (59) extended the method to beam columns, using a more analytic treatment of the equations.

Another example of incremental methods was given by Mendelson, Hirschberg and Manson (64); as before any variable stress creep law could be used, but in this case an iterative feature was introduced to take account of the variation of creep strain during the time increment. The method could be generalised to multiaxial problems, and another recent example of its application has appeared (62).

2.3.5 Sanders et al, Schlechte

A variational theorem for creep was developed by Sanders, McComb and Schlechte (80), which provides a powerful tool for plate and column problems. In it's most general form, considerable computation would be necessary: accordingly the authors made some simplifying assumptions regarding deflection and stress distribution. The resulting equations for a rectangular column were rather similar to those of Kempner (53), differences being due to the one point collocation of Kempner as compared with the averaging process of the variational theorem. Further applications of the theorem are described by Schlechte (81), who considered rectangular and idealised H-sections. In the case of the rectangular section, comparison was made with the lifetime calculated on an assumed linear stress distribution, as opposed to the more rigorous method of calculating the actual distribution. The analysis showed that there were no significant differences between the linear and nonlinear solutions, except for very large initial deflections and values of the creep exponent; further, the very considerable amount of extra computation was not justified by the improvement in accuracy of prediction. It appeared that the tangent modulus theory of Shanley was in most cases more reliable for lifetime predictions than the variational method.

2.3.6 Hu, Sidebottom, Bleich.

Hu and Triner developed dimensionless isochronous moment-stress curves for rectangular sections, and tested the theory by application to beam-columns. The results were not self consistent, and the author believes that this may be due to the unrealistic creep law used. A very similar method was described by Sidebottom and Dewhurst (83), who obtained reasonable agreement with experiment.

A limit analysis for the curvature rate of rectangular columns was developed by Bleich and Dillon (10), which eliminates the need to follow changes in stress distribution. However, the bounds are rather wide and no experimental confirmation is available: they are also not particularly easy to derive.

2.3.7 Alexander, Blackburn

Another approximate method was proposed by Alexander (1). This was based on the assumption that the creep strain rate in the column could be assumed to be proportional to the local stress; further it was assumed that the factor of proportionality was the slope of the stress-strain rate curve at the mean stress. Considering secondary creep strains only, he derived particularly simple equations relating the tangent rate modulus (called $\dot{E}$) to the applied bending moment and the rate of change of curvature:

$$\dot{K} = M/\dot{E}I$$

From this, the time to achieve a given bow could be readily obtained; comparisons with an actual stress distribution calculated iteratively for a cylindrical shell, showed that the approximate method was very adequate. The analysis was extended in a further paper (2) to take account of primary creep as well. The range of validity of the method when the direct load is combined with an applied bending moment was investigated by Young (89). In a later paper he showed good experimental agreement with predicted bowing rates for some simulated fuel elements (90). Another attempt was made to provide some experimental support for the theory by Webster and Alexander (95). Although the experiments were consistent with the theory, they were not conclusive on account of the considerable scatter in the tensile data. It seemed that more careful tensile experiments were indicated.

An almost identical theory was derived independently by Blackburn (7), by neglecting second order terms in the stress distribution. The resulting equations are then equivalent to those of Alexander, being derived under the same assumptions; they were used to predict the behaviour of a fuel element tilted across the channel, including the effect of thermal cycling and radial temperature gradients. When the weight of the element is included in the calculations, the equations become complex and a computer solution was used to calculate the time at which contact is no longer at the ends of the element.

2.3.8 Conclusions

Most of the interest in imperfect columns has been centered on the collapse - or critical - times; the object of this survey however was to compare methods for the prediction of deformation histories, but because most of the experimental data has been exclusively concerned with critical times, one has to assess the theories on this basis. This is not particularly rewarding, as even the rigorous Hoff-de Veubeke (19) theory for the collapse of imperfect columns, which can be deduced from stability considerations, can in some circumstances be unreliable (55, 60).

Apart from the limitations inherent in the theories, it is also well known that any of the familiar equations for variable stress are likely to be seriously in error in some situations (49, 6, 66). Another consideration influencing the assessment of any creep experiment, is the undue sensitivity to small excursions in the test variables: this results from nonlinearities in the creep laws and gives rise to considerable scatter. These factors taken together make the relative merits of the creep buckling theories difficult to compare.

The rigorous theory of Higgins (33) was very far from being in agreement with the experimental result quoted in that reference; a similar conclusion is inferred from the calculations of Lin (58).

The formulae derived by Kempner (51), which closely paralleled those of Schlechte (81), were also not in good agreement with experiment: the tangent modulus of Shanley (which cannot be readily applied to deflection history calculations) was often more reliable.

The simple H-section equations of Hoff (36) have not been used directly to predict experimental column deflection rates. It is shown elsewhere however by the author (section 10.2) that the method of equivalent H-sections and the linearisation of the stress-creep strain rate relations (used by Alexander and Blackburn) lead to identical moment-curvature rate equations for $n = 1, 2$; the theories are approximately equivalent for $n \geqslant 3$.

As noted previously, encouraging agreement had been found for the

simple theory of Alexander (95); the Hoff-de Veubeke theory, which used the H-section equations to predict the time to attain the critical deflection, appeared to be in better overall agreement than the more rigorous theories of Higgins and the variational methods. It seemed therefore reasonable to attempt to use the linearised equations in this problem, and to hold the more generalised incremental theories of Lin (58) and Mendelson et al (64) in reserve.

2.4 Restrained bowing

As indicated in section 1.2, all the work on restrained bowing had originated among the nuclear power consortia, much of it in unpublished reports. It will therefore be useful to describe the relevant work in some detail.

2.4.1 Young

The first report discussing restrained bowing was the work of Young (90), at English Electric. Using the tangent modulus method of Alexander, he set up a partial differential equation for the deflected shape.

Writing $\dot{K} = \dot{M}/\dot{EI}$, and noting the force and co-ordinate systems of Fig. 2, we have

$$\dot{EI}\,\frac{\partial}{\partial t}\left(\frac{\partial^2 y}{\partial x^2}\right) = -Py + \frac{R}{2}x \qquad (2.1)$$

This equation was replaced by it's finite difference equivalent

$$\frac{\dot{EI}}{\delta t \delta x^2}\left[(y_{m+1} - 2y_m + y_{m-1})_t - (y_{m+1} - 2y_m + y_{m-1})_{t-\delta t}\right] = \left[-P + Rx/2\right]_{t-\delta t} \qquad (2.2)$$

and solved numerically. It was assumed in this solution that the element merely flattened progressively against the channel without developing a reverse bow. It can be shown however from the boundary conditions at the point of contact (section 4.2.1), that the element is unstable when curvature disappears at the point of contact, and that therefore this condition is passed through instantaneously. Further the analysis was performed assuming that $\dot{E}$ was independent

of stress and time - i.e. itwas for linear viscoelastic materials only. This solution must therefore be regarded as being approximate.

2.4.2 Blackburn and Percy

A much more comprehensive analysis of the problem by Blackburn and Percy (8) appeared during the course of the present work. Using a linearised theory mentioned earlier, they considered both point- and continuous restraint for the symmetric problem. From the condition that the element remains tangential to the wall, a differential equation for dr/dt (see Fig. 2) was derived (see section 4.2.1). This was solved numerically, simultaneously with the bending moment-curvature equation.(2.1) above. They were also able to show that after first contact with the wall, dr/dt became indeterminate when the curvature became zero. The subsequent behaviour then depended on the third derivative of the shape. Some errors were made in the analysis and these are discussed in section 4.2.1. They were able to show that the effects of elasticity were likely to be small during the phase of initial flattening, and neglected it during the analysis on subsequent deformation. The solution was presented in terms of doubling times (defined in section 4.4.1.1).

2.4.3 Fudge, Haigh

A very similar analysis was presented by Fudge (22), using the E method of Alexander, to consider the case of point restraints. Like that of Blackburn and Percy, the solution was for secondary creep only.

In another report issued simultaneously with the above, Fudge and Haigh (23) took cognizance of the fact that the bowing would in practice be three dimensional; all the previous treatments had been two dimensional. They assumed that the three braces at the quarter points constituted point restraints, and that the initial shapes in the two coordinate planes were first and second harmonics of a sine wave. Equations essentially similar to eqn. (2.1) were written down for the two planes and the reactions calculated from geometric considerations.

A simplified three-dimensional representation was considered for

point restraints by Haigh (29). The channel was now assumed to be square, which meant that the bows and reactions in the two directions could be assumed to be independent of one another[+]. An interesting feature of this analysis was that the deformation was resolved into two components: the first was that produced by the end load and the second produced by the wall reactions. (This superposition is valid as the equations are linear). The method of forward integration in time however, as in their previous papers, seemed rather inaccurate and potentially unstable.

2.4.4 Blackburn

In an extensive and as yet unpublished analysis, which became available to the author towards the end of this investigation, Blackburn (9) extended his previous work on continuously restrained bowing to various asymmetric shapes; he also took account of the reactor condition where the pin jointed end is allowed to tilt freely across the channel. In this case the deformation was bounded by both sides of the channel — however his calculations show that the element will not in general be in contact with both sides simultaneously during the design life. It was also shown that initial shapes which are slightly asymmetric approached a symmetric form after some time. A stability analysis of the effect of asymmetric perturbations on various initial symmetric shapes was presented, and equations derived for the time rate of change of the perturbation component. As in the previous papers, this analysis was for secondary creep only and in terms of a parameter which is equivalent to the E modulus.

2.4.5 English Electric experiments

The only previous experimental work on restrained bowing known to the author is a lead bar bowing test at the English Electric Co. Ltd.[x] This work was undertaken to support the theoretical study of Young (90), but was never fully written up. However the data available is reproduced elsewhere (section 7.3.4) and analysed according to the

[+] The conditions under which this will be true are derived in section 10.3.

[x] G.P. Clark - personal communication.

theory of section 4.2. This experiment consisted of an axially loaded bar, bowing against a plane restraint. Minor plane bowing was prevented by pins fixed into the restraint. The deformation was approximately symmetrical, and the percentage length in contact with the restraint was measured at various times. The theoretical comparison is based on only four tensile tests, and so must be considered to be only tentative.

2.4.6 Conclusions

All the analytical work on restrained bowing had been performed using the linearised methods of Alexander or Blackburn. This supported the conclusions of section 2.3.8 that these presented the best compromise between analytical convenience and reality.

Most of the defects in the method used by Young (90) had been rectified by Blackburn and Percy; the work of Fudge and Haigh was not of direct interest as it was restricted to the special case of point restraints. This is a less general problem than that of continuous restraint.

The later paper by Blackburn (9) considered asymmetric two dimensional shapes, but as in the previous papers was restricted to secondary creep only.

The existing experimental work was obviously inadequate to confirm the preceding theory.

It appeared therefore that it was necessary to assess theoretically the significance of elastic and primary creep deformation during restrained bowing, and if possible to develop solutions which (like the existing secondary creep solutions) could be translated in terms of any material data without additional computation.

Further, it appeared that there was a very considerable need for some experimental work, which would lend some substance to the lengthy numerical computations required to solve the equations characterising the problem.

3.0 Detailed object of investigation

From the discussion of previous work given in section 2, it is now possible to formulate more precisely the object of this investigation.

3.1 Theoretical work

3.1.1 Extension of the tangent modulus theory

In their original forms, the linearised theories of Alexander and Blackburn did not include elastic strains. It was considered that these may be significant in the small deflection type of problem under consideration, and it was therefore attempted to incorporate elastic strains into the original equations.

Some similarity between the above theories and those of Hoff had been noted previously by Young (89): it was therefore deemed worthwhile to attempt to derive the conditions under which these theories became equivalent, as the Hoff theories have been widely used.

3.1.2 Modification of existing symmetrical solutions to include elasticity and primary creep

The most rigorous theory of continuously restrained bowing had been that of Blackburn and Percy, and with some small reservations (see section 4.2) the solution derived by these authors for symmetric steady state creep appeared to be a valid one.

It seemed therefore necessary to refine the symmetric theory to include all phases of creep and elasticity, in a manner which would enable designers to assess the effects of temperature or material changes without having to repeat the solution.

3.1.3 Derivation of the equations for asymmetric bowing

It soon became apparent that the symmetric column was as much a fiction as the classically straight column; it was therefore required to derive equations valid for asymmetric restrained bowing, including all phases of deformation as above.

3.2 Experimental work

3.2.1 Verification of the E modulus

The experimental work of Webster and Alexander had not been conclusive. It was therefore decided to attempt a more precise series of experiments, with a view to obtaining a quantitative assessment of the tangent modulus theory under conventional bowing conditions. This would provide a firm basis for the use of the theory under the more complex conditions of restrained bowing.

3.2.2 Restrained bowing

The sum total of experimental work on restrained bowing known to the author was one experiment on lead at English Electric. This was obviously unsatisfactory, considering the volume of theoretical work which had gone before. It was therefore decided to undertake a comprehensive series of experiments, designed to provide data on force and deflection histories over a range of stresses.

Using derived tensile creep data, it was intended to compare experimental deflection and force histories with those predicted from theoretical considerations, and also to examine the lead bowing data in the light of the present theory.

It was hoped in this way to provide solutions of value to reactor designers.

4.0 Derivation of equations

4.1 Incorporating elastic strains in Alexander's equation[+]

The following assumptions are made in the derivation:

1) Plane sections remain plane.

2) Deflections are small.

3) The axis of zero bending stress coincides with the centroidal axis - this will be termed the "neutral axis".

4) The creep strain rate is a function of current stress, temperature and time only.

5) The creep properties in compression are identical with those in tension, and the strain rates in the fibres of the column can be predicted from uniaxial behaviour in constant stress experiments.

Assumption (1) is well based on experiment; the second assumption is a realistic one from engineering considerations, as most structures cease to be functional beyond a small amount of deformation. This assumption also leads to the linear relation between curvature and the second derivative of the deflected shape. The third assumption would only be strictly valid for a linear stress distribution, and implies that the centre of internal and external moments coincide. It is believed however that this will be sufficiently accurate provided the stress distribution does not become seriously non-linear.

The fourth assumption is the subject of perennial discussion amongst engineers, and is invoked by the need for considering variable stress conditions. Under simple stress variations, it is said (20) that the 'strain-hardening' relation[x] may be more accurate, but a comprehensive examination of these theories and others under a variety of multiaxial conditions by Johnson (49) and Berkovits (6) has shown that neither strain- nor time-hardening is invariably reliable. This

[+] This section is based on Freed and Seyna (21).

[x] Assuming strain rate a function of current stress, strain and temperature.

has been verified by other investigators (66). In the special case of creep buckling, Johnson et al (48) have obtained excellent agreement with a time-hardening law: other theoretical studies (62) have shown that where there is a stress which remains substantially constant in magnitude and position, there is little to choose between the two theories.

The fifth assumption is perhaps the most questionable. In the study reported above (48), tensile data was used exclusively in experiments where the stress distribution was both tensile and compressive, without prejudicing the results. Other more comprehensive studies of this question (78, 79) have shown that in some circumstances the data may not be interchangeable.

From assumptions (1) and (2), we have the relation (see Fig. 1)

$$\dot{e} = \dot{\varepsilon}_o + \dot{K}z \tag{4.1}$$

where the suffix refers to the neutral axis.

We also assume a creep law of the form

$$\dot{e} = \dot{\sigma}/E + \dot{\varepsilon}(\sigma, t, T) \tag{4.2}$$

where $\dot{\varepsilon}$ is the creep rate function.

The first approximation made by Alexander (1) was that the stress distribution, which is in practice non-linear, can be represented by the simple relation $\sigma = Mz/I$.

From this it also follows that

$$\dot{\sigma} = \dot{M}z/I \tag{4.3}$$

Substituting from eqn. (4.3) into (4.2), and equating with (4.1), we have

$$\dot{K} = \dot{M}/EI + \frac{\dot{\varepsilon} - \dot{\varepsilon}_o}{z} \tag{4.4}$$

By virtue of assumption (3)

$$\dot{e}_o = \dot{\varepsilon}_o$$

and also

$$\dot{\varepsilon} = \dot{\varepsilon}(\sigma, t, T) = \dot{\varepsilon}(z, t, T) \tag{4.5}$$

since stress is a dependent variable in this problem. Writing (4.5) as

$$\dot{\varepsilon}(z, t) = \dot{\varepsilon}(o, t) + z\dot{\varepsilon}'(o, t) + \frac{z^2}{2}\dot{\varepsilon}''(o, t) \quad (4.6)$$

where it will be permissible to neglect terms of second order and higher by virtue of the second assumption.

Substituting now in (4.4), we have

$$\dot{K} = \dot{M}/EI + \dot{\varepsilon}'(o, t)$$

Now $\partial\dot{\varepsilon}/\partial z = \partial\dot{\varepsilon}/\partial\sigma \cdot \partial\sigma/\partial z$

and $\partial\sigma/\partial z = M/I$

$$\dot{K} = \dot{M}/EI + (\partial\dot{\varepsilon}/\partial\sigma)_o \cdot M/I \quad (4.7)$$

The quantity $(\partial\dot{\varepsilon}/\partial\sigma)_o$, by assumption (5), can be evaluated from constant stress tests, and is the inverse slope of the isochronous stress-creep strain rate curves. Alexander called this quantity $(1/\dot{E})$, and writing eqn. (4.7) in a more familiar form

$$\dot{K} = \dot{M}/EI + M/\dot{E}I \quad (4.8)$$

This equation can be used for problems in which there is a finite stress on the neutral axis: as indicated by Young (89), the $\dot{E}$ modulus becomes infinite as the stress approaches zero. Young also showed that the validity of the approximation deteriorated as the bending moment of the axial load became small in comparison with other applied bending moments. This follows from the anomaly indicated above.

4.2 Symmetric restrained bowing

The restrained bowing phenomenon is of most interest to reactor designers, and therefore it is necessary to consider the axisymmetric shapes which are characteristic of all fuel element designs. It is not reasonable then to suppose that the deformation will remain two dimensional throughout the life of the element: this follows from the presence of three dimensional components in the initial shape or loading system.

A consideration of the three dimensional problem led to the following conclusions[+]:-

[+] A full description of this analysis is given in Appendix 10.3.

1) Within the assumption of a linear stress distribution, it is permissible to treat the bowing of an axisymmetric shape in two different planes independently.

2) When a cylindrical element is bowing inside a circular channel, and the point of contact remains on the same generator of the channel, there is no force interaction between the two planes, and the major plane deformation can still be analysed. There is a geometric interaction, but the problem remains soluble.

3) However there is every reason to believe that the condition required in (2) above is never satisfied in the present case, and that the point of contact moves round the channel in a condition of limiting friction. This implies an additional relation to be satisfied between the forces and the deflected shapes, which would make the solution extremely difficult to obtain.

It was therefore decided to restrict the analysis to two dimensional bowing, and the experiments were designed around axisymmetric specimens with predominantly two dimensional initial deflections. This would restrict the growth of the third dimensional component to a minimum. The analysis thus derived would be applicable to three dimensional bowing in a rectangular channel (see Appendix 10.3) or in a circular channel with large coefficient of friction. A rigorous solution of the general three dimensional problem appears to be a very large undertaking, and cannot at this stage be justified: it seems more logical to gauge the effectiveness of simpler analyses first.

The treatment of the problem will therefore be two dimensional. The behaviour of the element from first loading until contact with the restraining channel can be calculated from simple bowing theory (1, 95, 21); the main theoretical problem begins once contact has been established.

4.2.1 Creep only

The analysis that follows is based largely on that of Blackburn and Percy (8). It differs however in the introduction of additional dimensionless variables, and in the solution time; later, in the numerical

analysis sections (5.1.1, 5.1.2), improved interpolation formulae are introduced. The assumptions of section 4.1 are used once more.

The deformation may be conveniently divided into two phases. In the first, the element merely flattens against the wall, and in the second phase point contact splits and a shape similar to that of Fig. 2 is assumed. It is easier to derive the behaviour in the first phase from the more general equations of the second phase, and this is the procedure followed below.

Referring to Fig. 2, we have the following boundary conditions:

$$\left(\frac{\partial y}{\partial t}\right)_{x = o,\ a,\ L-a,\ L} = o, \quad t \geqslant o$$

also

$$\left(\frac{\partial y}{\partial x}\right)_{x = a,\ L-a,\ L/2} = o, \quad t \geqslant o$$

$$y\ (a,\ L-a) = \delta\ , \quad t \geqslant o$$

and

$$y = f(x), \quad t = o$$

We may express the tangency condition quoted above as

$$\frac{d}{dt}\left(\frac{\partial y}{\partial x}\right)_a = o$$

Expanding this

$$o = (\partial^2 y/\partial x \partial t)_a + \partial/\partial a\ (\partial y/\partial x)_a\ da/dt$$

Hence

$$da/dt = -\frac{\left(\frac{\partial^2 y}{\partial x \partial t}\right)_a}{\left(\frac{\partial^2 y}{\partial x \partial a}\right)_a}$$

Now

$$\partial^2 y/\partial x \partial a = \partial^2 y/\partial x^2$$

and we have

$$\frac{da}{dt} = -\frac{\left(\frac{\partial^2 y}{\partial x \partial t}\right)}{\left(\frac{\partial^2 y}{\partial x^2}\right)_a} \qquad (4.9)$$

Referring now to Fig. 2,
for $o \leq x \leq a$, with clockwise moments positive

$$M = Wx - Py \tag{4.10}$$

and for $a \leq x \leq L/2$, $M = Wa - Py$ [+] (4.11)

Equation (4.8) for creep only becomes

$$\dot{K} = M/\dot{EI} = \partial^3 y/\partial x^2 \partial t \quad \text{from}$$

assumption (2). Substituting in eqns. (4.10, 4.11) we have for $o \leq x \leq a$

$$\dot{EI}\, \partial^3 y/\partial x^2 \partial t + Py = Wx \tag{4.12}$$

and for $a \leq x \leq L/2$

$$\dot{EI}\, \partial^3 y/\partial x^2 \partial t + Py = Wa \tag{4.13}$$

From either of the above at $x = a$ and $y = \delta$,

$$W = 1/a \left\{ \dot{EI}\, (\partial^3 y/\partial x^2 \partial t)_a + P\delta \right\}$$

Substituting in (4.12, 4.13) and dividing by P

$$\frac{\dot{EI}}{P} \frac{\partial^3 y}{\partial x^2 \partial t} + y = \frac{x}{a} \left\{ \frac{\dot{EI}}{P} \left(\frac{\partial^3 y}{\partial x^2 \partial t}\right)_a + \delta \right\} \tag{4.14}$$

and

$$\frac{\dot{EI}}{P} \frac{\partial^3 y}{\partial x^2 \partial t} + y = \frac{\dot{EI}}{P} \left(\frac{\partial^3 y}{\partial x^2 \partial t}\right)_a + \delta \tag{4.15}$$

4.2.1.1 Introduction of dimensionless variables

Defining the non-dimensionless quantities

$$s = 2x/L, \quad r = 2a/L, \quad u = y/\delta$$

equations (4.14) and (4.15) become for $o \leq s \leq r$

$$\frac{4\dot{EI}}{PL^2} \left[\frac{\partial^3 u}{\partial s^2 \partial t} - \left(\frac{\partial^3 u}{\partial s^2 \partial t}\right)_r \cdot \frac{s}{r} \right] = \frac{s}{r} - u \tag{4.16}$$

and for $r \leq s \leq 1$

$$\frac{4\dot{EI}}{PL^2} \left[\frac{\partial^3 u}{\partial s^2 \partial t} - \left(\frac{\partial^3 u}{\partial s^2 \partial t}\right) \right] = 1 - u \tag{4.17}$$

[+] We need only consider half the element.

and (4.9) becomes

$$\frac{dr}{dt} = -\frac{\left(\frac{\partial^2 u}{\partial s \partial t}\right)_r}{\left(\frac{\partial^2 u}{\partial s^2}\right)_r} \qquad (4.18)$$

In ~~this~~ equations 4.16 + 4.17, the quantity $\dot{E}$ is a function of time since

$\dot{\varepsilon} = \dot{\varepsilon}(\sigma, t)$

and $\dot{E} = (\partial \sigma / \partial \varepsilon)_o = \dot{E}(\sigma, t)$

for non-steady creep. It is therefore highly desirable to eliminate the time dependence of the coefficients and the following method is proposed: inspection of equations (4.16 and 4.17) reveal that if we define a new variable v_c^+, called henceforth solution time, as follows

$$\frac{\partial}{\partial t} = \frac{PL^2}{EIQ} \frac{\partial}{\partial v_c} ,$$

where Q is an arbitrary constant, the solution becomes independent of L, P, $\dot{E}$ and I. This is a great advantage and from the rule

$$\frac{\partial}{\partial t} = \frac{\partial v_c}{\partial t} \cdot \frac{\partial}{\partial v_c} ,$$

we have that $\partial v_c / \partial t = PL^2 / QEI \qquad (4.19)$

We now have to specify the time dependence of the quantity $1/\dot{E}$, through a definition of $\dot{\varepsilon}$. Using a Graham-Walles (28)[x] formulation for constant stress and temperature

$$\varepsilon = c_1 \sigma^{n_1} t^{1/3} + c_2 \sigma^{n_2} t + c_3 \sigma^{n_3} t^3$$

from which $\dot{\varepsilon} = (\partial \varepsilon / \partial t) = \frac{1}{3} c_1 \sigma^{n_1} t^{-2/3} + c_2 \sigma^{n_2} + 3 c_3 \sigma^{n_3} t^2$

and neglecting tertiary creep

[+] Where the subscript indicates that creep only is being considered.

[x] See 7.1.1.

$$\frac{1}{E} = \frac{n_1}{3} C_1 \sigma_o^{n_1-1} t^{-2/3} + n_2 C_2 \sigma_o^{n_2-1}$$

Substituting in (4.19) and integrating

$$v_c = \frac{PL^2}{QI} (n_1 C_1 \sigma_o^{n_1-1} t^{1/3} + n_2 C_2 \sigma_o^{n_2-1} t) \qquad (4.20)$$

We may now arbitrarily choose Q; a convenient relation between v and t would be v_c directly equal to the doubling time+. This correspondence would be continuously true for secondary creep only, but only approximately true for primary and secondary creep; it is nevertheless a good means of estimating resistance to bowing. Discarding therefore the primary creep term for the purpose of fixing Q, putting $v_c = 1$ and

$$t = t_D = \frac{\pi^2 \dot{E} I \ln 2}{PL^2}$$

and noting that for secondary creep

$$1/\dot{E} = n_2 C_2 \sigma_o^{n_2-1}$$

we find $Q = \pi^2 \ln 2$; substituting in (4.19),

$$\frac{\partial}{\partial t} = \frac{PL^2}{\pi^2 \dot{E} I \ln 2} \cdot \frac{\partial}{\partial v_c} \qquad (4.21)$$

Using this transformation in (4.16, 4.17) we obtain the equations

$$\frac{4}{\pi^2 \ln 2}\left[\frac{\partial^3 u}{\partial s^2 \partial v_c} - \left(\frac{\partial^3 u}{\partial s^2 \partial v_c}\right)_r \cdot \frac{s}{r}\right] = \frac{s}{r} - u \qquad (4.22)$$

and

$$\frac{4}{\pi^2 \ln 2}\left[\frac{\partial^3 u}{\partial s^2 \partial v_c} - \left(\frac{\partial^3 u}{\partial s^2 \partial v_c}\right)_r\right] = 1 - u \qquad (4.23)$$

and

$$\frac{dr}{dv_c} = \frac{-\left(\frac{\partial^2 u}{\partial s \partial v_c}\right)_r}{\left(\frac{\partial^2 u}{\partial s^2}\right)_r} \qquad (4.24)$$

The dimensionless wall force $X = WL/2P\delta$, is now defined by the equation

+ The time for a column bowing in secondary creep to double it's deflection is constant for small deflections - see section 4.4.1.1.

$$X = \frac{1}{r}\left[\frac{4}{\pi^2 \ln 2}\left(\frac{\partial^3 u}{\partial s^2 \partial v_c}\right)_r + 1\right] \qquad (4.25)$$

The v_c - t relation then becomes

$$v_c = \frac{PL^2}{\pi^2 I \ln 2}\left(n_1 C_1 \sigma_o^{n_1 - 1} t^{1/3} + n_2 C_2 \sigma_o^{n_2 - 1} t\right) \qquad (4.26)$$

Thus solutions of eqns. (4.22 - 4.24) are now quite general for a particular initial shape and can be obtained without reference to problem geometry or creep properties. Once the solution is obtained, the relation between solution time and real time, which is the function (4.26), can be rapidly calculated by a graphical method; see Appendix 10.4.

4.2.1.2 Splitting of point contact

It is now pertinent to inquire how the shape depicted in Fig. 2, is arrived at from an approximately sinusoidal shape at first contact: i.e. how does the transition from the first to the second phase take place? This question was resolved in an elegant manner by Blackburn and Percy (8). The relevant analysis is lengthy but the essential details are contained in Appendix 10.5. By integrating equation (4.23) and substituting in the numerator of (4.24) the following equation is obtained

$$\frac{4}{\pi^2 \ln 2} \cdot \frac{dr}{dv_c} = \frac{\frac{3(1-r)}{r(2r-3)}\left[\int_o^r \int_o^s u \, dw \, dw - r\int_o^1 u \, dw\right] - \int_r^1 u \, dw}{\left(\frac{\partial^2 u}{\partial s^2}\right)_r} \qquad (4.27)$$

For shapes that are symmetrical but not in contact initially at the point of symmetry ($r \neq 1$), the numerator will be finite in general, and unless $(\partial^2 u/\partial s^2)_r = 0$, the motion will be defined by equation (4.24). This will be the most usual situation. If the curvature at first contact is zero, dr/dv will be infinite in general and the analysis of section 4.2.1.4 will be applicable. The above shapes ($r \neq 1$) are not likely to be typical: the most usual symmetric shape will be sinusoidal ($r = 1$ initially) or sinusoidal with some third

harmonic content. We restrict subsequent analysis to shapes having $r = 1$ initially.

For shapes having $\partial^2 u/\partial s^2 = 0$ at the instant of first contact (such as a sine wave + 1/9 third harmonic) there is no flattening phase: point contact splits immediately, and dr/dv is infinite (see section 4.2.1.4). For other shapes, eqn. (4.27) reveals that when $r = 1$, dr/dv_c is zero. This implies that when contact is first made with the wall at $r = 1$, the element continues to flatten: dr/dv can only become non-zero when the denominator also becomes zero, i.e. when curvature disappears at the point of contact. As the equation then takes the indeterminate form 0/0, it is necessary to differentiate numerator and denominator to obtain a finite limit for dr/dv. This yields the following at $s = r = 1$:

$$\lim_{r \to 1} \quad \frac{4}{\pi^2 \ln 2} \frac{dr}{dv_c} = \frac{1 - 3\int_0^1 s\,u\,d\,s}{\left(\frac{\partial^3 u}{\partial s^3}\right)_1} \qquad (4.28)$$

4.2.1.3 Rate of splitting finite

There are now two possibilities: if the third-derivative is non zero, there is a finite limit for dr/dv given by the above equation (4.28). Blackburn and Percy (8) assumed however that the third derivative would be zero for symmetrical cases, because in general the odd derivatives of symmetric analytic functions vanish at the point of symmetry. However in the case of functions where the second derivative is non-zero at the instant of first contact, like a symmetrical sine wave, a finite time elapses between first contact and the disappearance of curvature; there is therefore a finite force between the element and the wall. This implies that there is a discontinuity in the third derivative, which cannot therefore be zero. In this sense therefore, the analysis of Blackburn and Percy is in error at this point.

4.2.1.4 Rate of splitting infinite

The second of the possibilities mentioned above, is that the third derivative is also zero at the instant of curvature disappearing.

This is possible for shapes which have a zero second derivative at the point of first contact; the wall force and third derivative are both then zero, and point contact splits immediately. For this case, eqn. (4.28) shows that dr/dv will be infinite. However Blackburn and Percy were able to find a finite limit (see Appendix 10.5.1) for the indeterminate quantity $(1 - r)\, dr/dv_c$ by successive differentiation. They assumed that all functions could be treated in this way, but in fact the analysis is only valid for the type of function mentioned above. It is believed however that the error arising from such a procedure would be small and important only in the early stages of deformation.

4.2.1.5 Flattening phase

The deformation during the period between first contact and subsequent splitting of point contact, i.e. the first phase, is governed also by the three equations (4.22 - 25). In this case since $dr/dv_c = 0$ until curvature disappears, we have that r = 1 throughout the period; of the four equations only (4.22 and 4.25) are needed. The boundary conditions associated with this phase are slightly altered to become

$$(\partial y/\partial t)_{x=0,\frac{L}{2}} = 0 \text{ and } (\partial y/\partial x)_{x=\frac{L}{2}} = 0$$

Equation (4.22) takes the simple form (since r is constant and equal to 1)

$$\frac{4}{\pi^2 \ln 2}\left[\frac{\partial^3 u}{\partial s^2 \partial v_c} - s\left(\frac{\partial^3 u}{\partial s^2 \partial v_c}\right)_{s=1}\right] = s - u \qquad (4.29)$$

and (4.25) becomes $$X = \frac{4}{\pi^2 \ln 2}\left(\frac{\partial^3 u}{\partial s^2 \partial v_c}\right)_{s=1} + 1 \qquad (4.30)$$

It is apparent from (4.30) that as the curvature is increasing throughout this phase $-\left(\frac{\partial^3 u}{\partial s^2 \partial v_c}\right)_{s=1} > 0$,

a finite force ≥ 1 is predicted at the instant $v_c = 0$. This is obviously incorrect and is a defect in the analysis which is removed

by the inclusion of elastic deformation; the equation for the wall force then becomes more properly an initial value problem, and the force is initially zero.

If we were considering point restraint, these would be the governing equations throughout the deformation until the element came into point contact at some other position along it's length; the equation would then be slightly modified to take account of other forces.

The numerical analysis used in the solution of the equations of section 4.2.1 is presented in section 5.1.1. The computed solution of the flattening phase - eqn. (4.29) for an initially sinusoidal shape is given in Fig. 7. For generality both solution time and real time (calculated for a $\frac{1}{2}$ ins. specimen at 295°C, $P/P_E = 0.2$) are given. The dimensionless force-time relation, eqn. (4.30), was also computed and is shown in Fig. 12, 13. As indicated previously, this phase terminates when curvature disappears at the point of contact.

Fig. 8 shows the deformation after point contact has split - eqns. (4.22 - 24) for an initially sinusoidal shape - a continuation of Fig. 7. The force-time relation is on Figs. 12, 13.

Fig. 9 shows the deformation for a sinusoidal shape with third harmonic 1/9 the fundamental. In this case since the curvature is initially zero there is no flattening phase, and the time origin in Fig. 10 is zero. The forces for this initial shape are also given in Figs. 12, 13. The $\dot{r} - v_c$ relation for both the shapes is in Figs. 10, 11, and for the column specified above the $v_c - t$ relation is shown in Fig. 19.

4.2.2 Creep and elasticity

The equations derived in this section were intended to assess the significance of elastic strains in restrained bowing, by comparison with the easier solution of the 'creep only' problem given in the previous section.

Using eqn. (4.8), and differentiating (4.10) and (4.11) to obtain $\dot{M}$, the following are derived from Fig. 2:

$$\partial^3 y/\partial x^2 \partial t = \dot{W}x/EI - Py/EI + Wx/EI - \dot{P}y/EI$$

$$0 < x < a \qquad (4.31)$$

and $\partial^3 y/\partial x^2 \partial t = Wa/EI - Py/EI + Wa/EI + Wa/EI - Py/EI$

$a < x < L/2$ (4.32)

The boundary and tangency conditions are unchanged. It should be noted that in the preceding section we are able to write the curvature rate $\dot{K}$ as either

$$\partial^3 y/\partial t \partial x^2 \quad \text{or} \quad \partial^3 y/\partial x^2 \partial t,$$

since the quantity was continuous; however it is now evident that the presence of elastic deformation in the above equations causes a discontinuity to appear in $(\partial^3 y/\partial x^2 \partial t)_{x=a}$. Experience with the solution of eqns. (4.20, 4.21) showed that the maximum value of the discontinuity in the dimensionless quantity $(\partial^3 u/\partial s^2 \partial v)_r$, (which can be shown from (4.31, 4.32) above to be $\pi^2 P/P_E \cdot \frac{RL}{P\delta} \cdot \frac{dr}{dv}$), did not exceed 5 per cent of the quantity. It was thus not considered necessary to adopt a more rigorous treatment, because of the large penalty in computational complexity. An example of a numerical scheme which does take this into account is shown in section 5.1.3.3.

4.2.2.1 Dimensionless equations

Using the same dimensionless variables as before, and the wall force

$$X = WL/\delta P \delta ,$$

we derive from (4.31) and (4.32) the equations

$$\frac{4\dot{E}I}{PL^2} \frac{\partial^3 u}{\partial s^2 \partial t} = X\delta - u + \dot{X} \frac{\delta \dot{E}}{E} - \dot{u} \frac{\dot{E}}{E} \qquad (4.33)$$

$o < s < r$

and

$$\frac{4\dot{E}I}{PL^2} \frac{\partial^3 u}{\partial s^2 \partial t} = Xr - u + \frac{\ddot{X}rE}{E} + \dot{X} \frac{r\dot{E}}{E} - \dot{u} \frac{\dot{E}}{E} \qquad (4.34)$$

$r < s < 1$

Following reasoning identical to that given in section 4.2.1, we introduce the relation[+]

$$\frac{\partial}{\partial t} = \frac{PL^2}{\pi^2 \dot{E}I \, (1 - P/P_E) \ln 2} \frac{\partial}{\partial v_{ce}} \qquad (4.35)$$

the term in P_E being introduced because of the presence of Youngs

[+] The subscript indicates that creep and elasticity are considered.

modulus in the equation. Using (4.35) in (4.33, 34) for $o < s < r$

$$\frac{4}{\pi^2(1 - P/P_E) \ln 2} \frac{\partial^3 u}{\partial s^2 \partial v_{ce}} = Xs - u + \frac{P/P_E}{(1 - P/P_E) \ln 2} \cdot s \frac{\partial X}{\partial v_{ce}}$$

$$- \frac{P/P_E}{(1 - P/P_E) \ln 2} \frac{\partial u}{\partial v_{ce}} \qquad (4.36)$$

and for $r < s < 1$

$$\frac{4}{\pi^2(1 - P/P_E) \ln 2} \frac{\partial^3 u}{\partial s^2 \partial v_{ce}} = Xr - u + \frac{P/P_E}{(1 - P/P_E) \ln 2} \cdot X \frac{\partial r}{\partial v_{ce}}$$

$$+ \frac{P/P_E}{(1 - P/P_E) \ln 2} \cdot r \frac{\partial X}{\partial v_{ce}} \qquad (4.37)$$

The terms in X can be eliminated by invoking the boundary conditions at r; and setting

$$B = \frac{P/P_E}{(1 - P/P_E) \ln 2} \text{ , and } C = \frac{4}{\pi^2 (1 - P/P_E) \ln 2}$$

for $o < s < r$

$$C \frac{\partial^3 u}{\partial s^2 \partial v_{ce}} = C \frac{s}{r} \left(\frac{\partial^3 u}{\partial s^2 \partial v_{ce}}\right)_r + \frac{s}{r} - u - B \frac{\partial u}{\partial v_{ce}} \qquad (4.38)$$

and for $r < s < 1$

$$C \frac{\partial^3 u}{\partial s^2 \partial v_{ce}} = C \left(\frac{\partial^3 u}{\partial s^2 \partial v_{ce}}\right)_r + 1 - u - B \frac{\partial u}{\partial v_{ce}} \qquad (4.39)$$

It is now evident that for the case of no elasticity ($P_E \to \infty$), equations (4.35, 4.38, 4.39) become identical with (4.21, 4.22, 4.23) as would be expected.

The appropriate equation for the wall force is

$$\frac{\partial X}{\partial v_{ce}} = \frac{C}{Br} \left(\frac{\partial^3 u}{\partial s^2 \partial v_{ce}}\right)_r + \frac{1}{rB} - \frac{X}{B} \qquad (4.40)$$

From equation (4.35) we find

$$v_{ce} = \frac{AL^2}{\pi^2 I\,(1 - P/P_E)\,\ln 2}\,(n_1 C_1 \sigma_o^{n_1} t^{1/3} + n_2 C_2 \sigma_o^{n_2} t) \quad (4.41)$$

This relation is readily evaluated by a graphical method (see Appendix 10.4).

One immediate result of the introduction of elasticity in the equations above is some loss of generality: we now obtain a solution as a function of v_{ce}, which is valid only for the value of P/P_E chosen. This is rather restrictive, and it would be worthwhile to know whether the importance of elastic deformation justifies it's inclusion: the results of this investigation are discussed in section 8.2.1.3.

4.2.2.2 Splitting of point contact

Identical arguments to those used in section 4.2.1.3, 4.2.1.4 apply, and the detailed analysis for the limits on dr/dv is outlined in Appendix 10.5.2.

4.2.2.3 Flattening phase

As in the 'creep only' case, the equation for the flattening phase is found from (4.38)

$$C\,\partial^3 u/\partial s^2 \partial v_{ce} = Cs\,(\partial^3 u/\partial s^2 \partial v_{ce})_{s=1} + s - u - B\,\partial u/\partial v_{ce} \quad (4.42)$$

and the force equation is

$$\partial X/\partial v_{ce} = \frac{C}{B}\left(\frac{\partial^3 u}{\partial s^2 \partial v_{ce}}\right)_1 + \frac{1}{B} - \frac{X}{B} \quad (4.43)$$

The numerical analysis used in the solution of the equations of section 4.2.2 is shown in section 5.1.2; the computed solutions showed that when the results were presented in terms of real time for $P/P_E = 0.2$, the effect of elasticity on the deflections was negligible. These computations are therefore not illustrated; however there was some noticeable effect on the forces and this is shown in Fig. 12.

4.3 Asymmetric restrained bowing

During the course of the experimental work, it soon became apparent that small but unavoidable asymmetric components were present in the initial shapes of the specimens. This type of function cannot be treated using the equations of section 4.2, and new equations were evolved.

In the symmetric case, the point of contact remains stationary until curvature disappears, and the element flattens against the channel. However in the asymmetric case, it is found that the point of contact begins to move immediately after touching the channel. Deformation then continues and the element usually flattens into two point contact; this second phase of the deformation will not be entered if the asymmetric component is very large. In this case the element will probably snap away from the channel without ever being in two point contact. This can however be treated by the first phase analysis.

We consider here only the case of creep and elastic deformation. The extension of the equations to the case of creep only is readily performed.

4.3.1 First phase of deformation

Fig. 3 illustrates the first phase of deformation.

From moment equilibrium

$$R'' = a\,R/L, \quad R' = (1 - a/L)\,R$$

The boundary conditions are now

$$\left.\begin{aligned} &(dy/dt)_{x=0,\ a,\ L} = 0 \\ &(dy/dx)_{x=a} = 0 \\ &y(a) = \delta \end{aligned}\right\} \quad t \geqslant 0$$

Writing the bending moments in terms of R, and incorporating these in eqn. (4.8), for $a < x < a$

$$\frac{\partial^3 y}{\partial x^2 \partial t} = (1 - a/L)\,\dot{R}x/EI - \dot{P}y/EI + \frac{x}{EI}(1 - a/L)\frac{dR}{dt} - \frac{Rx}{EIL}\frac{da}{dt} - \frac{P}{EI}\frac{\partial y}{\partial t} \qquad (4.44)$$

and for $a < x < L$

$$\frac{\partial^3 y}{\partial x^2 \partial t} = (1 - x/L)\, Ra/EI - Py/EI + \frac{R(1 - \frac{x}{L})}{EI}\frac{da}{dt} + \frac{a}{EI}\frac{dR}{dt}(1 - \frac{x}{L}) - \frac{P}{EI}\frac{\partial y}{\partial t} \tag{4.45}$$

The discontinuity in $(\partial^3 y/\partial x^2 \partial t)a$ is once more neglected.

Introducing dimensionless variables, now in terms of the whole length,

$$s = x/L,\ r = a/L,\ u = y/\delta\ ,\ v_{ce} \text{ as before,}$$

and eliminating R, dR/dt by methods analagous to section 4.2.2, the equations become[+] for $o < s < r$

$$D\frac{\partial^3 u}{\partial s^2 \partial v} = D\frac{s}{r}\left(\frac{\partial^3 u}{\partial s^2 \partial w}\right)_r + \frac{s}{r} - u - B\frac{\partial u}{\partial v} \tag{4.46}$$

and

$$D\frac{\partial^3 u}{\partial s^2 \partial v} = D\frac{1 - s}{1 - r}\left(\frac{\partial^3 u}{\partial s^2 \partial v}\right)_r + \frac{1 - s}{1 - r} - u - B\frac{\partial u}{\partial v} \tag{4.47}$$

for $r < s < 1$

$$D = \frac{1}{\pi^2(1 - P/P_E)\ln 2} \tag{4.48}$$

and

$$B = \frac{P/P_E}{(1 - P/P_E)\ln 2} \tag{4.49}$$

The equation for the wall force $Y = RL/P\delta$ is given by

$$\frac{\partial Y}{\partial v} = \frac{D}{Br(1 - r)}\left(\frac{\partial^3 u}{\partial s^2 \partial v}\right)_r + \frac{Y}{1 - r}\frac{dr}{dr} - Y/B + \frac{1}{rB(1-r)} \tag{4.50}$$

The tangency condition (4.24) applies once more; in this case dr/dv is in general determinate at all times, but the analysis of 4.2.1.2, 4.2.1.3 could be applied if necessary to treat a case of zero curvature. This condition was not encountered in the experiments or in any of the analytic shapes, and will not be considered in detail.

[+] As henceforth we shall be including elastic deformation in all the analysis, we shall write v for v_{ce}.

Equations (4.46, 4.47, 4.50) are applicable until either snap buckling occurs, as evidenced by the wall force decreasing to zero, or when the deflection in the element becomes equal to the channel clearance elsewhere, i.e. $u(s) = 1$, $s \neq r$.

The latter condition was the one of most interest and is analysed in the next section.

The theory was applied to two asymmetric analytical shapes, chosen to be comparable with those presented by Blackburn (9). As elastic effects were again found to be negligible, the results are given in terms of v_c. The first case considered was a sine wave with second harmonic in the ratio 34/3, and the second case was a sine wave and second harmonic in the ratio 2/1. This solution is depicted in Figs. 14, 15, and the forces and $r - v_c$ data are given in Figs. 16, 17.

The theory was also applied to the asymmetric experimental initial shapes. In all cases the theory showed that the specimens would flatten until two point contact was established; the shape at this instant is shown on the Figs. 24 - 55. In all cases the material data derived from the buckling experiments was used in computing the $v_c - t$ relations. This was done because there seemed to be some doubt as to the interchangability of tensile and compressive creep data (see section 8.1.2).

4.3.2 Second phase of deformation

With reference to Fig. 4, we have the following relations for bending moments: for $o < x < a_1$

$$M_1 = \frac{Rx}{3} - Py$$

for $a_1 < x < a_2$

$$M_2 = \frac{Rx}{3} - R_1 (x - a_1) - Py$$

and for $a_2 < x < L$

$$M_3 = \frac{Rx}{3} - R_1 (x - a_1) - R_2(x - a_2) - Py$$

Expressing R_3 in terms of R_1 and R_2 from moment equilibrium, substituting in eqn. (4.8) and eliminating the wall forces through the use of the boundary conditions on y and $\partial y/\partial t$ at the points of contact, we have for $o < s < r$,

$$D\frac{\partial^3 u}{\partial s^2 \partial v} - D\frac{s}{r_1}\left(\frac{\partial^3 u}{\partial s^2 \partial v}\right)_{r_1} + B\frac{\partial u}{\partial v} = \frac{s}{r_1} - u \qquad (4.51)$$

and for $r_1 < s < r_2$

$$D\frac{\partial^3 u}{\partial s^2 \partial v} - \frac{(r_2 - s)}{(r_2 - r_1)}\left(\frac{\partial^3 u}{\partial s^2 \partial v}\right)_{r_1} + \frac{(r_1 - s)}{(r_2 - r_1)}\left(\frac{\partial^3 u}{\partial s^2 \partial v}\right)_{r_2} + B\frac{\partial u}{\partial v} = 1 - u \qquad (4.52)$$

and for $r_2 < s < 1$

$$D\frac{\partial^3 u}{\partial s^2 \partial v} - D\frac{(1 - s)}{(1 - r_2)}\left(\frac{\partial^3 u}{\partial s^2 \partial v}\right)_{r_2} + B\frac{\partial u}{\partial v} = \frac{(1 - s)}{(1 - r_2)} - u \qquad (4.53)$$

in terms of the same dimensionless variables and constants as before.

It will be noted that equations (4.46, 4.51) and (4.47, 4.53) are identical as would be expected.

The equations defining the dimensionless wall forces $Y_1 = R_1 L/P\delta$, $Y_2 = R_2 L/P\delta$, can be shown to be

$$B(1 - r_1)\dot{Y}_1 + B(1 - r_2)\dot{Y}_2 = BY_1\dot{r}_1 + BY_2\dot{r}_2 + \frac{D}{r_1}\left(\frac{\partial^3 u}{\partial s^2 \partial v}\right)_{r_1} + \frac{1}{r_1} - Y_1(1 - r_1) - Y_2(1 - r_2) \qquad (4.54)$$

and

$$B\dot{Y}_1 r_1 + B\dot{Y}_2 r_2 = D\left(\frac{1}{1 - r_2}\right)\left(\frac{\partial^3 u}{\partial s^2 \partial v}\right)_{r_2} - BX_2\dot{r}_2 - BX_1\dot{r}_1 + \left(\frac{1}{1 - r_2}\right) - X_1 r_1 - X_2 r_2 \qquad (4.55)$$

Equations (4.51 - 4.55) define the deformation during this phase, together with the tangency conditions as before

$$\frac{dr_1}{dv} = -\left(\frac{\frac{\partial^2 u}{\partial s \partial v}}{\frac{\partial^2 u}{\partial s^2}}\right)_{r_1}, \quad \frac{dr_2}{dv} = \left(\frac{-\frac{\partial^2 u}{\partial s \partial v}}{\frac{\partial^2 u}{\partial s^2}}\right)_{r_2} \qquad (4.56, 4.57)$$

It is not anticipated that the tangency relations could become either indeterminate or infinite. If this were the case, an analysis of the type presented in section 10.5 would be applicable.

The numerical method of solution is illustrated in section 5.1.3.2. A computation—continuing from the first phase of deformation, section 4.3.1, on a sine wave with second harmonic in the ratio 34/3, is shown in Fig. 14, and the displacement of the points of contact in Fig. 16.

The computation was also applied to one of the experimental shapes - Test 55, Fig. 38. More were not attempted because the calculation was exceedingly lengthy: this resulted from the very short step length dictated by stability requirements (see section 5.1.3.2). It was also obvious that the asymmetric component was decaying rapidly, and that this type of computation was not really warranted for such small degrees of asymmetry.

4.4 Miscellaneous equations

The use of the general equation (4.8) is illustrated in deriving relations for use in the free bowing phase, and also for testing the sensitivity of the buckling experiments to eccentricity in the loading system: it was hoped in this way to identify some of the scatter in the buckling data.

4.4.1 Free bowing phase

4.4.1.1 Doubling times

The method of solution for the sinusoidal column given here is essentially the one-point collocation method of Alexander (1), satisfying the equations at the mid-height of the column only. It is known that more precise variational methods (80), satisfying the equations in an average way over the length of the column, do not yield significantly different results.

From Fig. 5, we have the following moment relations

$$M = -Py, \quad \dot{M} = -\dot{P}y,$$

and from equation (4.8),

$$\partial^3 y/\partial x^2\,\partial t = -Py/EI - \dot{P}y/EI \qquad (4.58)$$

If the deflected shape is assumed to be $y = b(t) \sin \pi x/L$, substitution in the above equation at $x = L/2$ yields

$$-\frac{\pi^2}{L^2}\frac{db}{dt} = -\frac{Pb}{EI} - \frac{\dot{P}b}{EI}$$

Separating the variables and integrating

$$\log_e \left(\frac{b_2}{b_1}\right) = \frac{PL^2}{\pi^2 I \left(1 - P/P_E\right)} \int_o^t \frac{\dot{w}}{E} \qquad (4.59)$$

where b_1 and b_2 are initial and current deflections. A similar equation was derived by Webster and Alexander (95) from incremental analysis. For the purpose of defining the doubling time we assume $\dot{E}$ constant (secondary creep only) and setting $b_1/b_2 = 2$

$$t_D = \frac{\pi^2 \dot{E} I \left(1 - P/P_E\right) \ln 2}{PL^2}$$

4.4.1.2 Non sinusoidal shape

For the more general shapes encountered during the experiments, the general eqn. (4.58) was used. In terms of the same dimensionless variables as for the asymmetric shapes (section 4.3).

$$D \partial^3 u / \partial s^2 \partial v + B \partial u / \partial v \checkmark = \dot{u} \qquad (4.60)$$

The numerical solution is given in section 5.2. This equation was used for the deformation history subsequent to the application of load, until contact was made with the channel. The resulting correlation with experiment is shown in Fig. 66.

4.4.2 Effect of eccentricity

When the self-weight of the column is negligible in comparison with the direct load, as in the buckling experiments performed to assess the $\dot{E}$ theory, it is possible to calculate the effect of small eccentricities on the bowing rates quite simply. If the weight of the column is appreciable, a more complex equation arises (7).

From Fig. 6, for moment equilibrium and $L \gg q$,

$$Z = Pq/L$$

$$M = -Py + Zx = -Py + Pq\, x/L$$

$$\dot{M} = -P\dot{y}$$

and from substitution in eqn. (4.8)

$$\frac{\dot{E}I}{P} \frac{\partial^3 y}{\partial x^2 \partial t} + y + \dot{y} \frac{\dot{E}}{E} = \frac{qx}{L}$$

Introducing the dimensionless variables $s = x/L$, $c = y/q$, and the solution time v_{ce} defined previously,

$$D\,\partial^3 c/\partial s^2 \partial v + c + B\,\partial c/\partial v = s \qquad (4.61)$$

with boundary conditions

$$(\partial c/\partial v)_{s = 0,\ 1} = 0$$

and $c = c(s),\ t = o$

This equation is analytically soluble for a certain class of initial shapes $c(s)$, but a numerical solution was used, and is described in section 5.3.

The resulting c - v data for $q = .03$ ins., $b_1 = .025$ ins., $P/P_E = 0.2$ (shown in Fig. 59) on a $\frac{1}{2}$ ins. Magnox specimen, was converted into c - t data using the creep data of Figs. 62, 63. When the deflections are processed in the same way as the experimental data, it is found that the results are a function only of the increments in deflection (section 7.2); it was also found that the effect of the eccentricity on the increments in deflection was negligible, whether positive or negative. The result shown on Figs. 62, 63 therefore represents other errors in the analysis - e.g. curve fitting, truncation errors etc.

4.4.3 Initial elastic deflections

It is required to determine the elastic deflection of the column under the weight of the loading system and immediately after the application of the load. For sinusoidal shapes, well known formulae exist for this purpose, but to treat the more general asymmetric experimental shapes encountered, the following equation was used

$$\frac{M}{EI} = K_2 - K_1 ,$$

where the suffices 1 and 2 refer to initial and final curvatures.

Since (Fig. 5) $M = -Py$, we have

$$d^2y_2/dx^2 + Py/EI = d^2y_1/dx^2 \qquad (4.62)$$

A numerical solution was used, and is shown in section 5.4.

5.0 Numerical analysis+

5.1 Restrained bowing equations

As all the restrained bowing equations appeared intractable to analytical methods, numerical solutions were used in all cases. This also enabled the specimen to specimen variations in initial shape to be accounted for.

5.1.1 Symmetric equations, creep only

5.1.1.1 Flattening phase

The equation governing the deformation of this phase, when r = 1, is (4.29) viz.

$$\frac{4}{\pi^2 \ln 2}\left[\frac{\partial^3 u}{\partial s^2 \partial v_c} - s\left(\frac{\partial^3 u}{\partial s^2 \partial v_c}\right)_{s=1}\right] = s - u$$

$$\text{for } o \leqslant s \leqslant 1 \qquad (5.1)$$

with the boundary conditions

$$u = f(s), \quad v_c = o$$

and

$$(\partial u/\partial v_c)_{s=o,1} = (\partial u/\partial s)_{s=1} = o, \quad v_c \geqslant o$$

The dimensionless wall force from (4.30) is

$$X = \frac{4}{\pi^2 \ln 2}\left(\frac{\partial^3 u}{\partial s^2 \partial v_c}\right)_{s=1} + 1 \qquad (5.2)$$

The numerical solution for this phase is considerably simpler than the following phase, because the point of contact is stationary and there is only one variable u(s,v) (this is analagous to the case of point restraint). The most convenient and accurate method of solution is to convert equations of the type above into a series of initial value problems, one for each space mesh point; once this has been done it is possible to use the Runge-Kutta method of forward integration. These have leading error terms of the order $(\delta t)^5$, and are therefore much more accurate than the alternative backward or

+ As this section is concerned purely with the numerical solution of equations derived in Section 4, it may be omitted in a first reading if desired.

forward difference relation for the time derivative as used by Young (90) and Fudge and Haigh (22, 23, 29).

There are in principle two methods of eliminating the space derivative. The first and most elegant, is to remove the derivatives by analytical integration, as shown by Blackburn (9). A typical equation of this type would then be (by integrating eqn. (4.36))

$$C \frac{\partial u}{\partial v_c} = \frac{Xs^3}{6} - \int_o^s \int_o^s u \, dw \, dw + \frac{\dot{B}Xs^3}{6} - B \int_o^s \int_o^s \frac{\partial u}{\partial v_c} \cdot dw \, dw +$$

$$B s \int_o^1 \frac{\partial u}{\partial v_c} dw + s \int_o^1 u \, dw - X r s \left(1 - \frac{r}{2}\right) - \dot{B}Xrs \, (1 - r) + \dot{B}Xrs(1 - r/2)$$

$$\text{for } o < s < r \qquad (5.3)$$

In this case if the space region had been divided into M segments, there would be M initial value problems of the type shown above, and equation (4.40) for the force X. For the creep only solution given by Blackburn (9), all the terms with coefficients B in (5.3) would disappear, which implies that the equations are explicit in $(\partial u / \partial v)$, as required for Runge-Kutta integration. However for the more general solution of the problem including elasticity, the implicit nature of equation (5.3) would make the solution inaccurate, and difficult to start; the analytic method is attractive in the case of creep only. It is only required to perform repeated numerical quadrature to evaluate the integrals, in comparison with the less accurate numerical differentiation required by the alternative method below.

Consider the space region divided into M segments, and replace the continuous variable s by the finite difference variable $m \delta s$, where $\delta s = 1/M$, and m = 0, 1, ... M. Equation (5.1) then becomes

$$\frac{4}{\pi^2 \ln 2} \left[M^2 \left\{ \frac{\partial u}{\partial v_{m-1}} - 2 \frac{\partial u}{\partial v_m} + \frac{\partial u}{\partial v_{m+1}} \right\} - M m G \left(\frac{\partial u}{\partial v} \right)_M \right] = \frac{m}{M} - u \qquad (5.4)$$

$$\text{for } m = 1, 2 \ldots M - 1.$$

The second derivative $(\partial^3 u / \partial s^2 \partial v_c)_m$ has been replaced by its equivalent central difference approximation, and the quantity

$(\partial^3 u/\partial s^2 \partial v_c)_M$ by an operator $M^2 G(\partial u/\partial v_c)$ - see Appendix 10.6.1. In this case we would incorporate in G the information that the function is symmetric about the point m = M.

Equations (5.4) form a set of linear simultaneous equations in $(\partial u/\partial v)_m$, which can be solved by matrix inversion and matrix vector multiplication. When the $(\partial u/\partial v_c)_m$ are known, Runge-Kutta (5) integration can be performed. The inversion of the matrix need only be done once: stepping ahead of the solution involves merely repeating matrix vector multiplication with the new vectors+.

Rewriting eqn. (5.4) as

$$\frac{\partial u}{\partial v_{m-1}} - 2\frac{\partial u}{\partial v_m} + \frac{\partial u}{\partial v_{m+1}} - \frac{m}{M} G\left(\frac{\partial u}{\partial v}\right)_M = \frac{m}{M^3 D'} - \frac{u}{M^2 D'} \qquad (5.5)$$

for m = 1, 2, ... M - 1

and the boundary conditions are

$$(\partial u/\partial v)_{o,M} = (\partial u/\partial s)_M = 0$$

and $$D' = \frac{4}{\pi^2 \ln 2}$$

For G we use the operator (4)

$$G\,(\partial u/\partial v)_M = \left(\frac{1}{45}\frac{\partial u}{\partial v_{M-3}} - 0.3\frac{\partial u}{\partial v_{M-2}} + 3\frac{\partial u}{\partial v_{M-1}}\right)$$

since $(\partial u/\partial v)_M = 0$

The equation can then be written in the matrix-vector form:-

+ Another powerful argument in favour of the matrix and Runge-Kutta technique, is that they are available in machine language on the London University Atlas.

$$\begin{bmatrix} -2 & 1 & . & . & \frac{-1}{45M} & \frac{0.3}{M} & \frac{-3}{M} \\ 1 & -2 & 1 & . & \frac{-2}{45M} & \frac{0.6}{M} & \frac{-6}{M} \\ . & . & . & . & -\frac{M-2}{45M}+1 & \frac{0.3\,(M-2)}{M}-2 & \frac{-3\,(M-2)}{M}+1 \\ . & . & . & . & -\frac{M-1}{45M} & \frac{0.3\,(M-1)}{M}+1 & \frac{-3\,(M-1)}{M}-2 \end{bmatrix}$$

$$\begin{bmatrix} \partial u/\partial v_1 \\ \partial u/\partial v_2 \\ \partial u/\partial v_m \\ \partial u/\partial v_{M-2} \\ \partial u/\partial v_{M-1} \end{bmatrix} = \begin{bmatrix} \frac{1}{M^3D'} - \frac{u_1}{M^2D'} \\ \frac{2}{M^3D'} - \frac{u_2}{M^2D'} \\ \frac{m}{M^3D'} - \frac{u_m}{M^2D'} \\ \frac{M-2}{M^3D'} - \frac{u_{M-2}}{M^2D'} \\ \frac{M-1}{M^3D'} - \frac{u_{M-1}}{M^2D'} \end{bmatrix}$$

or more shortly as

$$\left[A\right]\left[\partial u/\partial v_m\right] = \left[B\right] \qquad (5.6)$$

hence

$$\left[\partial u/\partial v_m\right] = \left[A^{-1}\right] \cdot \left[B\right] \qquad (5.7)$$

Once the constant matrix $\left[A\right]^{-1}$ has been evaluated, $\left[B\right]$ is a function of the current shape only. Hence using the initial shape to calculate $\left[B\right]$, and the algorithm (5.7), we can calculate the $\left[\partial u/\partial v_m\right]$. Using Runge-Kutta integration, we now step ahead to calculate $u(s, v + \delta v)$. This is then used to calculate $\left[B\right]_{v+\delta v}$ etc. For the flattening phase, the calculation would be terminated when the second derivative (i.e. the curvature) at the point of contact is zero.

A convenient numerical expression for this condition, to an error $(\delta s)^8$ (4) is

$$\left(\frac{\partial^2 u}{\partial s^2}\right)_m = 4\,u_{M-3} - 54\,u_{M-2} + 540\,u_{M-1} - 490\ ;$$

advantage has been taken of the symmetry to obtain a very accurate formula. The force is readily calculated by writing eqn. (5.2) as

$$X = \frac{4M^2}{\pi^2 \ln 2}\ G\ \ (\partial u/\partial v)_M\ +\ 1$$

The solution was tested with M ranging from 8 to 40, and it was found that the time to the disappearance of curvature remained sensibly constant. However, as the next phase of the solution required M = 40, the data presented in Fig. 7 for a sine wave is calculated with M = 40, $\delta v = .125$.

5.1.1.2 Splitting of point contact

In the case of the initially sinusoidal shape, the third derivative is finite at the instant of the curvature disappearing, and eqn. (4.28) is applicable

$$\lim_{r \to 1} \frac{4}{\pi^2 \ln 2} \frac{dr}{dv_c} = \frac{1 - 3\int_0^1 s\,u\,ds}{\left(\frac{\partial^3 u}{\partial s^3}\right)_{s=1}} \qquad (4.28)$$

Using numerical quadrature to evaluate the integral from the shape at the end of the first phase, and a backward difference[+] (since there is a discontinuity at s = 1 in the third derivative) for the third derivative, we can readily evaluate dr/dv at the instant of point splitting. As the value of dr/dv thus obtained is only instantaneously correct, we choose a very small initial time step ($\delta v = .005$) and assume that eqn. (4.28) is valid during this small interval. The subsequent values of dr/dv will be defined by eqn. (4.24).

For the case of the sine wave plus third harmonic 1/9 th of the fundamental, the third derivative is zero at the instant of contact, and dr/dv is infinite. It is possible however to find a finite limit for (1 - r) dr/dv, as shown in Appendix 10.5.1.

This is

$$\lim_{r \to 1} \frac{d(1-r)^2}{dv_c} = \frac{4 - 12\int_0^1 s\,u\,ds}{\frac{4}{\pi^2 \ln 2}\left(\frac{\partial^4 u}{\partial s^4}\right)_1} \qquad (5.8)$$

[+] See Appendix 10.6.2.

By evaluating the integrals it is possible to find an average value of dr/dv_c during the first small time step ($\delta v = .005$).

5.1.1.3 Final phase of deformation

Once point contact has split, the element deforms according to eqns. (4.22 - 4.25). The varying point of contact now becomes a moving boundary within the system, and because of this the matrix of coefficients is no longer constant. It is also necessary to evaluate the interpolated derivatives in the equations.

Using the same numerical method of the previous section, (4.22) becomes

$$\frac{\partial u}{\partial v}_{m-1} - 2\frac{\partial u}{\partial v}_{m} + \frac{\partial u}{\partial v}_{m+1} - \frac{m}{Mr} H \left(\frac{\partial u}{\partial v}\right)_r = \frac{m}{M^3 rD'} - \frac{u}{M^2 D'},$$

$$\text{for } 1 \leqslant m \leqslant J \qquad (5.9)$$

and (4.23) becomes

$$\frac{\partial u}{\partial v}_{m-1} - 2\frac{\partial u}{\partial v}_{m} + \frac{\partial u}{\partial v}_{m+1} - H \left(\frac{\partial u}{\partial v}\right)_r = \frac{1}{M^2 D'} - \frac{u}{M^2 D'}, \qquad (5.10)$$

$$\text{for } J+1 \leqslant m \leqslant 1$$

where the boundary conditions are

$$(\partial u/\partial v)_{o,\,r} = (\partial u/\partial s)_{s=1} = 0$$

and J is the greatest integer $\leqslant r M$. The operator H is defined (Appendix 10.6.4) as

$$M^2 \; h_1 (\partial u/\partial v)_{J-1} + h_2 (\partial u/\partial v)_J + h_3 (\partial u/\partial v)_{J+1} + h_4 (\partial u/\partial v)_{J+2}$$

This is modified suitably to take account of symmetry when $J = M - 1$.

Also when $m = M$, we can replace the central difference operator by one which takes account of the symmetry at this point:

$$(\partial^3 u/\partial s^2 \partial v)_M = M^2 \left[\frac{1}{45} \left(\frac{\partial u}{\partial v}\right)_{M-3} - 0.3 \left(\frac{\partial u}{\partial v}\right)_{M-2} + 3 \left(\frac{\partial u}{\partial v}\right)_{M-1} - \frac{49}{18} \left(\frac{\partial u}{\partial v}\right)_M \right]$$

A typical matrix of equations would be (for J = M - 3)

m \ i	1	2	3	.	.	J - 1	J	J + 1	J + 2	M
1	-2	1	.	.	.	$-\frac{h_1}{Mr}$	$-\frac{h_2}{Mr}$	$-\frac{h_3}{Mr}$	$-\frac{h_4}{Mr}$	.
2	1	-2	1	.	.	$-\frac{2h_1}{Mr}$	$-\frac{2h_2}{Mr}$	$-\frac{2h_3}{Mr}$	$-\frac{2h_4}{Mr}$	.
J	.	.	.	.	.	$1-\frac{Jh_1}{Mr}$	$-2-\frac{Jh_2}{Mr}$	$1-\frac{Jh_3}{Mr}$	$-\frac{Jh_4}{Mr}$	.
J + 1	.	.	.	.	.	$-h_1$	$1-h_2$	$-2-h_3$	$1-h_4$	.
M	.	.	.	.	.	$-h_1$	$\frac{1}{45}-h_2$	$-0.3-h_3$	$3-h_4$	$-\frac{49}{18}$

$$\times \begin{bmatrix} \partial u/\partial v_1 \\ \partial u/\partial v_2 \\ \vdots \\ \partial u/\partial v_{J-1} \\ \\ \\ \partial u/\partial v_M \end{bmatrix} = \begin{bmatrix} \frac{1}{M^3 rD'} - \frac{u}{M^2 D'} \\ \frac{2}{M^2 rD'} - \frac{u}{M^2 D'} \\ \vdots \\ \frac{J-1}{M^3 rD'} - \frac{u}{M^2 D'} \\ \frac{J}{M^3 rD'} - \frac{u}{M^2 D'} \\ \frac{1}{M^2 D'} - \frac{u}{M^2 D'} \\ \frac{1}{M^2 D'} - \frac{u}{M^2 D'} \end{bmatrix}$$

or more compactly as before

$$\left[\frac{\partial u}{\partial v}\right]_m = \left[A^{-1}\right] \cdot [B] \qquad (5.11)$$

where $\left[A\right]^{-1}$ is a function of r. In the Runge-Kutta method of solution, the r.h.s. of (5.11) is evaluated four times within the step length. Rigorously speaking, $\left[A\right]^{-1}$ must also be evaluated four times per step. This could be dispensed with if less accuracy was permissible (see section 5.1.3.3).

The initial condition for this calculation is the shape at the

end of the flattening phase for a sine wave, or the initial shape for a sine wave with 1/9 third harmonic. During the first time step (dr/dv) is calculated from either (4.28) or (5.8); subsequently equation (4.24) is used, viz.

$$\frac{dr}{dv} = \frac{-\left(\frac{\partial^2 u}{\partial s \partial v}\right)_r}{\left(\frac{\partial^2 u}{\partial s^2}\right)_r} = \frac{-E\left(\frac{\partial u}{\partial v}\right)_r}{F(u)_r}$$

where the Lagrangian operators E and F are defined in Appendices 10.6.5, 10.6.6.

The flow of calculation is shown in a simplified manner in Fig. 22. It is not necessary for calculation purposes to evaluate the force at the end of each step, but if it is required the finite difference form of (4.25) is

$$X = \frac{1}{r}\left\{D' M^2 H \left(\partial u/\partial v\right)_r + 1\right\}$$

The computed results shown in Figs. 8, 9 were obtained with M = 40 initially, and after 5 steps with M = 20. It was not found possible to reduce the number of meshes further. The time step δv was held constant at 0.125, once the first three steps at $\delta v = .005$ had been traversed. The $r - v_c$ data and forces are given in Figs. 10, 11, 12.

5.1.2 Symmetric equations, including elasticity

5.1.2.1 Flattening phase

The same geometric conditions obtain for this phase as in section 5.1.1.1.

The relevant equation is (4.42)

$$C\,\partial^3 u/\partial s^2 \partial v_{ce} = Cs\left(\partial^3 u/\partial s^2 \partial v_{ce}\right)_{s=1} + s - u - B\,\partial u/\partial v_{ce}$$

for $o < s < 1$

with the boundary conditions

$$u = u(s), \quad v_{ce} = o$$

$$(\partial u/\partial v_{ce})_{s=0,\ 1} = (\partial u/\partial s)_{s=1} = 0,\ v_{ce} \geqslant 0$$

The same difference approximations are used

$$\partial u/\partial v_{m-1} + (B/M^2C - 2)\partial u/\partial v_m + \partial u/\partial v_{m+1} - \frac{m}{M} G \left(\frac{\partial u}{v}\right)_M = m/M^3\ C - u/M^2C \qquad (5.12)$$

The solution is now identical to the creep only case. It will be noted that $B/M^2C = \pi^2 P/4M^2 P_E \ll 1$, and therefore the effect of elasticity is likely to be small. This is born out by the solution, which was not significantly different from the creep only case. The solution of the force equation (4.43) however forms an initial value problem which is most conveniently solved simultaneously with the equations for $\partial u/\partial v_m$. This is shown in Fig. 11.

5.1.2.2 Splitting of point contact

The analysis of Appendix 10.5.2 reveals that identical considerations apply here, as for the creep only case. The evaluation of dr/dv_{ce}, from the expression

$$\frac{dr}{dv_{ce}} = \frac{1 - 3\int_0^1 s\,u\,ds - 3B\int_0^1 s\,\dot{u}\,ds}{C\left(\frac{\partial^3 u}{\partial s^3}\right)_{s=1} + 3BX}$$

now requiresa knowledge of the forces and $(\partial u/\partial v)$, as well as the deflection at the instant of zero curvature.

5.1.2.3 Final phase of deformation

Equations (4.36, 4.37) become

$$\partial u/\partial v_{m-1} + (B/CM^2 - 2)\partial u/\partial v_m + \partial u/\partial v_{m-1} - H(\partial u/\partial v)_r \cdot m/M_r = m/M^3 rC - u/M^2C$$

$$\text{for } 1 \leqslant m \leqslant J \qquad (5.13)$$

and

$$\partial u/\partial v_{m-1} + (B/Cm^2 - 2)\partial u/\partial v_m + \partial u/\partial v_{m+1} - H\,(\partial u/\partial v)_r = 1/M^2C - u_m/M^2C$$

$$\text{for } J + 1 \leqslant m \leqslant M \qquad (5.14)$$

with boundary conditions

$$(\partial u/\partial v)_{s=o,r} = (\partial u/\partial s)_{s=r,1} = 0$$

The flow of calculation is again as in Fig. 22. We note also that $B/CM^2 \ll 2$, and it was therefore expected that the effects of elasticity would be small, as proved to be the case. The variation of wall force from eqn. (4.40) is shown in Fig. 12.

5.1.3 Asymmetric equations, creep and elasticity

5.1.3.1 First phase of deformation

Equations (4.46, 4.47) become

$$\partial u/\partial v_{m-1} + (B/DM^2 - 2)\partial u/\partial v_m + \partial u/\partial v_{m+1} - H(\partial u/\partial v)_r \cdot m/Mr = m/M^3D - u_m/M^2D \quad \text{for } 1 \leq m < J \qquad (5.15)$$

and

$$\partial u/\partial v_{m-1} + (B/DM^2 - 2)\partial u/\partial v_m + \partial u/\partial v_{m+1} - \frac{1 - m/M}{1 - r} H \left(\frac{\partial u}{\partial v}\right)_r = \frac{1 - m/M}{(1-r)DM^2} - \frac{u_m}{DM^2} \quad \text{for } J + 1 \leq m < M \qquad (5.16)$$

with the boundary conditions

$$(\partial u/\partial v)_{o,\ r,\ M} = (\partial u/\partial s)_r = 0,$$

and equation (4.24) applies as before. Note that the dimensionless variables now refer to the whole length of the element.

In replacing (4.24) by it's finite difference equivalent, it was found that the previous operators E and F were unsuitable. This was attributed to the greater significance of high order derivatives in this case, causing some innaccuracy as $r - J/M \to 0$. The operator E was therefore replaced by $\mathcal{G}$ (see Appendix 10.6.7), a symmetrical Lagrangian operator.

For the curvature, $(\partial^2 u/\partial s^2)r$, the problem is more difficult, because the presence of the shearforce at r introduces a discontinuity in the third derivative; this implies that u(s) is not continuous at

r, and strictly speaking only backward - or forward - difference operators can be used. For symmetric deformation, it was found that this could be ignored; in the asymmetric cases however, the larger forces and higher derivatives precluded this approximate method. Various alternative Hermitian (34) and Newtonian (31) formulae were tried, but were not found to be suitable. Eventually an elegant solution to the problem was developed for the author by McConalogue,[x] using a symmetrical least squares approximation, which we will denote $\gamma'(u)_r$. For this phase then, equation (4.24) becomes

$$\frac{dr}{dv} = \frac{\varphi'(\partial u/\partial v)_r}{\gamma'(u)_r} \qquad (5.17)$$

The flow chart Fig. 22 is again applicable,[+] and a copy of the programme is included in the back of the thesis; solutions for a sine wave with second harmonic in ratio 3/34 are given in Figs. 14, 16, 17. This calculation would proceed until either the wall force became zero and the column snap-buckled away from the wall, or until the column came into contact with the wall at $s \neq r$. This was detected by searching along the deflected shape for a maximum at a point other than r, and stopping the calculation when $u_{s\neq r}$ max = 1. A more detailed flow chart is given in Fig. 23.

As all the experimental shapes were slightly asymmetric, they were used with this computation to predict the deformation histories in the phase prior to two point contact. A standard value of M = 72 was used for all the asymmetric programmes; the detection of the second maximum is very sensitive to mesh size, and whilst Blackburn's (9) results could be reproduced for M = 64, a 7 per cent increase in the time to attain 2-point contact was observed with M = 72. This figure also maintained cotabularity with the 18 measuring points used in the experiments.

The application of the calculation to the experimental shapes is shown in Figs. 24 - 55.

[x] McConalogue, D.J., Personal communication - see Appendix 10.6.8.
[+] In principle only.

5.1.3.2 Final phase of deformation

Once two point contact is established, the equations (4.52 - 4.57) must be solved simultaneously; these equations become, for $1 \leq m \leq 0$

$$\partial u/\partial v_{m-1} + (B/M^2D - 2)\,\partial u/\partial v_m + \partial u/\partial v_{m+1} - H(\partial u/\partial v)_{r_1} \cdot m/Mr_1 = m/M^3 r_1 D - u/M^2 D \qquad (5.18)$$

and for $0 + 1 \leq m \leq J$

$$\partial u/\partial v_{m-1} + (B/M^2D - 2)\,\partial u/\partial v_m + \partial u/\partial v_{m+1} - \frac{r_2 - m/M}{r_2 - r_1} H \left(\frac{\partial u}{\partial v}\right)_{r_1} + \frac{r_1 - m/M}{r_2 - r_1} H \left(\frac{\partial u}{\partial v}\right)_{r_2} = 1/M^2D - u/M^2D \qquad (5.19)$$

and for $J + 1 \leq m \leq M - 1$

$$\partial u/\partial v_{m-1} + (B/M^2D - 2)\,\partial u/\partial v_m + \partial u/\partial v_{m+1} - \left(\frac{1 - m/M}{1 - r_2}\right) H \left(\frac{\partial u}{\partial v}\right)_{r_2} = \frac{1 - m/M}{M^2 D(1 - r_2)} - \frac{u}{M^2 D} \qquad (5.20)$$

with the boundary conditions

$$(\partial u/\partial v)_{s = o,\ r_1,\ r_2,\ 1} = (\partial u/\partial s)_{s = r_1,\ r_2 = o}$$

where 0 is the greatest integer $< r_1 M$

and J is the greatest integer $< r_2 M$.

For the tangency conditions (4.56, 4.57), the symmetrical Lagrangian operator $\mathcal{L}$ was not found to be suitable, due to interactions when $r_1 \approx r_2$. This was replaced by the less accurate but more stable Newtonian operator η (see Appendix 10.6.9). The tangency equations then become

$$\frac{dr_1}{dv} = \left(\frac{\eta(\partial u/\partial v)}{\gamma(u)}\right)_{r_1} \qquad (5.21)$$

and

$$\frac{dr_2}{dv} = \left(\frac{\eta(\partial u/\partial v)}{\gamma(u)}\right)_{r_2} \qquad (5.22)$$

The equations for the wall forces (4.54, 4.55) were too cumbersome

to invert manually, and a small routine was written into the programme to transform them into Runge-Kutta equations, solved simultaneously with (5.18 - 22).

The application of this programme to the case of the sine wave with 2nd harmonic in the ratio 3/34 is shown in Figs. 14, 16, 17. The integration could continue until either the element comes into contact with the opposite side of the channel through reverse bow, or until snap buckling occurs. In practice it is believed that neither will occur during the design life of the fuel element.

The programme was also applied to the experimental shape shown in Fig. 39, Test 55. Only one experiment was processed in this way, using M = 72 and gradually increasing δv from .005 to 0.5.

Whilst the computation for this phase was perfectly stable when the moving boundaries at the points of contact remained within the tabular points, a considerable perturbation was introduced each time a tabular point was crossed. This could only be attenuated by holding $\delta v < 0.1$ for the next few integration steps, and then allowing it to increase again. The computation could be held stable in this way, but became exceeding lengthy. To traverse 4 doubling times can take up to 20 minutes on the London Atlas, which is obviously impractical. However the computation which was performed indicated that a return to the symmetric mode could be observed almost immediately.

5.1.3.3 Improvements to solution

The Runge-Kutta method, being explicit, is known (5) to be subject to instability: the critical step length is inversely proportional to the square of the number of space meshes i.e. M^2, but difficulty was only experienced in the computation of section 5.1.3.2. If more extensive use of this computation was required, it would be necessary to change to the creep only solution of Blackburn (9), or to redesign the numerical method around an implicit scheme, as suggested below.

Equation (4.38) in implicit form is

$$\left[\partial^2 u/\partial s_m^2 - (\partial^2 u/\partial s^2)_r \cdot s/r + Bu_m/C - m\,\delta s\,\delta v/r + \delta v.u_m/C\right]_{v+\delta v} = \left[\partial^2 u/\partial s_m^2 - (\partial^2 u/\partial s^2)_r\, s/r + Bu_m/C\right]_v$$

where v represents present known values and $v + \delta v$ is the unknown values for the next time step. The r.h.s. is completely known, and by the usual finite difference methods one could solve the linear equations for the $u_{m,v+\delta v}$. The use of an implicit scheme will almost invariably give rise to a stable solution, which can be obtained with a large value of δv.

As mentioned previously, it may not be necessary to invert the matrix $[A]$ 4 times during each time step, when using the Runge-Kutta method; in the implicit method above, this is also the case, and normally only one inversion per step would suffice. If greater accuracy were required, one or two iterations might be performed.

5.2 Free Bowing

A numerical solution of eqn. (4.60) was required for the measured experimental shapes. The equation becomes

$$\partial u/\partial v_{m-1} + (B/M^2 D - 2)\,\partial u/\partial v_m + \partial u/\partial v_{m+1} = -u/M^2 D\,, \quad \text{for } 1 \leq m \leq M-1 \qquad (5.23)$$

with the boundary condition $(\partial u/\partial v)_{s=o,\,1} = 0$.

The solution was obtained as before by matrix inversion and then through Runge-Kutta integration; this was then continued until the maximum of the curve (as located by 5-point Lagrangian interpolation (31) through the central portion of the curve) exceeded unity: this corresponds to contact with the restraint. From the actual value of the maximum, the previous integration was repeated with a step length δv calculated to give $u_{max} = 1$. This could be achieved in practice to an accuracy of 0.1 per cent with $\delta v = 0.125$.

The initial shape for the application of eqn. (5.23) was obtained as follows: the 18 points measured in the initial shape were interpolated to 72 points, using 7-point least squares parabolic interpolation

(34). This had the dual purpose of smoothing experimental errors and expanding the data to the required mesh length. The effect of the initial elastic deflection was then calculated from eqn. (4.62).

The use of eqn. (5.23) to calculate the times to contact the channel, is illustrated in Fig. 66.

5.3 Effect of eccentricity

The numerical solution of eqn. (4.61) is very similar to that used for the free bowing phase. Writing the eqn. (4.61) in finite difference form,

$$\partial c/\partial v_{m-1} + (B/DM^2 - 2)\partial c/\partial v_m + \partial c/\partial v_{m+1} = m/M^3D - c/M^2D \quad (5.24)$$

for $1 \leq m < M - 1$ and $(\partial c/\partial v)_{s=o,\,1} = o$

The method of solution is identical and results shown in Fig. 59 are for $q = .03$ ins., $b_1 = .025$ ins. (where $c = y/q$).

5.4 Elastic deflections

Writing (4.62) in terms of dimensionless variables $s = x/L$, $u = y/\delta$, we have

$$\frac{1}{L^2}\, d^2u_2/ds^2 + Pu/EI = \frac{1}{L^2}\, d^2u_1/ds^2$$

which in terms of finite differences is

$$u_{2_{m-1}} + (PL^2/M^2EI - 2)\, u_{2_m} + u_{2_{m+1}} = u_{1_{m-1}} - 2u_{1_m} + u_{1_{m+1}}$$

for $1 \leq m < M-1$, with boundary conditions

$$u_{o,\,M} = o.$$

The r.h.s. is known from the initial shape, and it remains only to invert the matrix of the l.h.s. to obtain the solution. This calculation was used in establishing initial data for the free bowing phase.

6.0 Description of apparatus and experiments

6.1 Conventional creep buckling experiments[+]

These experiments were undertaken to reinforce the findings of Webster and Alexander (95), as regards the accuracy of the tangent modulus method. They were performed in the main by F. Seyna under the author's direction, and consisted in essence of repeating the experiments of Webster (94). Some additional factors were investigated however: firstly, two different specimen sizes ($\frac{1}{2}$ ins. and $\frac{3}{4}$ ins. diameter) were used, to see whether the results could be correlated in a consistent manner, without reference to tensile data. Secondly, measurements of actual eccentricity in the buckling furnaces were made, as the method of centring was somewhat subjective. Thirdly, the push-rod extensometer legs used in the tensile creep experiments by Webster (94) were felt to be unsatisfactory, and were believed to have contributed to the considerable scatter in his data. A redesign of these was undertaken by the author in conjunction with S.B. Mathur, using as a basis the grooved specimen and extensometer legs developed at the National Gas Turbine Establishment.

6.1.1 Apparatus

For the conventional creep buckling experiments, 2 of the furnaces designed by Webster (94, 95) were used. They are described in full in the references quoted, and only the briefest details are given below. The tensile creep testing machines (Denison T47 x 1 ton) and recording equipment ~~was~~ also discussed in these references.

6.1.1.1 Buckling furnaces

The axiality of loading depends on the accuracy with which the upper spider of the loading system remains central in the furnace tube, and also on the centring of the specimen support stool with respect to the upper spider. As this latter operation has to be done with a plumbline, the accuracy is rather limited; the former depends

[+] This section is based largely on Freed and Seyna (21).

on the straightness of the tube and accuracy of the fit of the spider in the tube. Accurate measurements of internal diameter of the tube were made, and it was found that there was a variation of .005 ins. in diameter along the length of each tube. This meant that the spider often had .005 ins. lateral motion, and that any subsequent alignment would be in error by this amount at least.

The specimens (95) were 17¼ ins. long by ½ ins. and ¾ ins. diameter; the material was 'Magnox' AL80, and the specification is given in Table 1. All the specimens came from one billet, and were consecutively taken from the centre of the extrusion. The ½ ins. bars were extruded originally as 1 ins. bars, and then machined down to size to obtain uniform properties across the diameter; the ¾ ins. specimens were similarly extruded as 1½ ins. bars through a 3-hole die. All the extrusion was done at 425°C, and the bar was then reeled to straighten it. The specimens were sprayed with a .005 ins. coating of alumina, to prevent metallic interaction in the restrained bowing experiments. The specimens also had tapped, counter bored holes to receive the end fittings, making a total effective length of 18 ins. It was observed that the end fittings were often up to .003 ins. off centre due to the tapped hole, which thus constituted a further source of error of alignment.

An 'Ether' temperature controller was used together with a chromal alumel control thermocouple; by adjustment of the power supply through a 'Variac', the temperature could be maintained at 295 ± 1°C.

6.1.1.2 Tensile Creep

The extensometer assembly is shown in Fig. 68. It was not possible to have the transducers completely independently mounted, but it is believed that the effect of bending in this configuration is small. The tensile specimen is shown in Fig. 69; these were machined from both ½ ins. and ¾ ins. bars.

Although the laboratory temperature was controlled at 66 ± 1°F, these fluctuations could be observed on the most sensitive scale of the amplifiers: at this level the resolving power was nomially ± 6 ins., and to attain stability it was necessary to use the 10:1 lever

arm of the machine, although the loads were occasionally very small[x]. To minimise errors, the lever arms were carefully balanced before application of load.

The furnaces had three independent windings to adjust the temperature distribution in the specimen, and this was observed to be uniform to 295 $\pm \frac{1}{2}^{o}$C, taking account of both axial and time dependent temperature variations.

6.1.2 Description of experiments

The experimental technique was identical to that of Webster, with some small modifications.

6.1.2.1 Buckling experiments

The temperature distribution inside the furnace was checked with a dummy specimen having 18 thermocouples at inch intervals. This distribution could be held constant to within $\pm 1^{o}$C. The actual test temperature was 295°C, which is that used by Webster (although he read it as 302°C).

The specimens were given an initial bow of approximately .03 ins. in a three point bending rig; this enabled the initial shape to be measured to a reasonable degree of accuracy, and also fixed the direction of bowing. The measurements were made by locating the lathe centres in the counterbored holes, thereby dispensing with the end fittings and the error associated with their use. Deflections were read at five equally spaced points, where the alumina had been removed. This permitted the use of the electrical contact system.

The specimen was then given a 24 hour soaking at test temperature, to allow complete recrystallisation to take place. The material as received (Fig. 70)[+] showed signs of heavy deformation, and it was intended to remove if possible the effect of different cold working histories by this treatment. Once the initially deformed grains had been removed, no grain growth was observed; the subsequent grain size was in fact stable even at 400°C, and uniform along the length and across the diameter.

[x] Webster (94) had used direct loading for this reason.

[+] The author is indebted to Mr. F.Seyna for these photographs.

The micrometer probes are only accurate when measuring increments in deflection (because of reproducibility errors in centring the specimen), and the initial readings are then related to the deflections measured in a lathe.

The load was applied gently by a hydraulic jack, and deflection readings taken as required. The tests were carried on until a deflection of 0.3 ins. had been attained. The range of testing is given in Table 2, and the analysis of the experimental results is described in section 7.1.2.

6.1.2.2 Tensile creep experiments

As all the test specimens were produced on an automatic lathe, the gauge length and diameter were found to be adequately determined by batch sampling. This was done on a projection microscope and variations among the specimens were found to be negligible.

Three copper constantan thermocouples were attached along the length of the specimen, and the temperature distribution was adjusted with reference to these readings. As in the case of the buckling specimen, a 24 hour soaking period was used. The tests were continued until a strain of 1 per cent or 1,000 hours had been reached. Details of test stresses are given in Table 2, and the analysis of the data is shown in section 7.1.3.

6.1.2.3 Eccentricity experiments

As described previously, the method of aligning the loading system with respect to the specimen support stool was rather subjective; also other errors are present due to slackness in the upper spider and inaccuracies in the location of the end fittings. It was therefore deemed necessary to measure the effective eccentricity and evaluate the possible effect on bowing rates.

The most convenient method of achieving this appeared to be the modified Southwell plot (88); through a knowledge of the initial shape and applying successive load increments, a plot of deflection versus deflection/load enables the eccentricity and critical load to be determined+. These tests were performed at room temperature, as it was found necessary to control both the position of the specimen and the loading spiders during successive load increments, in order

+ See section 7.2.

to obtain consistent results. Both tended to rotate with load application, and as the eccentricity was thereby varied the analysis would not be applicable.

It was found that the eccentricity varied from .002 ins. to .060 ins., according to the position of the specimen; in the position where all the bowing tests were performed, the eccentricity was found to be .03 ins. The tests were performed on one furnace only, but it is believed that this would be a typical figure for the other furnace.

Having found the effective eccentricity, the analysis of section 4.4.2 was applied to estimate it's significance in the free bowing experiments. Full details are given in section 7.2.

6.1.2.4 Hot elastic properties

Webster (94) used the initial elastic deflection of the column specimens to determine Youngs modulus of the material ~~and~~ at the test temperature; this was however considered by the author to be unsatisfactory, as the scatter in these experiments was very large and the deflections often too small to measure accurately.

An alternative method was used, which involved incremental loading of the tensile creep specimens. The slow chart recorder was replaced by a fast potentiometric recorder (2 seconds full scale), the apparatus being otherwise just that used for tensile creep testing. The recrod showed that it was easily possible to differentiate between the instantaneous elastic deformation and the subsequent time-dependent creep deformation, and the tests were continued up to 2000 p.s.i. This was believed to be a representative upper limit of stresses attained during the buckling experiments.

Twenty experiments were performed on specimens machined from both ~~for~~ bar sizes, and the mean modulus was found to be $4.1 \pm 0.2 \times 10^6$ p.s.i.; this was significantly different from that obtained by Webster (3.2×10^6).

6.2 Restrained bowing experiments

It was decided to attempt to use the apparatus as designed by Webster with as little modification as possible.

The five point measuring system had to be dispensed with, and replaced by one capable of continuous deflection measurement; this resulted from the fact that complex shapes were expected in these experiments. It was also necessary to fit a restraining channel inside the furnaces, together with devices for measuring the force between the specimen and the channel. Thirdly, it was thought that the design of the loading system could be improved, by replacing the "floating" specimen support stool by one in which the specimen support point was machined centrally with respect to the end plate, which is a close fit in the furnace bore.

Three of Webster's furnaces were modified; two for $\frac{3}{4}$ ins. specimens and one for $\frac{1}{2}$ ins. specimens. An exact half-scale experiment for a typical reactor fuel element (L = 36 ins., δ = 0.144 ins.) would have meant a clearance of 0.072 ins.; this was however considered to be rather small in relation to the accuracy of measurement, and so it was decided to use a clearance δ = 0.144 ins. for both bar sizes.

6.2.1 Apparatus

6.2.1.1 The measuring system

Various means of deflection measurement were considered; the most obvious is a transducer which could more vertically inside the furnace, giving a continuous record of horizontal displacement versus position along the specimen. A number of these were examined, but it was found that the requirements of long term stability and limits on size precluded those which could withstand the ambient temperature of 300°C.

The only device which appeared to be suitable was a direct mechanical lever system (see Figs. 71, 72, 73). A 9/16 ins. stainless steel bar was drilled and recessed to take a stainless steel lever, which carried a probe at one end. A micrometer is attached to the lower end of the bar, such that the displacement of the lower end of the lever can be measured. Light finger pressure is used to tilt the lever until contact is made with the specimen at the probe end, and an electrical contact system is used on the micrometer end to measure the horizontal movement of the lever. This was essential as the lever could not be made

very rigid because of space limitations. As discussed previously, it was not possible to have electrical contact between the specimen and the probe because of the alumina coating.

Two such measuring bars were used, mounted at right angles in order to allow for an arbitrary direction of bowing by vector addition. The bars are a close running fit in stainless steel rollers, which are mounted in the top and bottom end plates. These plates are in turn a close fit in the furnace bore, in order that the position of the measuring bar relative to the specimen may be accurately reproduced. The bars are grooved over the top portion, to register with a mating groove in one of the top rollers. This prevents rotation of the bars.

The vertical location of the measuring bar is achieved through 18 accurately machined conical holes along the length of the bar, spaced at inch intervals. A bevelled screw in a clamp outside the furnace locates with these holes, which are placed to correspond with the measuring intervals along the specimen. An operators view of the measuring bars can be seen in Fig. 72, and the assembly of the bars relative to the specimen is shown in Fig. 71.

The accuracy of this arrangement would obviously not be as high as a fixed probe, but it was found that readings were repeatable to $\pm$ .0015 ins. when the clamp had not been disturbed; it was however necessary to remove the clamp to withdraw the probe at the end of each test, and it was found that the reproducibility from one test to another with a dummy specimen was $\pm$ .0025 ins. It was initially intended to measure increments in deflection only, in which case the first figure for accuracy would be applicable. Subsequent experience showed that the plane of bowing rotated considerably and that it was necessary to measure angles as well; this requires reference to another setting[+] and in this case therefore the second figure was applicable.

In the present experiments, it was found that the alumina coating sometimes formed ridges of height .005 - .010 ins. under compressive

[+] See section 7.3.1.

strains, and that the deflection readings were sometimes in error by this amount. This implied that the error figure of $\pm$ .0025 ins. was not excessive in the circumstances, but if better accuracy were required and justifiable it is believed that a redesign of the clamp would reduce this source of error considerably.

6.2.1.2 The restraining channel and force measuring systems

It was found that a 90° segment of a circular channel would be the maximum that could be accommodated inside the furnace without interfering with the measuring and loading systems. Space considerations also limited the maximum depth of material behind the channel, and the highest stiffness which could be achieved was .0003 ins/lb., for a centrally applied load.

The force measuring device was required to have high stiffness and stability, and some commercially available load cells were found to be suitable. However the cost of these was prohibitive, and it was therefore decided to incorporate a strain-gauged section in the channel at each end. By simply supporting the channel (Fig. 73) the sum of the output from the two gauged plates would be proportional to the total wall force, and independent of the point of application.

Through the use of a full Wheatstone bridge (two gauges on each surface), complete temperature compensation could be attained. The maximum wall force was expected to be 20 lbs., and the plates are designed to attain .025 per cent strain under these conditions. It was hoped that this would be low enough to inhibit creep in the adhesive. Linear foil gauges of $\frac{1}{4}$ ins. gauge length and 90 ohms were used; a small gauge was desirable because of the high strain gradient on the plates. It was not expected that the gauge temperature would exceed 80°C, as both assemblies (Fig. 73) are well removed from the furnace, and insulated from conduction along the channel by a Sindanyo spacer; accordingly, the adhesive 'Araldite AY105' and hardener 'HY951' were chosen - being nominally suitable up to 100°C.

Gauge stability tests were conducted by varying the temperature of the assembly under no load from 50° - 80°C over one week, and no

significant thermal drift could be observed.

The gauged ends of the channel are supported top and bottom on self aligning ball bearings, which were degreased to reduce friction. Provision is made to rotate the channel assembly bodily through an angle of $\pm$ 14°, about a centre which coincides with that of the loading system; this enables the gauged plates to be kept normal to the plane of bowing. The plates are attached to the channel by dowels, which ensure repeatability in setting up; this is necessary because the upper plates must be disconnected from the channel in order to remove the 'Sindanyo' lid from the furnace.

The position of the gauged plates is such that any vertical friction forces between the specimen and the channel surface pass directly through the centre line of the plates, thus producing no bending moment. The resultant tensile or compressive forces or bending moments in the plane of the plate, do not produce any output from the bridge.

The overall view (Fig. 74) shows how the existing framework was extended by means of slotted angle. As the horizontal forces were low ($<$20 lbs.), the structure was sufficiently rigid.

6.2.1.3 Detection of first contact with the channel

The instant at which the specimen makes contact with the channel is one of the variables to be measured. This was achieved electrically, by insulating the channel from the rest of the furnace. The alumina coating was removed over the central inch of the specimen, and a piece of nickel foil .005 ins. thick spot welded in place to restore the original thickness, (see Fig. 67). A circuit incorporating a self-closing relay was designed to stop an electric clock at the instant of contact, and also provide visual indication through a green light.

6.2.2 Calibration of the apparatus

The presence of the measuring bars and channel assembly were found to modify the power requirements for an even temperature distribution, and some additional resistance was brought into the circuit to allow for this. It was also found that the lower section of the furnace had a considerably smaller heat capacity than the remainder,

and advantage was taken of this to relocate the control thermocouple in this zone. Good temperature control was achieved, and whilst the lower zone experienced cycles of $\pm$ 1°C, the temperature in the rest of the furnace remained sensibly constant. The limitation on the degree of control is undoubtedly due to mains variations, and as a result cycles of $\pm$ 2°C were frequently observed.

The radial distance between the centre of the furnace loading system and the inner surface of the restraining channel was set as follows: a cylindrical spacer of suitable dimensions was placed in the loading system, and a light pre-load applied. The channel (Fig. 73) is then moved radially in the slides top and bottom until contact is attained along the length of the spacer; the whole assembly is then bolted down, and the only subsequent adjustments are to rotate the assembly about the centre if required. It was not found practical to adjust the radial distance at test temperature.

An attempt was made to attach thermocouples to the test specimens but it was found that these interfered with the measuring probes. It was not possible to attach the thermocouples to the channel as the life of the thermocouple was not sufficiently long; the procedure was therefore adopted of checking the temperature distribution after every two experiments using a dummy specimen. No systematic changes in distribution were observed, provided care was taken to pack the insulation over the top end plate in the same way each time.

The furnaces were levelled, and the reference-zeroes of the measuring system found by inserting straight steel bars of $\frac{1}{2}$ ins. and $\frac{3}{4}$ ins. respectively into the loading system. This too was re-checked frequently during the course of the experiments.

The force measuring system was calibrated at test temperature by the device shown in Fig. 75. When this is placed in the loading system, the pivot being in contact with the channel, the resultant horizontal force is a known linear function of the vertically applied load. Some typical calibration curves are shown in Fig. 76.

6.2.3 Description of experiments

6.2.3.1 Round specimens

After prebending, measurements of initial shape are taken at one inch intervals. The specimen is then placed in the loading system, with the maximum bow directed towards the centre of the channel. The rest of the components are then assembled, and a 24 hour soaking at test temperature was allowed.

The initial readings can now be made, and the load then applied. From the increments in deflection, the plane of bowing can be determined and the channel rotated suitably. This was not always satisfactory, as the plane of bowing sometimes appeared to rotate even in the period before contact with the wall.

Once the channel position is fixed, the initial readings on the strain gauges and energising voltage were noted. Further readings of deflection and gauge output were made as required; the tests were continued in all cases until the deformation of the specimen made movement of the measuring bars impossible. This usually came about through the occurrence of considerable deformation at right angles to the initial major plane (see section 7.3.1).

A considerable proportion of the tests were spoilt by the specimen escaping from the channel and collapsing, but details of those tests which were successful are given in Table 3.

Analysing the measurements according to the method of section 7.3.1, the experimental data is presented in Figs. 24 - 56, together with some predictions from symmetric and asymmetric theory.

Some remarks on the technique for making the deflection measurements are in order, because the measuring bars move in a large temperature gradient, and the errors arising from this must be assessed. The greatest difference in length between the upper and lower sections of the measuring lever, assuming a hypothetical temperature difference of 300°C, is 0.3 per cent; the error in deflection measuring arising out of unequal lever ratios is then also 0.3 per cent. This figure

is however neither realistic nor appreciable in comparison with the other errors mentioned previously. Another error arises from variations in the vertical position of the probe due to thermal expansion. These could be more severe, as although the actual maximum positioning error of the probe could only be 0.04 ins., this could constitute an appreciable deflection error in a region of large deflection gradient.

To obviate this a consistent deflection measuring routine was evolved, which ensured that the probes experienced an identical temperature history each time a measurement was made. This meant that measurements could not be taken more frequently than at hourly intervals, which was the period required for the probes to cool down to the starting temperature.

6.2.3.2 Rectangular specimen

As noted previously, the two dimensional behaviour analysed by the theory was rather obscured in the main body of the experiments by considerable minor bowing: further, a rigorous three dimensional treatment did not seem practical. An experiment was therefore designed in which the minor bowing was inhibited by having a rectangular specimen with a favourable aspect ratio.

The 0.25 x 0.5 ins. specimen was machined out of one of the $\frac{1}{2}$ ins. diameter specimens, and prebent in the weaker plane. A test was then performed at $P/P_E = 0.46$, and the deflected shape at the end of the test measured in a lathe. It was not possible to make intermediate measurements during the experiment as the rectangular shape made normal interpretation of the data impossible. The result of this experiment together with some theoretical predictions is given in Fig. 57.

7.0 Analysis of experimental results and processing of data

7.1 Free bowing and tensile data

From a knowledge of the initial shape, and by vector addition of the increments in shape measured in the buckling furnace, it is possible to calculate the ~~deflected~~ deflected shape at any instant of time. To check the hypothesis that the deflections remained sinusoidal, the data from a number of experiments was studied. The computed solution (Fig. 59), for the effect of eccentricity, showed unambiguously that even in the presence of a considerable (.030 ins.) eccentricity, increments in deflection remained symmetrical.

It was therefore surprising to note that the experiments (Fig. 77) revealed continuously varying degrees of asymmetry in the increments of deflection. This could only be ascribed to variations in eccentricity during the test, and is believed to occur as the specimen rotates during the course of the experiment. However the midspan deviation from the best (least-squares) sine wave was not in excess of 2 - 3 per cent, so that the error in treating the deflections as sinusoidal should not be significant.

7.1.1 Choice of a creep law

On the basis of the preceding analysis, the sinusoidal assumption was used in deriving eqn. (4.59)

$$\ln (b_2/b_1) = \frac{PL^2}{\pi^2 I (1 - P/P_E)} \int_0^t \frac{\dot{w}}{E} \qquad (7.1)$$

where $1/\dot{E} = (\partial\dot{\varepsilon}/\partial\sigma)_o$, and $\dot{\varepsilon} = \dot{\varepsilon}(\sigma, t, T)$.

The choice of the creep law has not yet been discussed in detail. The most important criteria for the choice of an empirical law would be firstly that it fit the material data well, and secondly that it be readily amenable to interpolation and extrapolation.

The phenomenological law proposed by Graham (27) and used extensively by Graham and Walles (28, 92, 93) on a variety of materials, fits both these requirements admirably. The relation of this method to

other well-known techniques - Norton, Larson and Miller, Manson and Haferd, has been discussed in detail elsewhere (28), and need not be expanded upon here. Briefly, it consists in expressing creep strain in the form

$$\varepsilon = \sum_i C_i \sigma^{n_1} t^{K_i} |T_i - T|^{\pm 20K_i}$$

where C_i, n_i, K_i and T_i are constants. K_i takes only the values 1/3, 1, 3 and K_i/n_i take values from the series 1, $\frac{1}{2}$, $\frac{1}{4}$, 1/8 etc. The equation for creep strain can then be written

$$\varepsilon = \alpha t^{1/3} + \beta t + \gamma t^3 \qquad (7.2)$$

which is reminiscent of the equation derived by Andrade (3). At a constant temperature, as in this series of tests, the problem is to evaluate the stress dependence of the constants α, β and γ. The usefulness of this law has been demonstrated by it's originators for a wide range of alloys (28, 93) and Webster (94) had shown that it seemed also to describe the creep of magnox and commercially pure aluminium EIC - M. The graphical method of data analysis developed by Walles was particularly convenient, and so it was decided to use this technique in the present analysis.

7.1.2 Reduction of bowing data[+]

On the basis of assumption (5) of section 4.1, we generalise eqn. (7.2) for varying stress:

$$\partial\varepsilon/\partial t = \dot{\varepsilon} = 1/3\,\alpha t^{-2/3} + \beta + 3\gamma t^2$$

from which

$$\frac{1}{\dot{\sigma}} = (\partial\varepsilon/\partial\sigma)_0 = \frac{1}{3}\left(\frac{\partial\alpha}{\partial\sigma}\right)_0 t^{-2/3} + \left(\frac{\partial\beta}{\partial\sigma}\right)_0 + 3\left(\frac{\partial\gamma}{\partial\sigma}\right)_0 t^2$$

Substituting in eqn. (7.1) yields on transposing

$$\frac{\pi^2 I\,(1 - P/P_E)}{PL^2} \ln\left(\frac{b_2}{b_1}\right) = \left(\frac{\partial\alpha}{\partial\sigma}\right)_0 t^{1/3} + \left(\frac{\partial\beta}{\partial\sigma}\right)_0 t + \left(\frac{\partial\gamma}{\partial\sigma}\right)_0 t^3$$

which can also be written

[+] This has been described in detail by Webster (94) and Webster and Alexander (95).

$$\frac{\pi^2 I\,(1 - P/P_E)}{AL^2}\ \ln\left(\frac{b_2}{b_1}\right) = (n_1 c_1 \sigma_o^{n_1} + n_1' c_1' \sigma_o^{n_1'} + \ldots\ldots)\, t^{1/3} + (n_2 c_2 \sigma_o^{n_2} + n_2' c_2' \sigma_o^{n_2'} + \ldots)\, t + (n_3 c_3 \sigma_o^{n_3} + n_3' c_3' \sigma_o^{n_3'} + \ldots)\, t^3 \qquad (7.3)$$

which is similar in form to eqn. (7.2). This equation is valid if the whole length is active in the bowing. In the actual experiments, however, the specimen is 17¼ ins. long and has end fittings ¼ ins. and ½ ins. long respectively. An approximate correction for these rigid fittings was therefore made, assuming a sinusoidal shape and that each fitting was 3/8 ins. long: the parameter

$$(.936 - \frac{P}{P_{E'}}) \cdot \frac{\pi^2 I}{AL'^2}\ \ln\ (\frac{b_2}{b_1})$$

resulted. The dashed quantities refer to the reduced (actual length). This was the actual parameter used in correlating the data, and the calculated results are only 1 - 2 per cent different from the uncorrected data.

The similarity between (7.2) and (7.3) lead Alexander and Webster (2) to propose that the Graham-Walles method of data analysis be applied to the bowing data, plotting

$$\frac{\pi^2 I\,(1 - P/P_E)}{PL^2}\ \ln\ (\frac{b_2}{b_1})$$

against time. The method of analysis is then identical with that for tensile creep. The creep strain is resolved into three components, by determining the times $t_{1/3}$, t_1, t_3 for each to contribute the arbitrary standard strain ε^*; eqn. (7.2) can then be written

$$\frac{\varepsilon}{\varepsilon^*} = (\frac{t}{t_{1/3}})^{1/3} + (\frac{t}{t_1}) + (\frac{t}{t_3})^3$$

from which by definition

$$t_{1/3} = (\varepsilon^*/\alpha)^3 = \varepsilon^{*3}(c_1 \sigma^{n_1} + \ldots)^{-3} \qquad (7.4)$$

$$t_1 = (\varepsilon^*/\beta) = \varepsilon^*(c_2 \sigma^{n_2} + \ldots)^{-1} \qquad (7.5)$$

$$t_3 = (\varepsilon^*/\sigma)^{1/3} = \varepsilon^{*1/3} (c_3 \sigma^{n_3} + \ldots)^{-1/3} \qquad (7.6)$$

It is found from experience that K_i/n_i take on the values 1, $\frac{1}{2}$, $\frac{1}{4}$ etc., and therefore a log-log plot of eqns. (7.4 - 6) will be a succession of straight lines; as $K_1 = 1/3$, $K_2 = 1$, $K_3 = 3$, we can then from the slopes determine the n_i, and the c_i from the intercepts.

The values of $t_{1/3}$ etc. corresponding to each stress level are most readily determined using the perspex curves supplied by Graham and Walles. These are designed for use with the graph scales given in Fig. 78, which shows typical curves for some buckling data. The standard value of $\frac{\pi^2 I}{AL^2}(1 - P/P_E) \ln(\frac{b_2}{b_1})$ was chosen as .001; in analysing the data from bowing experiments, the tertiary component was found to be negligible, or only occurring in the region of large deflections. The result of the analysis of eighteen bowing experiments is shown in Figs. 62, 63. It was found in each case that only one K/n ratio appeared, and the best least squares straight line having the appropriate standard slope is drawn. The standard deviations of these lines, and also that of the best fitting lines (not having standard slopes) are shown in Table 4.

It was found that for the $t_{1/3}$ component $K/n = \frac{1}{4}$, and for t_1 $K/n = \frac{1}{2}$. From this it follows that $n_1 = 4/3$ and $n_2 = 2$, and the creep buckling equation for Magnox at 295°C becomes

$$\frac{\pi^2 I}{AL^2}(1 - P/P_E) \ln(\frac{b_2}{b_1}) = 0.55 \times 10^{-7} \sigma_o^{4/3} t^{1/3} + 3.035 \times 10^{-10} \sigma_o^2 t \qquad (7.7)$$

By adjusting eqn. (7.3) for the constants n_1, n_2, we derive from (7.7) the uniaxial creep equation, as predicted from the buckling data

$$\varepsilon = 0.416 \times 10^{-7} \sigma^{4/3} t^{1/3} + 1.51 \times 10^{-10} \sigma^2 t \qquad (7.8)$$

7.1.3 Reduction of tensile data

The method of attack is just the normal Graham and Walles analysis. The results of 11 tensile creep experiments are summarised in Figs. 64, 65. Once again only one K/n ratio was found to be present in each

of the $t_{1/3}$, t_1 cross-plots. As the tensile tests did not go beyond 1 - 2 per cent strain, no tertiary component was observed. The standard value of strain was $\varepsilon^* = .001$, and the values of n_1 and n_2 were the same as in the case of the buckling data.

A least squares analysis of the data using the nearest Graham-Walles standard slopes was performed, and the following equation for the tensile creep of Magnox at 295°C was obtained.

$$\varepsilon = 1.03 \times 10^{-7} \sigma^{4/3} t^{1/3} + 1.66 \times 10^{-10} \sigma^2 t \qquad (7.9)$$

The lines drawn in Figs. 64, 65 are those predicted from eqn. (7.8). The lines which would represent eqn. (7.9) have been omitted for the sake of clarity. The statistical data relating to these figures is given in Table 4.

A very large quantity of creep data on Magnox has been collated by Harris and Jones (30), and it was therefore of interest to compare the secondary creep rate from eqn. (7.9) with that given by the Harris and Jones equation. The comparison is restricted to the range of stresses (100 - 1,000 p.s.i.) covered in the present series of experiments, and is shown in Fig. 79.

7.2 Analysis of computations on the eccentricity equation

For a column with initial sinusoidal amplitude b_1 subject to the load P, the increment in amplitude δb is given by (88)

$$\delta b = \frac{bP}{P_E - P}$$

Further, for a straight column with initial eccentricity q, the increment in amplitude b' is (88)

$$\delta b' \doteq \frac{4q}{\pi} \left(\frac{P}{P_E - P}\right)$$

Superimposing the two effects, for a column having both initial amplitude and eccentricity, the increment in amplitude b" is

$$\delta b'' = (b + 4q/\pi) \left(\frac{P}{P_E - P}\right)$$

From which

$$\frac{\delta b''}{P} = \frac{1}{P_E} \left(b'' + \left(b + \frac{4q}{\pi}\right)\right)$$

This equation forms the basis of the Southwell plot (88). When $\delta b''/P$ is plotted as a function of $\delta b''$, the inverse slope is P_E, and the intercept on the $\delta b''$ axis is $b + 4q/\pi$. In the present case, the column was subject to a small preload due to the weight of the loading system P_L, and reworking the analysis to take account of this yields

$$\frac{\delta b''}{P} = \frac{\delta b'' + c}{P'_E}$$

where $P'_E = P_E - 2P_L$, and P is the total load increment in the normal way.

As mentioned in section 6.1.2.3, the median value of eccentricity q found in this way was .03 ins. A computer solution of eqn. (4.59) with b_1 = .025 ins., and q = .03 ins. was performed, and the resulting changes in deflected shape are shown in Fig. 59.

The first surprising feature of this solution, is that increments in deflection remained symmetrical. This was true even at larger eccentricities (q = 0.1 ins.), and has been used in section 7.1 in interpreting the bowing data. The eccentricity could be either additive, as in the solution shown, or of opposite sign to the deflected shape. It was therefore expected that this would provide upper and lower bounds on the scatter in the buckling data: however, this was not the case. When the computer solution was analysed in the way that the experimental data had been treated, viz.

$$\ln (b_2/b_1) = \ln \left(\frac{b_1 \text{ (nominal)} + \delta b}{b_1 \text{ (nominal)}}\right)$$

the results for positive and negative eccentricity were identical. This implied that the increments in midspan deflection were the same for both cases, independent of the sign of the eccentricity. This is only true for small eccentricities.

The resulting $\ln (b_2/b_1)$ - time data for this sdution was analysed like the experimental data, and the result is shown in Figs. 62, 63. Since the result is independent of the sign of the eccentricity, it follows that the effect of this order of eccentricity is negligible on the bowing rates: the deviations shown in Figs. 62,

63, are therefore not due to eccentricity, but represent errors in the numerical solution and in the curve fitting process. These latter errors arise in the solution of the v - t relation, and in the analysis of the ln (b_2/b_1) - t curve.

7.3 Restrained bowing

7.3.1 Round specimens

It was assumed in the design of the apparatus that the bowing would remain predominantly two dimensional, as in the free bowing experiments; in this event, the scalar addition of the initial deflection and subsequent increments will be permissible. If however the increments have a substantially different associated angle from the initial bow, the scalar addition is likely to be considerably in error. This was in fact found to be the case and a different procedure had to be adopted.

The first quantity to be evaluated is the radius vector $\underset{\sim}{b}$, to the centre of the specimen from the centre of the furnace. (The lines of action of the two measuring probes intersect at this point). Referring to Fig. 80, from the cosine rule,

$$|\underset{\sim}{b}| = \sqrt{|\underset{\sim}{b}_o|^2 + |\underset{\sim}{r}|^2 - 2|\underset{\sim}{b}_o||\underset{\sim}{r}| \cos\theta}$$

where $\underset{\sim}{b}_o$ is the initial deflection at the point

$\underset{\sim}{r}$ is the current increment

θ = arc tan R/L

R and L are increments on right and left probes

α = angle included between $\underset{\sim}{r}$ and $\underset{\sim}{b}$.

ϕ' = initial angle after application of load, associated with $\underset{\sim}{b}_o$

γ = angle associated with $\underset{\sim}{b}$

and $\alpha = \pi + \theta - \phi'$

The angles all vary along the length of the column, although ϕ' was almost constant along the length.

The measurement of angle θ poses no problem, as it is defined accurately by the increments R and L. The angle ϕ', can only be measured if the 'zeroes' of the measuring system are known, and the

coordinates of b_o known relative to them. This can be found, but as described in section 6.2.1.1 the insertion of the same specimen twice might incur reproducibility errors of $\pm$ .0025 ins. This is the order of error to be associated with the calculation of angle φ'. The calculation of δ is subject to the same limitations.

A number of different interpretations can be put on the observed rotation of $\underset{\sim}{b}$: it could be assumed as in Fig. 81a that the original plane of maximum bow and specimen rotate bodily. Secondly, Fig. 81b, it might be assumed that the specimen rolls around the channel, under the influence of the couple indicated. Thirdly, Fig. 81c, the original plane would remain fixed in direction, but lateral translation could take place under the influence of minor plane (at right angles to the major plane) bowing.

The second possibility could be disposed of by an inspection of the specimen: if rolling had taken place at some points, originally straight lines would become helical and be displaced from the upper surface - no evidence of this could be found. Of the first and third hypotheses, the third was more economical in that it did not require to explain how the specimen could rotate bodily, and there are in fact no forces which could cause this rotation. This hypothesis was therefore adopted, and the terms 'major' and 'minor' bow are defined quantitatively in Fig. 82.

Once it has been established that no rotation takes place, the axes of the bending moments remain fixed in their original position with respect to the fibres of the column. From Fig. 82, the deflection with respect to the major bending axis is then $|\underset{\sim}{b}| \cos(\varphi' - \gamma)$, and that with respect to the minor axis is $|\underset{\sim}{b}| \sin(\varphi' - \gamma)$.

It will be noted that the clearance for major bowing decreases as the minor bow increases and vice versa. When the non dimensional parameter $u = y/\delta$ is introduced, and the maximum clearance is then unity, the reduced clearance for minor and major bowing is $\sqrt{1 - |\underset{\sim}{b}|^2 \cos^2(\varphi' - \gamma)}$ and $\sqrt{1 - |\underset{\sim}{b}|^2 \sin^2(\varphi' - \gamma)}$. These clearances were useful to know as they indicate where the minor bow has enforced

a reduction in the major bow, thus causing a deviation from one dimensional behaviour[+]. Further, they constituted a useful indication of experimental error in cases where the deflection had apparently exceeded the permitted maximum at the point.

A computer programme was written to process the data, as the amount of calculation was considerable. The clearance used in computing non-dimensional deflections was adjusted for the fact that it had been set at room temperature.

The results of this data processing are given in Figs. 24 - 55, which show the major plane deflections, and in some cases the minor plane and polar plots.

An examination of the experimental results for force measurement, revealed that for each furnace the upper set of strain gauges had become unreliable due to being overheated by controller failures. However as the channel was statically determinate, the wall force could be calculated from a knowledge of the point of contact and the lower reaction (this assumed that there was one point contact only).

The increments in output of the bridge, corrected for the changes in battery voltage, were converted to forces through the appropriate calibration curve - e.g. Fig. 76. The results are shown in Fig. 56.

7.3.2 Rectangular specimen

The measurement of deflection during this test was not possible, because any slight rotation of the plane of buckling made the deflection underdetermined. The initial deflection was therefore measured in a lathe, and finally at the end of the test. Some inaccuracy was caused by the deflection of the specimen under the dial gauge pressure, but this was not appreicable. The results are shown in Fig. 57.

7.3.3 Consistency correlations

An examination of the non dimensional eqns. (4.46, 4.47) and (4.51 - 53) reveals that the solution is a function of the initial shape, the Euler loading ratio, and the solution time v_{ce}. This implies that the results of experiments on two different diameter specimens, having equal Euler loading ratios, should be identical

[+] See Appendix 10.3.3.

at equal values of the solution time v_{ce}; this would of course correspond to different values of real time. An examination of Table 3 shows that correlations of this kind should exist between Tests 52 and 70, 71: 53 and 72 - 74: 54 and 75, 76: 55 and 77. As the initial shapes were nominally identical, it would be expected that all the above-mentioned correlations should be valid. However it was soon apparent that other factors[+], such as minor bowing and the small tilting of the loading system, were also influencing the behaviour; consequently, since a number of different types of deflected shapes were observed, the correlations would only be valid where the shapes were similar. These are shown in Figs. 43, 48, 50.

If the effects of elasticity are small, as was indicated by the computations on the theoretical shapes, then the terms including $1 - P/P_E$ can be dropped from the equations; this implies that all the tests should be comparable at equal values of the solution time v_c, subject to the same restrictions on the similarity of deflected shapes. Numerous such correlations were found and are shown in Figs. 24 - 55.

7.3.4 Lead bowing experiments

A restrained bowing experiment had been performed by Clark[x] at the English Electric Co. Ltd., using lead bars. Four tensile creep experiments had been performed, to derive supporting data at room temperature. An analysis of the data performed by the author yielded $\epsilon = 2.52 \times 10^{-11} \sigma^{2.13 \pm 0.86}$ t: the standard deviation of the isochronous stress strain plot was 0.5 cycles of log strain. The experimental result together with the predictions from the theory of section 4.21, is given in Fig. 58.

[+] See 8.3.2.2.

[x] Clark, G.P. Personal communication.

8.0 Discussion

8.1 Accuracy of the tangent modulus method

The experiments designed to investigate the validity of the tangent modulus method rested mainly on the comparison between measured tensile data and that predicted from the buckling experiments. This comparison is based on the applicability of a Graham-Walles type of law (27, 28) to both sets of data, and it will therefore be appropriate to examine this first.

8.1.1 Reliability of the Graham-Walles method

The usefulness of this method in examining tensile data has been demonstrated by it's originators for a wide range of alloys (92, 93), but not for magnox. A statistical study of the cross-plots Figs. 64, 65, was therefore undertaken to determine the significance of the "standard slopes": this is shown in Table 4.

For the primary component, the Graham-Walles line had the same standard deviation as the best least squares line, and a similar conclusion is reached for the secondary data. It therefore follows that the Graham-Walles lines fit both sets of data as well as those with the best least square slopes. The standard deviations in both cases were of the same magnitude as those quoted by Walles and Graham (93) in testing Nimonic alloys; the larger value for the primary data is probably due to the greater sensitivity of this component to curve fitting errors, and also to its smaller relative magnitude.

A comprehensive survey of the available tensile creep data on magnox was produced by Harris and Jones (30), and a comparison of the line given by equation (7.8) with their data is shown in Fig. 79. This degree of agreement is well within the scatter of the data (Fig. 8 of ref. (30)) used to arrive at their correlation, and it was concluded that satisfactory agreement had been obtained.

The use of the Graham-Walles curve in fitting the buckling experiments is shown in Fig. 78. Here the very small random correction for

the zero error has resulted in a reasonably good fit to the data, and the degree of deviation from the mean experimental data is small. A statistical analysis of the crossplots, Figs. 62, 63, given in Table 4, results in the same conclusion as for the tensile data: hence it was concluded that the use of the Graham-Walles method was justified in both cases.

8.1.2 Comparison between buckling and tensile data

The lines drawn in Figs. 64, 65 are those predicted from the buckling data, Figs. 62, 63. For the secondary data, reference to the appropriate terms in equations (7.7), (7.8) indicates that the predicted line is also the best fitting line, for practical purposes.

In the case of the primary data, there is a displacement of one cycle in log time between measured and predicted data. This is a significant amount because the standard deviations of Table 4 indicate that only a very small percentage of the points would lie within the common 34 per cent confidence limits.

A necessary condition for the coincidence of these lines would be the interchangeability of tensile and compressive creep. A survey of the literature indicated that no general conclusions could be drawn on this subject: it therefore appears that the deviation shown in Fig. 64 may be due to differences in tensile and compressive creep.

Another possible source of error may be variations in eccentricity during the experiments. The theoretical work of section 4.4.2 had shown that the constant eccentricities which were found to be present could have had no discernible effect on the bowing rates. However the rotation of the specimens during loading for the Southwell plot (section 6.1.2.3), which was also observed in the creep buckling experiments, was usually accompanied by increases in eccentricity. It is evident that the apparent increase in deflection caused in this way would lead to larger values of deflection, and hence smaller values of $t_{1/3}$ and t_1. This leads to errors opposite in sign[x] to those of Fig. 64, which on

[x] Freed and Seyna (21) are incorrect on this point.

this basis must therefore be due to decreases in eccentricity. As the six typical experiments (of which Fig. 77 is one) all exhibited increasing eccentricities, it appears likely that the rotation of the specimen was not an important source of error in these experiments.

8.1.3 Time to contact channel

A further application of the tangent modulus theory is seen in Fig. 66, which depicts theoretical and experimental times for first contact with the channel. The data for this calculation was derived directly from the buckling material data, as were all the v-t calculations. The agreement is notgood, and some of the data appears to be displaced with respect to the theoretical line by an amount which is too large to be due to temperature errors.

However, as this phase of deformation was dominated by primary creep, it is to be expected (see Fig. 62) that the scatter would be considerable: it is not therefore possible to draw any definitive conclusions from Fig. 66.

8.1.4 Conclusions

The very good agreement in the secondary data Fig. 65, and the consistency of the results of two diameters when correlated according to the basis of Figs. 62, 63 indicated that the theory was satisfactory. The significance of the disparity in Fig. 64 was assessed by comparing a hypothetical mean buckling experiment with one predicted from tensile data, as would be done in practice. This showed that the error decreased from 0.8 cycles of log time in the initial stage to 0.1 cycles towards the end. In a component designed well into the secondary creep range, this implies that the time to achieve a given bow can be predicted within 20 per cent. There is no reason to suppose that theerror of Fig. 64 is due to limitations in the theory, which should in fact be more accuratte in the primary creep region.

The analysis of section 10.3, comparing the predictions of the Hoff H-section theory with the tangent modulus theory, showed them to be exactly equivalent for stress exponents of 1 and 2, and approximately

equivalent for small deflections for higher exponents. As the exponent for magnox was found to be 2, no advantage would have accrued from the use of an equivalent H-section.

8.2 Symmetric restrained bowing

It is unlikely to meet in practice a column having an exactly symmetric shape; however the theory of symmetric columns is of interest as it is evident from the stability analysis of Blackburn (9), and also from the authors computations on slightly asymmetric shapes (Figs. 24 - 55), that most small asymmetric perturbations tend to be attenuated. The final shapes can then be calculated from symmetric theory. This is a considerable advantage in cases where the amount of asymmetry is very small or unknown, as an asymmetric computation then becomes much more difficult or even impossible. We shall consider the theoretical results first.

8.2.1 Computations on analytical shapes

8.2.1.1 General results

The results of computations on a sine wave, and on a shape of a sine wave with 1/9th third harmonic are shown in Figs. 7 - 13. This showed that the effect of the third harmonic was to accelerate the deformation; conversely if a third harmonic of opposite sign had been chosen, the effect would have been to sharpen the point of contact and hence delay the instant at which point contact split. The shape considered is not necessarily a reliable upper bound on the rate of deformation: it is possible to devise shapes which would be in two point contact at the instant of first touching the channel, and hence deform at much higher rates.

The results of the computation are in good agreement with those of Blackburn and Percy (8), except where the latter's deflected shape exceeded the physical constraint. This is due to inaccurate interpolation and was corrected by Blackburn in his later paper (9).

The calculations reveal that the total wall force reaches a maximum of $8P\,\delta/L$, whilst the element is in contact with one restraining wall. In an actual reactor, where another contact can be established

due to reverse bow with the opposite side of the channel at $v_c = 43$, (for a sinusoidal element), the forces may begin to rise again. However present practice is to discharge the element after $v_c > 25$, so this condition is not of practical significance. The maximum non-dimensional curvature[x] would be 20 at the instant of contact with the opposite wall: the maximum strain at this time would be 1 per cent.

8.2.1.2 Significance of primary creep

The contribution of primary creep is readily assessed through the use of the solution time parameter. The v_c - t relation is calculated firstly for secondary creep only, and then for primary plus secondary creep. Corresponding solutions are then plotted against real time, as in Fig. 11.

As expected, the error in neglecting primary creep decreases rapidly: an initial error of 10 per cent in r is attenuated to 3 per cent after 140 hours, or $v_c = 23$.

Nevertheless, this technique would be extremely useful where either the primary or tertiary phase of creep is significant in comparison with the secondary phase.

8.2.1.3 Effect of elastic deformation

The additional deformation due to elasticity was found to be negligible, and is therefore not depicted on the figures.

In the force calculations however, the neglect of elasticity is important in assessing initial transients, as the force is zero at the instant of first contact. The 'creep only' solution wrongly predicts a finite force at the instant of first contact - Fig. 12.

For an Euler loading ratio 0.2, the subsequent forces are adequately predicted from the creep only solution. When the loading is rather higher at 0.46, the creep only solution becomes less adequate.

It appears therefore that the neglect of elasticity will give rise to conservative design and is therefore justifiable. The degree of error would of course vary with material, temperature and stress rate, but some guide to the importance of elastic deformation could be

[x] This is $\frac{L^2}{4\delta}$ x actual curvature.

formulated through the use of viscoelastic models.

8.2.2 Correlations with experiment

The series of experiments on axisymmetric columns depicted in Figs. 24 - 55, did not produce results which could be compared with symmetric theory: this was due to the geometrical interaction between the minor and major bows in the circular channel. However one experiment was designed with a rectangular specimen - section 7.3.2 - in which the bowing was nearly symmetric; this is considered below together with a lead bar experiment performed by English Electric Co. Ltd.

8.2.2.1 Rectangular specimen

The experimental result for this test is shown in Fig. 57, together with the predicted theoretical deformation under various assumptions. The slight amount of asymmetry is due to the small amount of minor bowing which took place.

The nominal disparity in the predicted time to achieve the deformation shown, is only 14 hours or 20 per cent. This is good agreement for problems of this nature. Using the temperature dependence of creep rate found by Harris and Jones (30), the effect of a $\pm$ 3°C error ~~in~~ test temperature was assessed. This showed that the error quoted above could be accounted for entirely by a 3°C error in temperature. The figure also shows that this amount of disparity can be caused through neglect of primary creep.

8.2.2.2 Lead bar experiment

Experimental and theoretical displacements of point of contact are shown in Fig. 58. The agreement is quite reasonable, considering the scatter in the tensile data (see section 7.3.4); there is little doubt that the use of the upper tolerances on the creep rate data would have brought the curves into close coincidence.

Lead is not particularly well suited to quantitative creep stress analysis, as it exhibits succesive strain dependent recrystallisations at room temperature. Nevertheless the degree of success in the prediction was encouraging.

8.2.3 Conclusions

The use of the solution time parameter proved most convenient in assessing the effect of temperature and material property changes. Where they were comparable, the theoretical results were in agreement with those derived by Blackburn (9) and Blackburn and Percy (8).

The effect of elasticity on deformation was found to be negligible in these experiments, but the use of the creep only solution was slightly conservative for the prediction of forces.

The limited amount of experimental evidence which could be invoked in support of the theory showed satisfactory agreement.

8.3 Asymmetric restrained bowing

The study of asymmetric columns was undertaken by the author and Blackburn (9) independently; in the present case it was desired to use the theory to predict the behaviour of the very slightly asymmetric shapes encountered in the experiments. As mentioned previously, the minor bowing and associated geometric changes obscured the asymmetric behaviour and the theory was only applicable during the early stages of deformation.

Some applications of the theory to analytical shapes were also investigated, to compare the present method of calculation with that of Blackburn. These are described below.

8.3.1 Computations on asymmetric shapes

The calculation on a sine wave with second harmonic 3/34 of the fundamental is shown in Fig. 14. The element flattens progressively until $v_c = 7.2^+$, when contact is established at two points; these then move apart in a manner analagous to the symmetric shapes. The forces and displacements are shown in Figs. 16, 17. There is good agreement with Blackburn.

Because of difficulties arising from numerical instability (see section 5.1.3.2) the integration was only carried as far as $v_c = 9.2$: it appears however that the asymmetric component is being attenuated,

+ A figure of 6.5 was found by Blackburn - the difference being due to his larger mesh size.

and this is confirmed by Blackburn's calculation.

The case of a sine wave with second harmonic ½ the fundamental is shown in Fig. 15. Here reverse bowing begins immediately until contact is established with the opposite wall at $v_c = 8.8$; forces and displacements are shown in Figs. 16, 17. The agreement with Blackburn is again good.

The result: of computations on the experimental shapes is discussed separately.

8.3.2 Experimental work

It was immediately obvious from the experiments that the two dimensional deformation initially imposed could not be maintained on axisymmetric sections. The random third dimensional components in the initial shape and loading system, or imperfections in the material, would not be important under normal free bowing conditions; under the restrained bowing condition however these components soon became appreciable. For example in Test 55, Fig. 41, a minor bow of 2nd harmonic shape and amplitude one half the major bow has developed by $v_c = 1.9$. The resultant effect on the deformation (see Fig. 81b) is to enforce a reduction in the magnitude of the major bow.

Whilst bowing in two planes can be treated independently in general (section 10.3), in the present case the geometric interaction renders this impractical; it is therefore natural to ask what can be achieved by way of the simpler two dimensional theory.

8.3.2.1 Correlations with theory

If the two dimensional behaviour had been significant, it would be expected that the deformation would either approximate that for the symmetrical shapes shown in Figs. 8, 9, or that of the slightly asymmetric shape Fig. 14[x]. A first examination of the experimental results Figs. 24 - 55, reveals that this expectation is not fulfilled to any extent. The only resemblance to two dimensional theory is to

[x] See also Blackburn, Fig. 2 of reference (9).

be found in the very early stages of the deformation ($v_c < 12$), where the minor bowing is generally not yet appreciable: the predictions of asymmetric theory are shown for the instant at which two point contact was first established. Quantitative agreement is reasonably found in only a few cases - Tests 70, 74, 75. In Test 70, the reduced clearances have depressed the actual curve below the theoretical, while in Tests 74 and 75 the minor bow was negligible at that stage.

The theoretical computation was carried past the establishment of two point contact in only one of the tests - Test 55, Fig. 39. The amount of asymmetry is hardly discernible and it is obvious that this computation would tend rapidly to a symmetric shape.

Some of the experiments did tend to an approximately symmetric shape - the appropriate prediction for Test 52 from the calculation of Fig. 8 is reproduced in Fig. 29: it is only qualitatively comparable. A better example is Test 75, where although the deformation is symmetric - Figs. 48, 49, the shape at $v_c = 23.5$ is totally different from the comparable time in Fig. 8. An explanation for this is apparent in the polar plot Fig. 18: the specimen is in fact outside the channel in the region of the midpoint. Other experiments which showed some symmetrical tendencies were Tests 51, 53 - 55, and 77.

8.3.2.2 Effect of minor bowing

It seemed reasonable to believe that the major plane deformation should be some systematic function of the minor bow, and to this end the tests were classified into groups having a common deformation mode, at some stage of the experiment. These were:-

1) 'Symmetrical' flattening only - Tests 70, 73, 75 - 77.

2) Positive second harmonic - Tests 51 - 55, 70, 72, 78.

3) Negative second harmonic - Tests 71, 74, 77.

The deformation of the first group can be thought of as being largely symmetrical, as expected, except where as indicated in the figures the clearance has been reduced by minor bowing.

The behaviour of the second group is rather more difficult to explain. In Test 51, Figs. 24 - 26, the minor bow was too small to

have affected clearance (see Fig. 31), and the initial 2nd harmonic component disappears as the symmetric mode predominates. On the other hand Test 52, Figs. 27 - 29, exhibited a considerable minor bow, Fig. 30, while showing similar deformation to 51. The behaviour in Test 53 is just the reverse of Test 51, and a complete transformation in the mode of minor bowing occurs during the test (Fig. 35). Further, a comparison of the minor bows of Tests 52, 54, 55, where all the major bows were similar, does not reveal any basis for comparison; the only common factor was that the peaks in the minor bows (Figs. 30, 38, 41) all appeared in the upper half of the specimen. Other tests in this group did not have appreciable minor bows, and the tests in the third group were equally disimilar.

It did not therefore appear possible to relate the deformation mode in any consistent way to the observed minor bow[x], taking the groups as a whole.

8.3.2.3 Measured wall forces

The measured wall forces are shown in Fig. 56, plotted in the same form as the symmetric calculations Fig. 13. These had indicated that a maximum value for $RL/4P\delta$ would be 2, but there is not enough consistency in the measurements to draw any conclusions.

Where rotation during a test had caused the specimen not to be aligned directly with the gauged plates, the measured force would be lower than the actual force. The minor bowing forces per se could not influence the readings, as the bridge is compensated for in-plane bending strains. However the resultant torsional moments could have a considerable effect on the readings, and may have caused some of the forces to apparently exceed 10 or 12[+].

Stability of the gauges was never a source of trouble, once the optimum cement, operating temperatures and battery voltage were

[+] These were excluded from the figure.

[x] There is one exception - see section 8.3.3.

established; it is believed that this technique is potentially very useful.

8.3.2.4 Consistency correlations

As explained in section 7.3.3, the elimination of real time from the equations through the use of the parameters v_c and v_{ce}, implies that the results of two different experiments with the same initial shape should be identical at equal values of the parameters. Such a correlation would only exist if the minor bowing had not seriously effected the deformation, or alternatively if it had produced similar effects in both cases. Despite these limitations, a considerable number of excellent correlations were found for both v_c and v_{ce} - and are indicated on each test in the Figs. 24 - 55, as they occurred. As expected, all the correlations were found between members of the same group, but their range and diversity gave excellent support to the theory.

It seemed then that some systematic effect was present in a particular group, despite the lack of any continued similarity in the minor bows.

8.3.3 Conclusions

The view that minor bowing is of small significance is substantiated by the similarity of major plane bowing in Tests 51, 52 and 55, where the minor bows were quite disimilar. The same argument can be applied to the existence of consistency correlations in tests not having similar minor bows. This also implies that geometric interaction was not important, and that the similarities in the deflected shapes are consistent with the independence of two plane bowing.

The origins of the two asymmetric groups are however difficult to explain on this basis: assuming that the computations were correct and that the very slight asymmetries in the initial shape would be attenuated[+], it must be concluded that the considerable initial deviations from symmetry were due to an extraneous factor such as minor bowing. These deviations were however attenuated in all of the tests for which $v_c > 20$, and a return to the symmetric mode could be observed.

[+] This view is supported by the stability analysis of Blackburn (9).

The deformation would obviously be affected by minor bowing where there had been reductions in clearance, or an escape from the channel restraint: it is also clear that this effect would not be localised. However there are cases (Test 52) where an asymmetric perturbation is apparent in the first readings after contact, whilst the minor bow is still negligible.

It appears then that once a mode of deformation has been established, the minor bow is of little importance: this follows from the good consistency correlations. A complimentary argument for the existence of these correlations is found in the fact that they must also be applicable to the minor bows; but this was evident only in the Figs. 30 and 41.

Two dimensional theory with constant clearance was shown to be inadequate in predicting the deformation: in some cas es the use of a reduced clearance would have improved agreement, but the overall rate of return to a symmetric mode was very much slower than that given by the theory.

9.0 Conclusions

9.1 Results of present study

It was concluded that the tangent modulus theory is adequate for engineering purposes in the prediction of conventional creep buckling behaviour: some uncertainties in the primary creep data correlations remain, and cannot be resolved without compressive creep data for this material.

A method was developed for predicting two dimensional column behaviour from one computed solution for a particular shape; the comparable solutions are valid for both conventional and restrained bowing over an arbitrary range of temperature and creep properties. Less generality was possible when elastic deformation was significant, and in this event the solution is valid only for columns having equal Euler loading ratios.

It was found that the significance of elastic deformation in restrained bowing was small for Magnox at 295°C: it's omission in any case gives rise to conservative design. The significance of the primary or tertiary creep phases, would vary according to the application.

The one restrained bowing experiment in which the deformation remained two dimensional, showed good agreement with the theory. In the experiments on axisymmetric shapes (simulating reactor fuel elements), considerable third dimensional deformation was noted. This rendered direct comparison with the theory impossible, but the application of consistency correlations within the data showed encouraging agreement. The experiments also showed that two dimensional symmetric theory was very conservative in predicting deformation of axisymmetric columns.

The problem of the reactor fuel element with five braces, in contact with point restraints only, is much simpler in three dimensions than the case of continuous restraint. Providing friction is neglected, a solution can be obtained (23) using the moment-curvature relations presented here. It is believed that the experiments gave justification for this approach.

9.2 Suggestions for further work

The linearised tangent modulus theory, and the equivalent H-section theory, are substantially identical for column buckling problems in materials exhibiting secondary creep only. Further work could assess their relative suitability for non steady creep laws. For creep bending applications however, and for combinations of bending moment and direct loading, only the H-section method remains valid; it appears that its simplicity and potential usefulness do not seem to have been fully appreciated. It is believed that a programme of experiments on creep bending of beams and beam columns would lend authority to the more general application of this technique as a design tool.

Various techniques for accelerating the method of computation used here for restrained bowing analysis have been suggested (section 5.1.3.3): it may be useful to compare these with the integral method of Blackburn (9).

The problem of continuously restrained three dimensional bowing could be studied under more tractable conditions in rectangular channels, and the independence of the bowing in two planes could then be verified.

Acknowledgements

The author is indebted to his supervisor, Professor J.M. Alexander, for his continued interest and encouragement.

Grateful thanks are due to the author's employers, The Atomic Energy Board, Pelindaba, Transvaal, in the Republic of South Africa, without whose generous financial support this project could not have been undertaken.

Due acknowledgement must also be made to Mr. D.J. McConalogue, of the Department of Electrical Engineering, Imperial College, whose assistance with the evaluation of the interpolated derivatives was invaluable.

Financial support for some of the equipment was provided by the Berkeley Nuclear Laboratories of the C.E.G.B.; the author is also grateful to the Atomic Power Division of the English Electric Co. Ltd. for their cooperation in the provision of otherwise inacessible reports.

The author would also like to thank Messrs. A. Graham and K.F.A. Walles, of the National Gas Turbine Establishment, for enabling him to learn the curve-fitting techniques and for advice on the design of the extensometers.

10.1 Bibliography

1) Alexander, J.M. 'Approximate theory for thermal and irradiation creep buckling of a uranium fuel rod and its magnesium can', J. Mech. Engng. Sci. 1959 1, 3, 211.

2) Alexander, J.M. and Webster, G.A. 'The creep buckling of composite members', J. Mech. Engng. Sci. 1960 2, 4, 342.

3) Andrade, E.N. da C. 'On the viscous flow of metals and allied phenomena' Proc. Roy. Soc. A, 1910 84, 1.

4) Anon. 'Interpolation and allied tables', 1956 (H.M.S.O.).

5) Anon. 'Modern Computing Methods', N.P.L. Notes on applied science No. 16, 1961 (H.M.S.O.).

6) Berkovits, A. 'Investigation of three analytical hypotheses for determining material creep behaviour under varied loads', N.A.S.A. 1961 TND-799.

7) Blackburn, W.S. 'Creep buckling of stacked fuel elements', Reactor Sci. Technol. (J. Nuc. Energy Pts. A and B) 1961 14, 1.

8) Blackburn, W.S. and Percy J. 'The symmetric creep bowing of stacked fuel elements', Reactor Sci. Technol. (J. Nuc. Energy Pts. A and B) 1963 17, 257.

9) Blackburn, W.S. 'Creep bowing of a fuel element against a continuous restraint', to be published in Reactor Sci. Technol.

10) Bleich, H.H. and Dillon, O.W. 'Nonlinear creep deformations of columns of rectangular cross-sections', J. Appl. Mech. 1959 4, 517.

11) Bodner, S.R. 'Mechanisms of creep buckling', Proc. 5th Israel Conference on Aviation and Astronautics, 1963 (Jerusalem Academic Press).

12) Calladine, C.R. 'Effect of cross section shape on the creep buckling behaviour of columns', Int. J. Mech. Sci. 1962 4, 387.

13) Carlson, R.L. and Schwope, A.D. 'Investigation of compressive creep properties of aluminium columns at elevated temperatures', W.A.D.C. 1952 TR52-251, Part 1.

14) Carlson, R.L. and Manning, G.K. Ibid, Part 2 1954, Part 3 1955.

15) Carlson, R.L., Bodine, E.G. and Manning, G.K. Ibid, Part 4 1956.

16) Carlson, R.L. 'An investigation of column creep' Batelle Memorial Institute, ARL 1961, 186.

17) Chapman, J.C., Erickson, B. and Hoff, N.J. 'A theoretical and experimental investigation of creep buckling', Int. J. Mech. Sci. 1960 1, 145.

18) Costello, G.A., Sidebottom, O.M. and Pocs, E. 'Inelastic design of load carrying members' W.A.D.D. 1961 TR60-580, Part 2.

19) de Veubeke, F.B. 'Creep Buckling' High temperature effects in aircraft structures (Ed. N.J. Hoff) 1958, A.G.A.R.D. (Pergamon Press).

20) Finnie, I and Heller, 'Creep of engineering materials', 1959 (McGraw-Hill).

21) Freed, N.H. and Seyna, F. 'Small deflection creep buckling of magnesium alloy (Magnox AL80) at 295°C', J. Mech. Engng. Sci. 1965 7, 3.

22) Fudge, D. 'The creep bowing of a five, brace fuel element in a single plane', English Electric Co. Ltd. 1963 TN 620.

23) Fudge, D. and Haigh, R.E. 'The creep bowing of a five brace fuel element in two planes', English Electric Co. Ltd. 1963 TN 641.

24) Gerard, G. 'A creep buckling hypothesis', J. Aero. Sci. 1956 23, 879.

25) Gerard, G. and Papirno, R. 'Classical columns and creep', J. Aerospace Sci. 1962 29, 6, 680.

26) Gjelsvik, A. and Bodner, S.R. 'An investigation of the energy criterion in snap buckling problems', Brown University, Division of Engineering 1962, TR No. 28.

27) Graham, A. 'The phenomenological method in rheology', Research 1953 6, 92.

28) Graham, A. and Walles, K.F.A., 'Regularities in creep and hot fatigue data', Aeronautical Research Council 1958 C.P. 379, 380 (H.M.S.O.).

29) Haigh, R.E. 'A theoretical study of the creep bowing of civil type stacked fuel elements', English Electric Co. Ltd. 1963 Report No. W/AT 1206.

30) Harris, J.E. and Jones, R.B. 'An analysis of 'Magnox' AL80 secondary creep data', C.E.G.B. Berkeley Nuclear Laboratories 1963 RD/B/R.144.

31) Hartree, D.R. 'Numerical analysis', 1952 (Oxford University Press).

32) Hedner, G. 'Total strain theory of creep including recovery', Trans. Roy. Inst. Tech. Stockholm 1963, 214.

33) Higgins, T.P. 'Weight-strength analysis of aircraft structures', Chap. 20 (Ed. F.R. Shanley) Rand Corp. 1952 (McGraw-Hill).

34) Hildebrand, F.B. 'Introduction to numerical analysis', 1956 (McGraw-Hill).

35) Hilton, H.H. 'Creep collapse of visco-elastic columns with initial curvature', J. Aero. Sci. 1952 19, 12, 844.

36) Hoff, N.J. 'Buckling and stability', J. Roy. Aero. Soc. 1954 58, 31.

37) Hoff, N.J. 'Creep buckling', Aero. Quart. 1956 7, 1.

38) Hoff, N.J. 'Buckling at high temperatures', J. Roy. Aero. Soc. 1957 61, 756.

39) Hoff, N.J. 'A survey of the theories of creep buckling', A.F.O.S.R. 1958 TN 60, 382.

40) Hoff, N.J. Ibid, Proc. 3rd U.S. Nat. Congr. Appl. Mechs., June 1958, New York, A.S.M.E.

41) Hoff, N.J. 'Reversed creep: a remark to the theory of Rabotnov-Shesterikov', J. Mech. Phys. Solids 1964, 12, 2.

42) Hult, J. 'Creep buckling' K.T.H. Publikation 1955, 111.

43) Hult, J. 'Critical time in creep buckling' J. Appl. Mech. 1955 22, 3, 432.

44) Hult, J. 'Creep buckling of plane frameworks', K.T.H. Publikation 1959, 136.

45) Hult, J. 'Oil canning problems in creep', I.U.T.A.M. Colloquium on creep in structures (Ed. N.J. Hoff), Stanford University, 1962 (Springer Verlag).

46) Jahsman, W.E. and Field, F.A. 'Comparison of theoretical and experimental creep buckling times of initially straight centrally loaded columns', J. Aerospace Sci. 1962 29, 4, 431.

47) Jahsman, W.E. and Field, F.A. 'Dynamic creep unstability of initially straight centrally loaded columns', J. Appl. Mech. 1962 29, 73.

48) Johnson, A.E., Mathur, V.D. and Henderson, J. 'The creep deflection of magnesium alloy struts', Aircraft Engng. 1956, 28, 419.

49) Johnson, A.E. 'Complex-stress creep of metals', Metall. Rev. 1960 5, 20, 447.

50) Kempner, J. and Pohle, F. 'On the non-existence of a finite critical time for linear viscoelastic columns', J. Aero. Sci. 1953 20, 8, 572.

51) Kempner, J. 'Creep bending and buckling of linear viscoelastic columns', N.A.C.A. 1954 TN 3136.

52) Kempner, J. and Patel, S. 'Creep buckling of columns' N.A.C.A. 1954 TN 3138.

53) Kempner, J. 'Creep bending and buckling of non-linear viscoelastic columns' N.A.C.A. 1954 TN 3137.

55) Lempriere, B.M. 'Comparison of the ranges of applicability of predictions of creep buckling time', I.U.T.A.M. Colloquium on creep in structures (Ed. N.J. Hoff) Stanford University 1962 (Springer Verlag).

56) Libove, C. 'Creep buckling of columns', J. Aero. Sci. 1952 19, 7, 459.

57) Libove, C. 'Creep buckling analysis of rectangular section columns' N.A.C.A. 1953 TN 2956.

58) Lin, T.H. 'Creep stresses and deflections of columns', J. Appl. Mech. 1956 23, 214.

59) Lin, T.H. 'Creep deflections and stresses of beam columns', J. Appl. Mech. 1958 25, 75.

60) Madsen, W.A. and Lempriere, B.M. 'Creep buckling experiments' S.U.D.A.E.R. 1962, 130.

61) Marin, J. 'Creep deflections in columns', J. Appl. Phys. 1947 18, 103.

62) Marriot, D.L. and Leckie, F.A. 'Some observations of the deflections of structures during creep', Conf. on thermal loading and creep, Paper 17, I. Mech. E. 1964.

63) Mathauser, E.E. and Brooks, W.A. 'An investigation of the creep lifetime of 75 S-T6 Al-alloy columns', N.A.C.A. 1954, TN 3204.

64) Mendelson, A., Hirschberg, M.H. and Manson. S.S. 'A general approach to the practical solution of creep problems', Trans. A.S.M.E. J. Basic Engng. 1959 81 D, 4, 585.

65) Odquist, F.K.G. 'Influence of primary creep on column buckling', J. Appl. Mech. 1954 21, 3, 295.

66) Ohji, K. and Marin, J. 'Creep of metals under non-steady conditions of stress', Conference on thermal loading and creep, Paper 18, I. Mech. E., 1964.

67) Papirno, R. and Gerard, G. 'Investigation of creep buckling of columns and plates', W.A.D.C. 1961 TR59-416, Part 3.

68) Patel, S.A. 'Buckling of columns in the presence of creep', Aero. Quart. 1956 7, 1.

69) Patel, S.A., Kempner, J., Erickson, B. and Mombassery, A.H. 'Correlation of creep-buckling tests with theory', N.A.C.A. 1956 RM56C20.

70) Patel, S.A. and Kempner, J. 'Effect of higher harmonic deflection components on the creep buckling of columns', Aero. Quart. 1957 8, 3, 215.

71) Pian, T.H.H. and Johnson, R. 'On the creep buckling of columns and plates', M.I.T. A.S.R.L. 1957 TR25-24.

72) Pian, T.H.H. 'Creep buckling of curved beams under lateral loading', M.I.T. A.S.R.L. 1958 TR25-26.

73) Pian, T.H.H. and Chow, C.Y. 'Further studies of creep buckling of curved beams under lateral loading', M.I.T. A.S.R.L. 1958 TR25-28.

74) Prentice, J.M. and Ross, A.D. 'Slender reinforced concrete columns', Concrete Constructional Engineer', 1948, 43, 261.

75) Rabotnov, G.N. and Shesterikov, S.A. 'Creep stability of columns and plates' J. Mech. Phys. Solids 1957 6, 1, 27.

76) Roberts, A.C. and Cotterell, A.H. 'Creep of Alpha Uranium during irradiation with neutrons', Phil. Mag. 1956 1, 711.

77) Rudnick, A., Carlson, R.L. and Manning, G.K. 'The compressive creep buckling of metal columns', W.A.D.C. 1958 TR52-251, Part 6.

78) Salmassy, O.K., MacDonald, R.J., Carlson, R.L. and Manning G.K. 'An investigation of the interchange of tensile creep for compressive creep', W.A.D.C. 1956 TR56-26, Part 1.

79) Ibid 1957, Part 2.

80) Sanders, J.L., MacComb, H.G. and Schlechte, F.R. 'A variational theorem for creep with applications to plates and columns', N.A.C.A. 1958 Rep. 1342 (TN4003).

81) Schlechte, F.R. 'Theoretical analysis of the creep collapse of columns' N.A.S.A. 1959 TND 95.

82) Shanley, F.R. 'Weight strength analysis of aircraft structures', Chap. 18. Rand Corpn. 1952 (McGraw-Hill).

83) Sidebottom, O.M. and Dewhurst, D.L. 'Theoretical and experimental creep analyses of beam columns', A.S.M.E. 1962 Pap. No. 62-WA-229.

84) Siegfried, W. 'Failure from creep as influenced by the state of stress', J. Appl. Mechs. 1943 10, 4, 202.

86) Stewart, J.C.C. 'Development and manufacture of 'Magnox' fuel', I. Mech. E. Paper P9/64, 1963.

87) Stowell, E.Z. and Wah, T. 'A unified theory for creep buckling under normal loads', J. Aerospace Sci. 1962 29, 6, 658.

88) Timoshenko, S.P. and Gere, J.M. 'Theory of elastic stability', 1961 (McGraw-Hill).

89) Young, A.G. 'Moment curvature-rate relations during steady creep for a beam under combined bending and direct load', English Electric Co. Ltd. 1959 Rep. No. W/AT 282.

90) Young, A.G. 'Creep bowing of the Hinkley Point fuel element', English Electric Co. Ltd. 1959 Rep. No. W/AT 353.

92) Walles, K.F.A. 'A quantitative presentation of the creep of nimonic alloys', N.G.T.E. 1959 Note no. N.T. 386.

93) Walles, K.F.A. and Graham, A. 'On the extrapolation and scatter of creep data', A.R.C. 1963 C.P. 680 (H.M.S.O.).

94) Webster, G.A. 'An investigation of thermal creep buckling', Ph.D. thesis, University of London, 1962.

95) Webster, G.A. and Alexander, J.M. 'An investigation of small-deflection creep buckling', Proc. I. Mech. E. 1963-64 178 (Pt. 3A), 2-1.

10.2 Relation between the $\dot{E}$ method and the equivalent H-section

Some similarity in the above methods had been noted for the case of linear viscoelasticity by Young (90), and in an indirect sense by Calladine (12).

It is intended to show here that the moment-curvature rate relations for the two methods are very closely analagous: this is to be expected as both are based essentially on the elastic behaviour of the column.

Consider the creep law

$$\dot{e} = c\sigma^n + \dot{\sigma}/E,$$

where n is an integer. For an equivalent H-section (36) of flange separation h, area A, and $\sigma_o = P/A$, the stresses in the compressive and tensile flanges σ_c, σ_t, under a deflection y are

$$\sigma_c = \sigma_o (1 + 2y/h)$$

$$\sigma_t = \sigma_o (1 - 2y/h)$$

The curvature rate is

$$\dot{K} = \frac{\dot{e}_c - \dot{e}_t}{h} = \frac{1}{h}\left[\sigma_o\, 2\dot{y}/Eh + c\sigma_o^n (1 + 2y/h)^n + \sigma_o\, 2\dot{y}/Eh - c\sigma_o^n (1 - 2y/h)^n\right]$$

$$= \frac{1}{h}\left[4\sigma_o\dot{y}/Eh + c\sigma_o^n \left(1 + 2ny/h + \frac{4y^2 n(n-1)}{2h^2} + \frac{n(n-1)(n-2)\,8y^3}{6h^3} + \ldots - 1 + 2ny/h - \frac{4y^2 n(n-1)}{2h^2} + \frac{n(n-1)(n-2)\,8y^3}{6h^3} - \ldots\right)\right] \quad (10.1)$$

Now for n = 1, 2, eqn. (10.1) becomes

$$\dot{K} = 1/h\left[4\sigma_o\dot{y}/Eh + c\sigma_o^n\, 4ny/h\right]$$

Now $4/h^2 = A/I$, $M = Py = \sigma_o Ay$

$$\dot{K} = \dot{M}/EI + cn\sigma_o^{n-1}\, Ay/I$$

$$= \dot{M}/EI + M/\dot{E}I, \text{ since } 1/\dot{E} = (\partial\dot{\varepsilon}/\partial\sigma)_{\sigma_0}$$

For these values of the stress exponent, the methods are therefore identical.

For n = 3, eqn. (10.1) becomes

$$\dot{K} = \dot{M}/EI + M/\dot{E}I + \frac{4\,\dot{M}}{3EI}\left(\frac{y}{h}\right)^2$$

In the range of small deflections, $y < h/2$, the effect of the third term (and others for higher values of n) will obviously be small. The relation between the $\dot{E}$ methods for the case of non-steady creep has not been examined: the $\dot{E}$ method is essentially a "time-hardening" theory, and it is not always possible to recast this type of creep law into a "strain-hardening" form. There will then be circumstances in which one or other of the methods will be more suitable.

10.3 On the independence of 2-plane bowing

Equations are derived below for the general two dimensional problem; after discussing possible methods of solution, it is shown under the assumptions inherent in the $\dot{E}$ method, that deformation in the two planes may be treated independently. Under the special conditions of restrained bowing in a circular channel however, some inter-action between the planes is found to exist.

10.3.1 General equations

Let $\dot{K}_y$, $\dot{K}_z$ be curvature in y- and z-directions, where y and z now originate in the centre of the section. Then from the assumption of plane strain, and assuming the geometrical centroid and axis of zero bending moment coincide,

$$\dot{e}\,(x, y, z) = \dot{e}_o + \dot{K}_y\,(x) \cdot y + \dot{K}_z\,(x) \cdot y \qquad (10.2)$$

and also

$$\dot{e}\,(x, y, z) = \frac{\dot{\sigma}\,(x, y, z)}{E} + \dot{\varepsilon} \qquad (10.3)$$

where $\dot{\varepsilon} = \dot{\varepsilon}\,(\sigma, t)$ or $\dot{\varepsilon}\,(\sigma, \varepsilon)$ etc.

From (10.3)

$$\dot{\sigma}\,(x, y, z) = E\,\dot{e}\,(x, y, z) - E\,\dot{\varepsilon}$$

i.e.

$$\dot{\sigma} = E\left[\dot{e}_o + \dot{K}_y \cdot y + \dot{K}_z \cdot z - \dot{\varepsilon}\right] \qquad (10.4)$$

Consider a cross-section with 2 axes of symmetry:-

$$\dot{M}_z = \iint_A \dot{\sigma}\,(x, y, z)\; y\; dz\; dy$$

and

$$\dot{M}_y = \iint_A \dot{\sigma}\,(x, y, z)\; z\; dy\; dz$$

From (10.4)

$$\dot{M}_z = E\iint_A (\dot{e}_o + \dot{K}_y \cdot y + \dot{K}_z \cdot z - \dot{\varepsilon})\; y\; dz\; dy$$

and

$$\dot{M}_y = E\iint_A (\dot{e}_o + \dot{K}_y \cdot y + \dot{K}_z \cdot z - \dot{\varepsilon})\; z\; dy\; dz$$

Now

$$\dot{e}_o \iint y\,dA = \dot{e}_o \iint z\,dA = \dot{K}_y \iint yz\,dA = \dot{K}_z \iint zy\,dA = 0$$

and

$$\iint y^2\,dA = I_z \quad \text{and} \quad \iint z^2\,dA = I_y$$

So $$\dot{M}_z = EI_z\dot{K}_y - E\iint \dot{\varepsilon}\, y\,dA \qquad (10.5)$$

and $$\dot{M}_y = EI_y\dot{K}_z - E\iint \dot{\varepsilon}\, z\,dA \qquad (10.6)$$

The numerical solution of (10.5, 10.6) presents no difficulty in principle. Knowing the initial (elastic) stress distribution and deflection, the double integral is evaluated from the creep law at each mesh point. The resulting equations in $\partial u_y/\partial t$, $\partial u_z/\partial t$ (where $\dot{K}_y = \partial^2 u_y/\partial x^2$ and $\dot{K}_z = \partial^2 u_z/\partial x^2$) are then solved in a manner analagous to the equations of section 4.2. From the new deflections, the curvature and hence the total strain at each point across the section is evaluated. By knowing the accrued creep strain, the change in stress is found from eqn. (10.4) and we are ready to proceed to the next time interval. Alternatively the process may be iterated to improve the accuracy. The method is valid for any creep law, as a knowledge of current creep strain is required in any case.

10.3.2 Implications of the E method

The assumption of a linear stress distribution, requires for consistency the assumptions of a linear distribution of both elastic and creep strains. The resulting simplification to the general equations (10.5, 10.6) is considerable.

Since under these conditions

$$\sigma(x, y, z) = \sigma_o + k_1 y + k_2 z$$

and $$\varepsilon = k_3 \sigma ,$$

the general equations become

$$\dot{M}_z = EI_z\dot{K}_y - Ek_3\iint_A (\sigma_o + k_1 y + k_2 z)\, y\,dA$$

and $$\dot{M}_y = EI_y\dot{K}_z - Ek_3\iint_A (\sigma_o + k_1 y + k_2 z)\, z\,dA$$

The product of inertia terms vanish and we have

$$\dot{M}_z = EI_z\dot{K}_y - EI_z k_1 k_3 ,$$

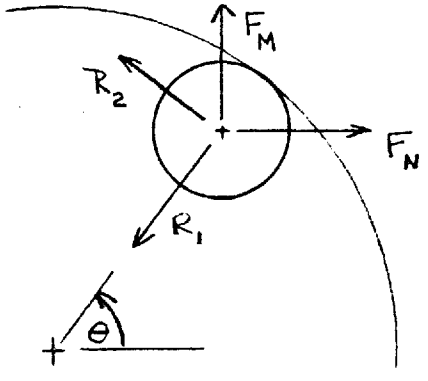
which is in fact another form of the equation (4.8): the deformation in each case is thus shown to be independent of the other plane.

10.3.3 Bowing in a circular channel

It was shown for a section with two axes of symmetry, that deformation in the two planes may be treated independently to a good approximation. There are circumstances however in which this will not be true: one of these is for restrained bowing in a circular channel.

The first factor responsible for this is the geometric interaction between the planes. The point of contact with the channel is a function of the deformation in the major plane only. Since the deflection in the minor plane must by definition be zero at this point, it follows that the major plane deformation, by influencing the point of contact, will indirectly be influencing the minor plane deformation. Also, as in Fig. 81c, a growth in the minor bow can enforce a reduction in the major bow. The problem would still be soluble in principle, given the initial shape in the minor plane and that the point of contact remained on the same generator of the channel.

The second consideration is that of force interaction due to friction. If the point of contact did not move round the channel, and the friction force was less than the limiting value, the following equations apply for the forces F_M and F_N in the major and minor planes



$$F_N = R_1 \cos\theta + R_2 \sin\theta$$

$$F_M = R_1 \sin\theta - R_2 \cos\theta$$

The forces are independent of each other and the solution can therefore be found. If however the friction is limiting and the point of contact moves circumferentially (this seemed to be the more likely), then the force R_2 becomes μR_1, and the following relations hold

$$\frac{F_M}{F_N} = \frac{\tan\theta - \mu}{1 + \mu\tan\theta}$$

The angle θ is now a function of F_M, F_N and μ, and an iterative process would be required to satisfy moment and force equilibrium in both directions simultaneously. This would be a very lengthy computation.

These considerations would not apply to a rectangular channel and in that case the bowing would be quite independent in the two planes.

10.4 Relation between solution time and real time

The similarity between eqns. (4.41, 4.26) and (7.3) led the author to the conclusion that the techniques used for analysing eqn. (7.3) could also be used for synthesising eqns. (4.41, 4.26). Rewriting (7.3) as

$$(1 - P/P_E)\frac{\pi^2 I \ln}{AL^2}(b_2/b_1) = n_1 c_1 \sigma_o^{n_1} t^{1/3} + n_2 c_2 \sigma_o^{n_2} t$$

and (4.41) as

$$v_{ce} \cdot (1 - P/P_E)\frac{2I}{AL^2} \ln 2 = n_1 c_1 \sigma_o^{n_1} t^{1/3} + n_2 c_2 \sigma_o^{n_2} t \qquad (10.7)$$

the similarity becomes apparent. Now the times for each term of the r.h.s. to attain the standard value of 10^{-3} are plotted against σ_o in Figs. 62 and 63; the appropriate standard value of v_{ce}^* is found by writing eqn. 10.7 as

$$C' \cdot v_{ce}^* = 10^{-3}, \text{ hence}$$

$$v_{ce}^* = 10^{-3}/C'$$

By using the values of $t_{1/3}$ and t_1 read off from Figs. 62, 63, and the value of v^* calculated as above, the Graham-Walles standard curve is used to construct the v – t relation, by a process which is the inverse of the graphical analysis.

10.5 Derivation of equations for dr/dv

10.5.1 Symmetrical creep only

Equations (4.22, 4.23) can be written

$$A'\partial^3 u/\partial s^2 \partial t + u = sX$$

$$o < s < r \qquad (10.8)$$

$$A'\partial^3 u/\partial s^2 \partial t + u = rX$$

$$r < s < 1 \qquad (10.9)$$

By integrating (10.8, 10.9) twice, and through use of the appropriate boundary condition, we obtain

$$A'\partial u/\partial t = \frac{sX}{6}(s^2 + 3r^2 - 6r) - \int_o^s\int_o^s u\,dw\,dw + s\int_o^1 u\,d\,s$$

$$\text{for } o < s < r \qquad (10.10)$$

and

$$A'\partial u/\partial t = \frac{rX}{6}(3s^2 - 6s + 6r - 6r^2) + \int_s^r\int_s^1 u\,dw\,dw$$

$$\text{for } r < s < 1 \qquad (10.11)$$

and since $\partial u/\partial t = o$ at $s = r$, eqn. (10.10) becomes

$$A'\partial u/\partial t = \left[\frac{\int_o^r\int_o^s u\,dw\,dw - r\int_o^1 u\,dw}{4r^3 - 6r^2}\right](s^3 + 3rs^2 - 6rs) - \int_o^s\int_o^s u\,dw\,dw + s\int_o^1 u\,dw \qquad (10.12)$$

Differentiating (10.12), and substituting in eqn. (4.24), setting $s = r$

$$A'\,dr/dt = \frac{\frac{3(1-r)}{r(2r-3)}\left[\int_o^r\int_o^s u\,dw\,dw - r\int_o^1 u\,dw\right] - \int_r^1 u\,d\,s}{\left(\frac{\partial^2 u}{\partial s^2}\right)_{s=r}} \qquad (10.13)$$

When $r = 1$, and the curvature is finite, no displacement of the point of contact occurs, since the numerator is zero. When the curvature at $s = r = 1$ becomes zero however, the above expression takes the form o/o and is indeterminate. To remove this, we differentiate top and

bottom w.r.t to t, noting that

$$df/dt = \partial f/\partial r \cdot dr/dt$$

we obtain

$$\lim_{r \to 1} A' \, dr/dt = \frac{1 - 3\int_0^1 s\,u\,ds}{\left(\frac{\partial^3 u}{\partial s^3}\right)_{s=r=1}}$$

If the third derivative is zero at the instant curvature disappears, then the r.h.s. is infinite. In the case of the initially sinusoidal shape, the third derivative is non-zero and the motion is defined during that instant by the above equations.

To treat the case where the third derivative is zero, we multiply eqn.(10.13) by $(1 - r)$, and differentiate top and bottom, obtaining

$$A' (1 - r)\, dr/dt = \frac{(1 - r)\,u + \left[\int_0^r \int_0^s u\,dw\,dw - r\int_0^1 u\,dw\right] \frac{3r^2 - 12r + 9}{r^2 (2r - 3)^2}}{\left(\frac{\partial^3 u}{\partial s^3}\right)_{s=r}}$$

$$+\frac{\int_r^1 u\,dw + \frac{3(1 - r)^2}{r(2r - 3)}\int_0^s u\,dw - \int_0^1 u\,ds}{\left(\frac{\partial^3 u}{\partial s^3}\right)_{s=r}}$$

which is still indeterminate. Differentiating again, we find

$$\lim_{r \to 1} A' (1 - r)\, dr/dt = \frac{6\int_0^1 s\,u\,ds - 2}{\left(\frac{\partial^4 u}{\partial s^4}\right)_{s=1}}$$

Since

$$A' (1 - r)\, dr/dt = -\tfrac{1}{2} A' \frac{d}{dt} (1 - r)^2$$

we find that

$$r = 1 - \sqrt{\frac{\left(4 - 12\int_0^1 s\,u\,ds\right) t}{A' \left(\frac{\partial^4 u}{\partial s^4}\right)_{s=1}}}$$

which is valid during the instant of point contact splitting.

10.5.2 Symmetrical creep and elasticity

Eqns. (4.38, 4.39) can also be written

$$C\,\partial^3 u/\partial s^2 \partial v = X s - u + B\dot{X}s - B\dot{u} \quad \text{for} \quad o < s < r \tag{10.14}$$

$$\text{and} \quad C\,\partial^3 u/\partial s^2 \partial v = X r - u + BX\,\partial r/\partial v + B\dot{X}r - B\dot{u} \quad \text{for} \quad r < s < 1 \tag{10.15}$$

Integrating (10.14, 10.15) and using the appropriate boundary conditions we find

$$C\,\partial u/\partial v = Xs^3/6 - \int_o^s\int_o^s u\,dw\,dw + \frac{B\dot{X}s^3}{o} - B\int_o^s\int_o^s \dot{u}\,dw\,dw + Bs\int_o^1 \dot{u}\,dw$$

$$+ s\int_o^1 u\,dw - Xrs\,(1 - r/2) - B\dot{X}rs(1 - r) - B\dot{X}\,r\,s(1 - r/2)$$

$$\text{for} \quad o < s < r$$

After using the condition $(\partial u/\partial v)_{s=r} = o$, and differentiating, we find

$$C\,(\partial^2 u/\partial s \partial v)_r = \int_r^1 u\,d\,s + B\int_r^1 \dot{u}\,d\,s + \left(\frac{r-1}{\frac{2}{3}r - 1}\right)\left[\frac{1}{r}\int_o^r\int_o^s u\,dw\,ds\right.$$

$$\left. + \frac{B}{r}\int_o^r\int_o^s \dot{u}\,dw\,ds - B\int_o^1 \dot{u}\,d\,s - \int_o^1 u\,d\,s + B\dot{X}rr/3\right]$$

Substitution in eqn. (4.24) yields

$$\frac{dr}{dv} = \frac{3(1-r)}{r(2r-3)}\left[\int_o^r\int_o^s u\,dw\,ds + B\int_o^r\int_o^s \dot{u}\,dw\,ds\right.$$

$$\left. - B\,r\int_o^1 \dot{u}\,d\,s - r\int_o^1 u\,d\,s\right] - \int_r^1 u\,d\,s - B\int_r^1 \dot{u}\,d\,s$$

$$\frac{}{C\left(\frac{\partial^2 u}{\partial s^2}\right)_{s=r} - \frac{3BXr(r-1)}{2r-3}} \tag{10.16}$$

When curvature becomes zero, and r = 1, this is indeterminate and differentiating top and bottom we find

$$\lim_{r\to 1} \frac{dr}{dv} = \frac{1 + B\,(\dot{u})_{r=1} - 3\int_o^1 s\,u\,d\,s - 3B\int_o^1 s\,\dot{u}\,d\,s}{C\left(\frac{\partial^3 u}{\partial s^3}\right)_r + 3BX}$$

This equation will apply where X and the third derivative are non zero at the instant the curvature disappears, as in the case of the sine wave. For the sine wave plus 1/9 third harmonic, where both force and third derivative are zero at the instant of first contact, we again multiply both sides of eqn. (10.16) by (1 - r), and differentiating twice, obtain after some simplification

$$\lim_{r \to 1} \frac{dr}{dv}(1 - r) = \frac{6 \int_0^1 s\,u\,ds + 6B \int_0^1 s\,\dot{u}\,ds - 2}{C \left(\frac{\partial^4 u}{\partial s^4}\right)_{s=1}}$$

from which we obtain a relation between r and v_{ce} as before.

10.6 Specification of finite difference operators

10.6.1 $G - (\partial^3 u/\partial s^2 \partial v)_{s=1}$

This was defined by the operators (4)

$$(\partial^3 u/\partial s^2 \partial v)_M = G\,(\partial u/\partial v)_M = M^2\,(1/45\;\partial u/\partial v_{M-3} - 0.3\,\partial u/\partial v_{M-2} + 3\;\partial u/\partial v_{M-1})$$

which incorporates the condition that $(\partial u/\partial s)_M = o$ and $(\partial u/\partial v)_M = o$.

10.6.2 $(\partial^3 u/\partial s^3)_{s=1}$

For this quantity, a backward difference operator (4) was used on account of the discontinuity at $s = 1$:

$$\left(\frac{\partial^3 u}{\partial s^3}\right)_M = M^3\,(4.25 - 17.75\,u_{M-1} + 29.5\,u_{M-2} - 24.5\,u_{M-3} + 10.25\,u_{M-4} - 1.75\,u_{M-5})$$

10.6.3 $(\partial^4 u/\partial s^4)_{s=1}$

For reasons as above, a backward difference operator (4) was also used

$$(\partial^4 u/\partial s^4)_M = M^4(-1 + 6u_{M-1} - 14u_{M-2} + 16u_{M-3} - 9u_{M-4} + 2u_{M-5})$$

10.6.4 $H - (\partial^3 u/\partial s^2 \partial v)_{s=r}$

This was represented by a Lagrangian operator (31), in order to incorporate accurately the condition $(\partial u/\partial v)_r = o$

$$\left(\frac{\partial^3 u}{\partial s^2\, v}\right)_{s=r} = M^2\,H\,\left(\frac{\partial u}{\partial v}\right)_r$$

where $H\,\left(\frac{\partial u}{\partial v}\right)_r = h_1\,\left(\frac{\partial u}{\partial v}\right)_{J-1} + h_2\,\left(\frac{\partial u}{\partial v}\right)_J + h_3\,\left(\frac{\partial u}{\partial v}\right)_{J+1} + h_4\,\left(\frac{\partial u}{\partial v}\right)_{J+2}$

and $$h_1 = \frac{4/M^2 - 12r/M + 12J/M^2 + 6r^2 - 12rJ/M + 6J^2/M^2}{6(1/M^2 + r/M - J/M^2)}$$

$$h_2 = \frac{6r^2 - 12rJ/M + 6J^2/M^2 - 8r/M + 8J/M^2 - 2/M^2}{2(J/M^2 - r/M)}$$

$$h_3 = \frac{6r^2 - 12rJ/M + 6J^2/M^2 - 4r/M + 4J/M^2 - 4/M^2}{2\,(r/M - J/M^2 - 1/M^2)}$$

$$h_4 = \frac{6r^2 - 12rJ/M + 6J^2/M^2 - 2/M^2}{3(4/M^2 - 2r/M + 2J/M^2)}$$

10.6.5 $E - (\partial^2 u/\partial s \partial v)_{s=r}$

A Lagrangian (31) was used here, for the same reason as above:

$$(\partial^2 u/\partial s \partial v)_{s=r} = E\,(\frac{\partial u}{\partial v})_r$$

where $E\,(\frac{\partial u}{\partial v})_r = e_1\,(\frac{\partial u}{\partial v})_{J-2} + e_2\,(\frac{\partial u}{\partial v})_{J-1} + e_2\,(\frac{\partial u}{\partial v})_J$

and $$e_1 = \frac{r^2 - 2Jr/M + J^2/M^2 + r/M - J/M}{-2/M^2\,(2/M + r - J/M)}$$

$$e_2 = \frac{r^2 - 2Jr/M + J^2/M^2 + 2r/M - 2J/M^2}{1/M^2\,(1/M + r - J/M)}$$

$$e_3 = \frac{2/M^2 + 3r/M - 3J/M^2 + r^2 - 2Jr/M + J^2/M^2}{2/M^2\,(J/M - r)}$$

10.6.6 $F - (\partial^2 u/\partial s^2)_r$

A Lagrangian (31) was used here, almost identical to that of 10.6.4:

$$(\partial^2 u/\partial s^2)_r = M^2 F\,(u)_{s=r}$$

where $F(u)_r = h_1(u)_{J-1} + h_2(u)_J + h_3(u)_{J+1} + h_4(u)_{J+2} + h_5$

where h_{1-4} are as before and

$$h_5 = \frac{12r^2 - 24rJ/M + 12J^2/M^2 - 12r/M + 12J/M^2 - 2/M^2}{(r^2 - 2rJ/M + J^2/M^2 + r/M - J/M^2)(r^2 - 2rJ/M + J^2/M^2 - 3r/M + 3J/M^2 + 2/M^2)}$$

10.6.7 $\varphi - (\partial^2 u/\partial s \partial v)_r$

A symmetrical Lagrangian (31) was in this case:

$$(\partial^2 u/\partial s\,\partial v)_r = \varphi' (\partial u/\partial v)_r$$

$$= \varphi'_1 (\partial u/\partial v)_{J-1} + \varphi'_2 (\partial u/\partial v)_J + \varphi'_3 (\partial u/\partial v)_{J+1}$$

$$+ \varphi'_4 (\partial u/\partial v)_{J+2}$$

10.6.8 $\gamma = (\partial^2 u/\partial s^2)_r$

The method described below was developed by Mr. D.J. McConalogue of the Department of Electrical Engineering, Imperial College, and is designed for the symmetrical evaluation of the second derivative, when the third derivative is known to be discontinuous. It also incorporates the information that $u_r = 1$, and $(\partial u/\partial s)_r = o$; the symmetrical approach, using values on both sides of the discontinuity, was found to be necessary for the attainment of sufficient accuracy.

Two polynomials of fourth order, $f_L(s)$ and $f_r(s)$ are defined, such that $f_L(s)$ exists in the range $s \leqslant r$, and $f_r(s)$ in the range $s \geqslant r$.

Incorporating the information $f(r) = 1$ and $(\partial f_L/\partial s)_r = (\partial f_r/\partial s)_r = o$, and also the continuity of the second derivative - $\partial^2 f_L/\partial s^2 = \partial^2 f_r/\partial s^2$ the two polynomials become

$$f_L(s) = f_r + (s - r)^2(\alpha s + \beta s^2)$$

and

$$f_r(s) = f_r + (s - r)^2(\alpha s + \beta rs + \gamma[s^2 - rs])$$ †

The only way of evaluating the coefficients in a symmetrical way is to require that the fitted polynomials $f_L(s)$ and $f_r(s)$ coincide with the actual function values as closely as possible.

Expressing this formally

$$\partial/\partial\alpha,\ \partial/\partial\beta,\ \partial/\partial\gamma\,(s_L + s_R) = o$$

where

$$s_L = \sum_{m=J-I}^{J} (f_m - f_L(m))^2$$

and

$$s_R = \sum_{m=J+1}^{J+I+1} (f_m - f_r(m))^2$$

This gives three linear equations for α, β, γ. The second derivative is then found by differentiating either f_l or f_r and is

† Where $\alpha, \beta,$ and γ are constants to be determined.

$2(\alpha r + \beta r^2)$.

The most suitable value of I was found from experience to be 1: greater values led to less accuracy.

10.6.9 $\eta - (\partial^2 u/\partial s \partial v)_r$

In this case a Newtonian interpolation was found to be the most consistently accurate:-

$$(\partial^2 u/\partial s \partial v)_r = M\ (\partial u/\partial v)_r = \eta_1(\partial u/\partial v)_{J-1} + \eta_2(\partial u/\partial v)_J + \eta_3(\partial u/\partial v)_{J+1} + \eta_4(\partial u/\partial v)_{J+2}$$

where

$$\eta_1 = -1/3 + rM - J - r^2M^2/2 + rMJ - J^2/2$$

$$\eta_2 = 3r^2M^2/2 - 3rMJ + 3J^2/2 - 2rM + 2J - \tfrac{1}{2}$$

$$\eta_3 = 1 + rM - J - 3r^2M^2/2 + 3rMJ - 3J^2/2$$

$$\eta_4 = r^2M^2/2 - rMJ + J^2/2 - 1/6$$

10.7 Temperature dependence of creep rate

10.7.1 Tensile data

The data used for this calculation was derived by Harris and Jones (30) in the form

$$\dot{\varepsilon} = f(\sigma) \exp(-32000/RT) \qquad (10.17)$$

where R = 1.98 cals/mole^{0}K

Now the creep tests showed that for Magnox at 295^{0}C, from eqn. (7.9)

$$\dot{\varepsilon} = 1.66 \times 10^{-10} \sigma^{2},$$

from which substitution in (10.17) yields that

$$\dot{\varepsilon} = 1.1 \times 10^{2} \sigma^{2} \exp(-32000/RT) \text{ at } 295^{0}\text{C}.$$

From which

$$\partial\dot{\varepsilon}/\partial T = 1.1 \times 10^{-2} \sigma^{2} \exp(-32000/RT) \cdot \frac{32000}{RT^{2}}$$

and $\delta\dot{\varepsilon}$ can be found from

$$\delta\dot{\varepsilon} \doteq \partial\dot{\varepsilon}/\partial T . \delta T$$

10.7.2 Bowing data

The dependence of the bowing data on small temperature excursions is found in the same way.

For the secondary data from eqn. (7.7)

$$\frac{\pi^{2} I (1 - P/P_{E})}{AL^{2}} \ln(b_{2}/b_{1}) = 3.03 \times 10^{-10} \sigma^{2} t$$

Separation of the r.h.s. into the product of the stress- and temperature-dependent factors as above yields

$$\frac{\pi^{2} I (1 - P/P_{E})}{AL^{2}} \ln(b_{2}/b_{1}) = 4.47 \times 10^{2} \sigma^{2} \exp(-32000/RT) \text{ at } 295^{0}\text{C}$$

from which $\delta \ln(b_{2}/b_{1})$ can be evaluated as above. For the primary data, the temperature dependence was assumed to be identical with the above.

Table 1 - 'Magnox' specification percentages

Al	Zn	Si	Cu	Mn
0.75	0.008	0.008	0.005	0.005
Fe	Sn	Ni	Be	Ca
0.005	0.005	0.002	0.007	0.005

Balance Magnesium

Table 2 - Details of free bowing and tensile test stresses

(a) Buckling experiments

Diameter in	Mean stress, lb/in^2	P/P_E
0.5	52.2	0.0256
	66.9	0.0327
	77.2	0.0378
	129.2	0.063
	131.3	0.064
	203.8	0.096
	324.3	0.159
	359.4	0.176
	413.2	0.202
	461.1	0.226
0.75	97.5	0.0219
	152.9	0.0344
	202.9	0.0455
	258.8	0.0582
	322.2	0.0725
	407.3	0.0916
	509	0.114
	612.6	0.138

(b) Tensile tests

Original diameter, in	Stress, lb/in^2
0.5	152.2
	300.7
	393.6
	601.1
	797.1
0.75	99.5
	202.7
	401.8
	505
	704
	787

Table 3 - Details of restrained bowing experiments

The tests on $\frac{1}{2}$ ins. specimens are prefaced 5, and the $\frac{3}{4}$ ins. specimens are prefaced 7.

Test Number	P/P_E	σ (lbs/ins^2)
51	.194	398
52	.156	320
53	.131	269
54	.1205	247
55	.1056	217
70	.156	696
71	.156	696
72	.139	618
73	.139	618
74	.137	611
75	.126	565
76	.121	543
77	.106	474
78	.0898	401

Table 4 - Statistical data relating to Figs. 62 - 65

		"Best" least squares		Graham-Walles	
		Slope	Standard Deviation	Slope	Standard Deviation
Tensile Data	Primary (Fig. 64)	-.22	0.46	-.25	0.44
	Secondary (Fig. 65)	-.54	0.26	-.5	0.28
Buckling Data	Primary (Fig. 62)	-.31	0.57	-.25	0.73
	Secondary (Fig. 63)	-.38	0.29	-.5	0.29

FIGURES:-

Relating to theoretical analysis - Figs. 1-23

Relating to experiments and apparatus - Figs. 24-82.

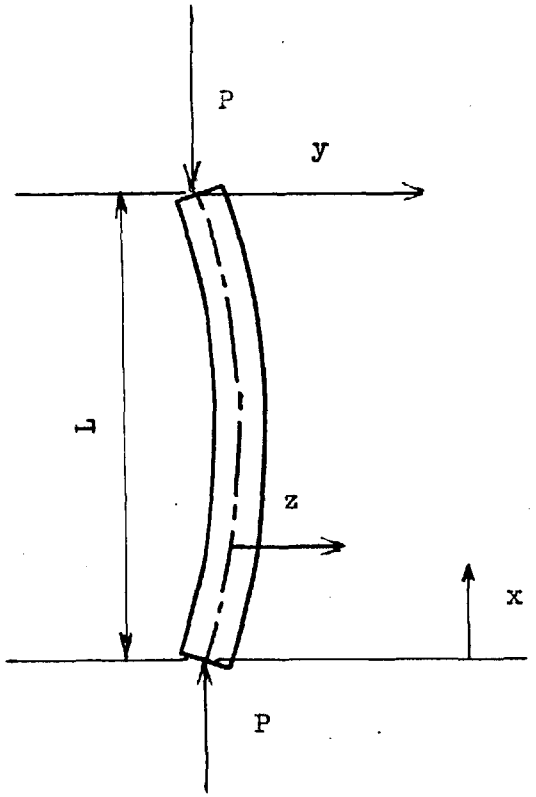


Fig. 1 Generalised column buckling.

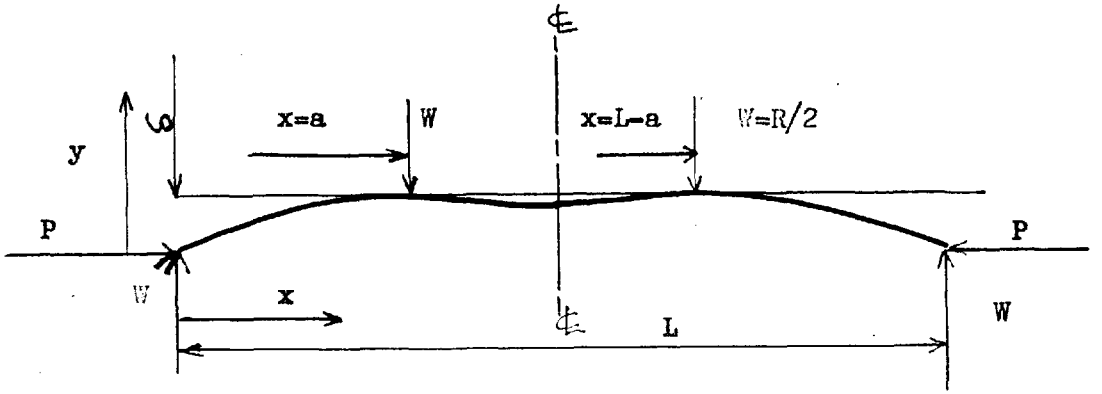


Fig.2 Symmetric Restrained Bowing.

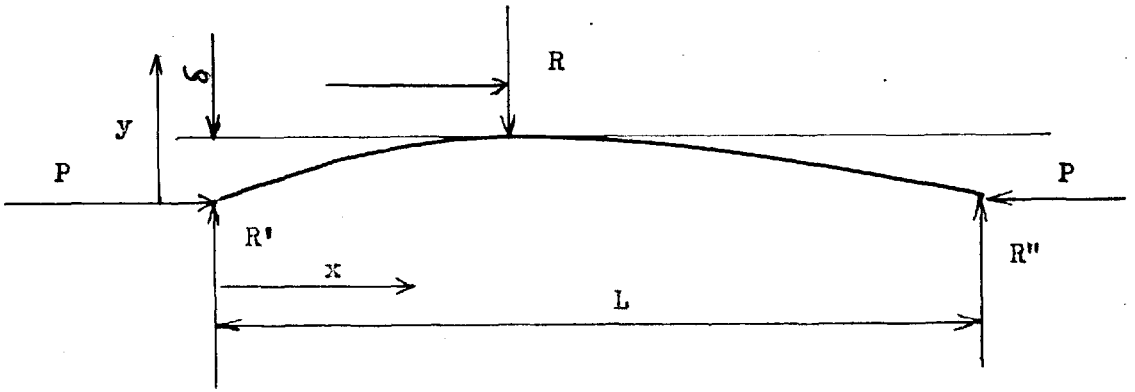


Fig. 3 Asymmetrical restrained bowing-first phase.

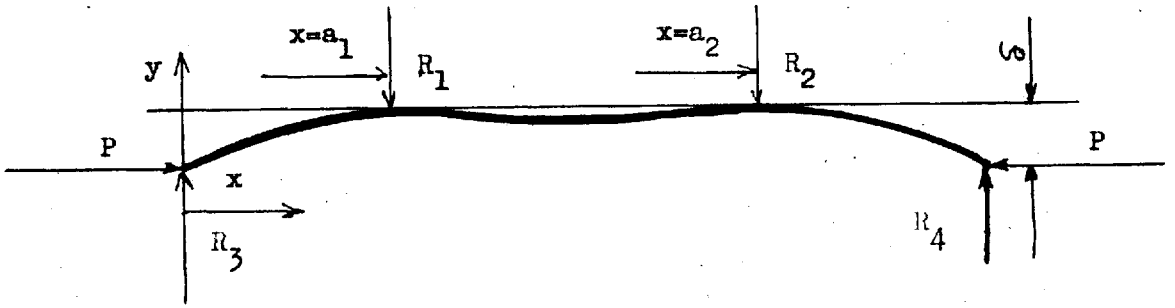


Fig. 4 Asymmetric bowing-second phase.

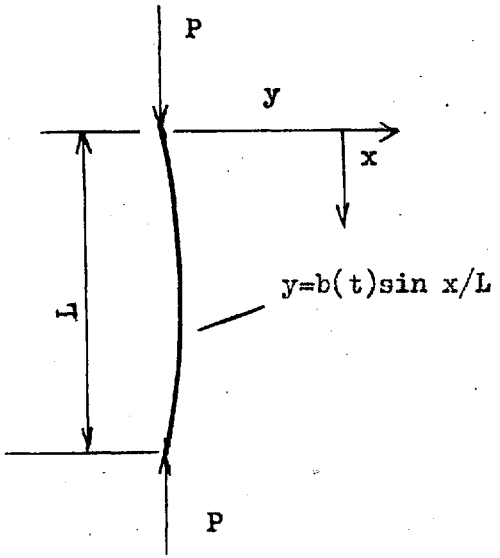


Fig. 5 Sinusoidal creep buckling.

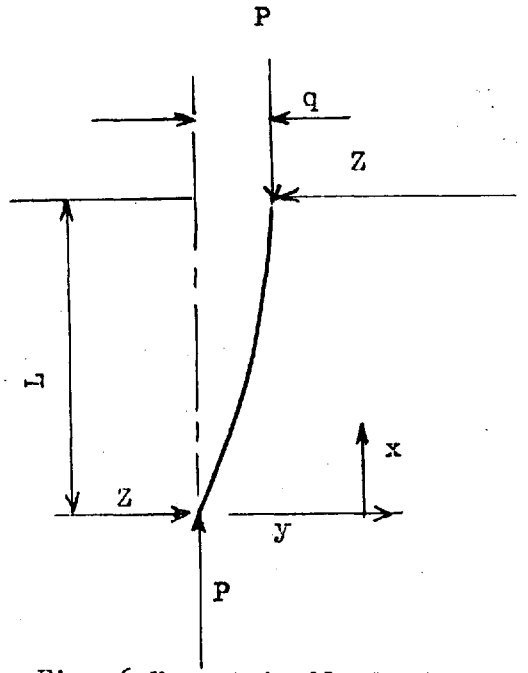


Fig. 6 Eccentrically loaded column.

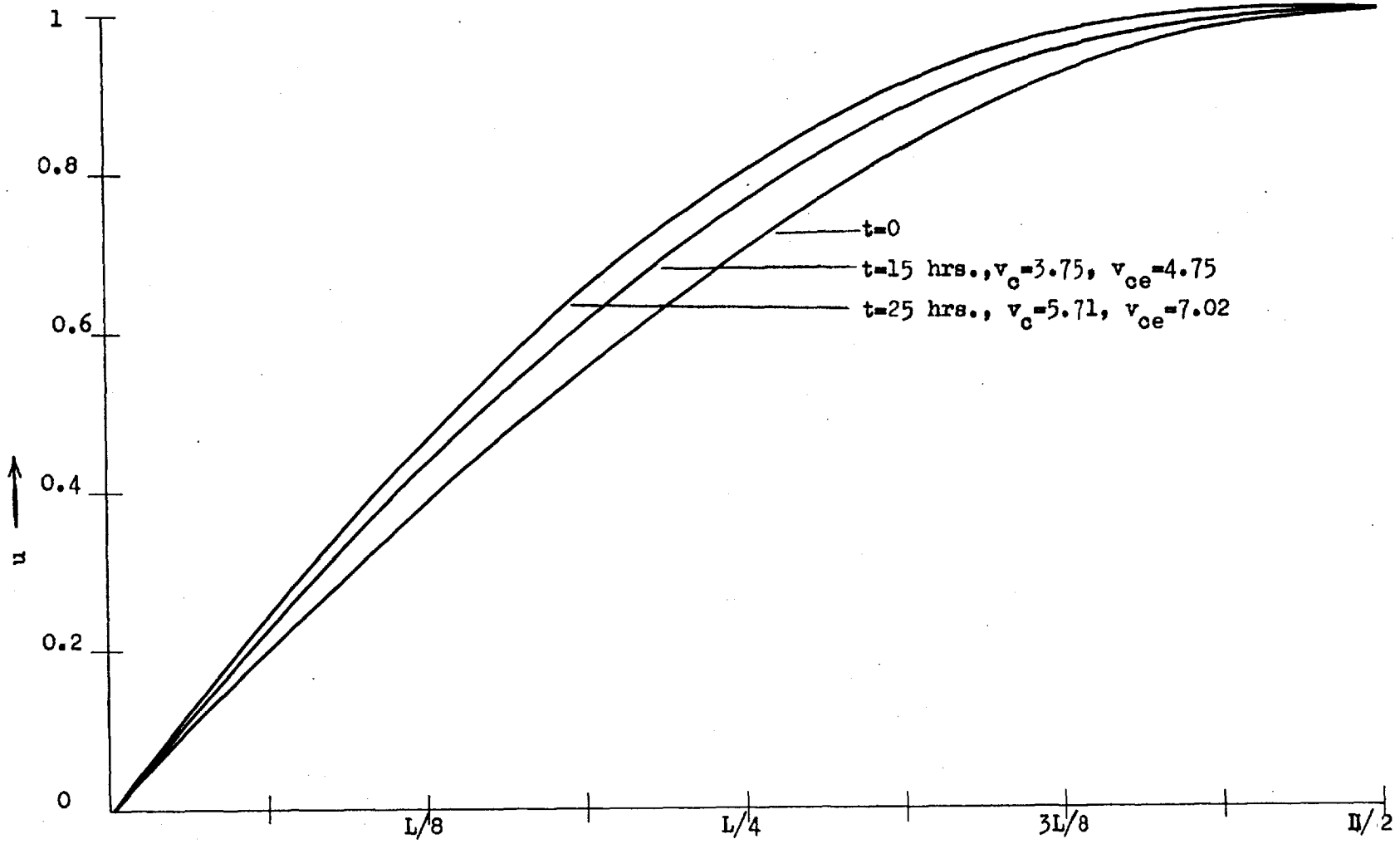


Fig. 7 Calculated deflections during the first phase of buckling of an initial sine wave for P/P_E =0.2, d=0.5 ins., L=18 ins.

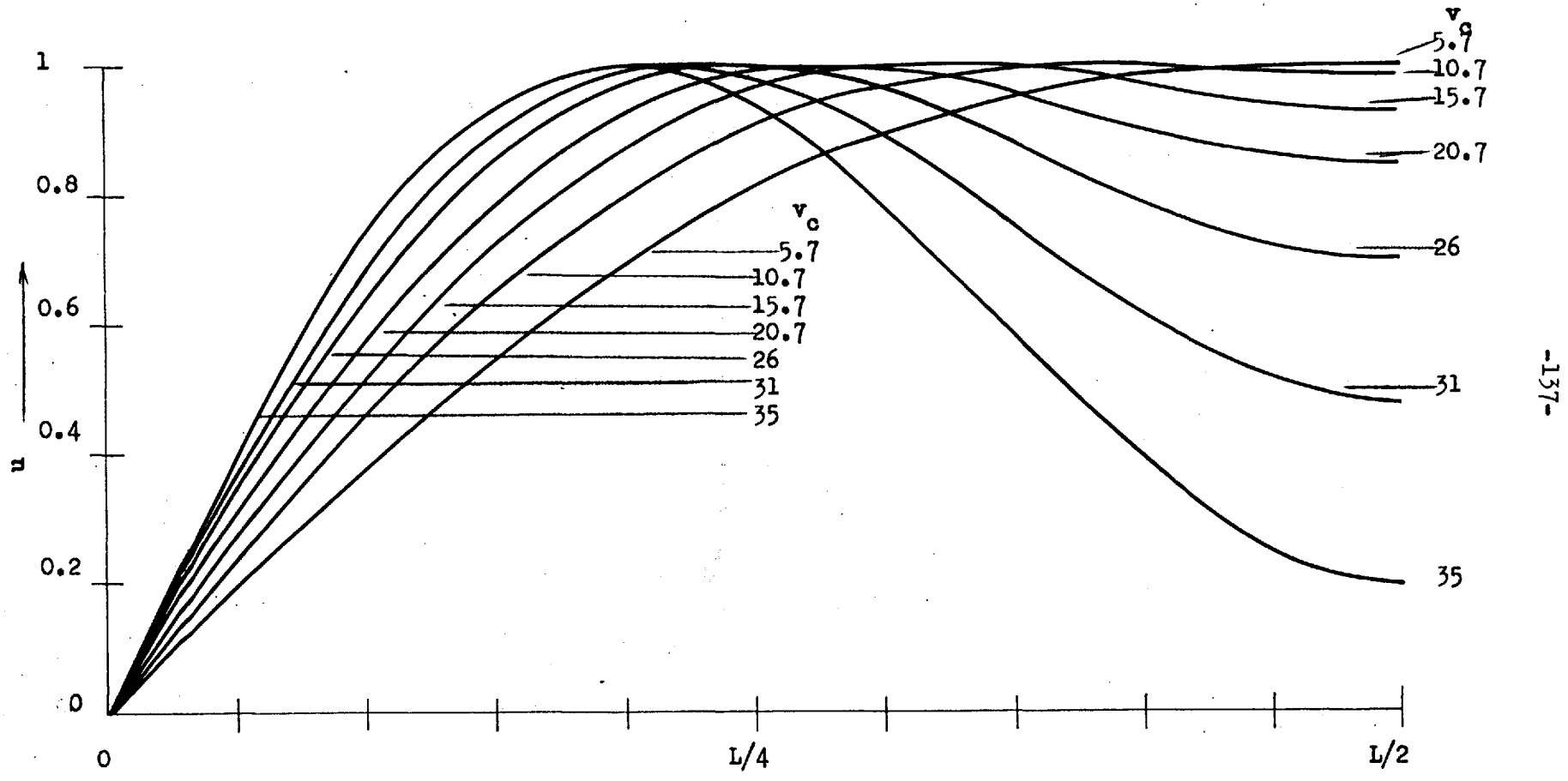


Fig. 8 Calculated deflection time curves for initially sinusoidal column - second phase of deformation.

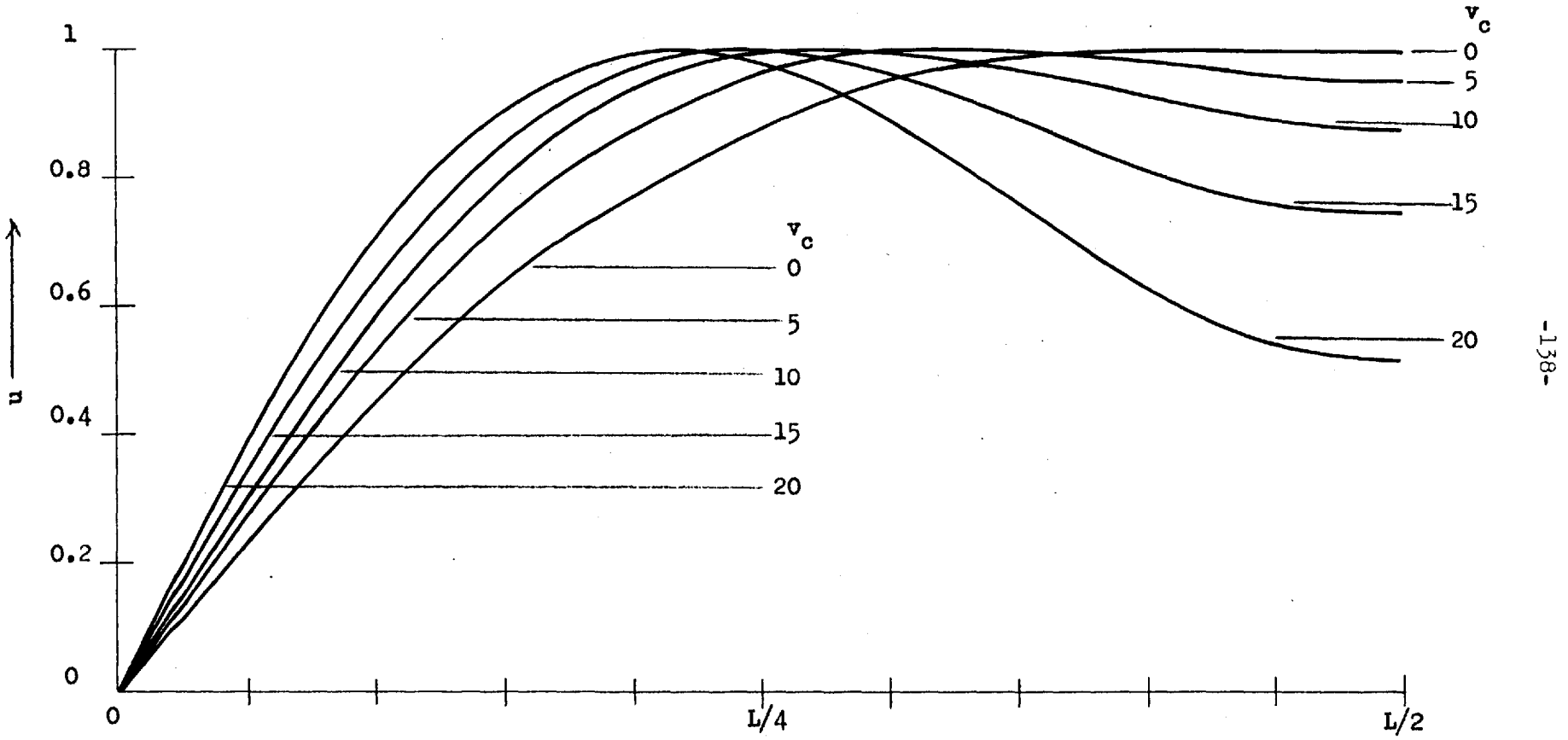


Fig. 9 Calculated deflection time curves for a sine wave with third harmonic 1/9 th the fundamental.

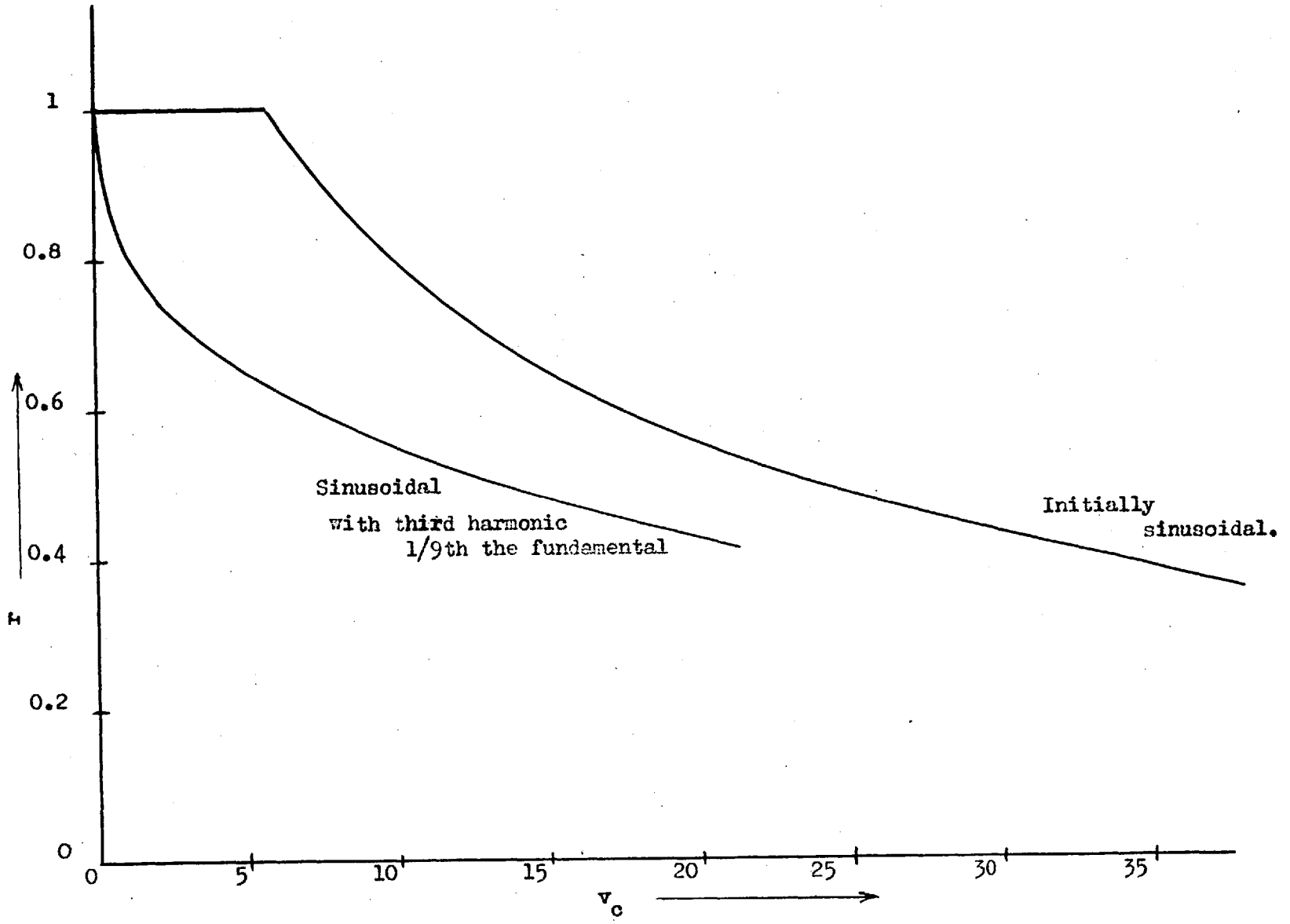


Fig. 10 Displacement of the point ofcontact versus v_c.

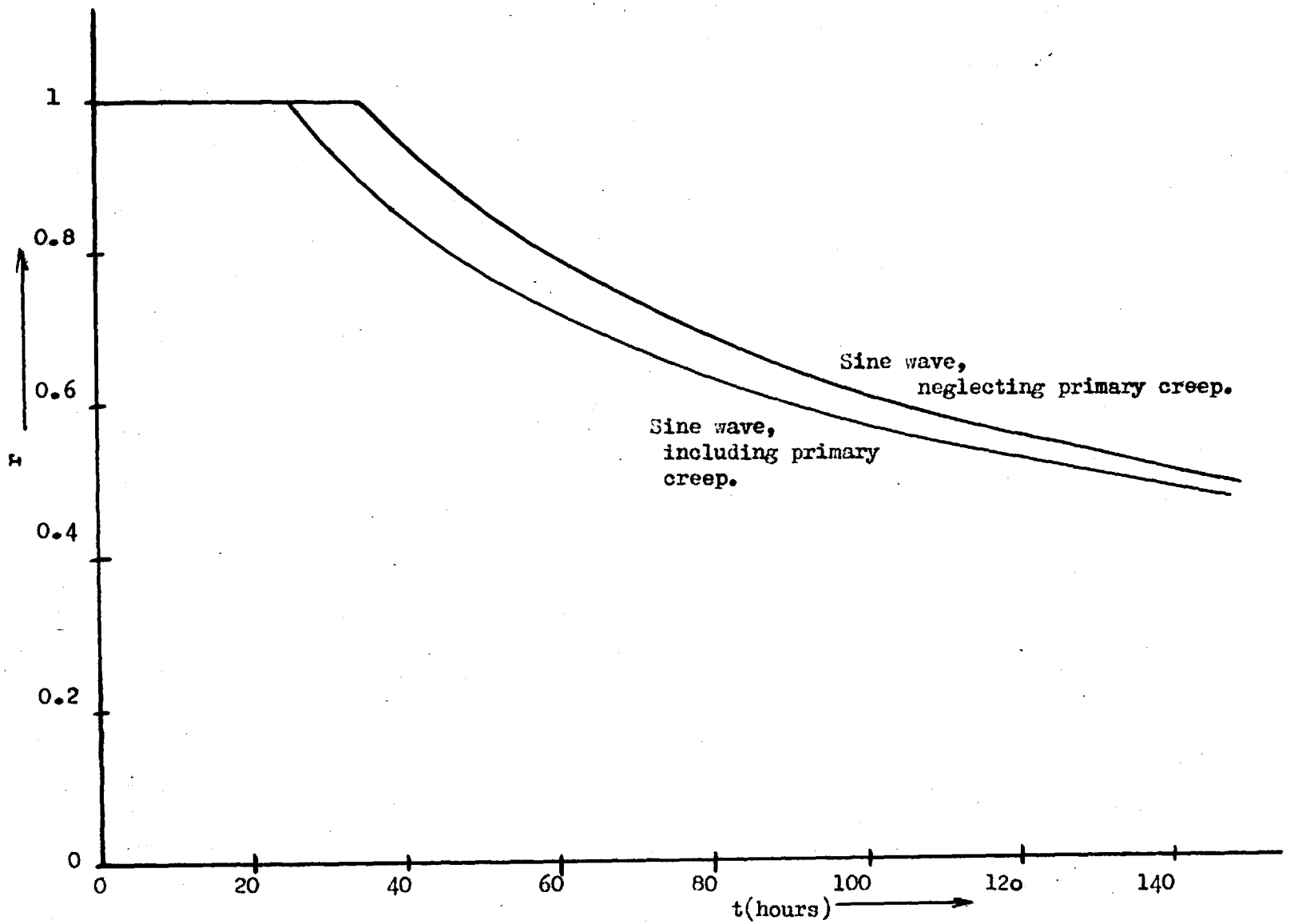


Fig. 11 Calculated displacement of the point of contact versus real time.

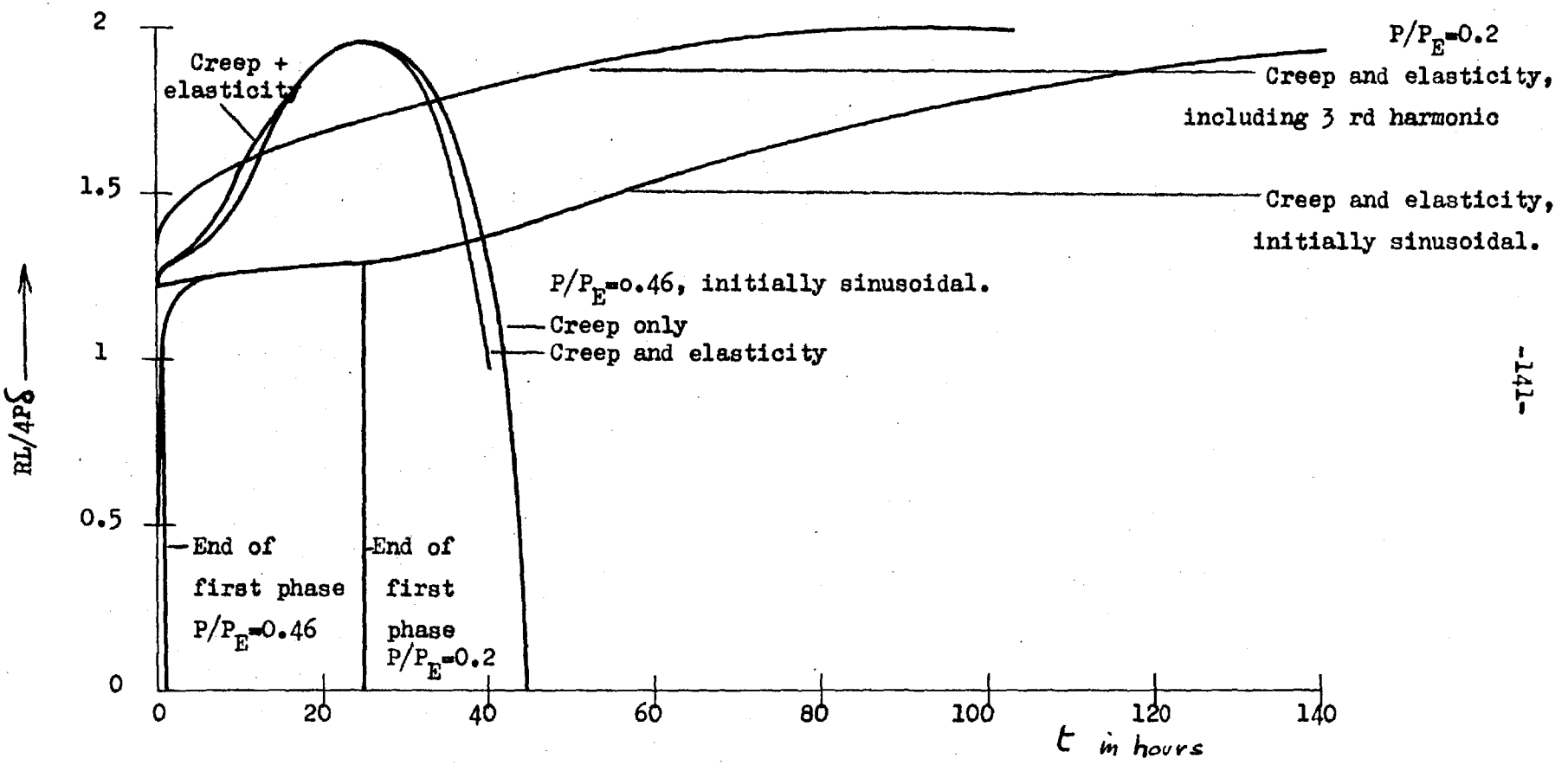


Fig. 12 Calculated force time relations for symmetric shapes: first and second phase of deformation.

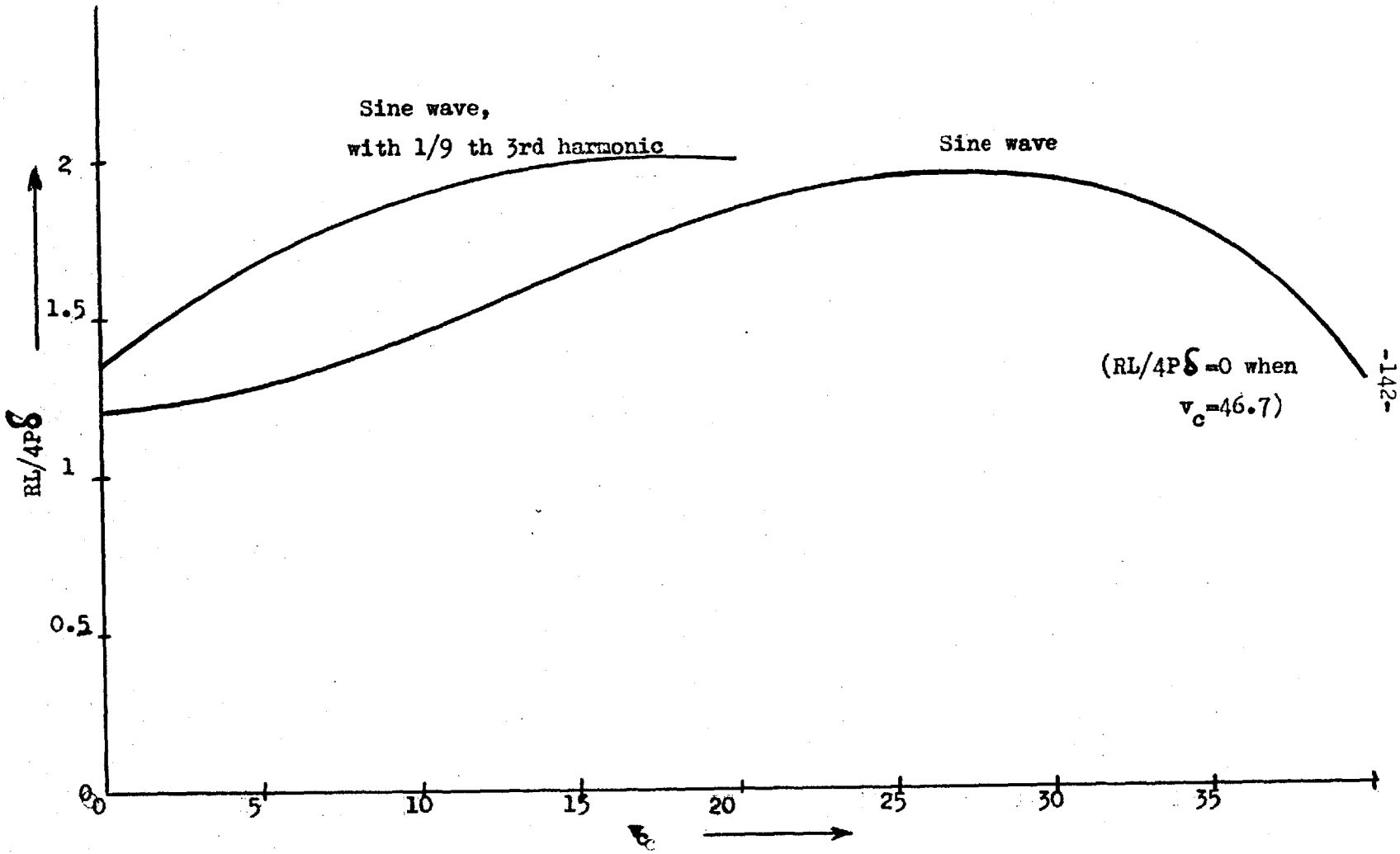


Fig. 13 Calculated force-v_c relations .

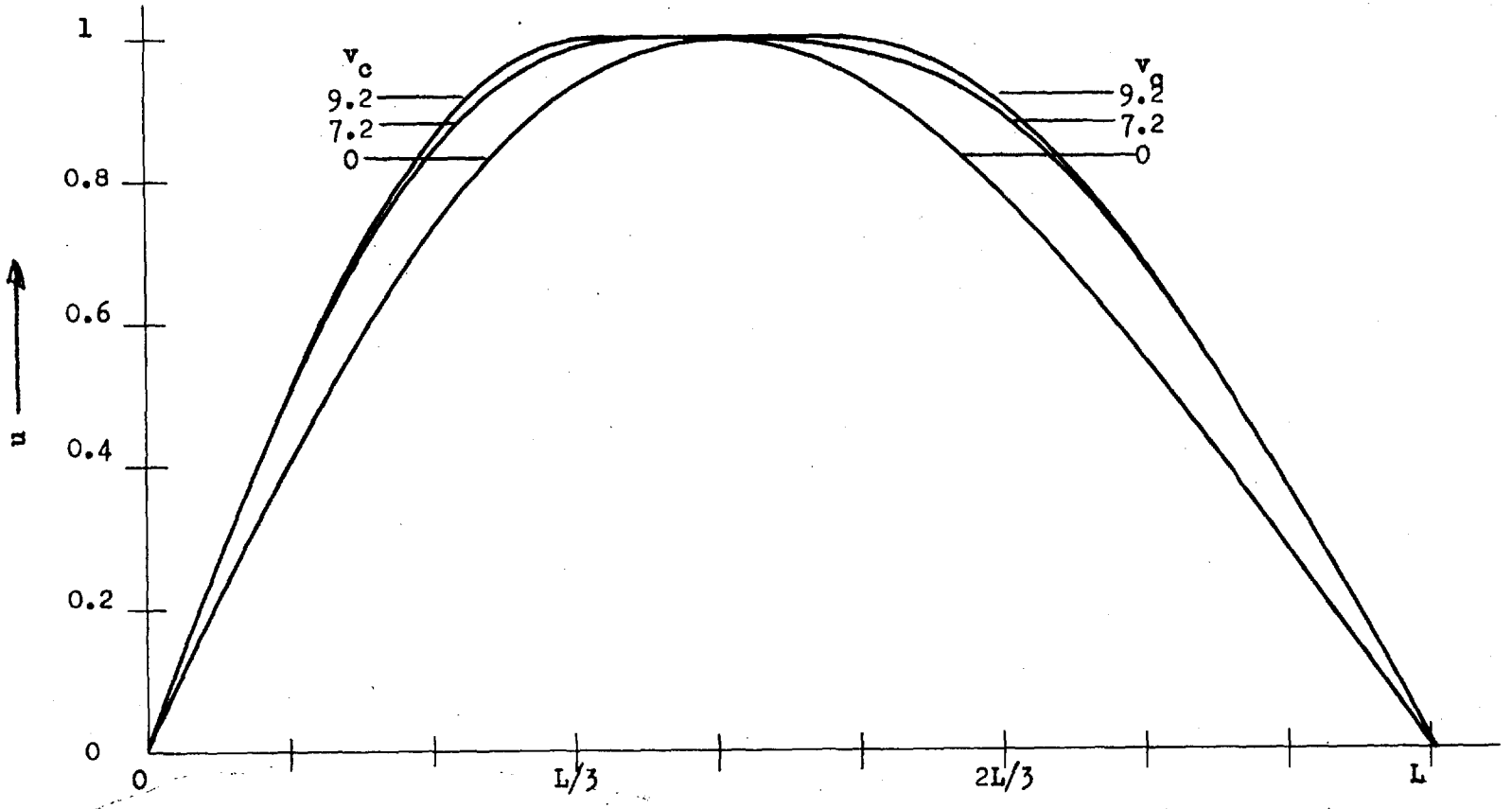


Fig. 14 Deflection - time curves for a sine wave with 2 nd harmonic in the ratio 34/3 .

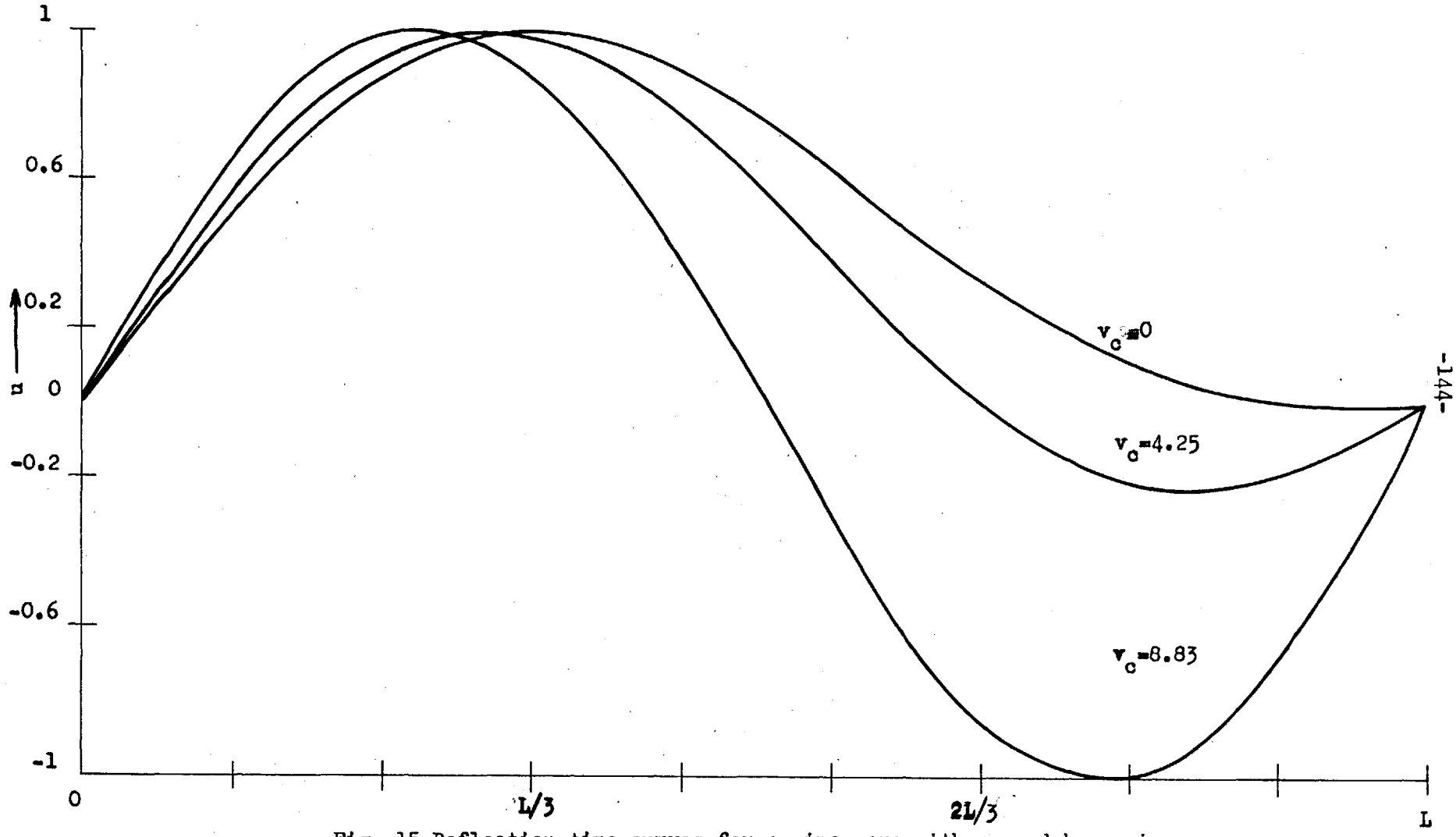


Fig. 15 Deflection-time curves for a sine wave with second harmonic in the ratio 2/ 1 .

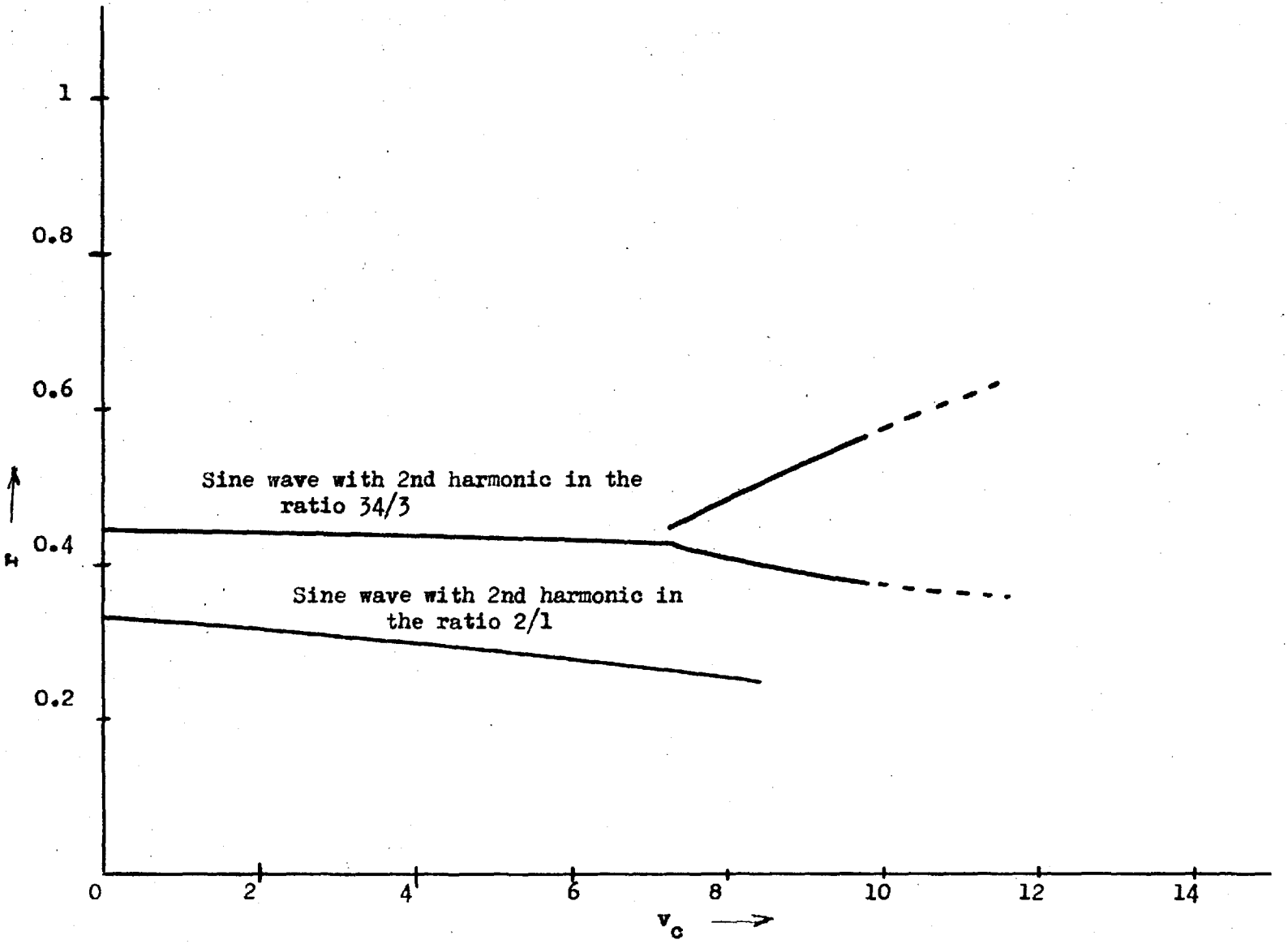


Fig. 16 Calculated displacement of the point of contact for two asymmetric cases.

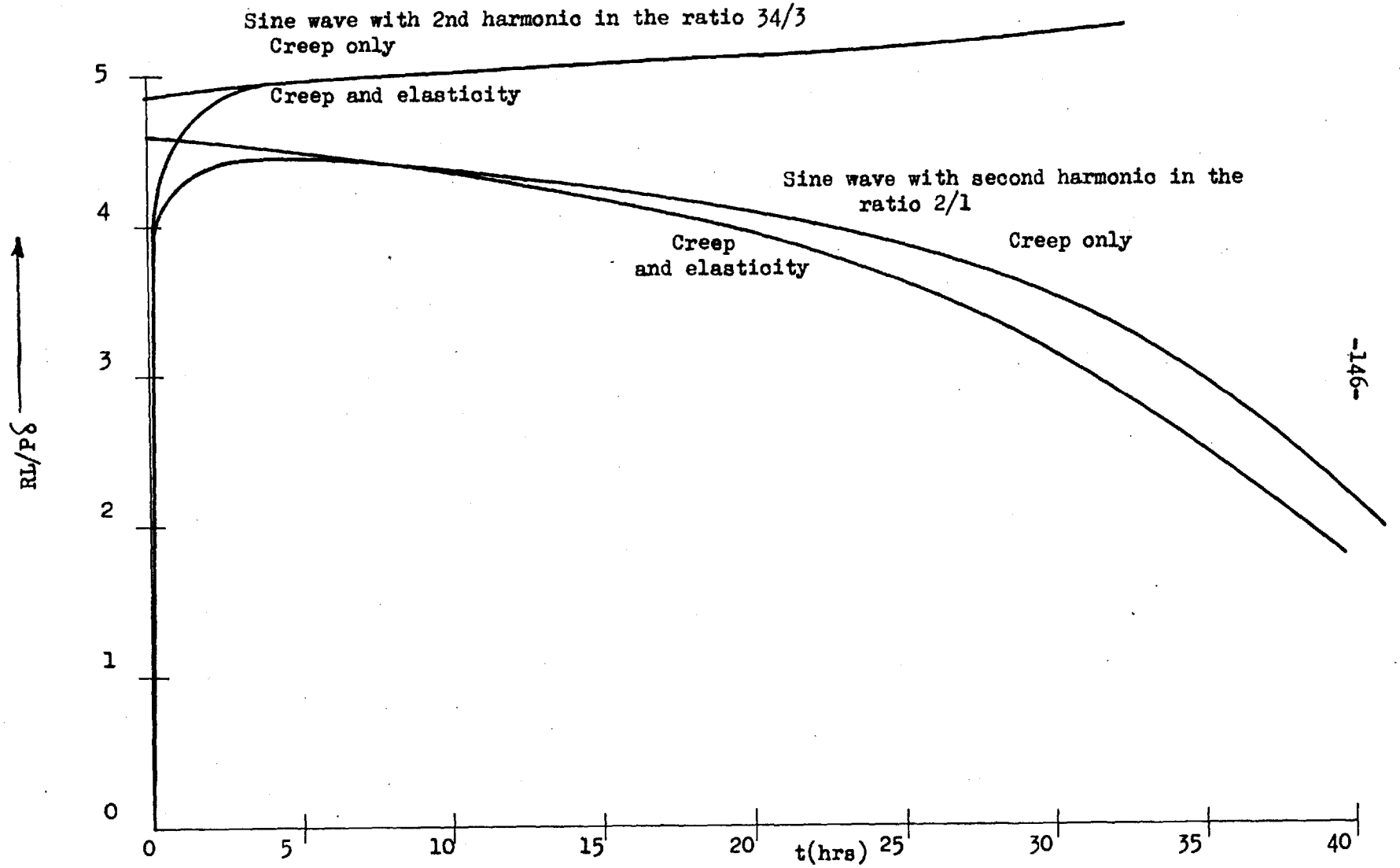


Fig. 17 Calculated force-real time curves for two asymmetric cases: P/P_E =0.2, d=0.5 ins.

Fig. 18 v_{ce} relations for $\frac{1}{2}$ ins. specimens

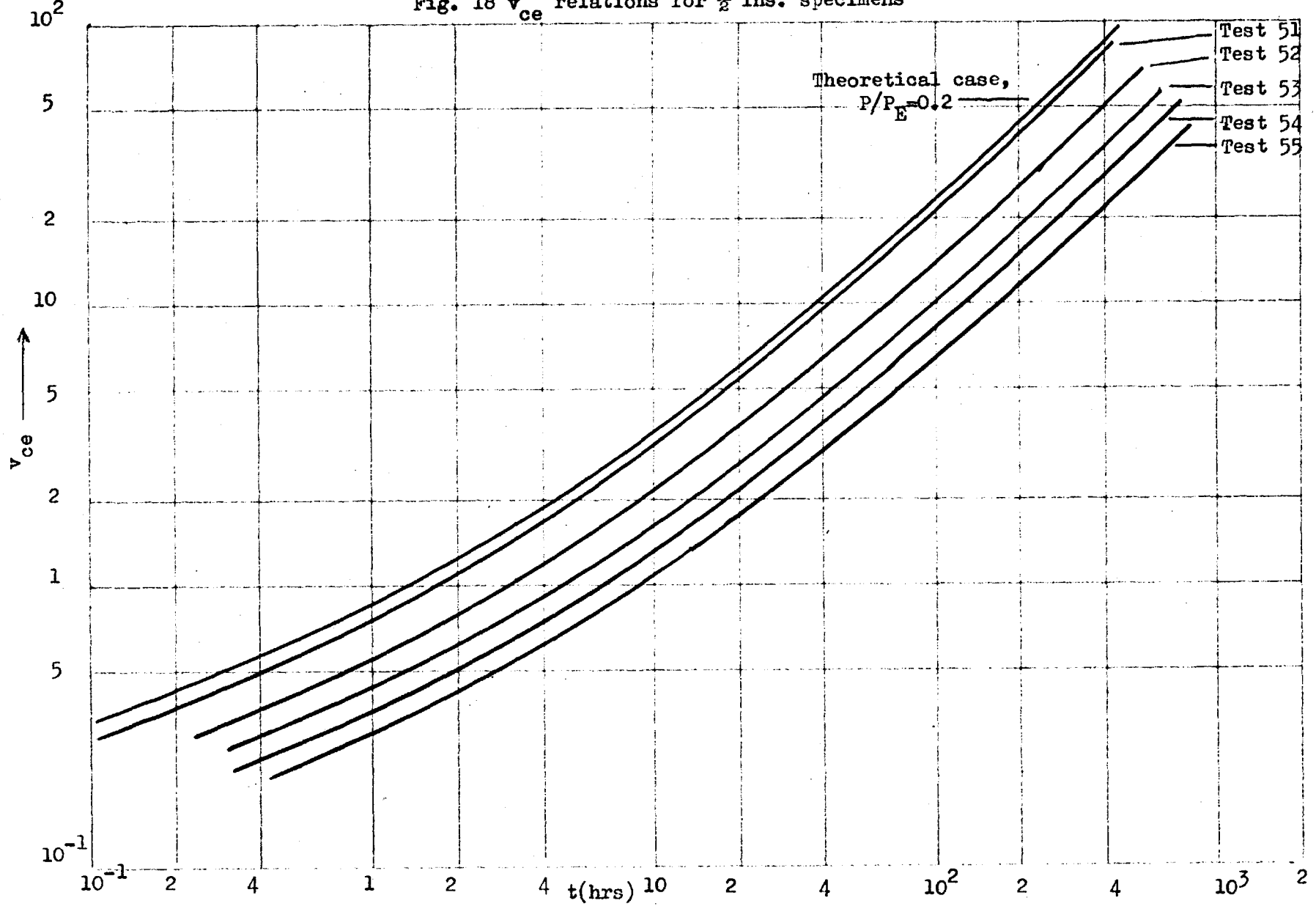


Fig. 19 v_c-t relations for $\frac{1}{2}$ ins specimens.

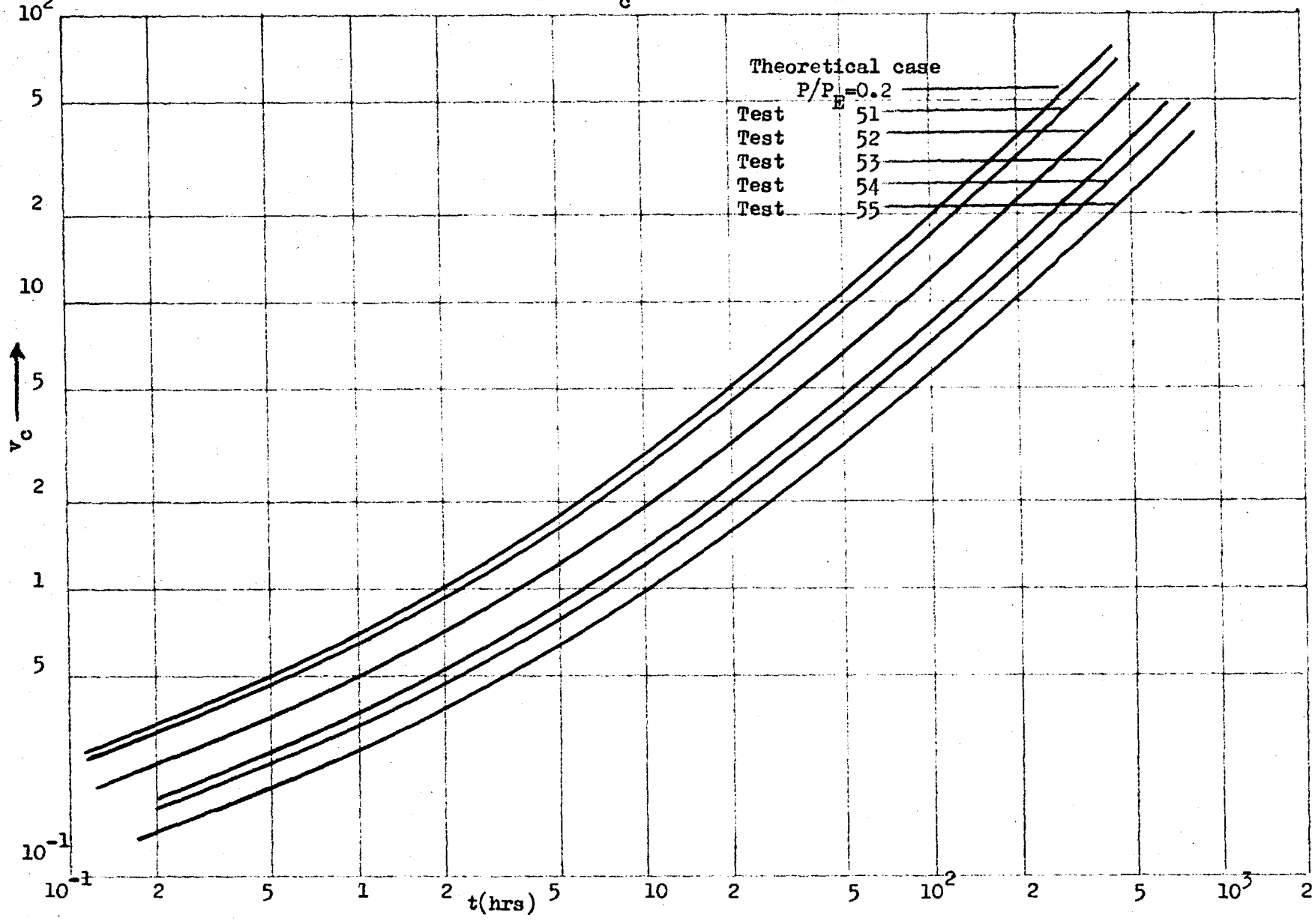


Fig. 20 v_{ce}-t relations for $\frac{3}{4}$ ins. specimens.

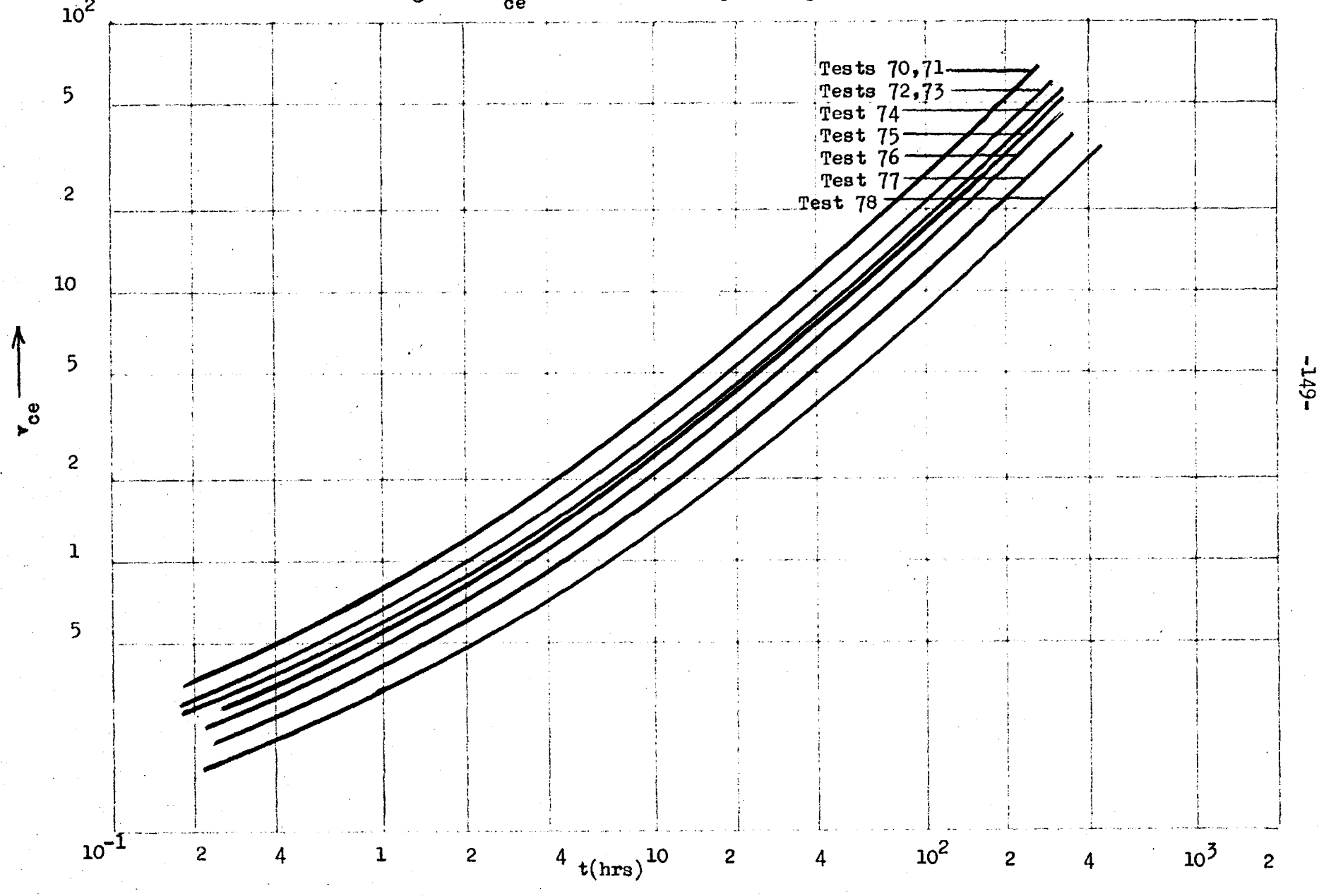
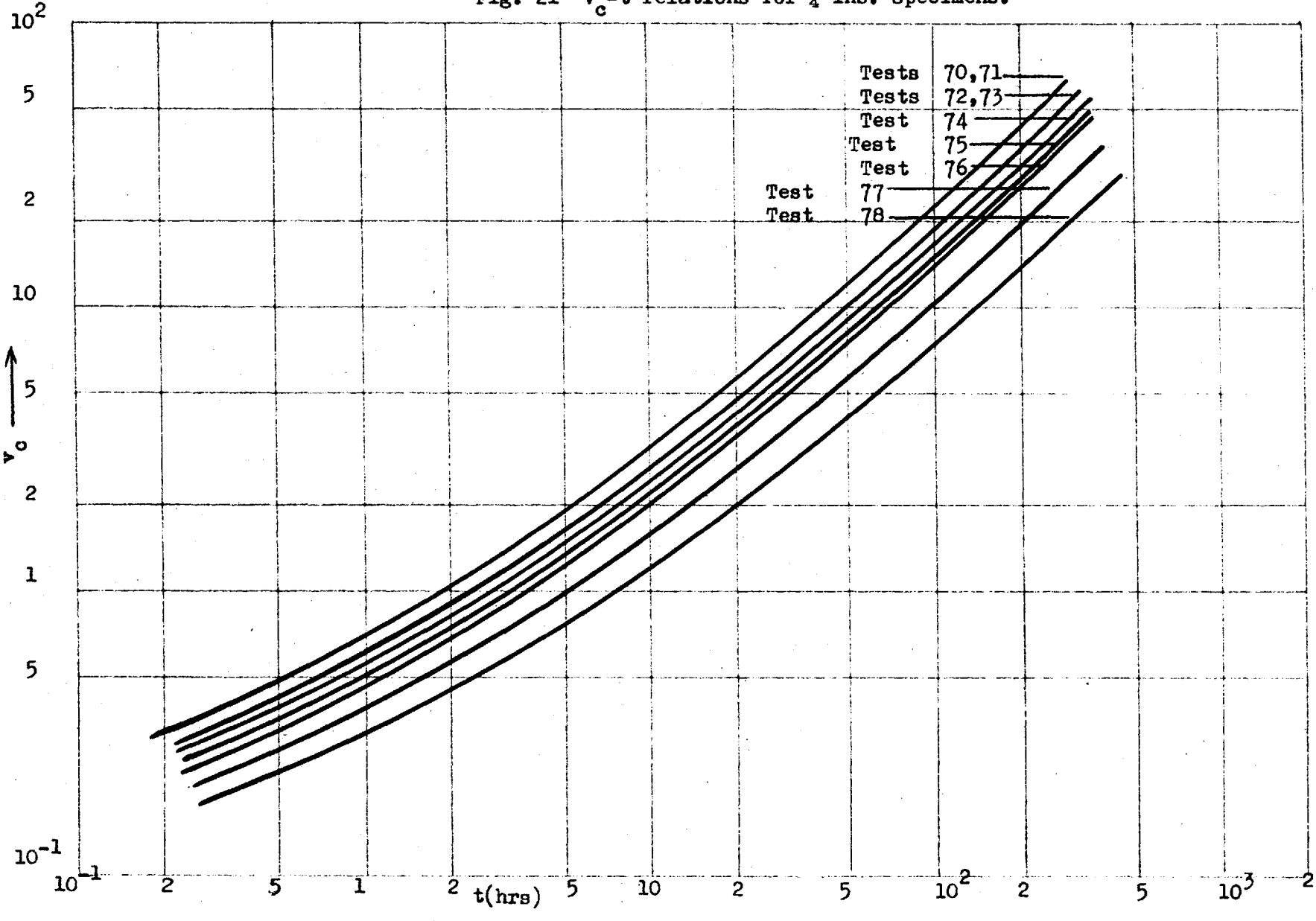


Fig. 21 v_c-t relations for $\frac{3}{4}$ ins. specimens.



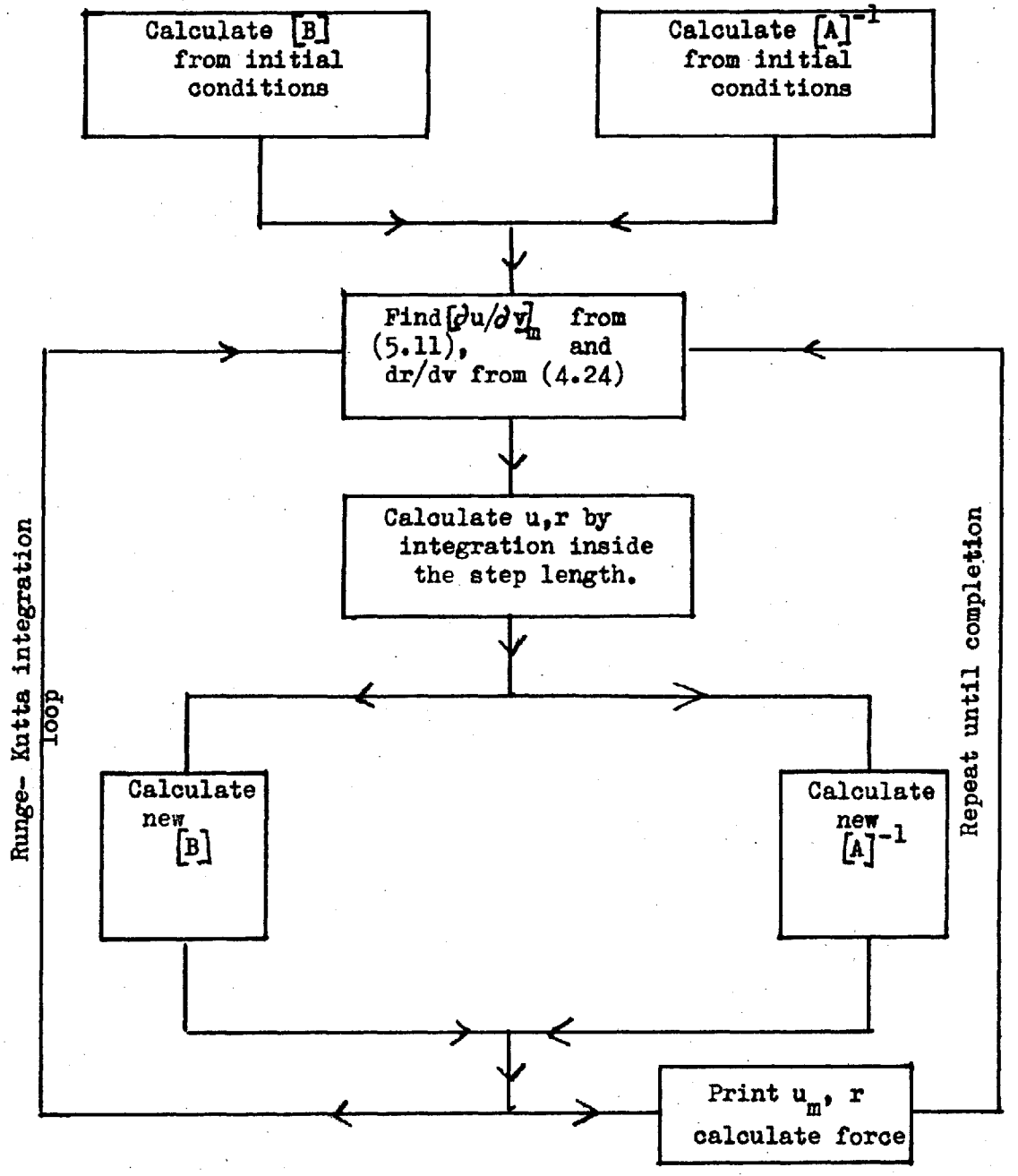


Fig. 22 Simplified flow chart for the numerical solution of section 5.1.1.3

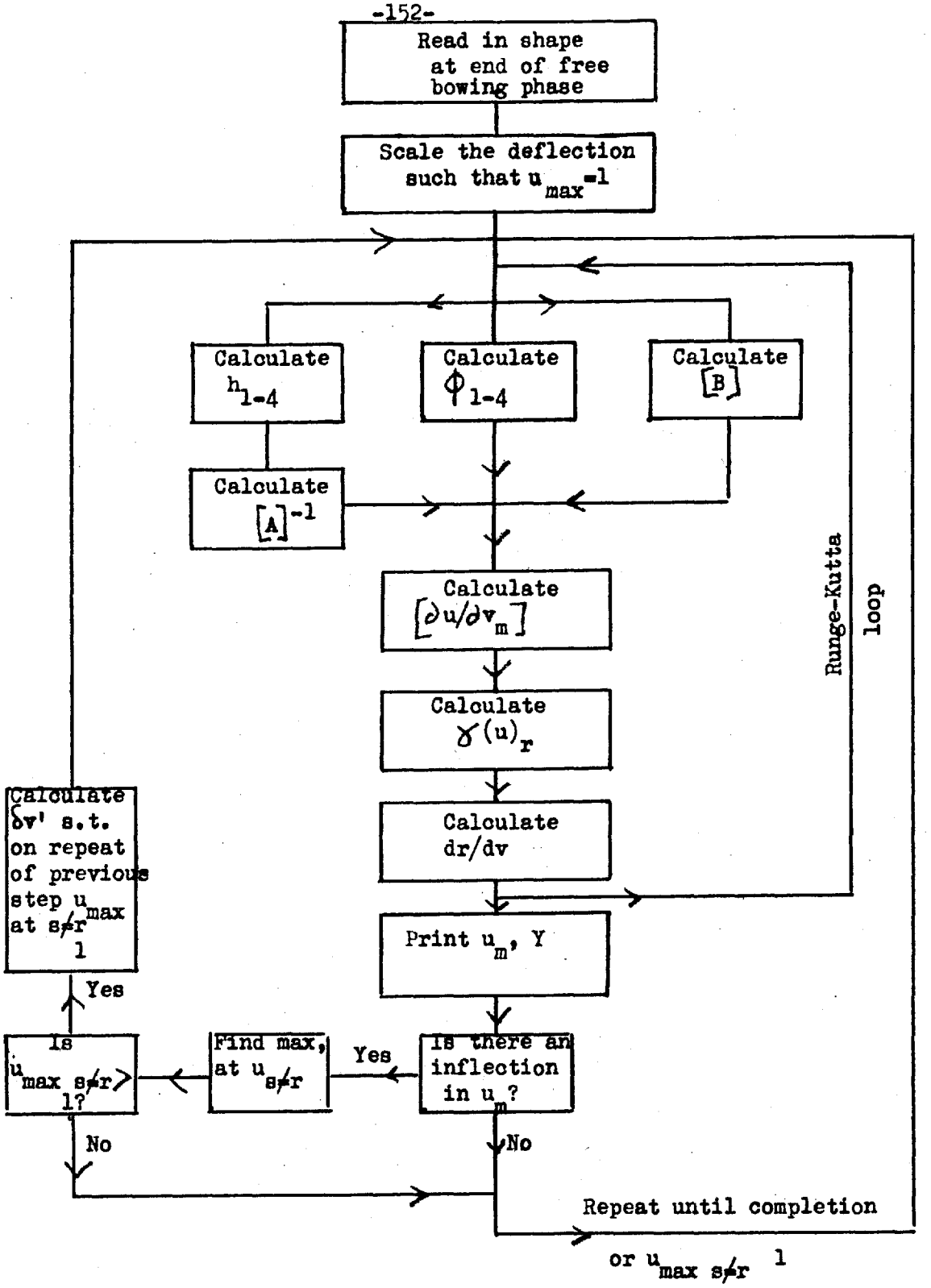


Fig. 23 Simplified flow chart for the asymmetrical calculation, section 5.1.3.1 .

Symbols used in presentation of experimental data on restrained bowing.

o	Measured experimental point
△ ▽	v_c correlations
□	v_{oe} correlations
———	Shape predicted from computations
t_{2p}	Time to achieve two point contact for asymmetrical shapes:(from theory)
—	Calculated clearance (see Fig. 82)
6 O	Polar coordinate at 6 ins. from upper loading point.
←——→	Circumferential limits of channel restraint.

Note: Details of test stresses appear in Table 3 (page 131) . All data is for Major bow, except where otherwise stated.

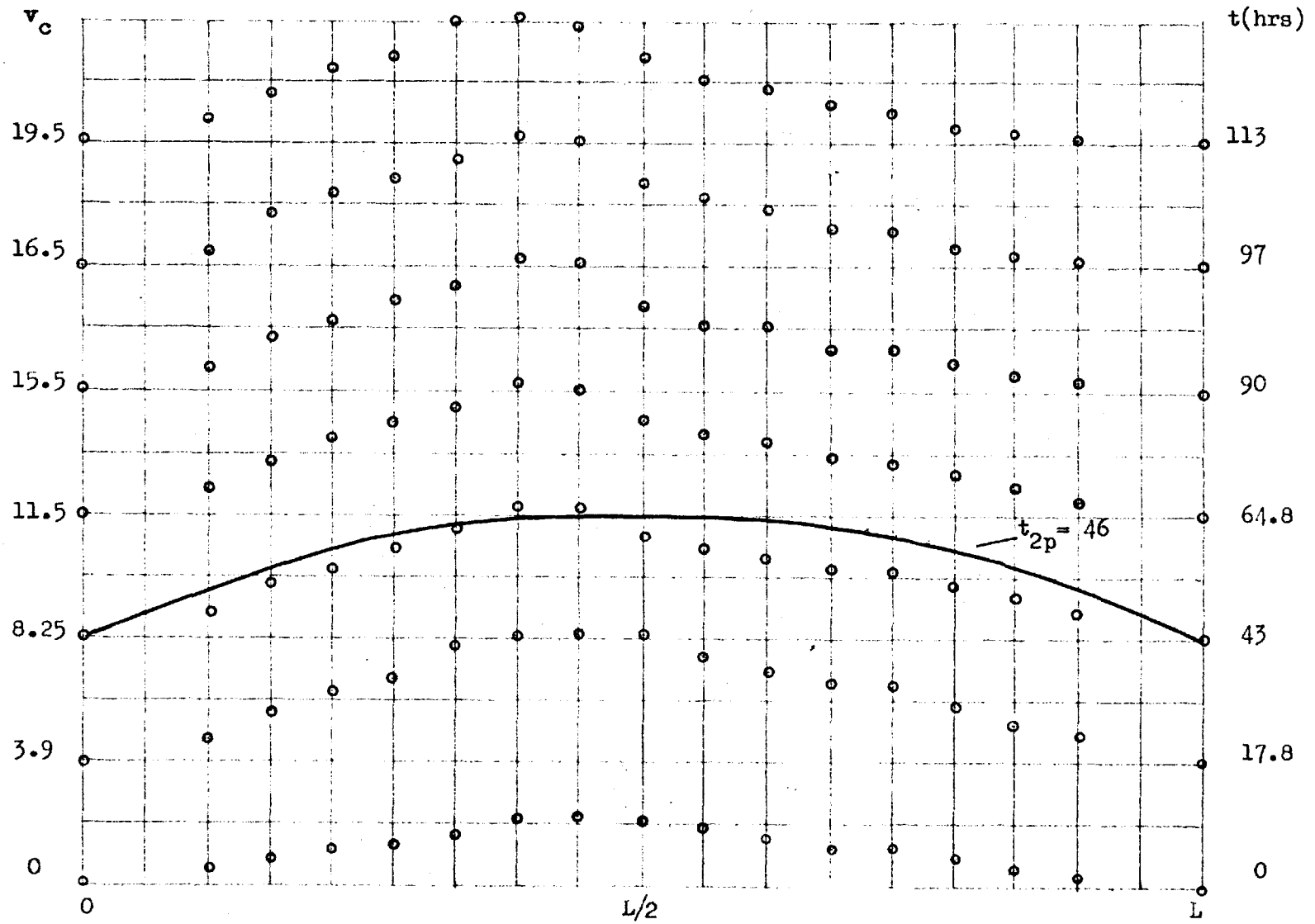


Fig. 24 Test 51

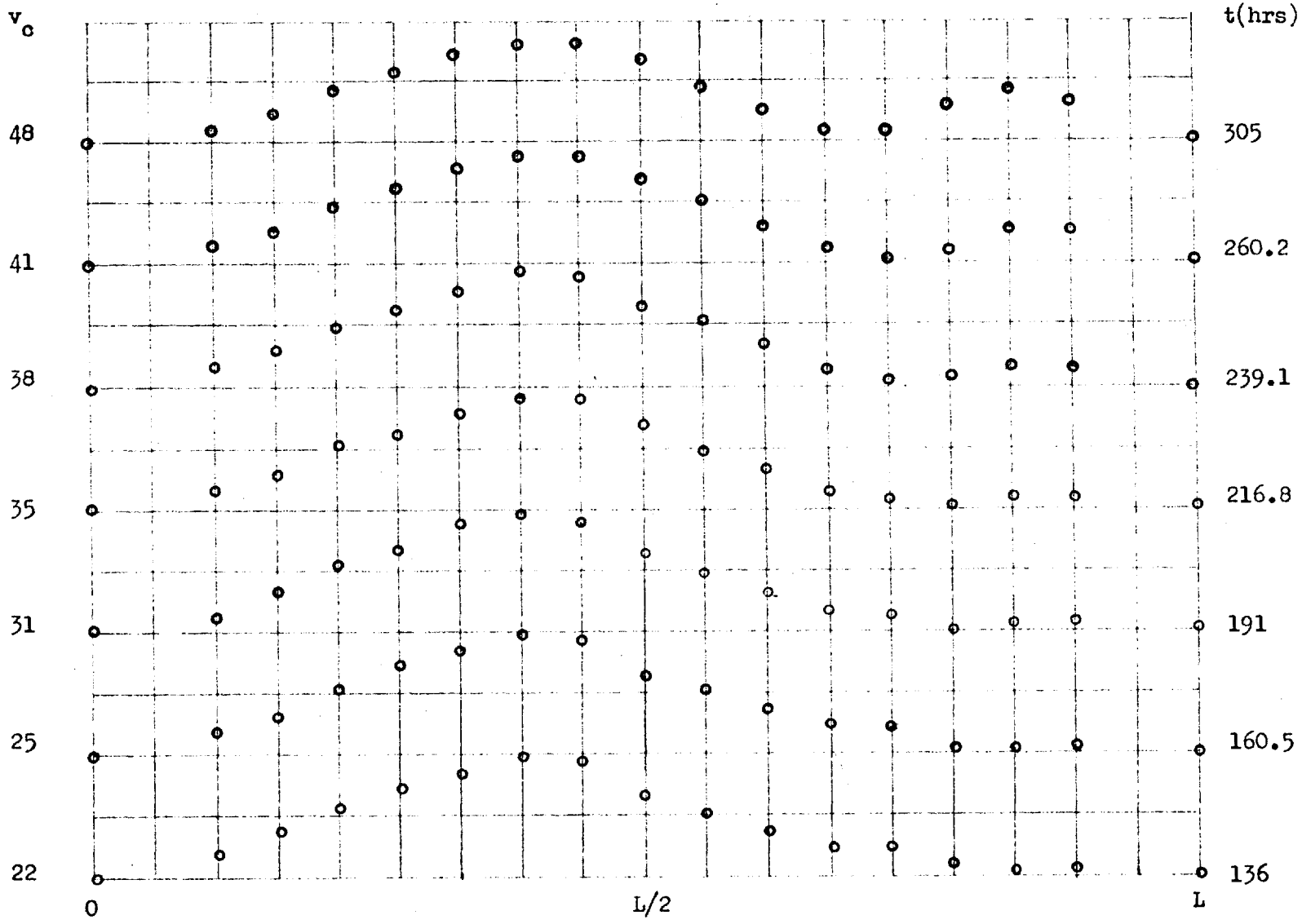


Fig. 25 Test 51 (contd.)

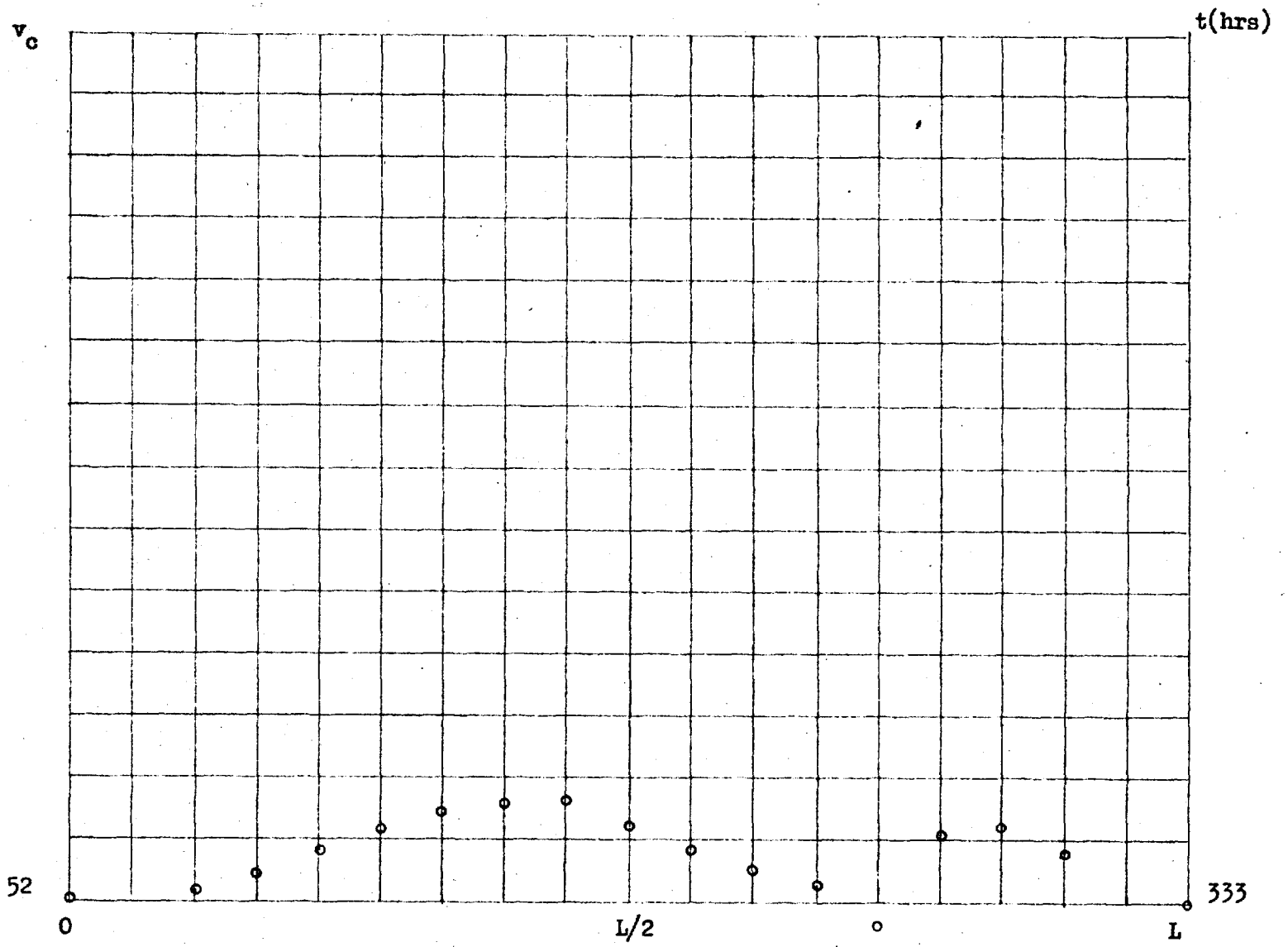


Fig. 26 Test 51 (concl.)

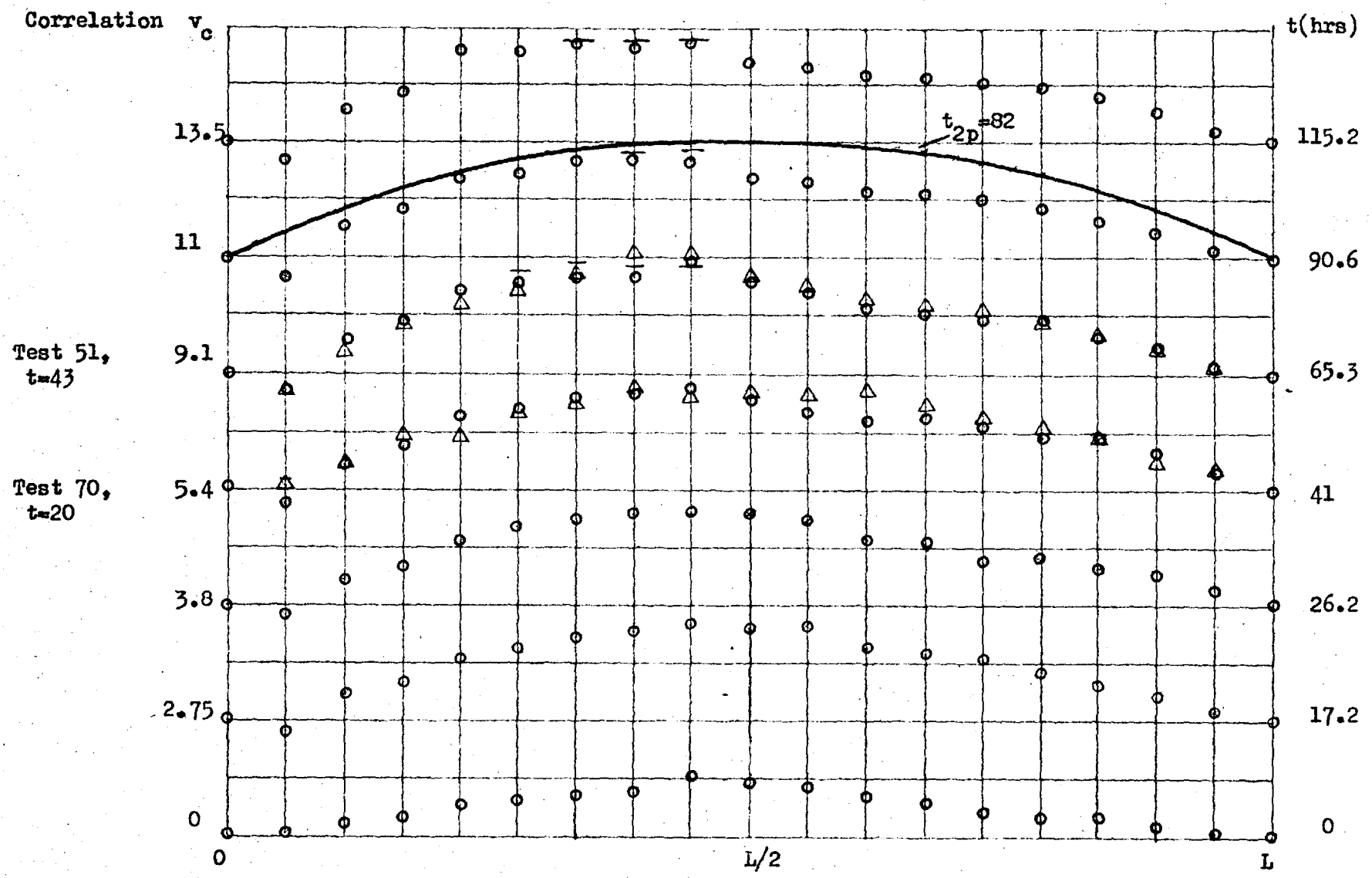


Fig. 27 Test 52

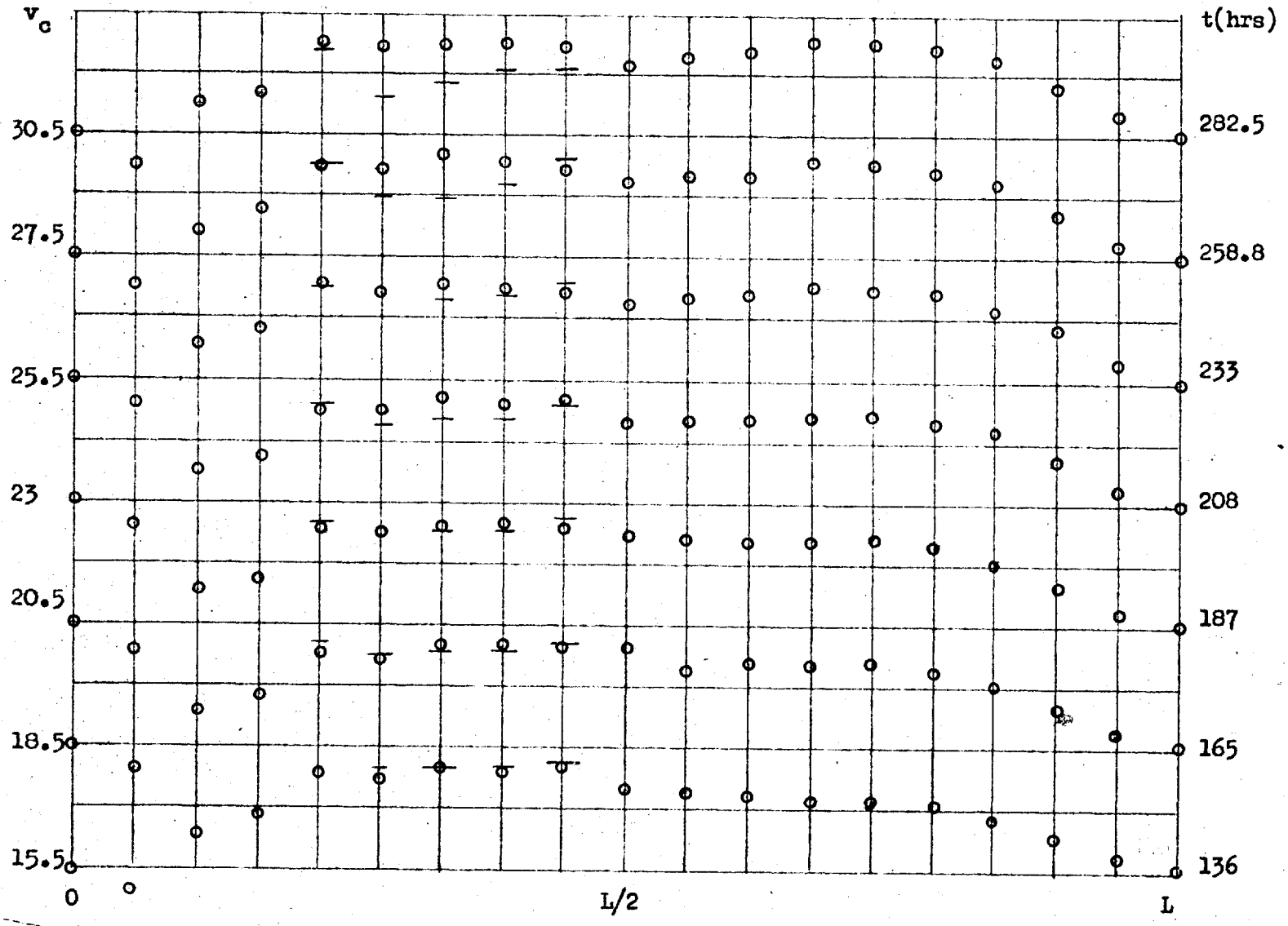


Fig. 28 Test 52 (contd.)

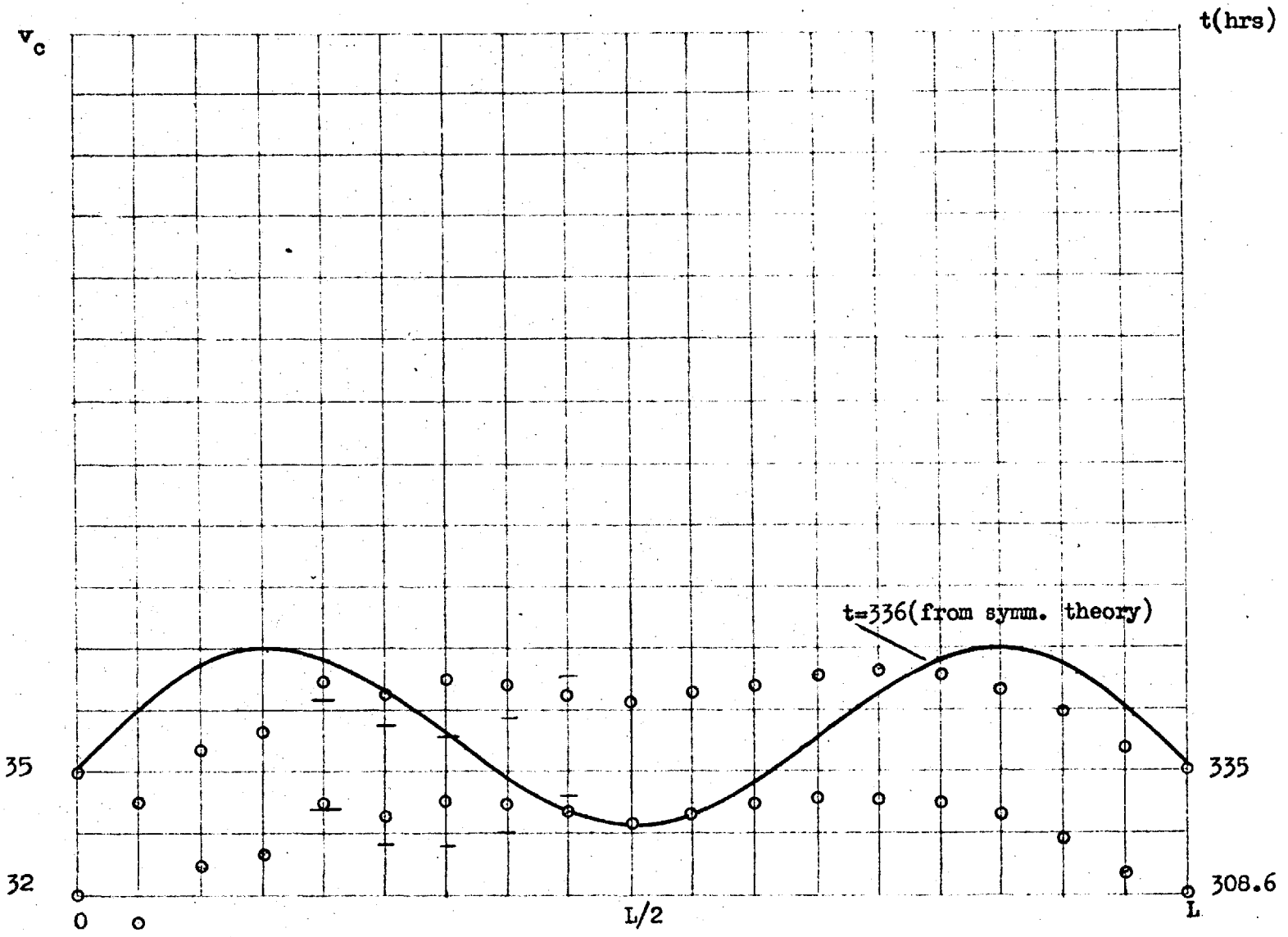


Fig. 29 Test 52 (concl.)

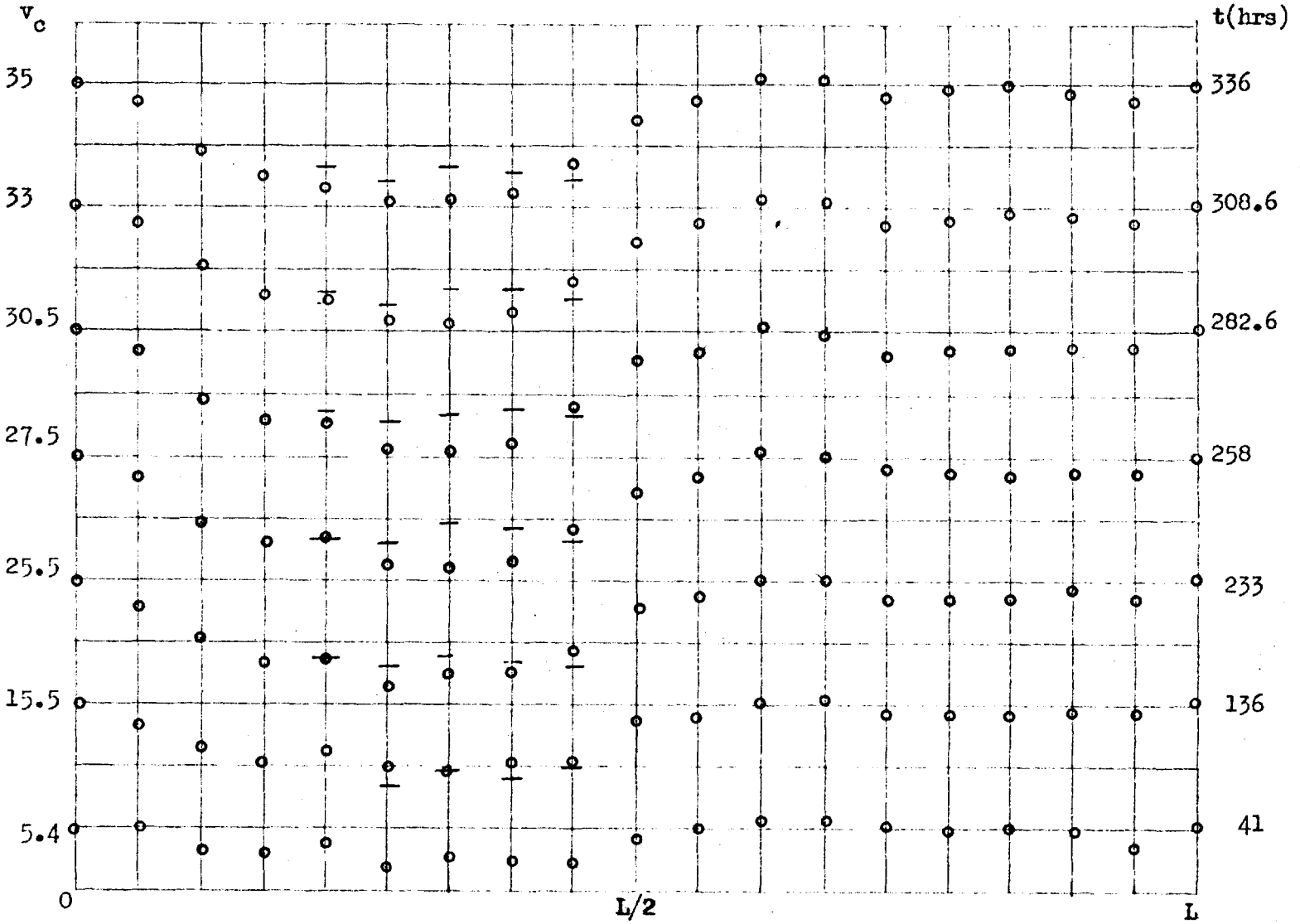
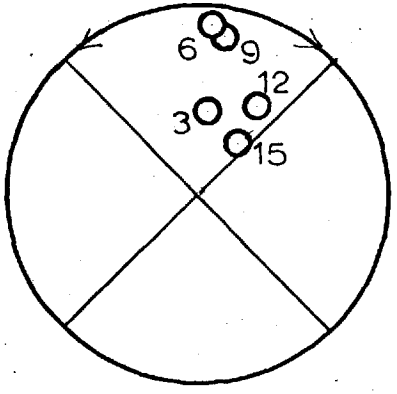
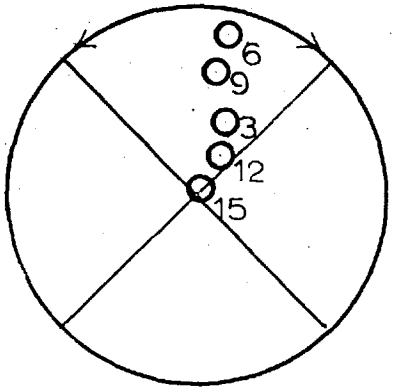


Fig. 30 Test 52 Minor bows.

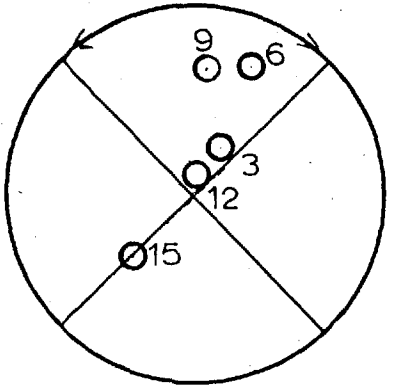


t=43

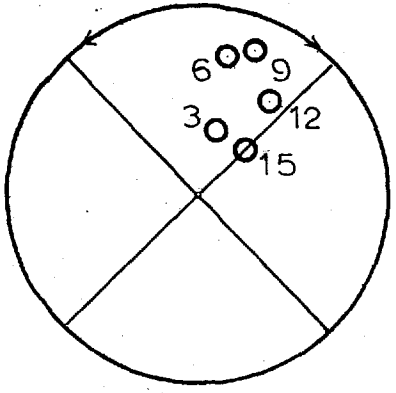


t=136

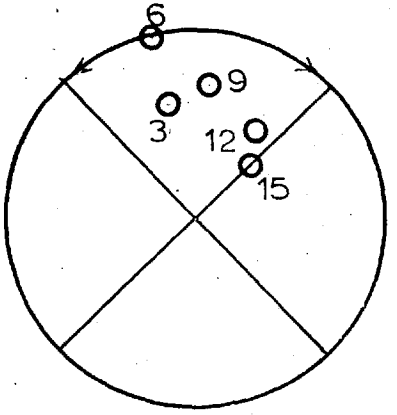
Test 51 .



t=305

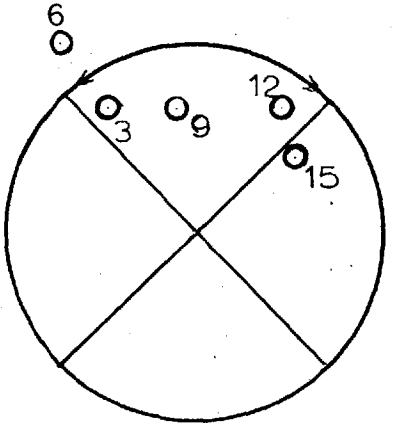


t=17.2



t=115.2

Test 52



t=336

Fig. 31 Polar plots of deflection for Tests 51, 52.

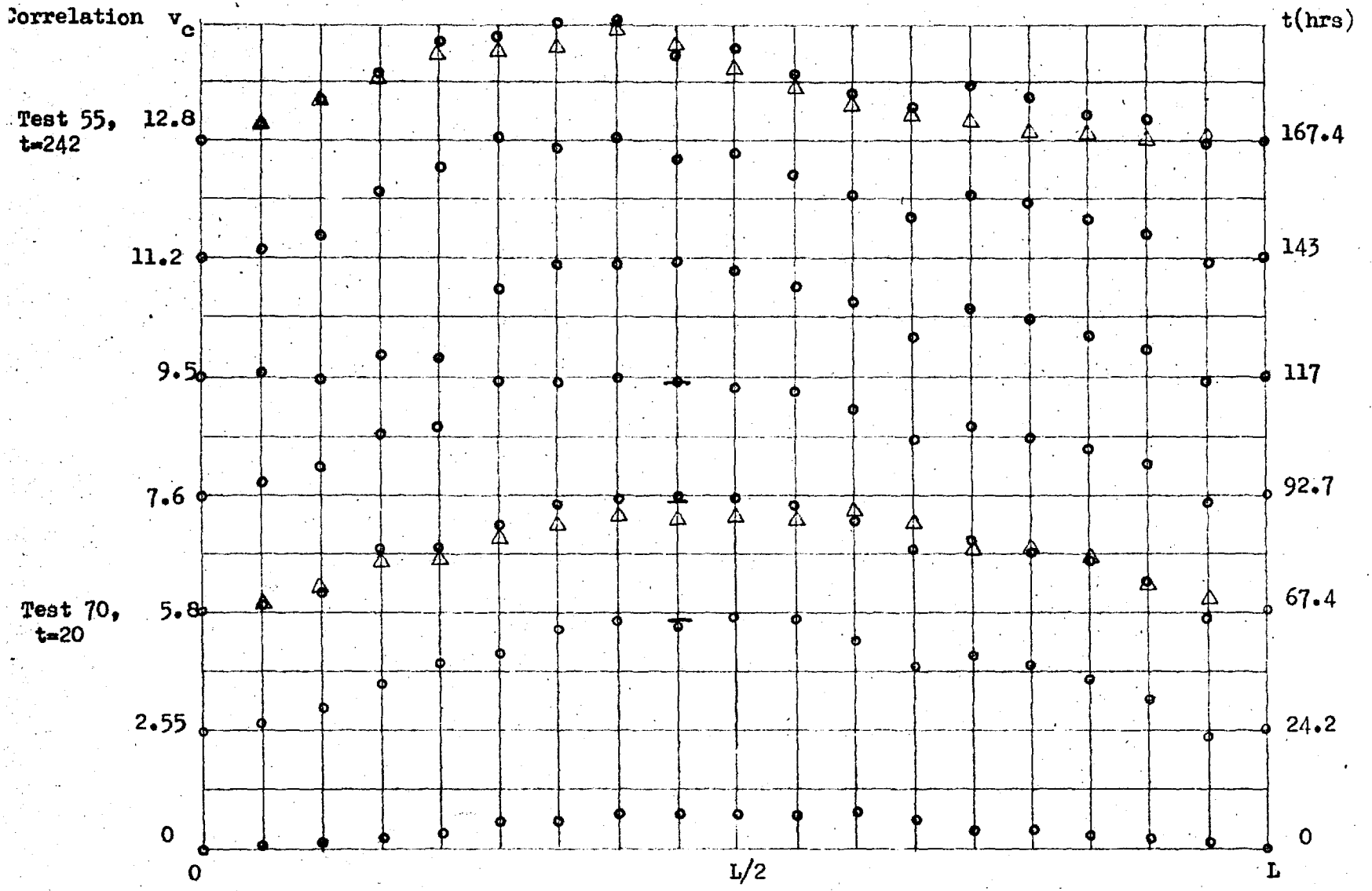


Fig. 32 Test 53

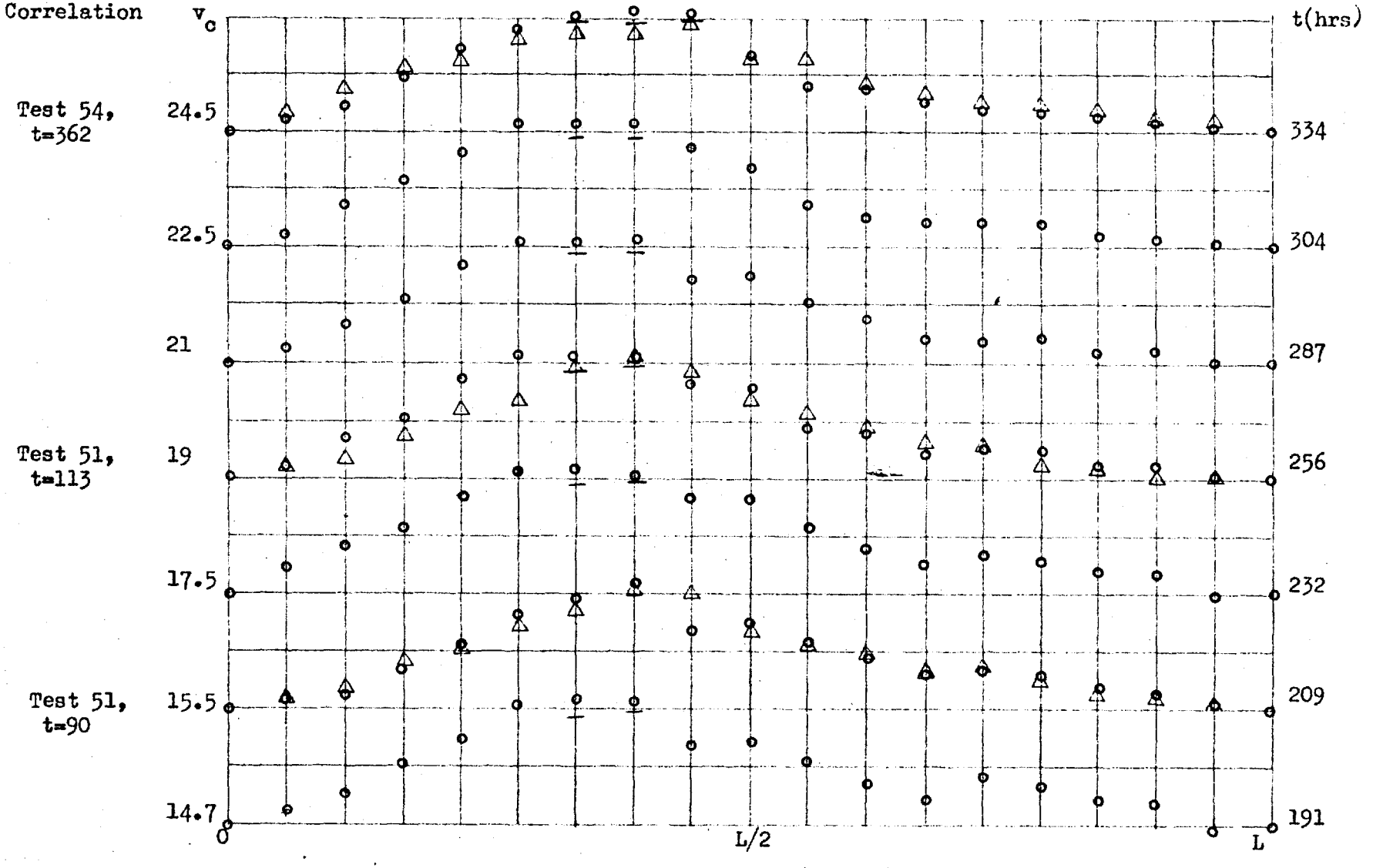


Fig. 33 Test 53 (contd.)

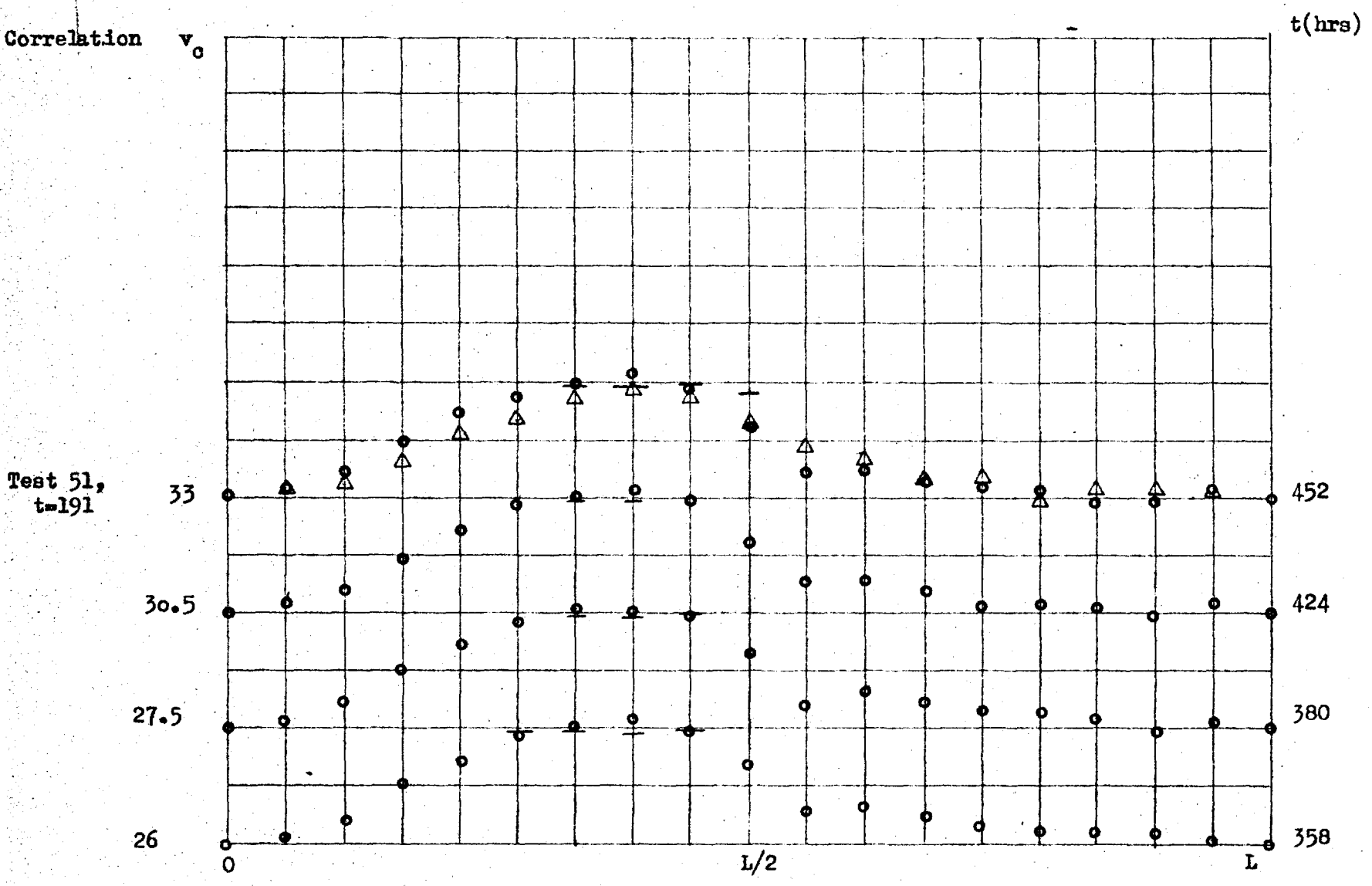
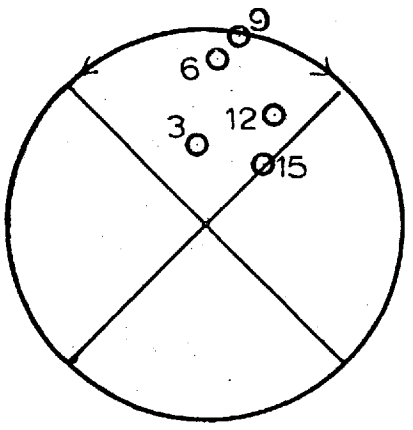
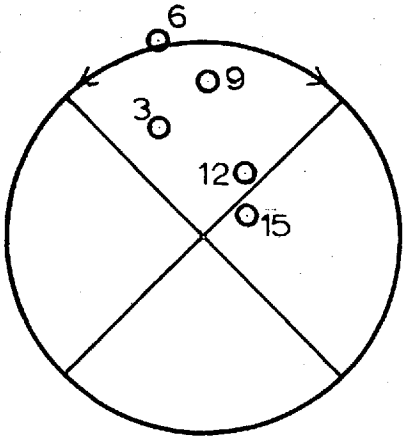


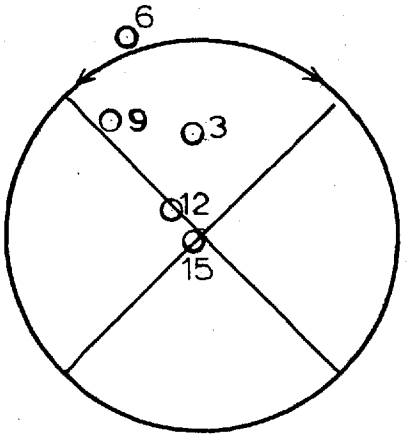
Fig. 34 Test 53 (concl.)



t=24.2

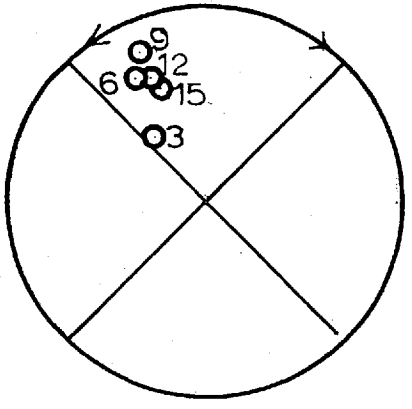


t=167

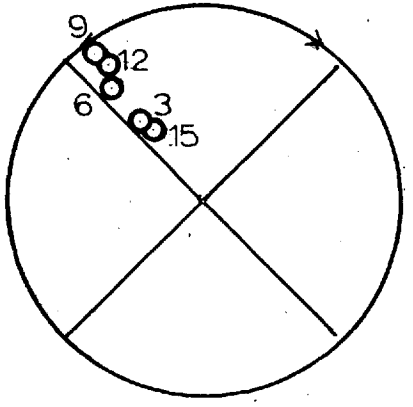


t=452

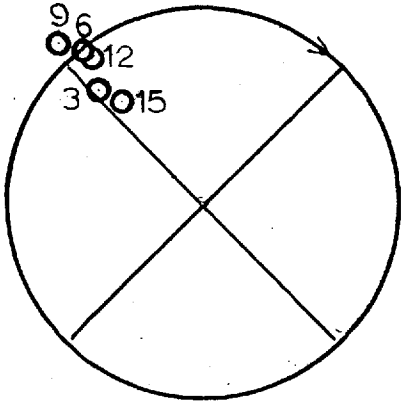
Test 53



t=23



t=93



t=167

Test 75

Fig. 35 Polar plots of deflection for Tests 53, 75.

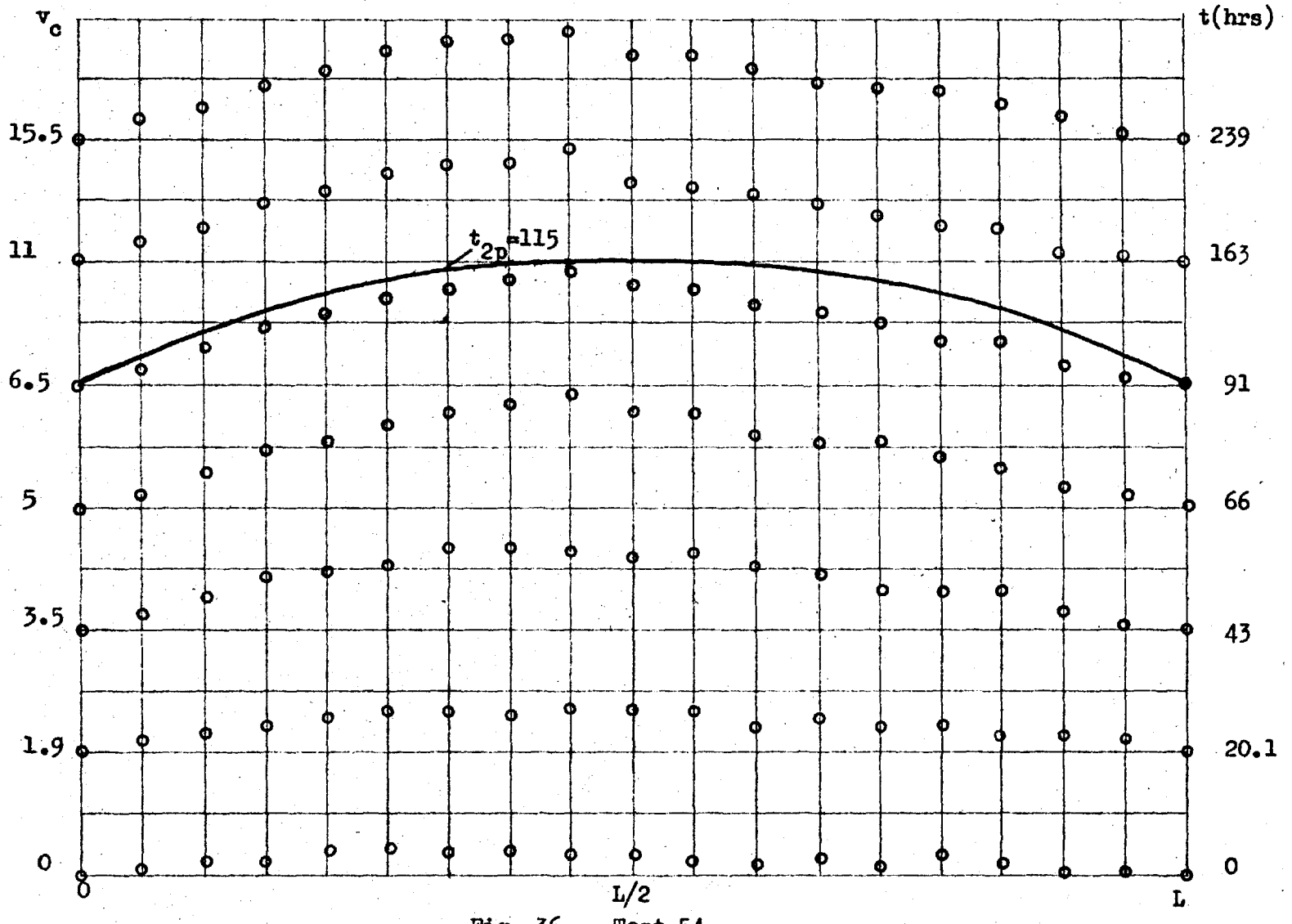


Fig. 36 Test 54 .

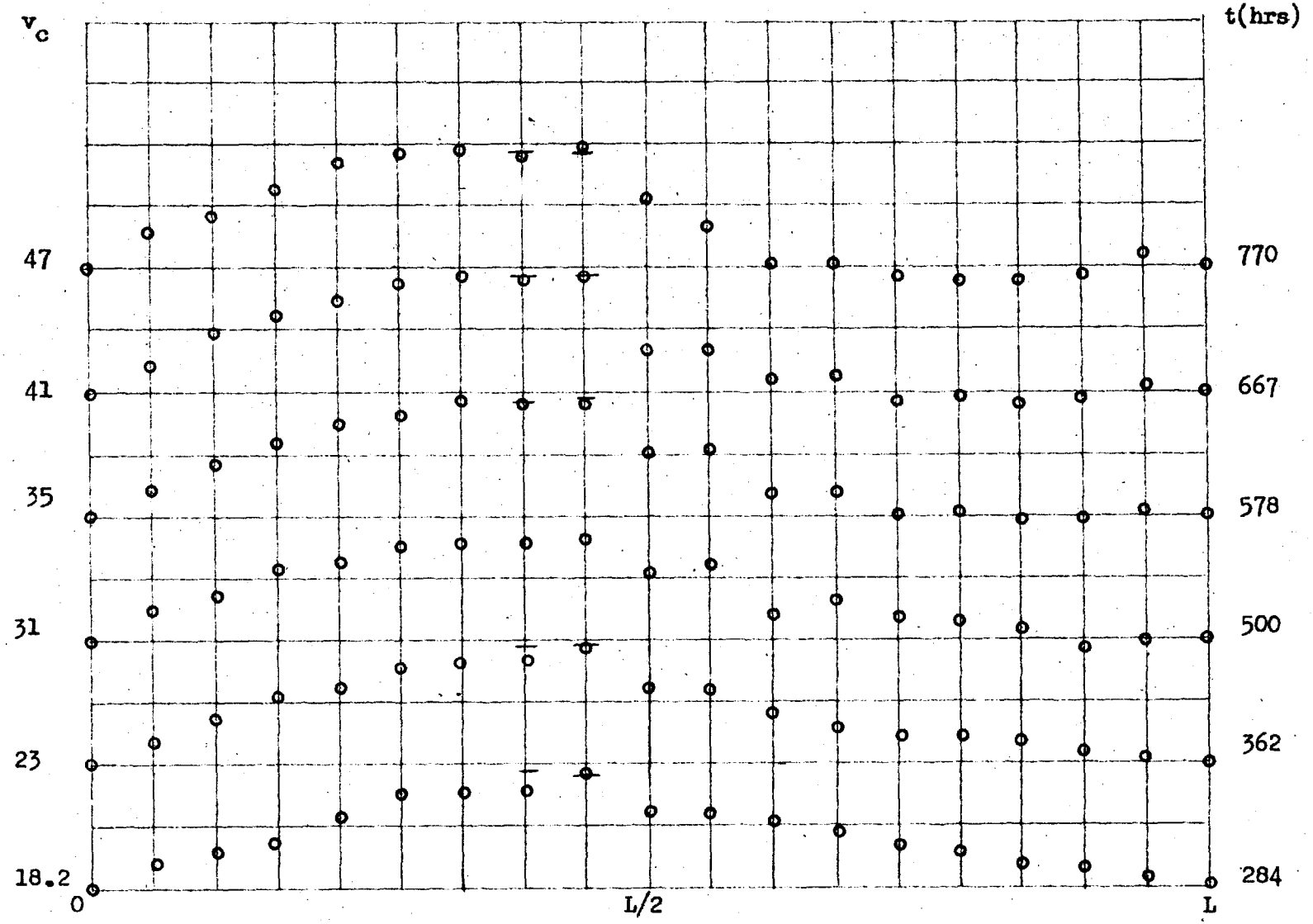


Fig. 37 Test 54 (contd.)

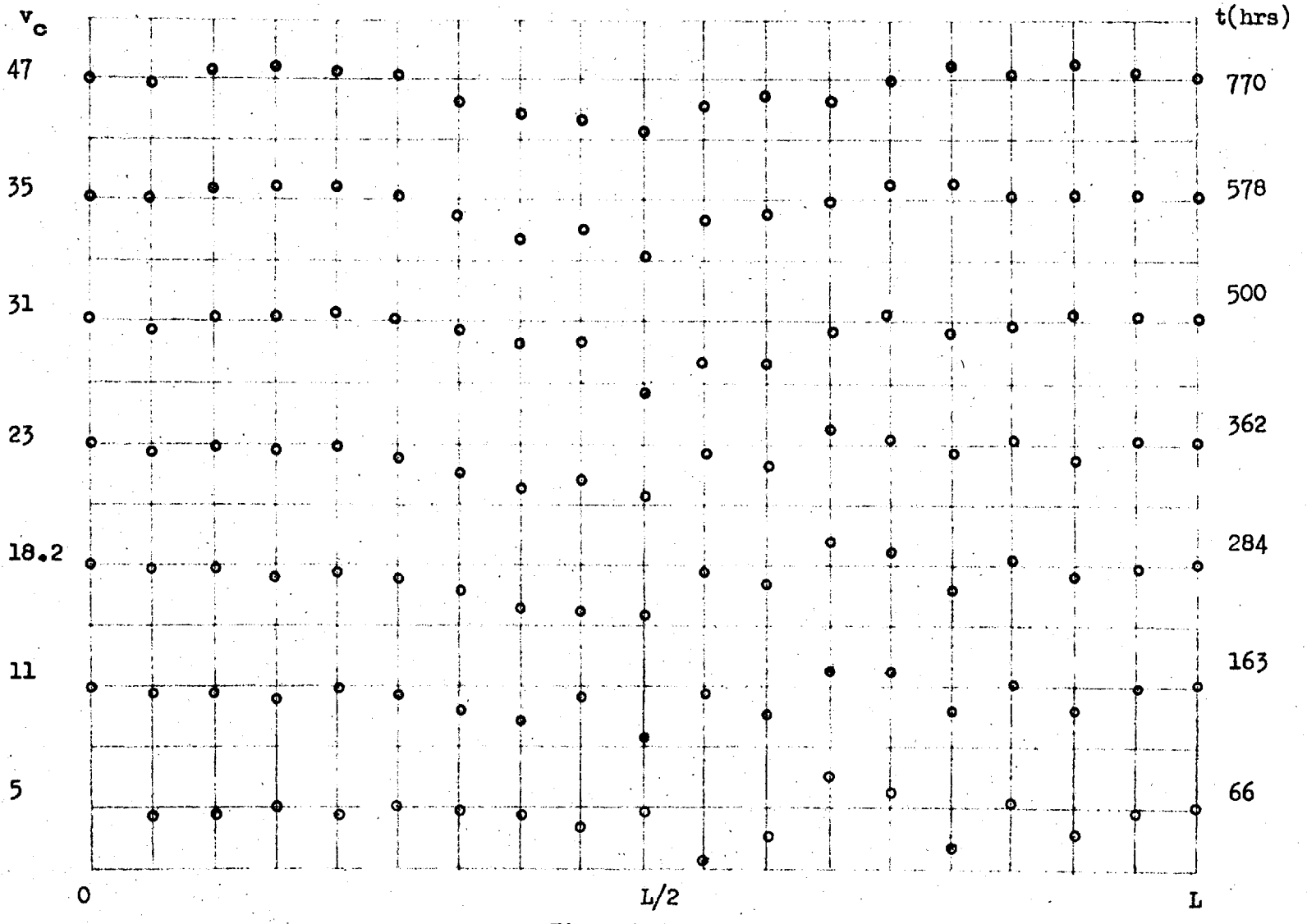


Fig. 38 Test 54 Minor bows.

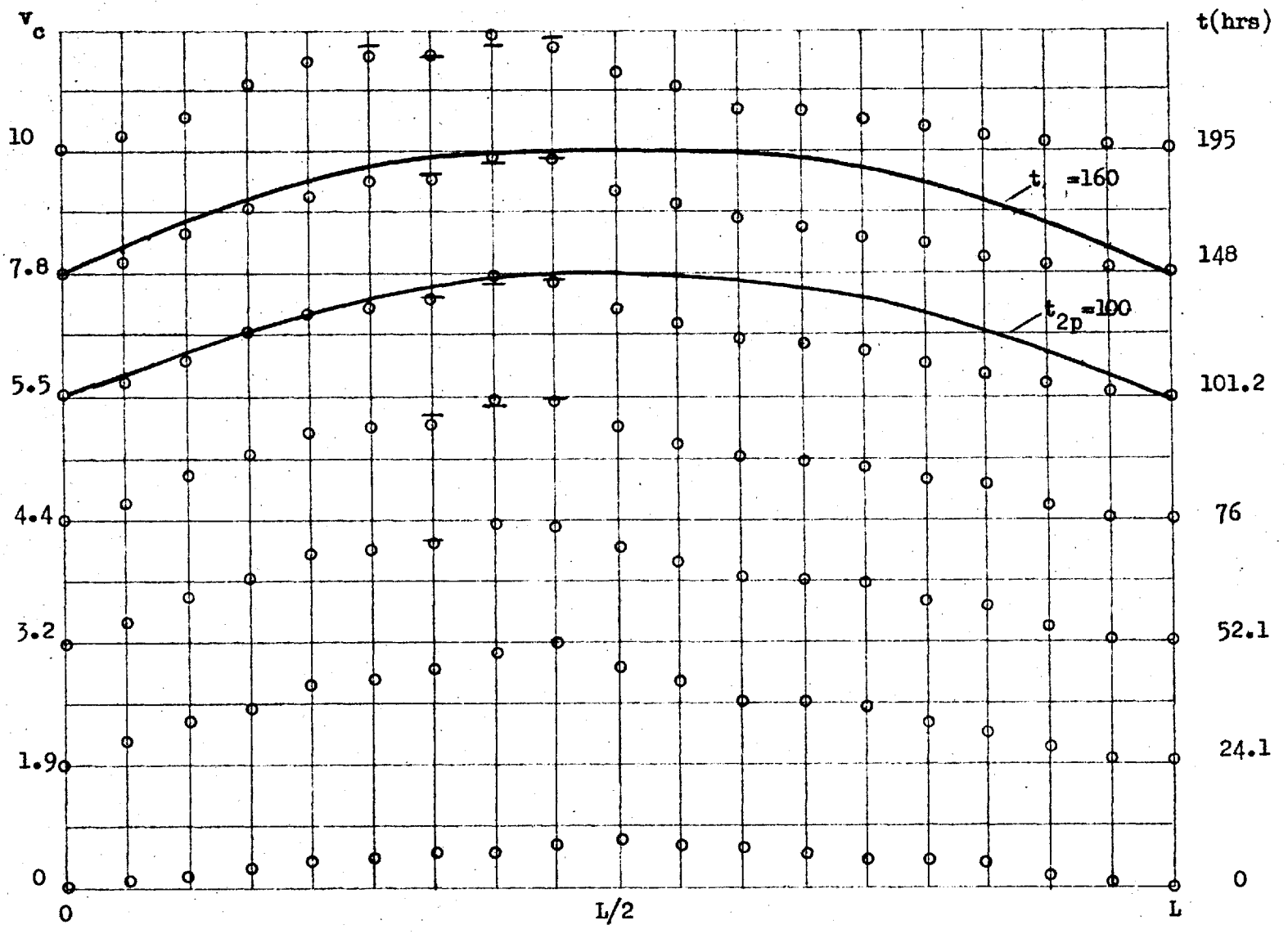


Fig. 39 Test 55.

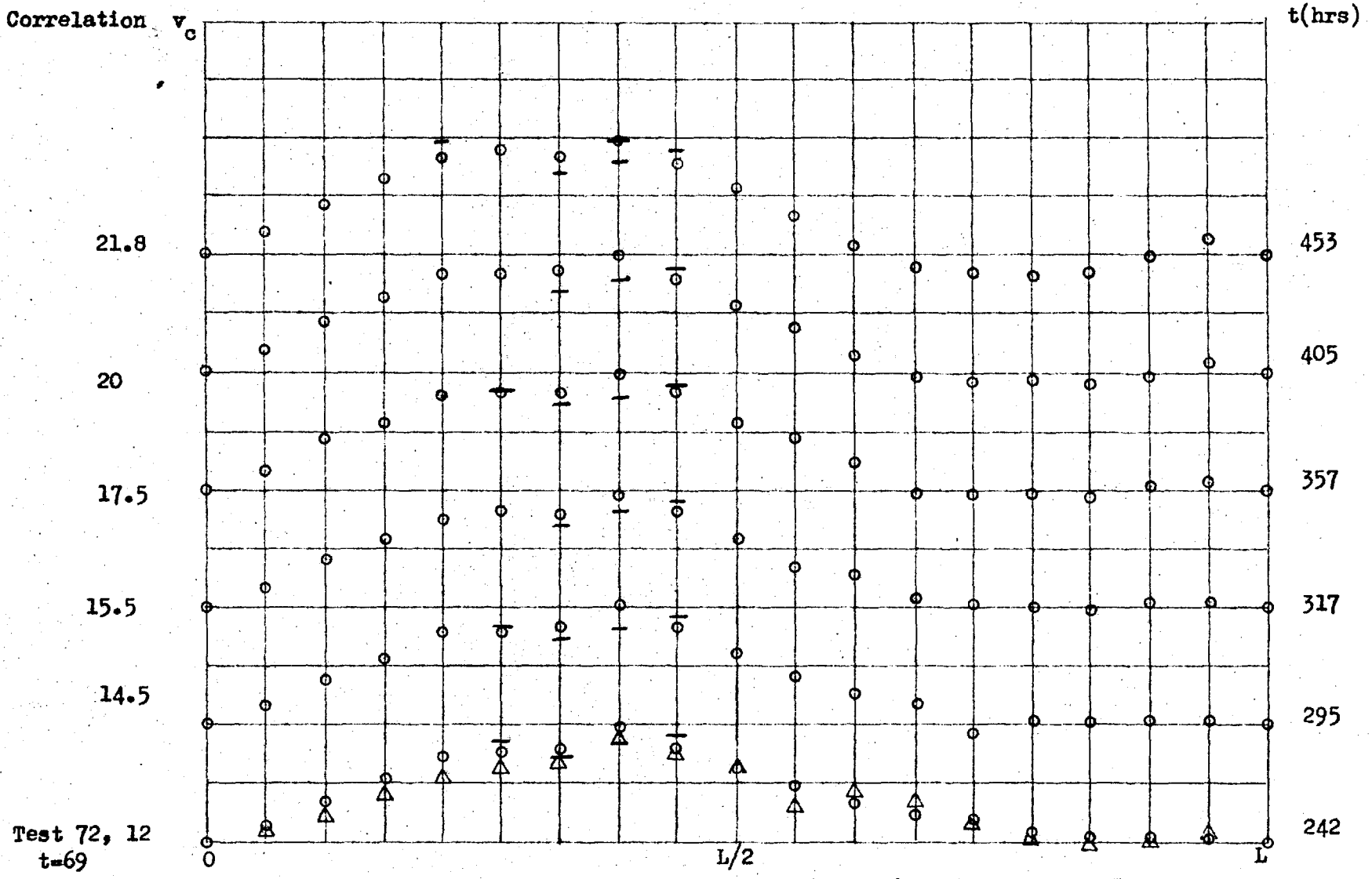


Fig. 40 Test 55 (contd.)

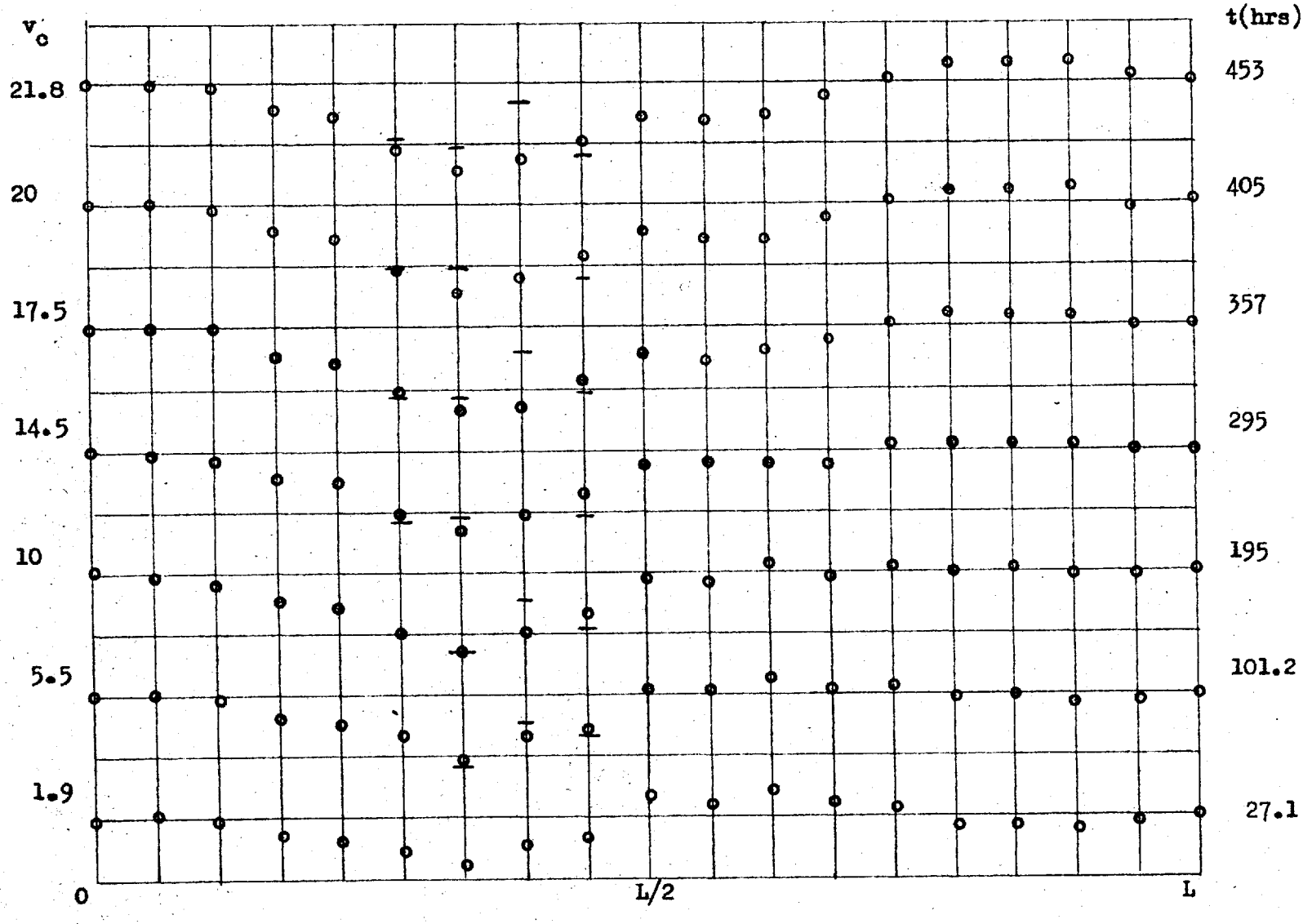
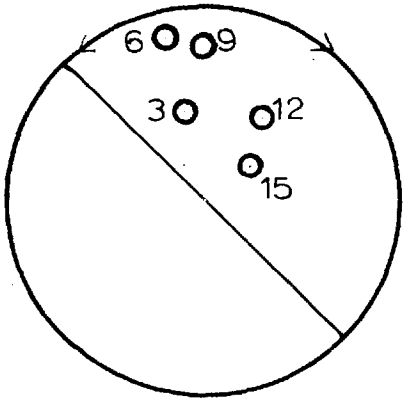
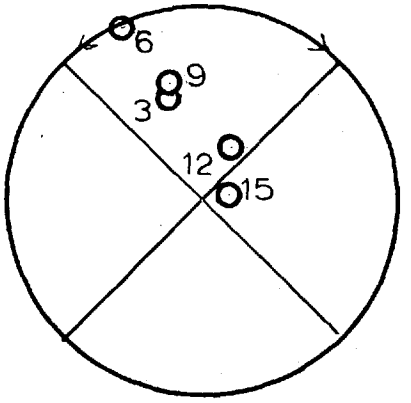


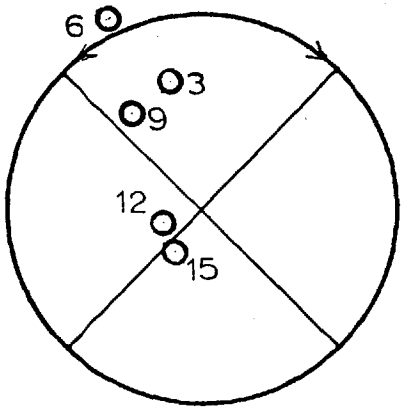
Fig. 41 Test 55 Minor bows.



t=27.1

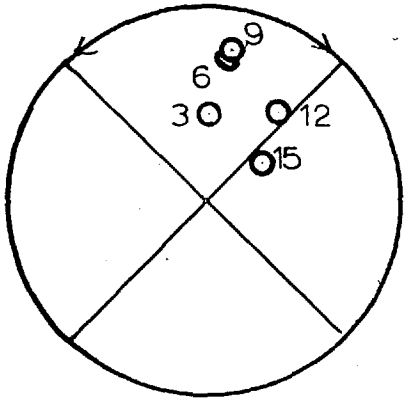


t=195

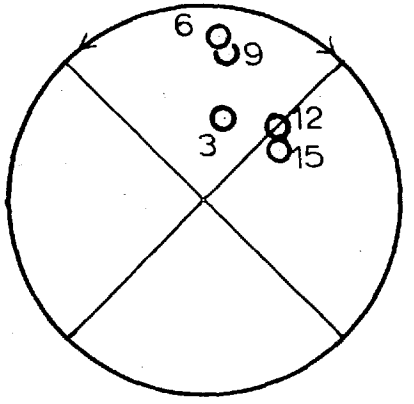


t=453

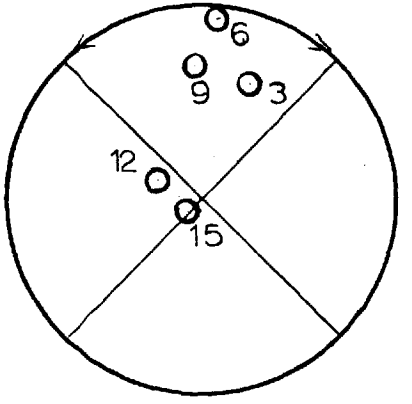
Test 55 .



t=66



t=239



t=770

Test 54

Fig. 42 Polar plots of deflections for Tests 55, 54.

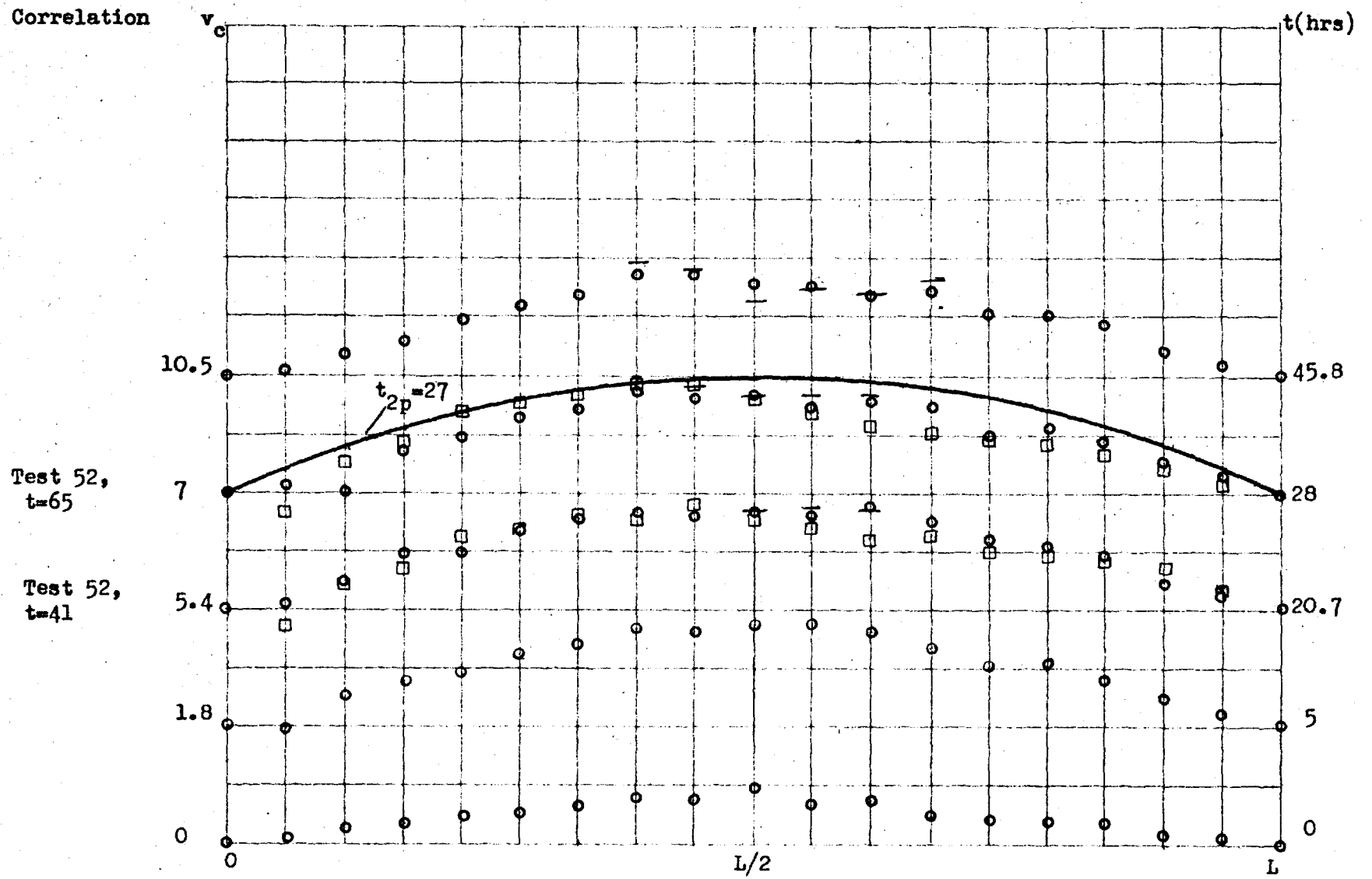


Fig. 43 Test 70 .

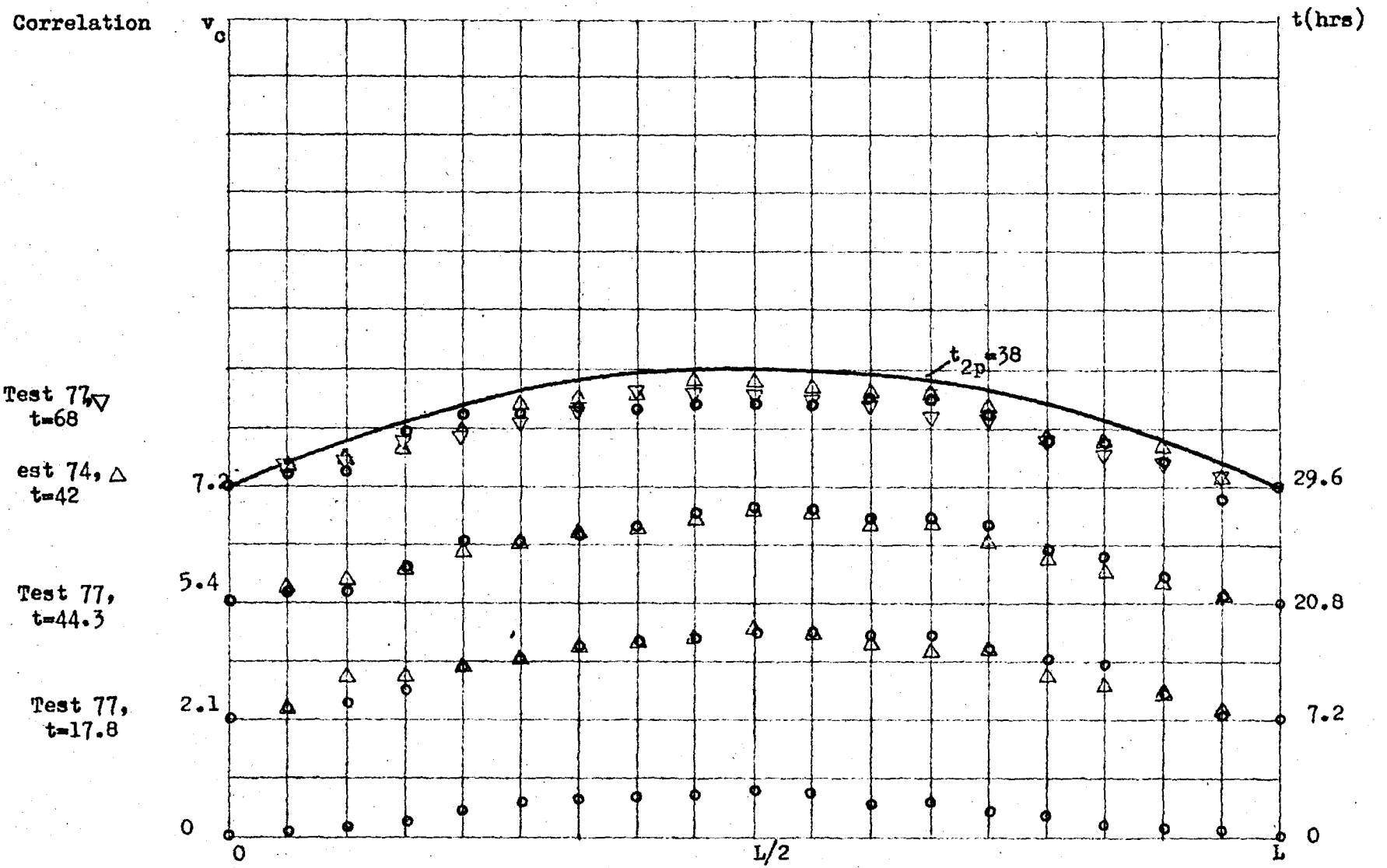


Fig. 44 Test 71 .

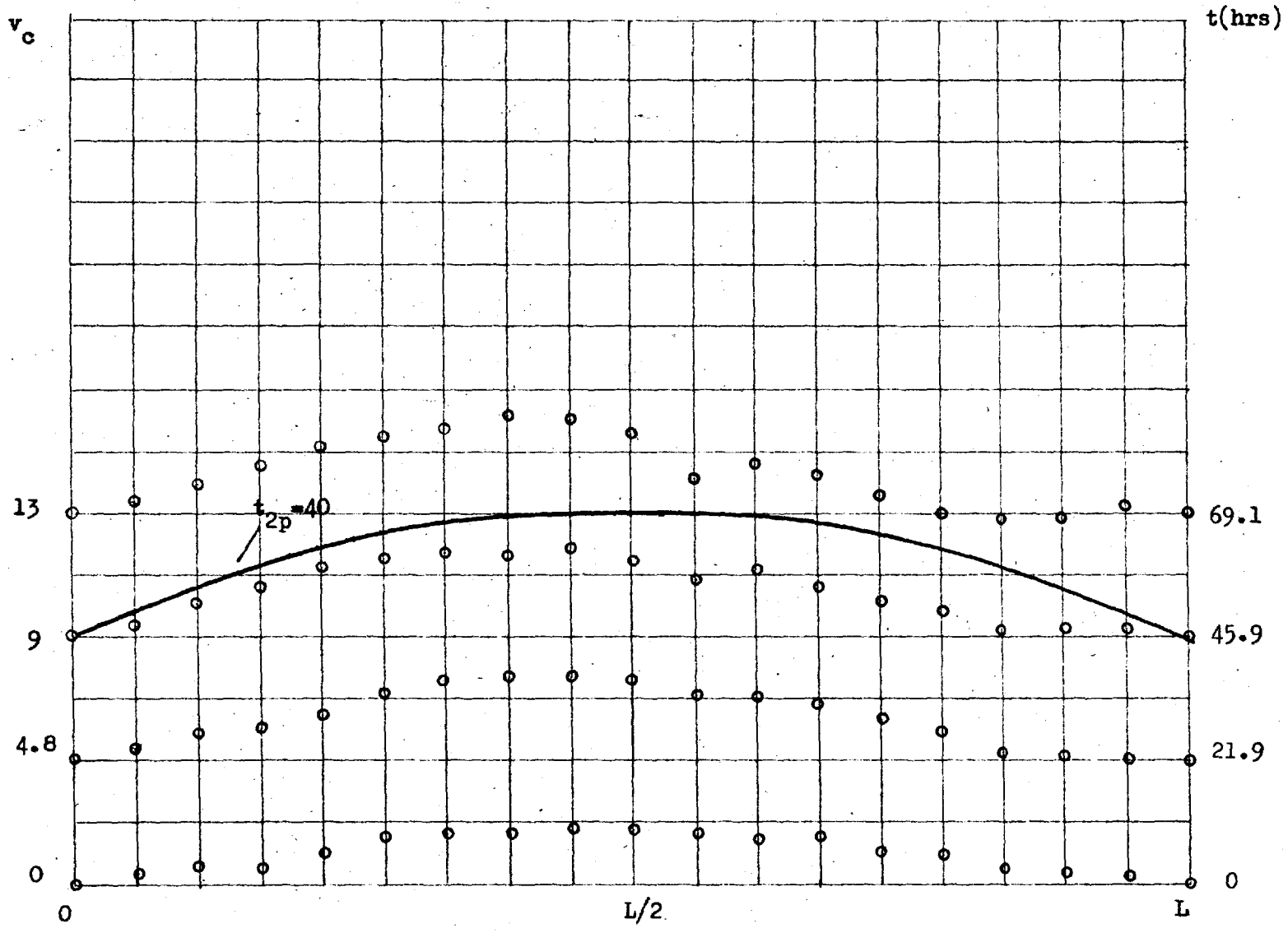


Fig. 45 Test 72 .

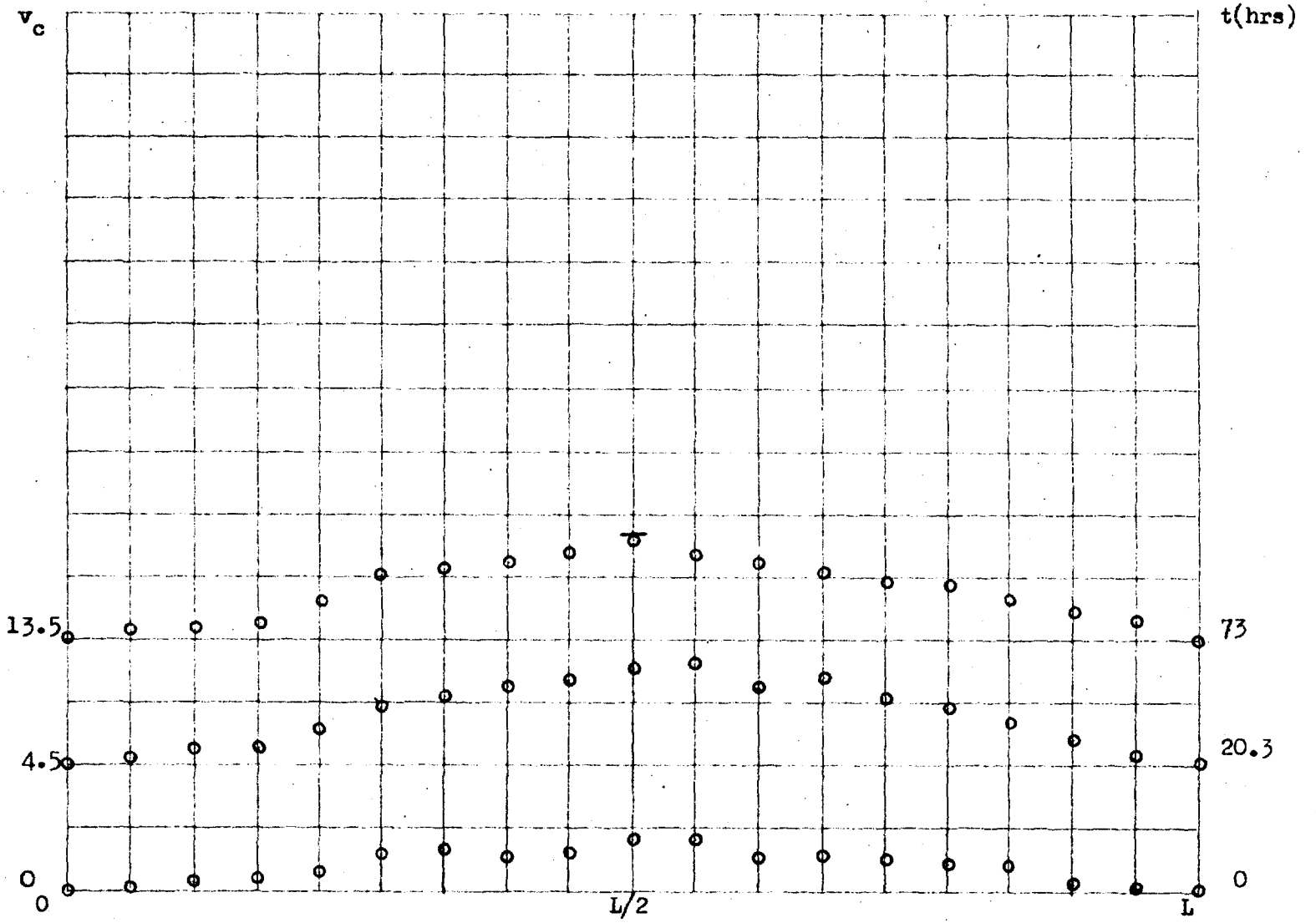


Fig. 46 Test 73 .

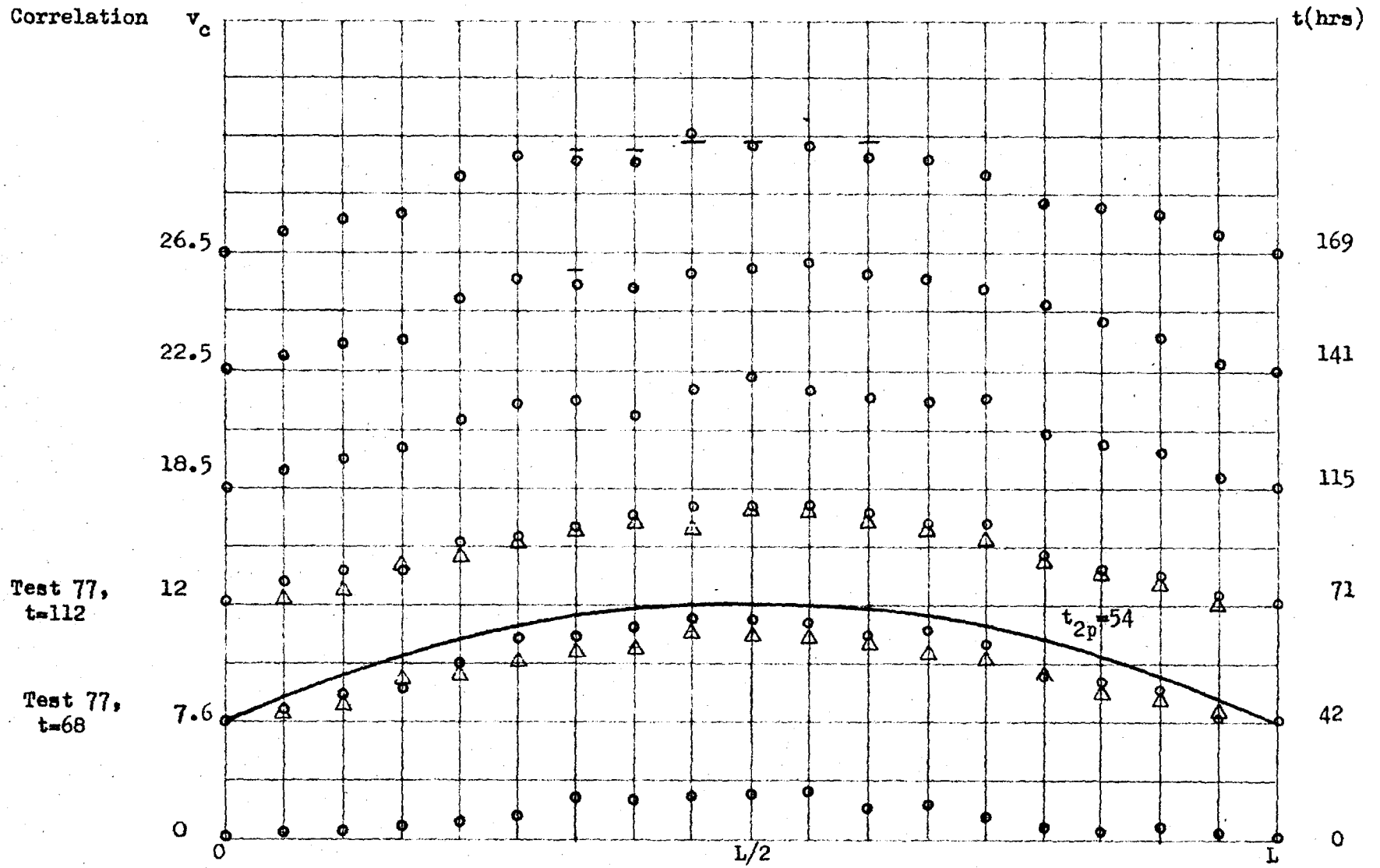


Fig. 47 Test 74 .

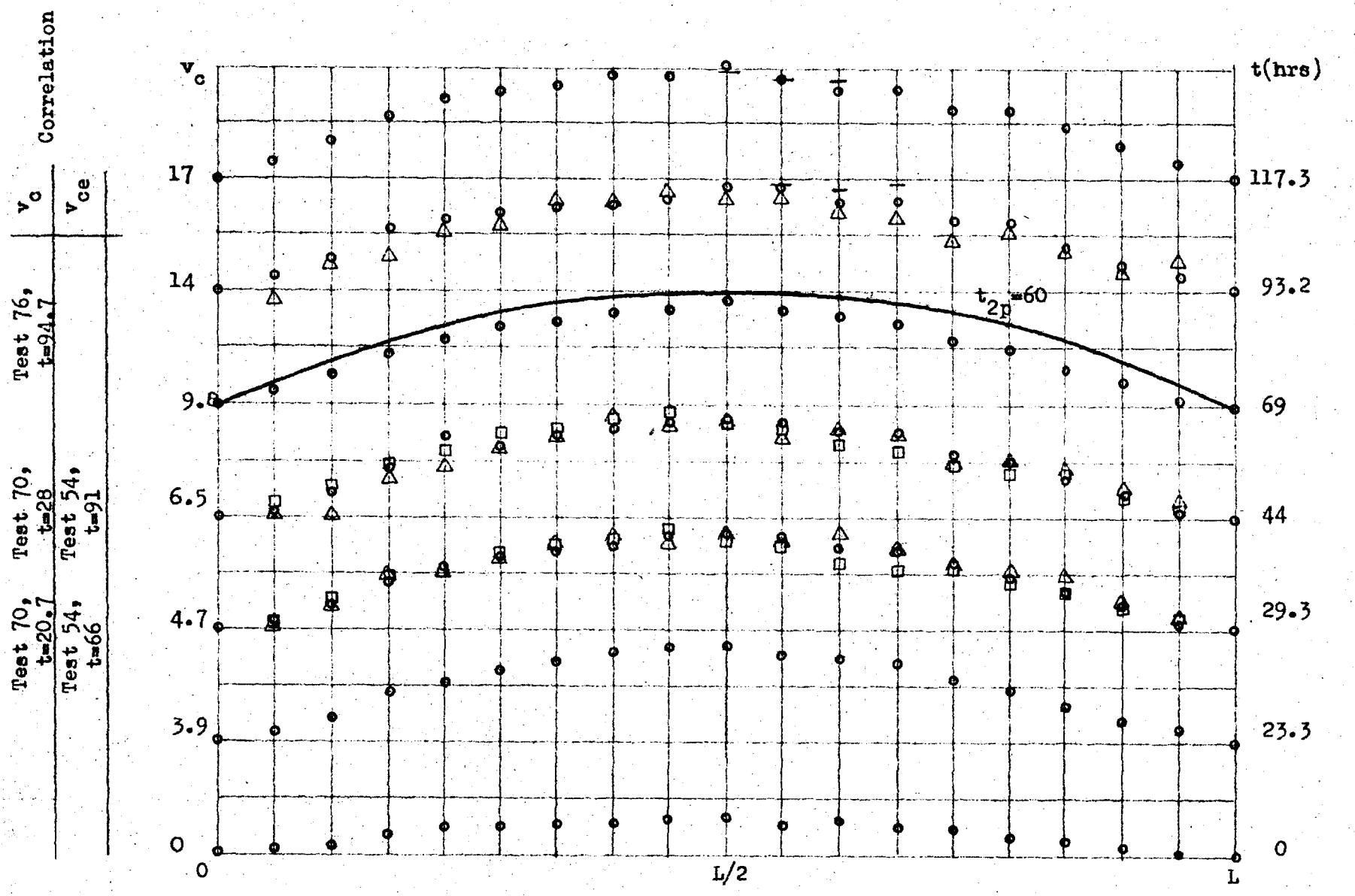


Fig. 48 Test 75 .

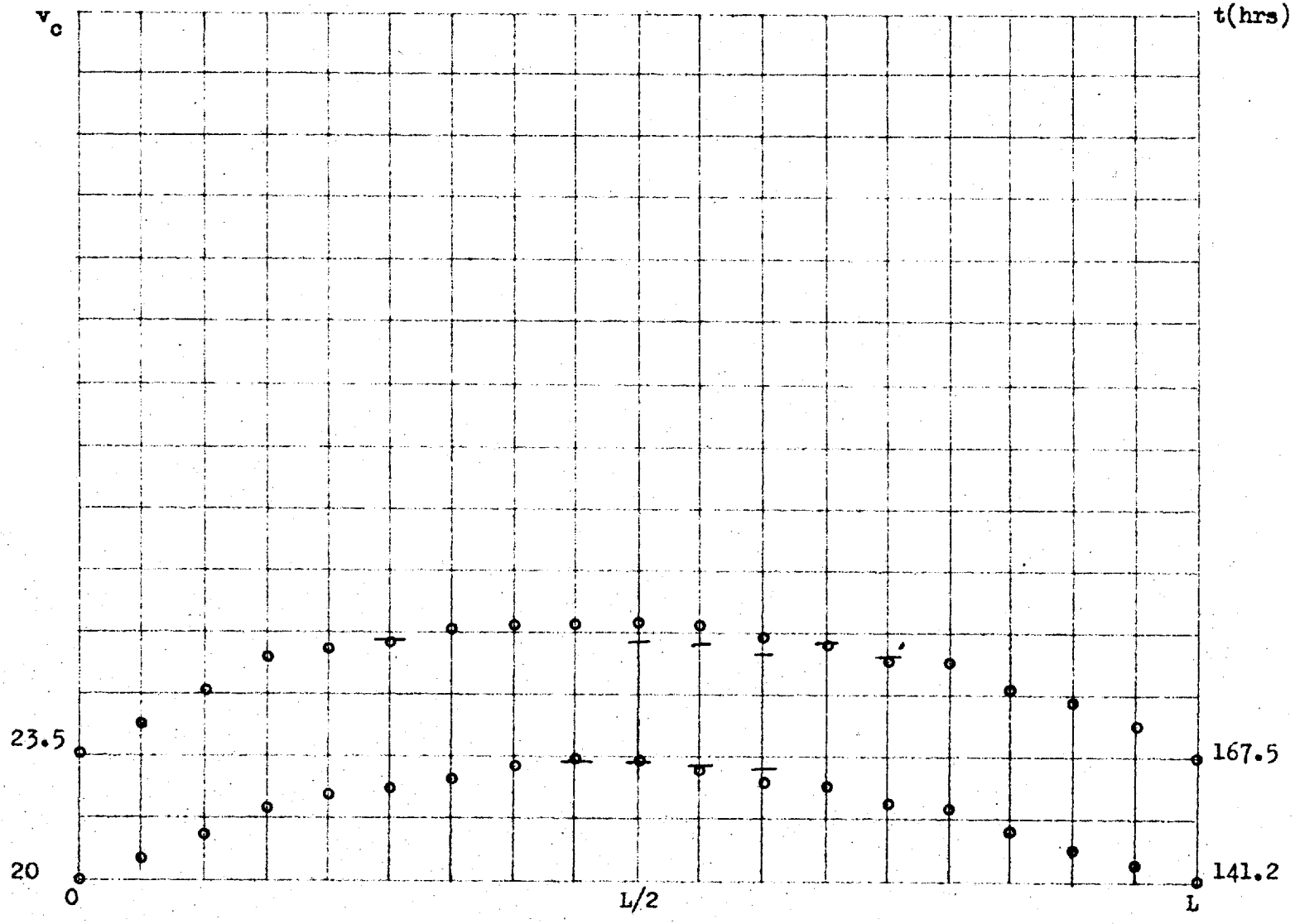


Fig. 49 Test 75 (contd.)

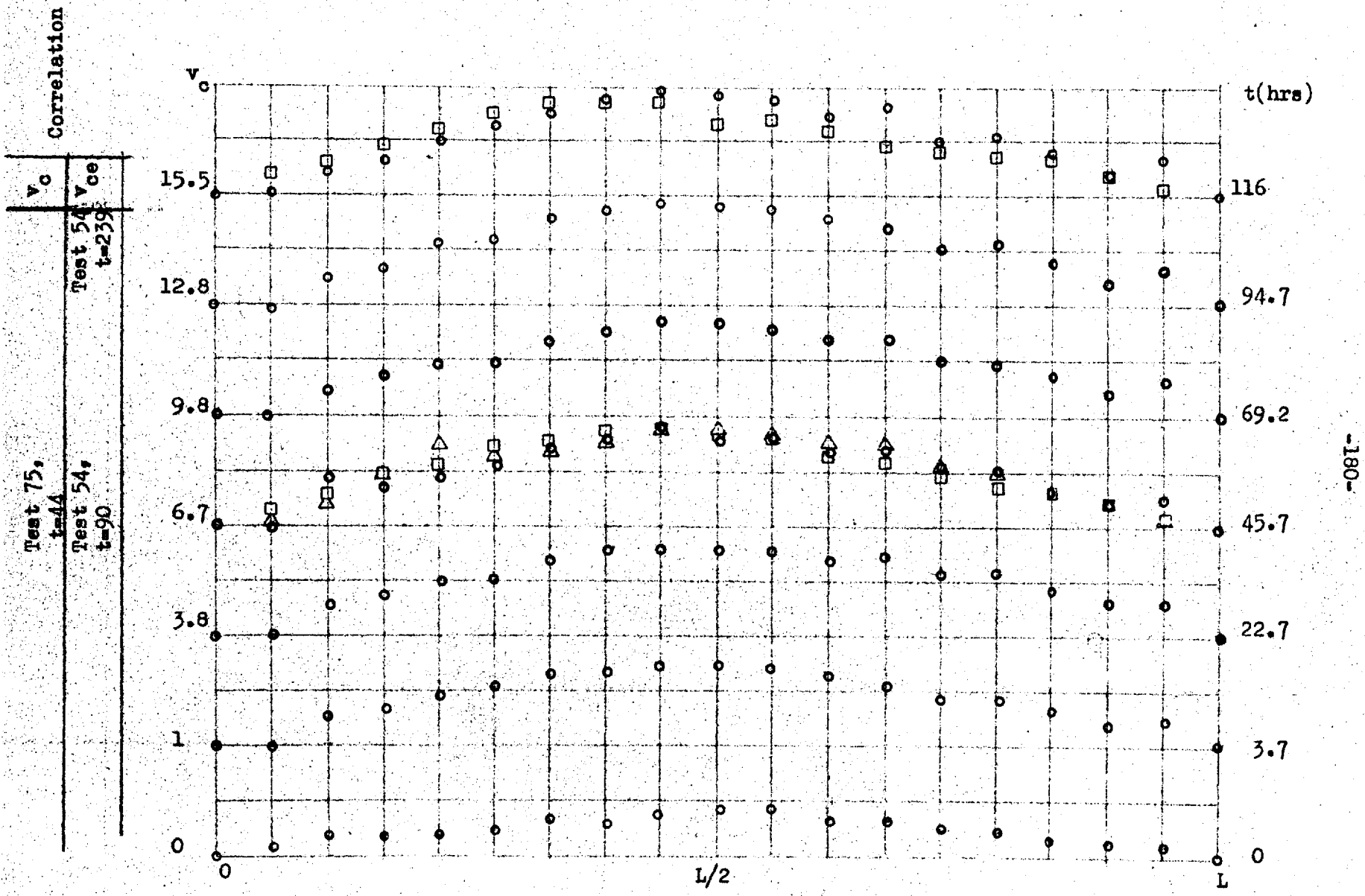


Fig. 50 Test 76.

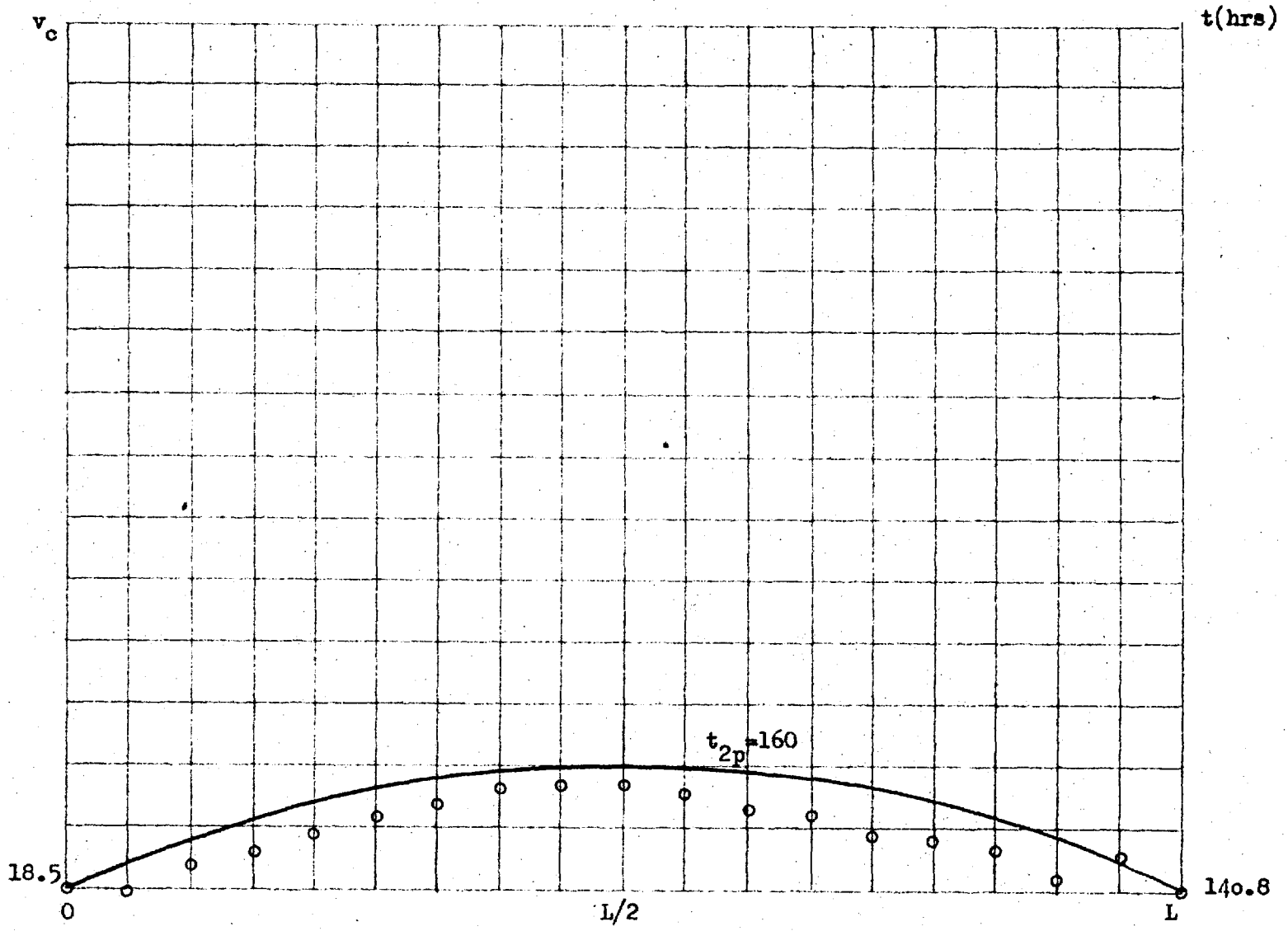


Fig. 51 Test 76 (contd.)

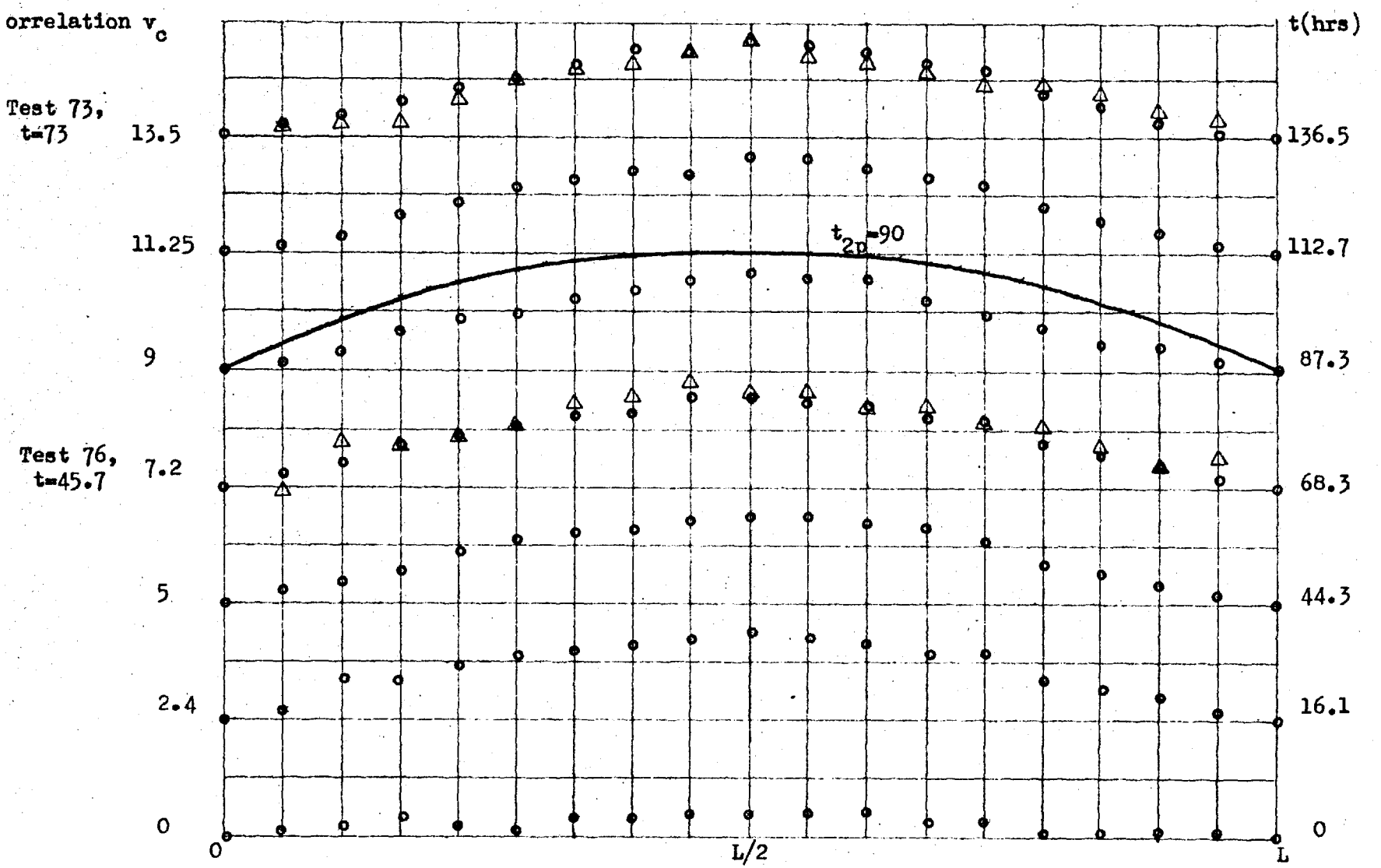


Fig. 52 Test 77

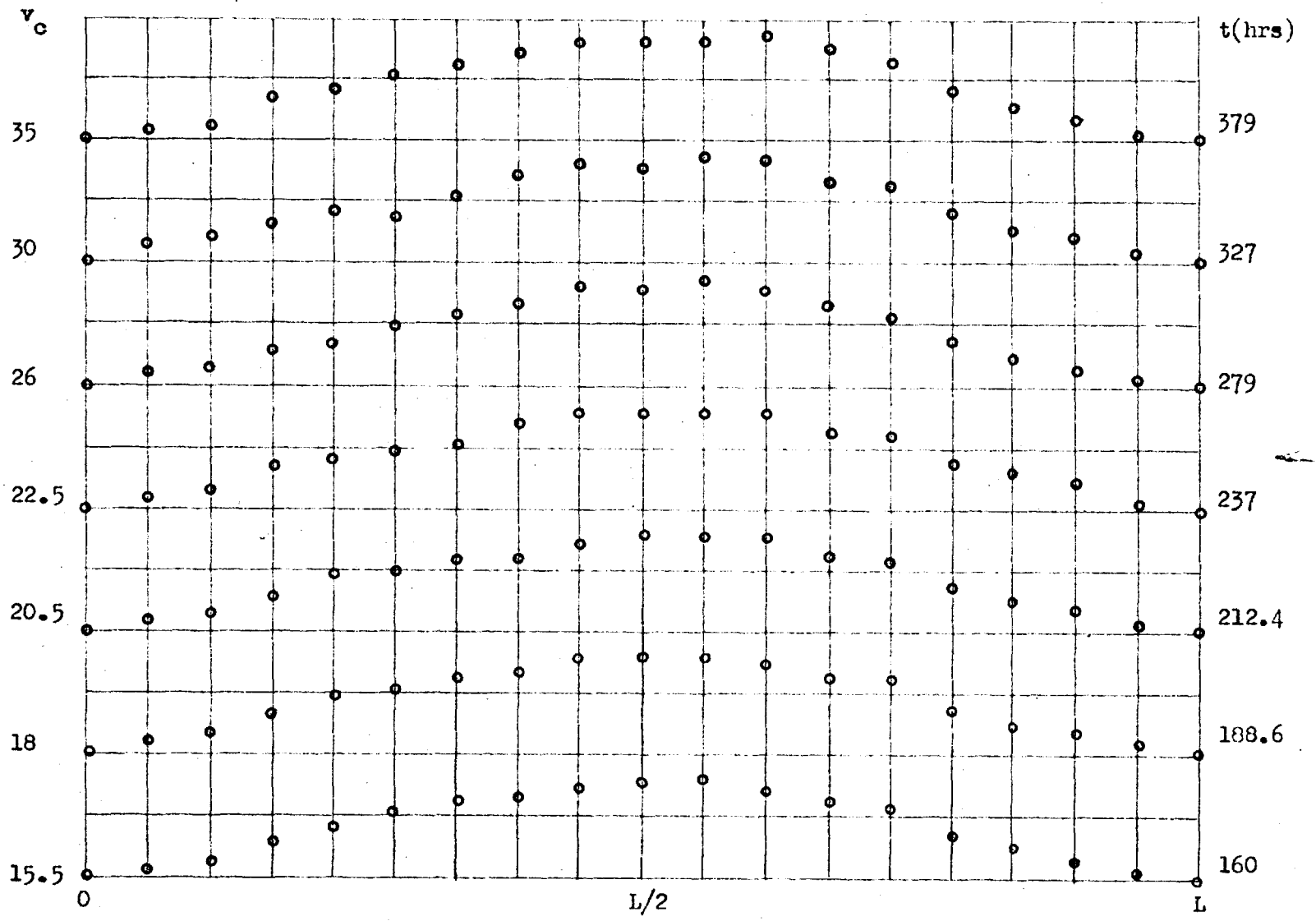


Fig. 53 Test 77 (contd.)

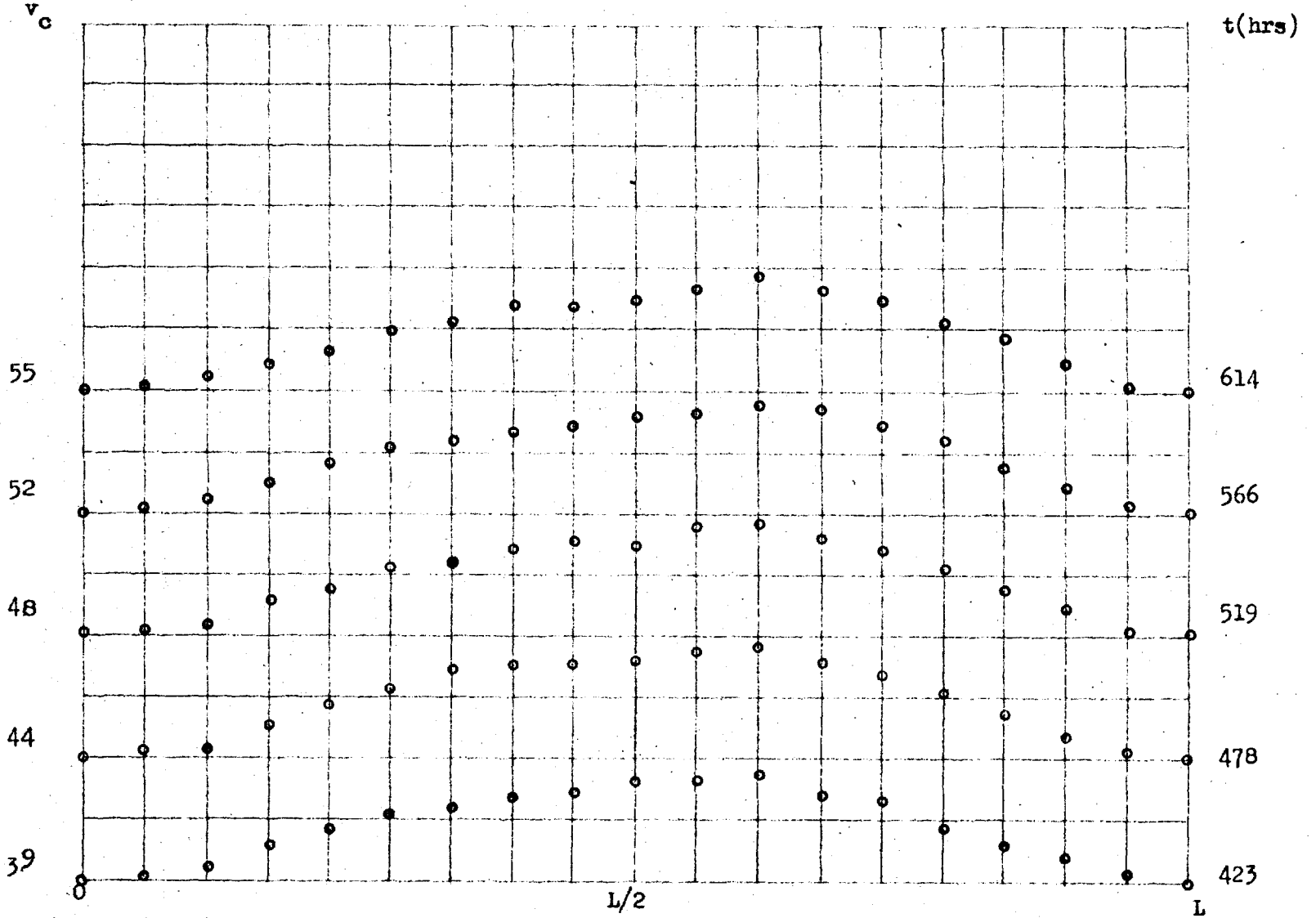


Fig. 54 Test 77 (concl.)

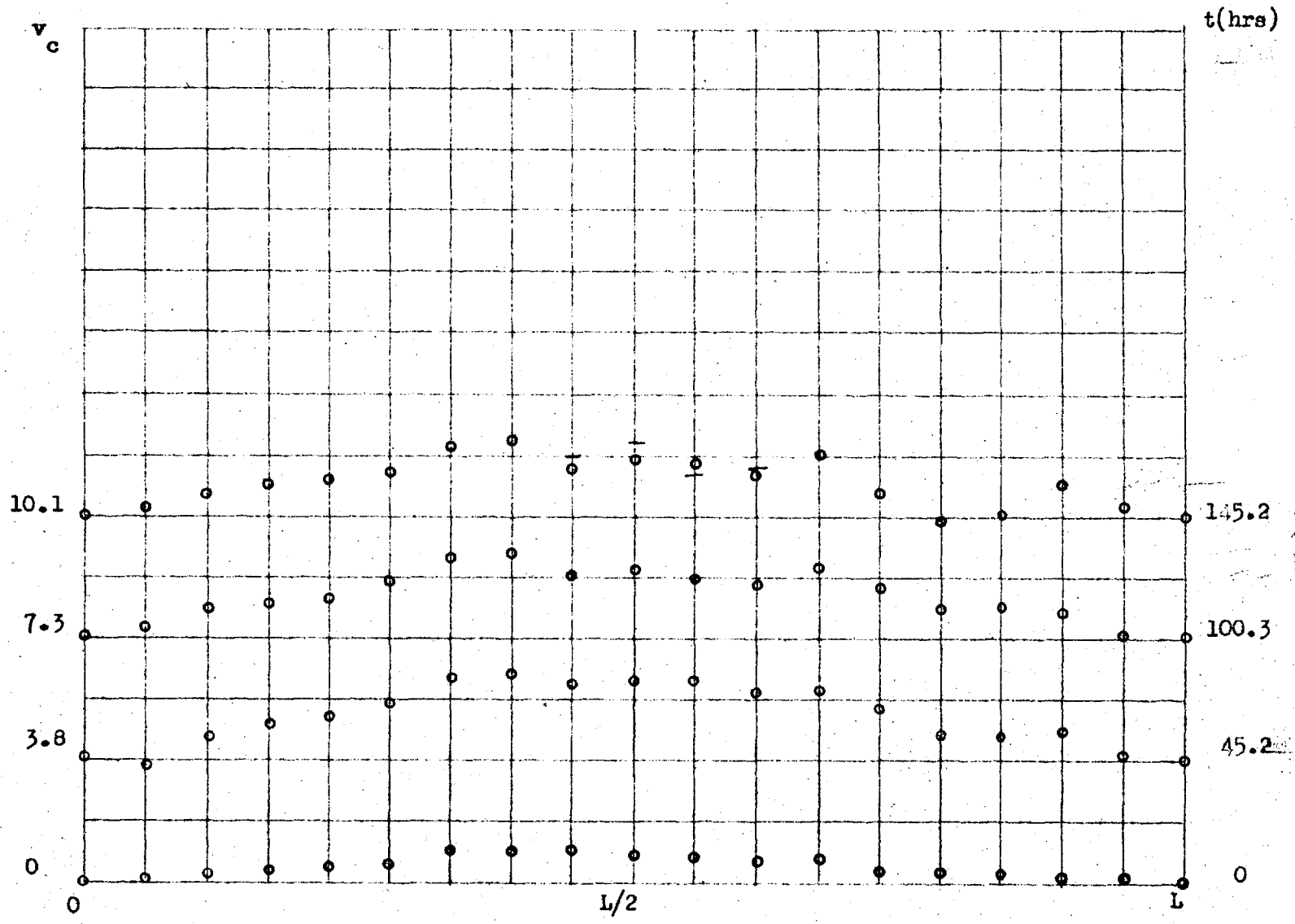


Fig. 55 Test 78

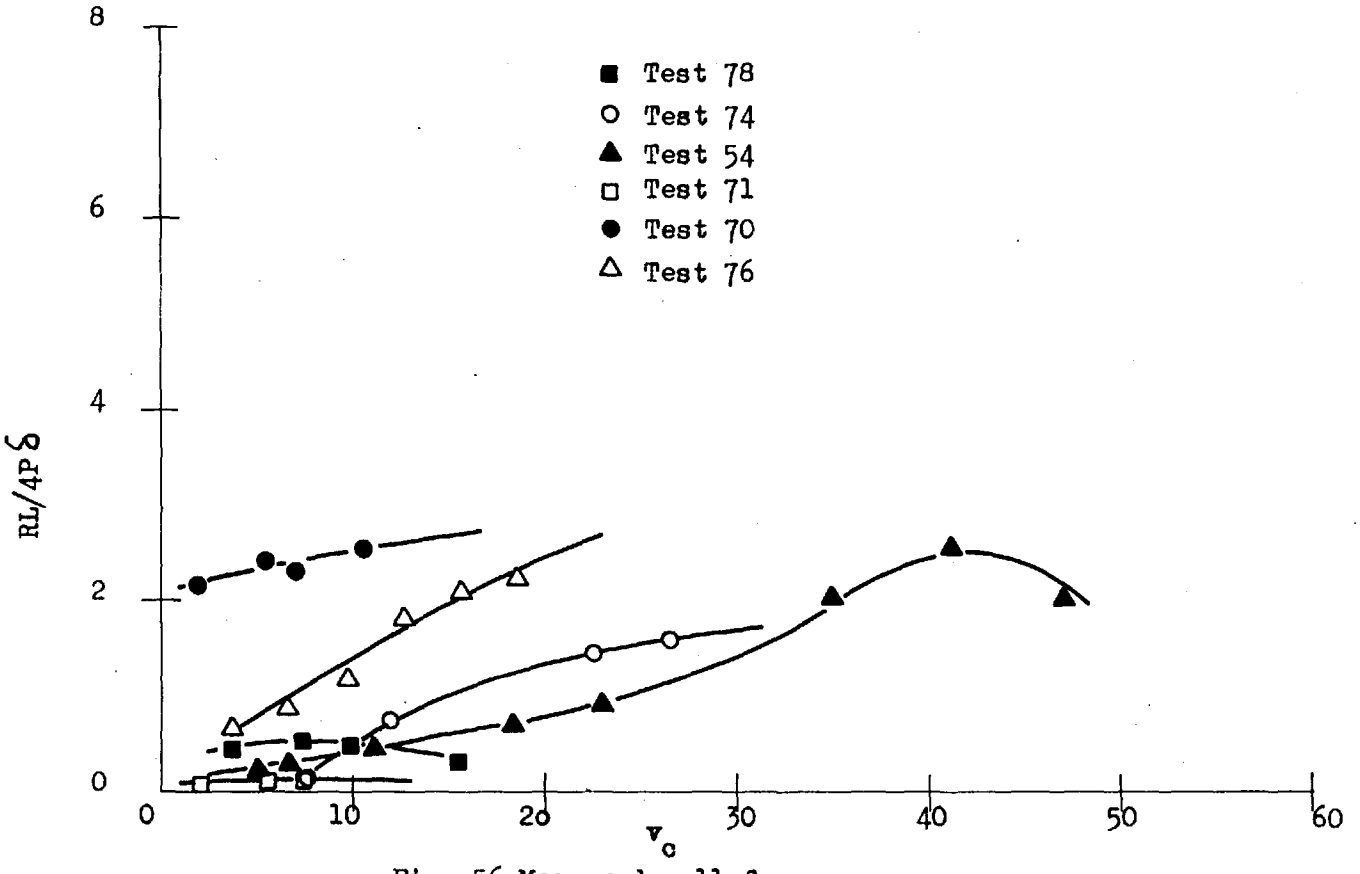


Fig. 56 Measured wall forces

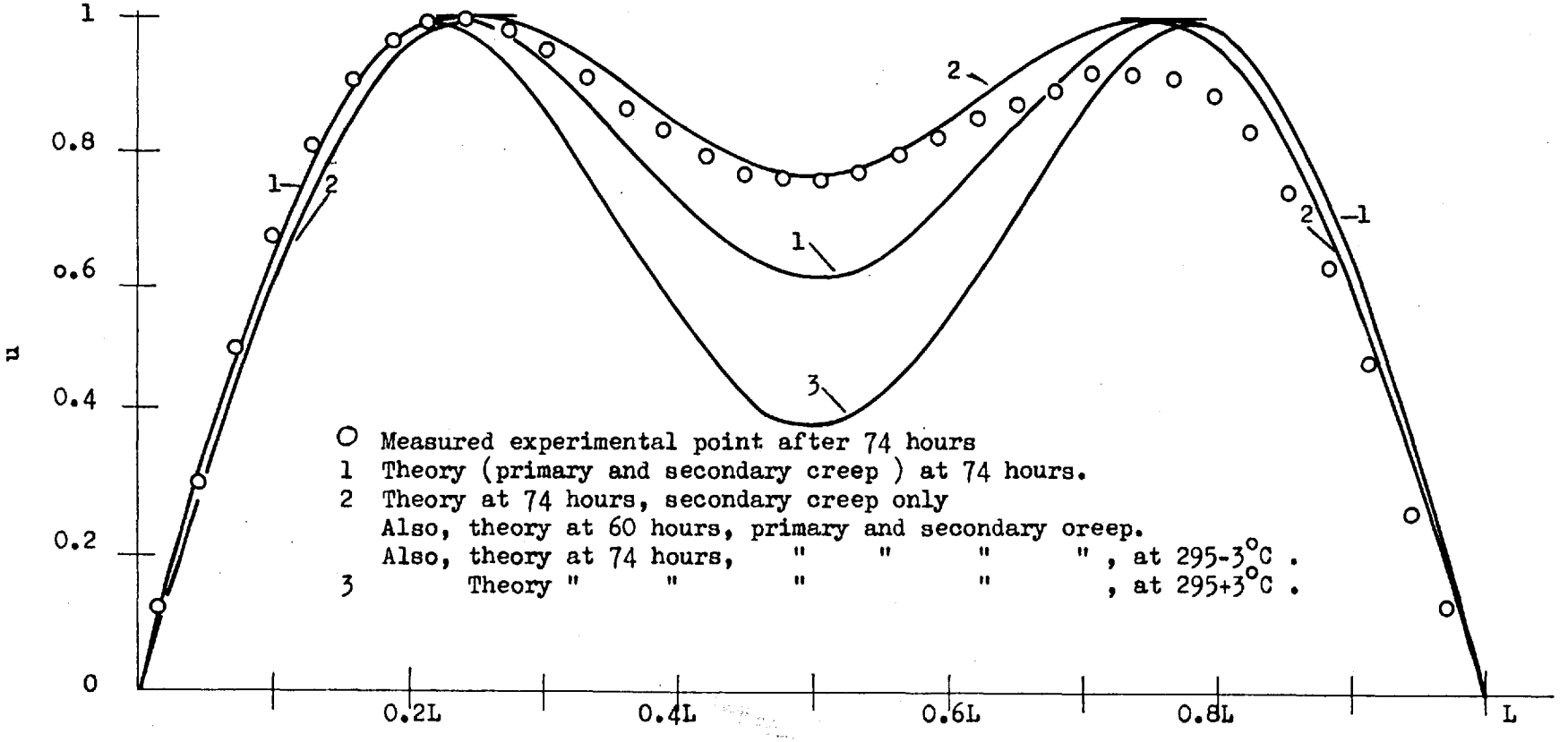


Fig. 57 Experiment on rectangular specimen showing prediction of the theory under various assumptions.

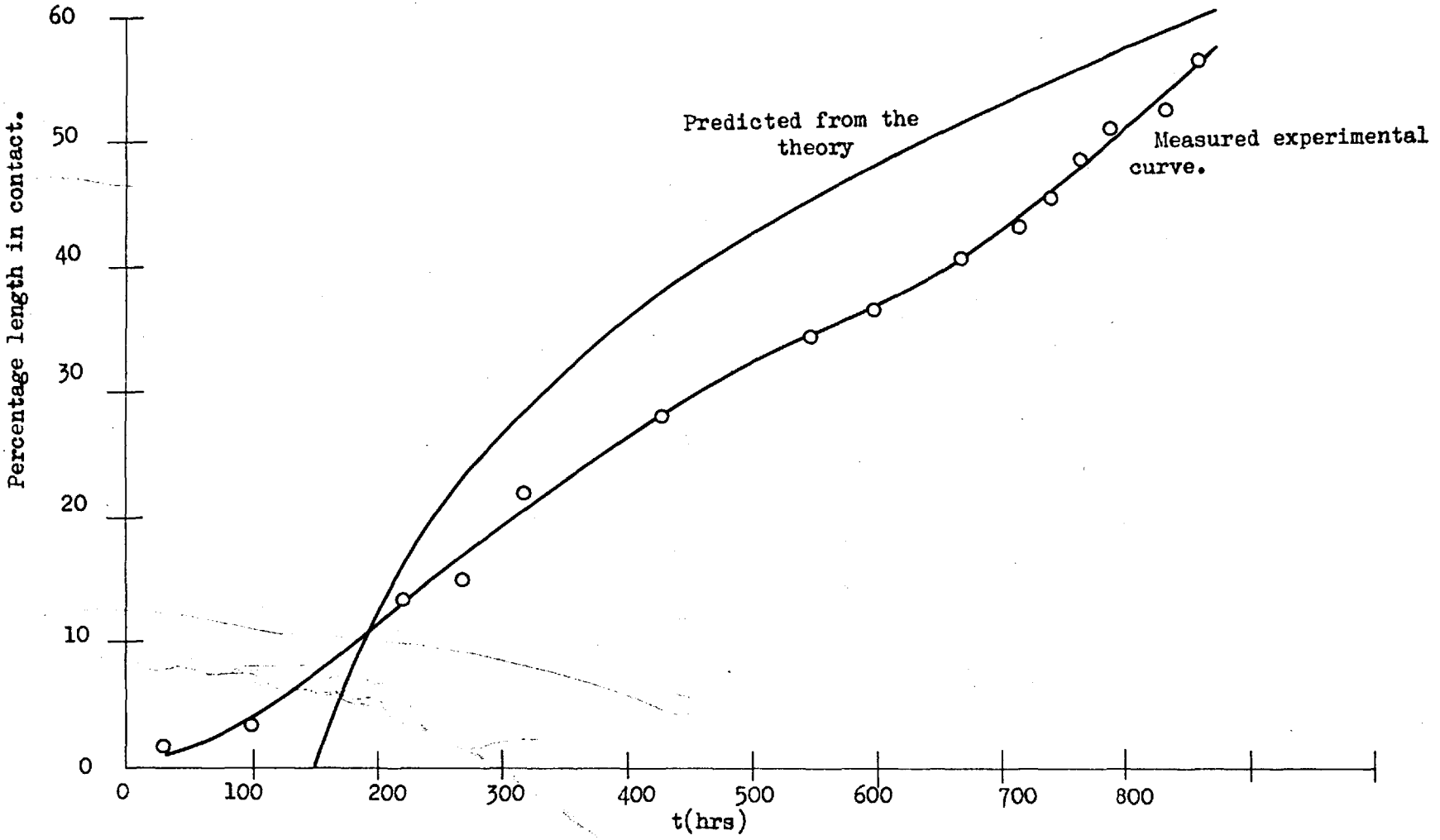


Fig. 58 Correlation of an English Electric Co. Ltd. lead bar experiment with the theory of section 4.2.1 .

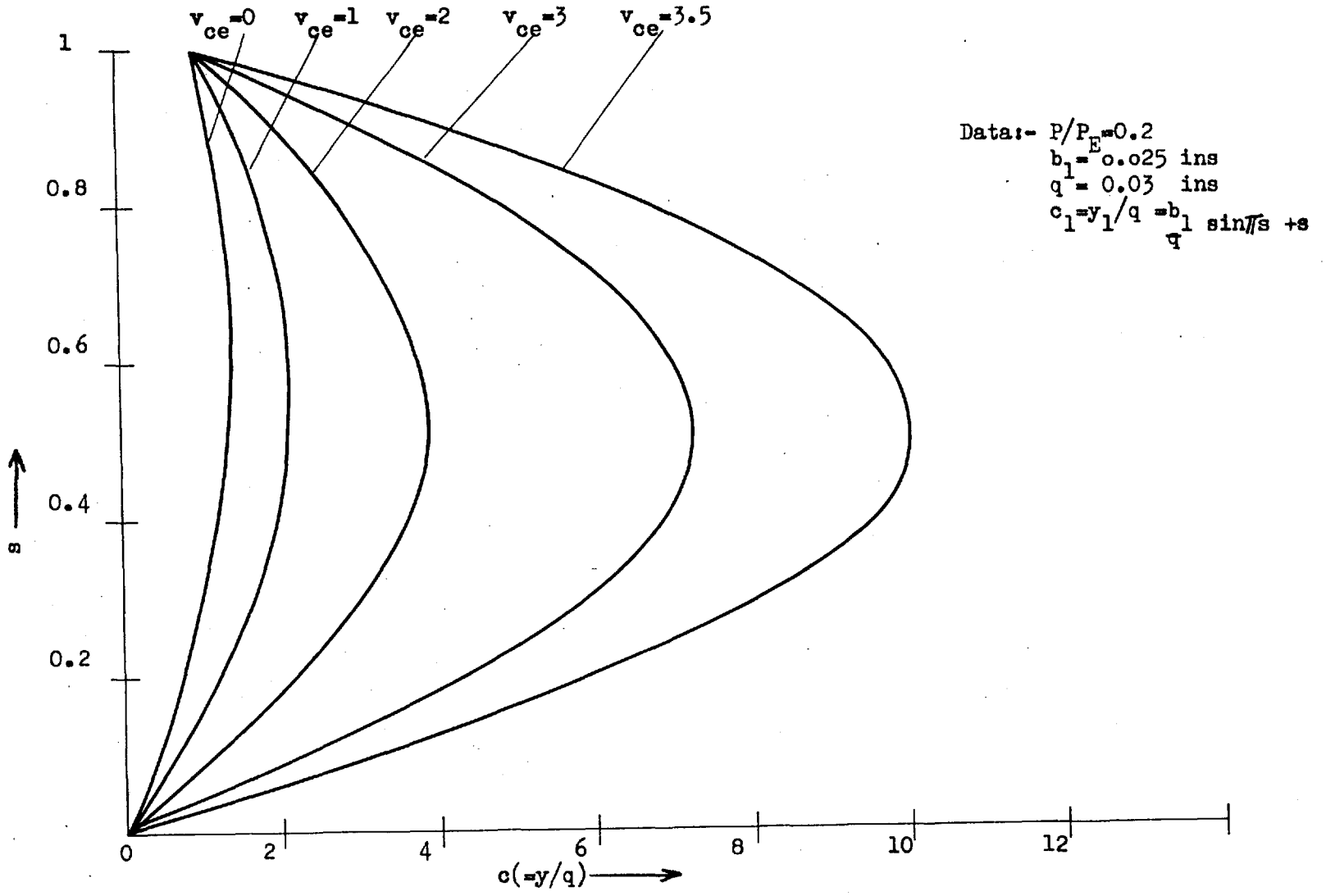
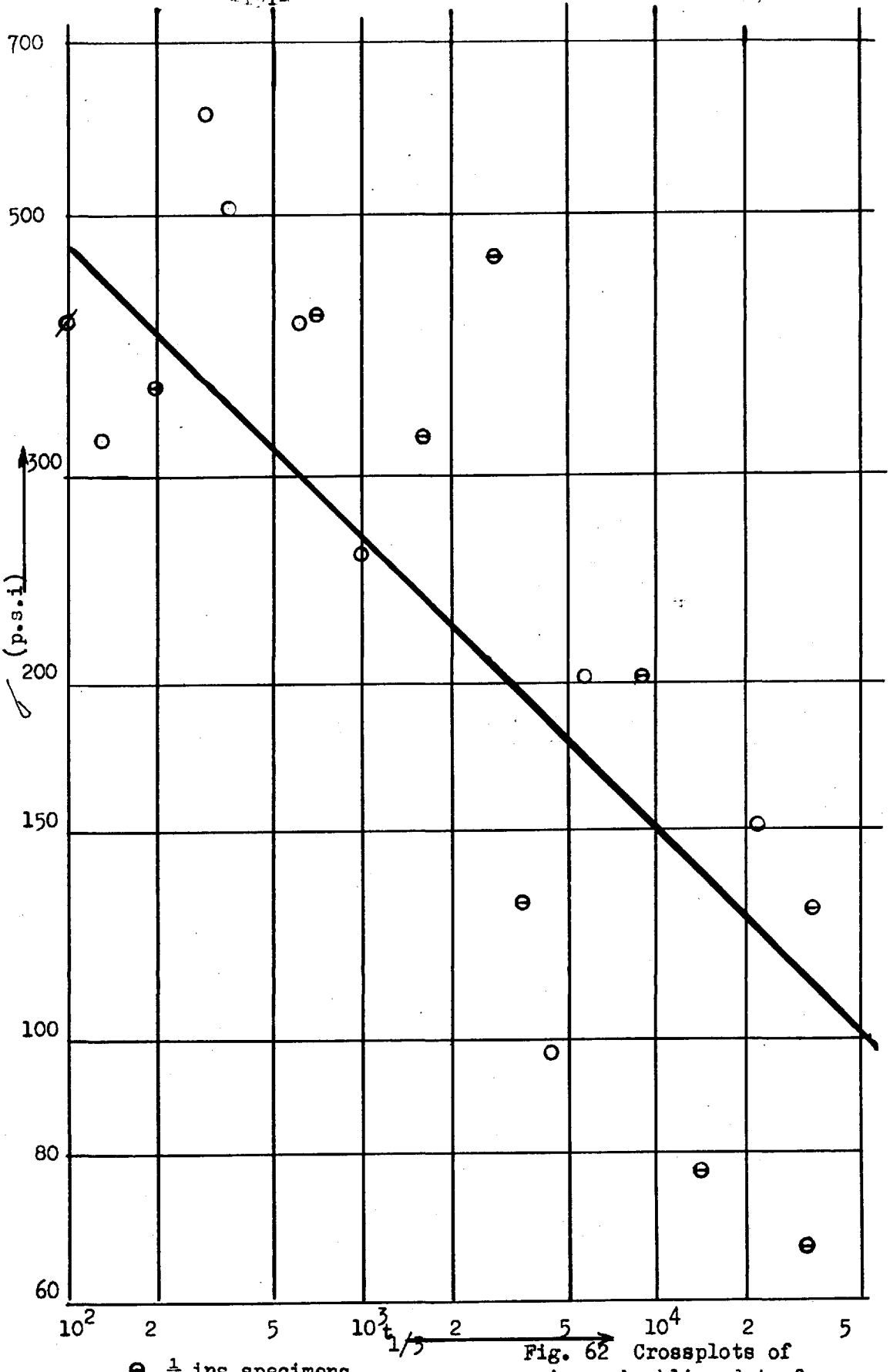


Fig. 59 Calculated effect of eccentricty



Fig. 60 } Showing the buckled rectangular specimen, and the
Fig.61 } minor bow in a cylindrical specimen.

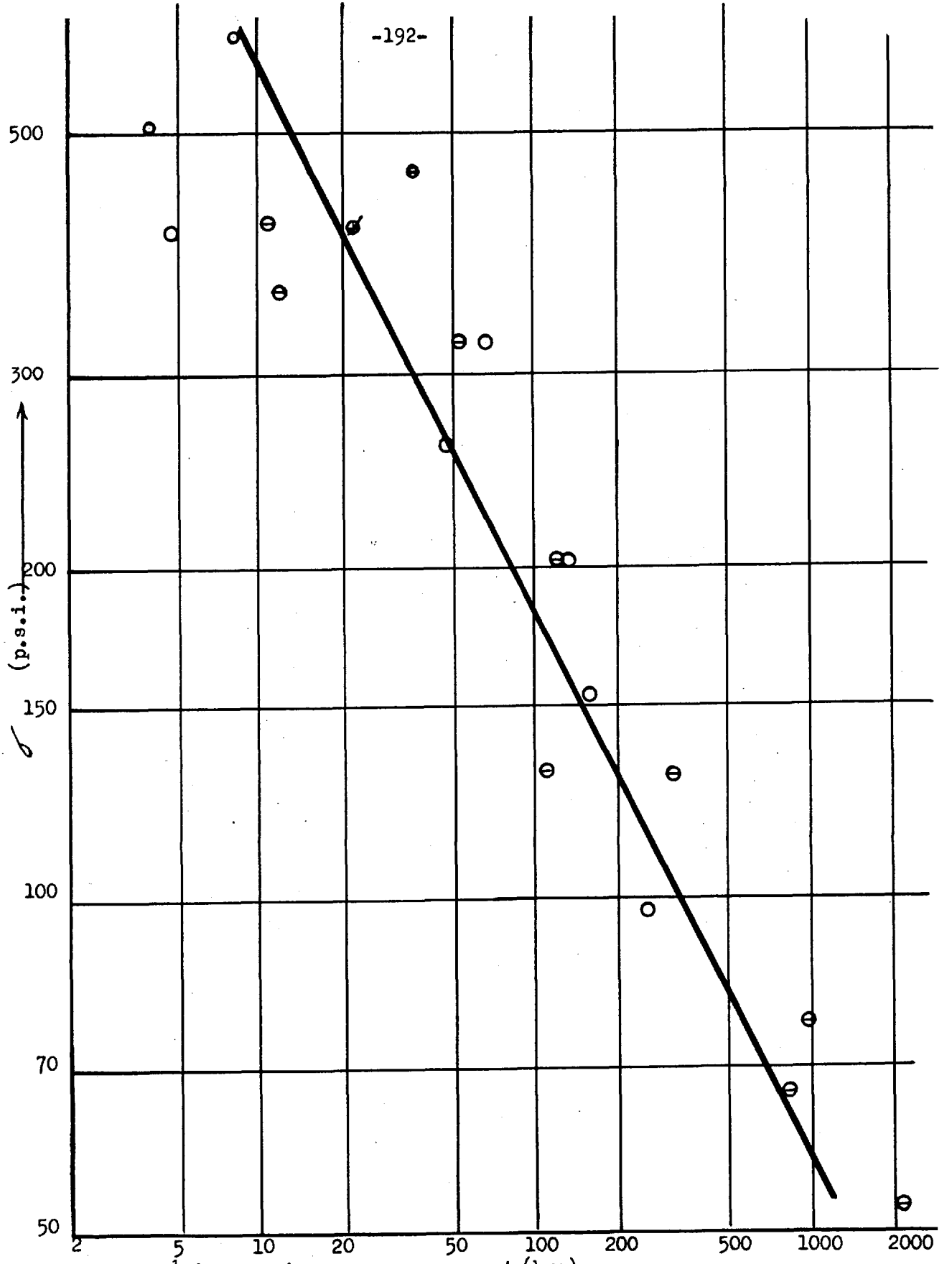


Θ $\frac{1}{2}$ ins specimens

O $\frac{3}{4}$ ins specimens

Ø Calculated for 0.03ins eccentricity.

Fig. 62 Crossplots of primary buckling data for $\frac{\pi^2 I(1-P/P_E)\ln(b_2/b_1)}{AL^2}$ * =.001



⊖ $\frac{1}{2}$ ins specimens

O $\frac{3}{4}$ ins specimens

⌀ Calculated for .03ins eccentricity

Fig. 63 Crossplots of secondary buckling data for $\frac{\pi^2 I(1-P/P_E)\ln(b_2/b_1)}{AL^2}$ = .001

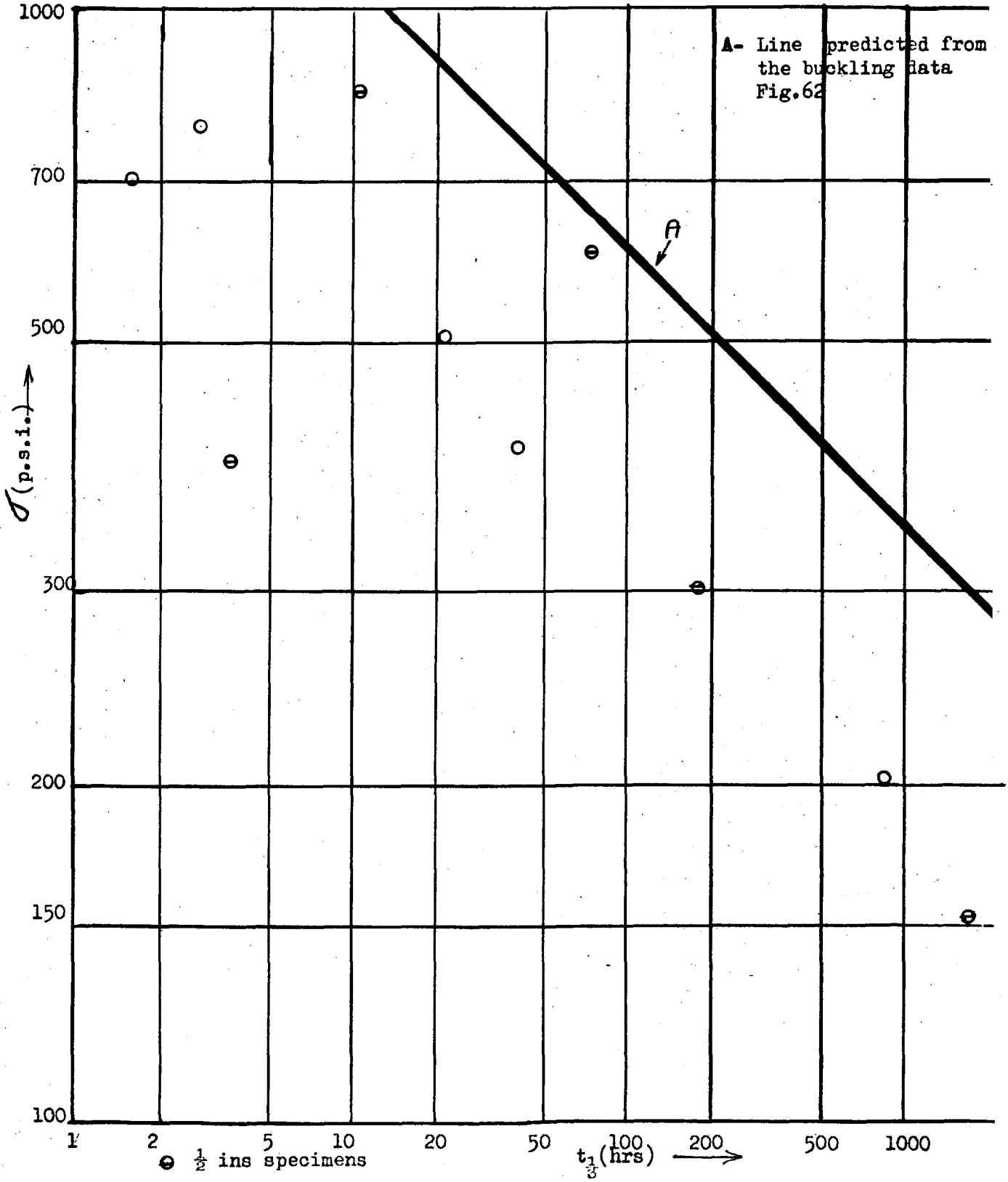


Fig. 64 Crossplot of primary tensile data for ε .001

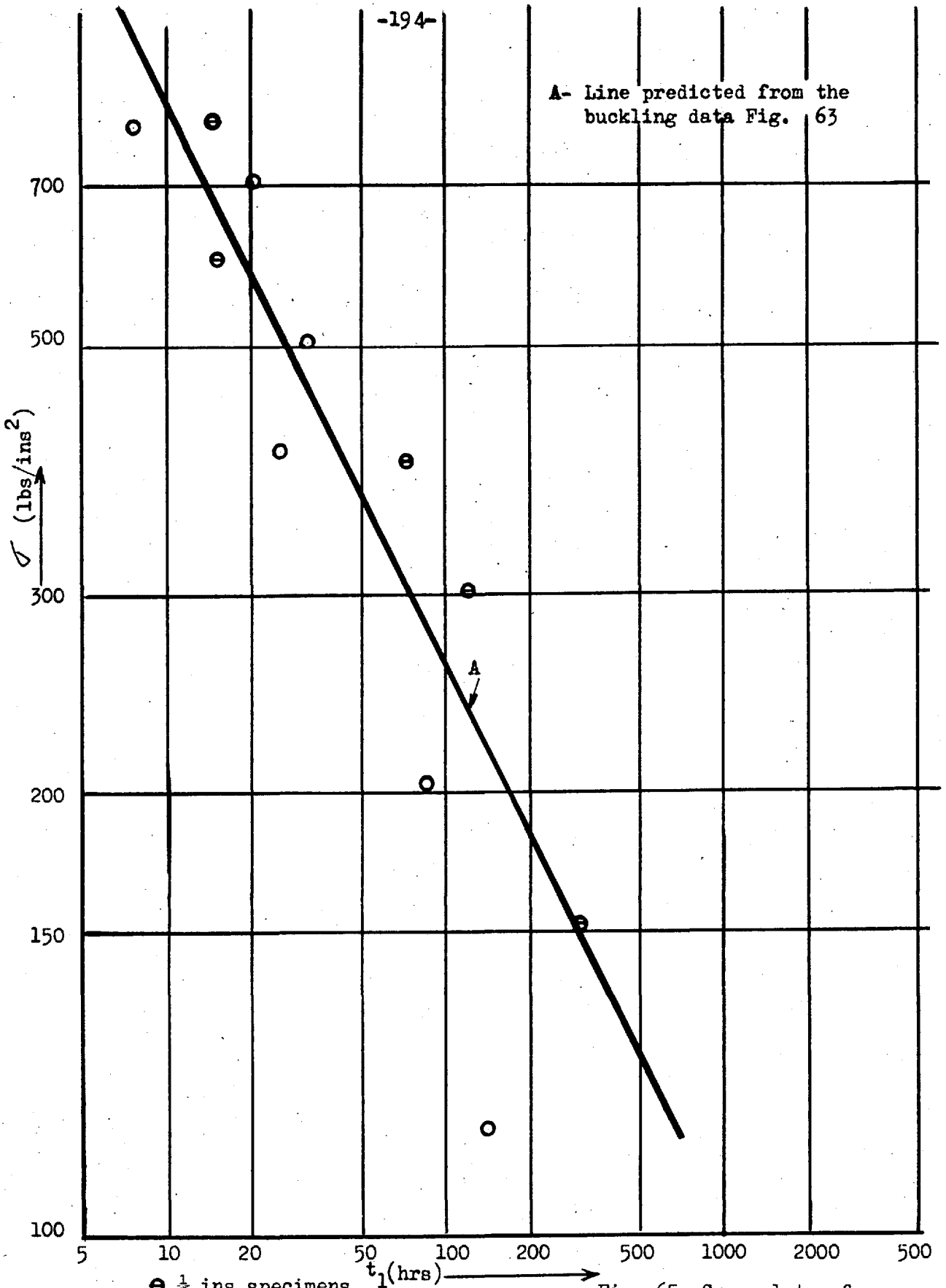
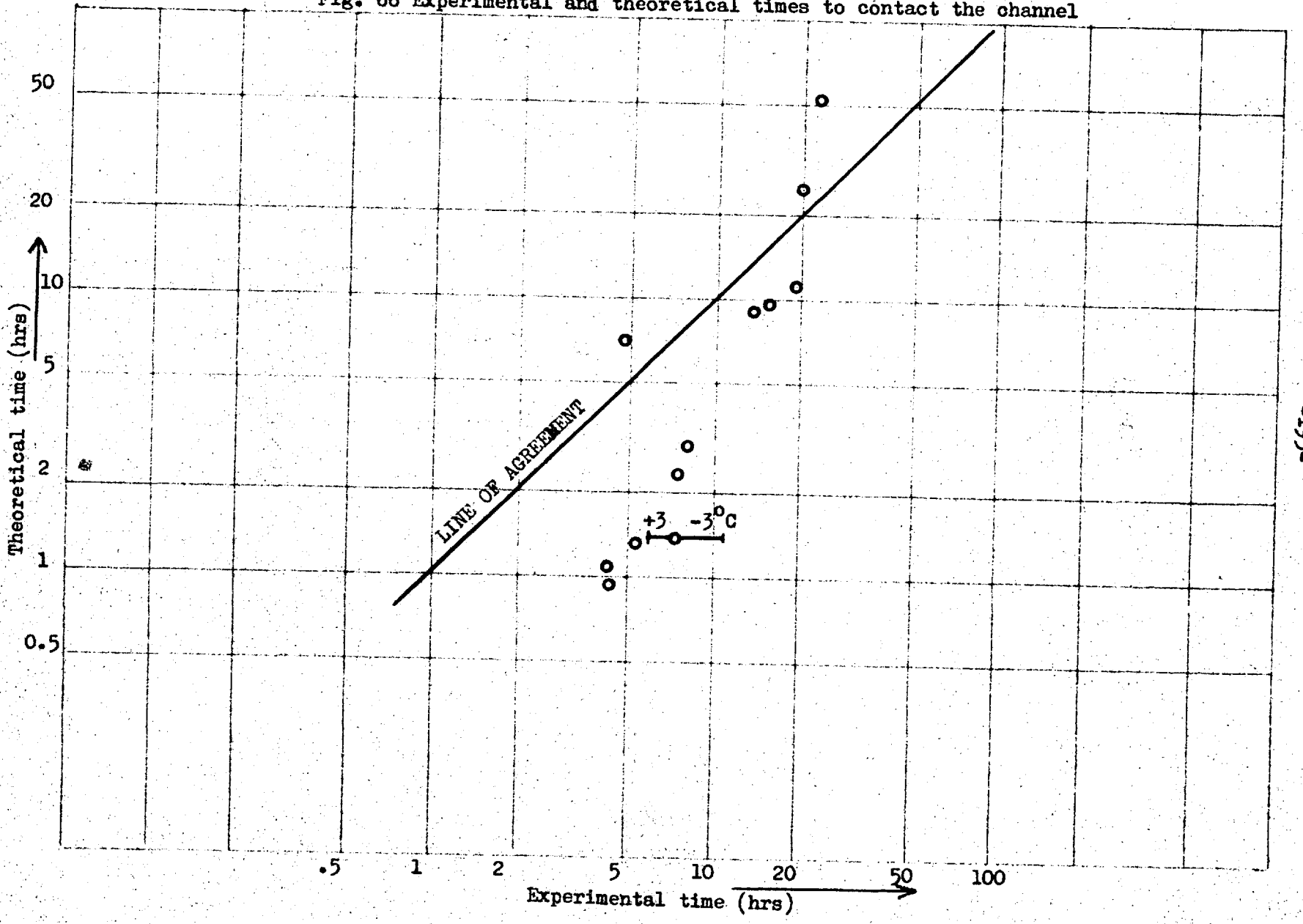


Fig. 65 Crossplots of secondary tensile data for $\dot{\varepsilon}^{*}$ =0.001

Fig. 66 Experimental and theoretical times to contact the channel



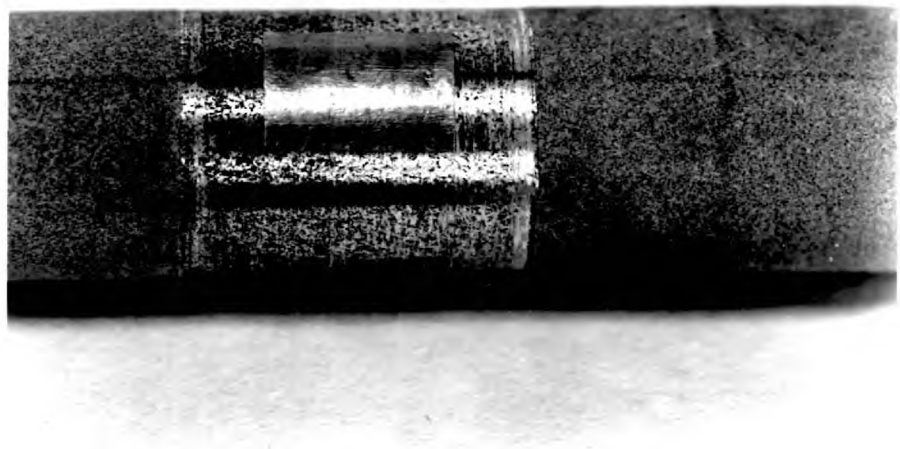


Fig. 67 Showing the nickel foil welded onto the buckling specimen



Fig. 68 Showing the extensometers and transducer assembly.

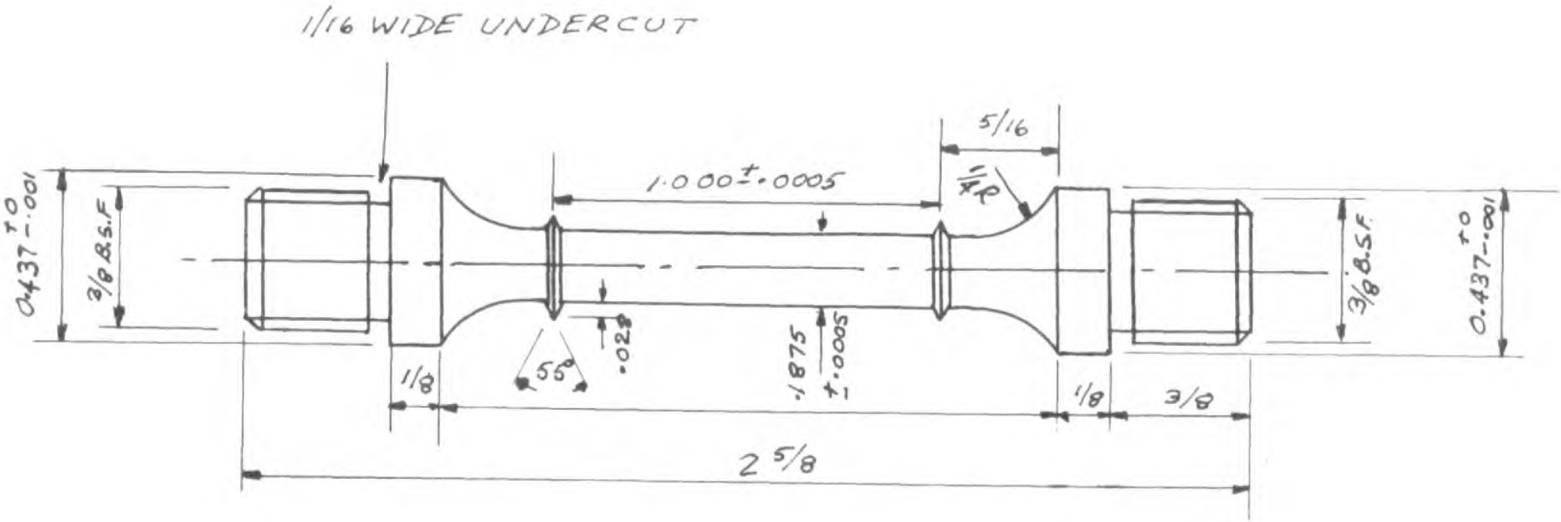
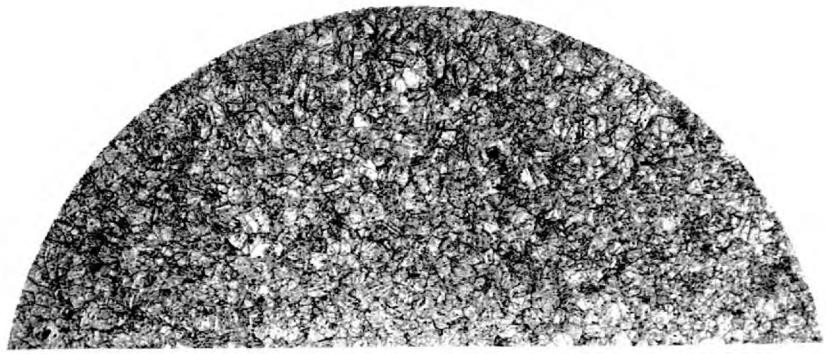
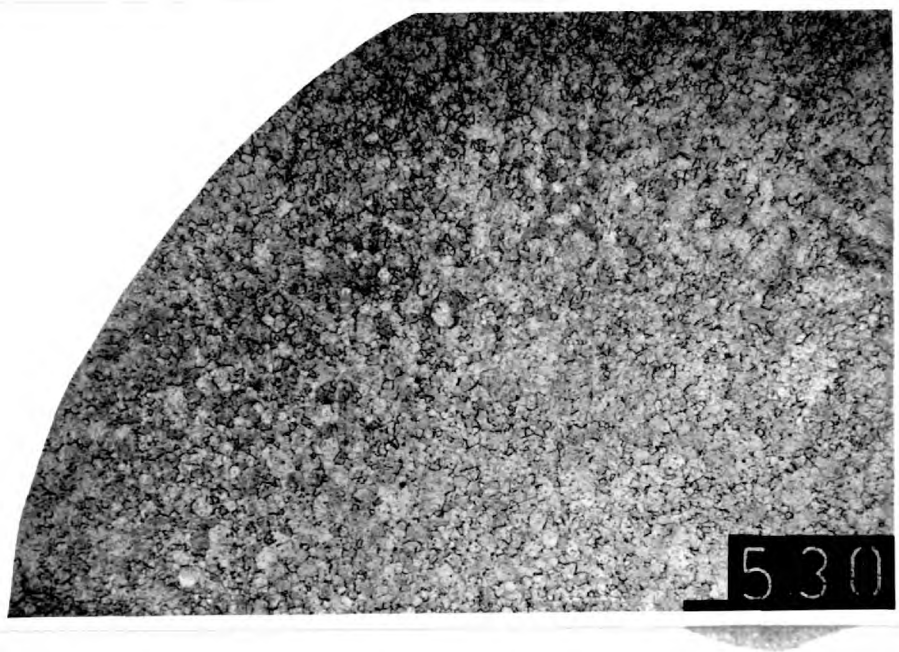


Fig. 69 Drawing of the tensile creep specimen (2x F.S.)



Initial macrostructure ($\frac{1}{2}$ins) x 8



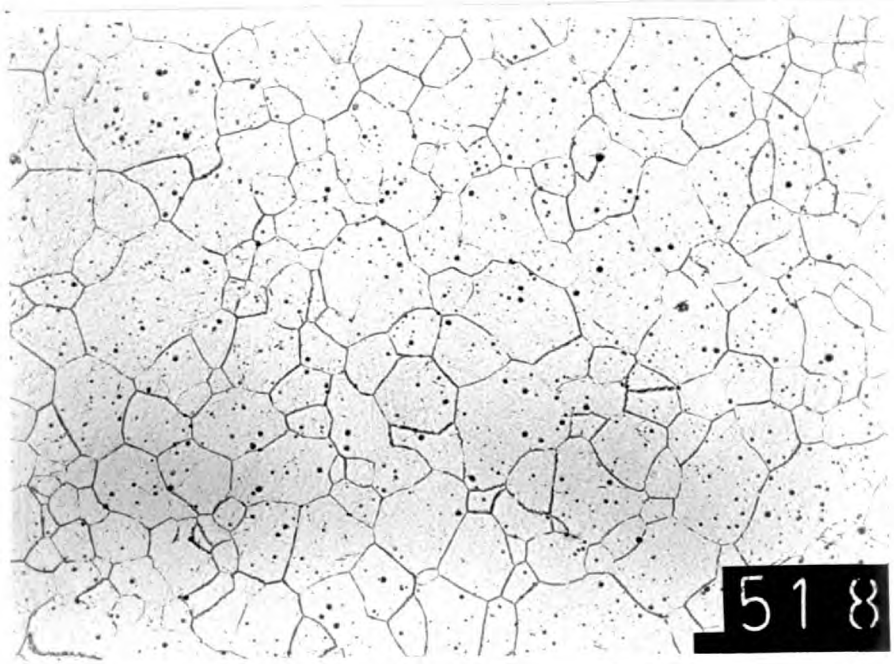
Initial macrostructure ($\frac{3}{4}$ ins) x 8

Fig. 70 Metallography

All specimens electro-polished and -etched in orthophosphoric acid(38 %) and ethyl alchlol (62 %)

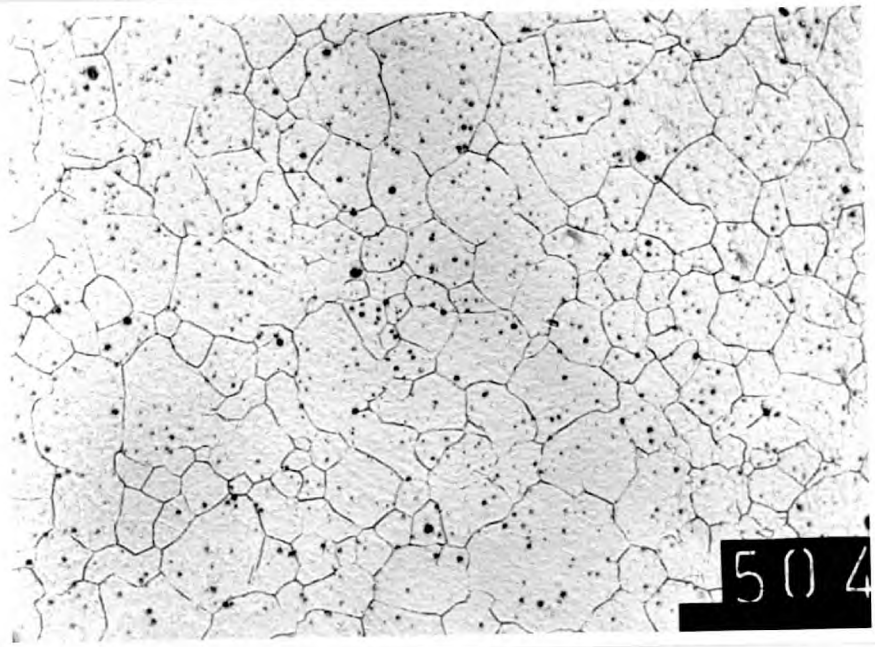


Initial microstructure ($\frac{1}{2}$ ins.) x 60

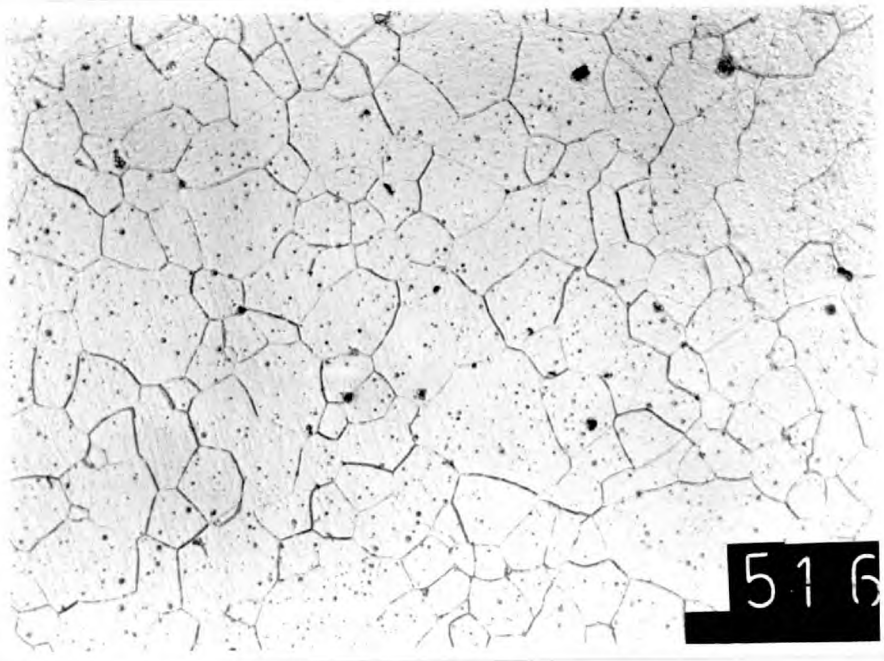


After 24 hours soaking at 295°C ($\frac{3}{4}$ ins) x 60

Fig. 70 Metallography (continued)



After tensile creep test (787 p.s.i.) x 60



After 24 hours soaking at 400°C x 60

Fig. 70 Metallography (Concluded)



Fig. 71 Showing the measuring probe assembly.



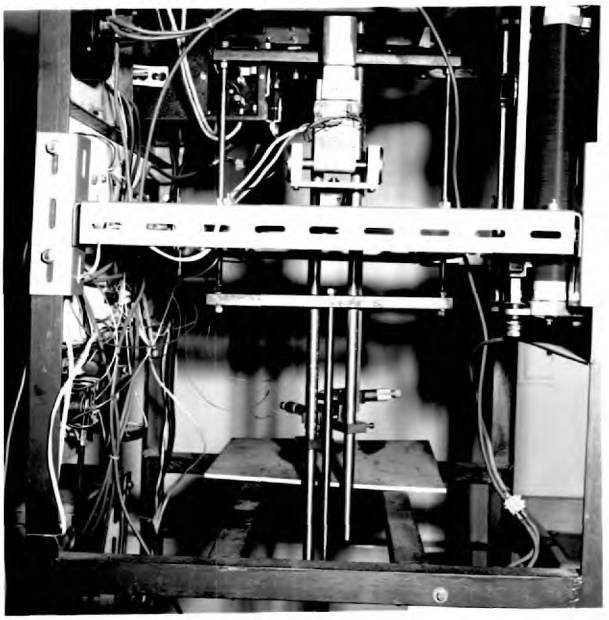
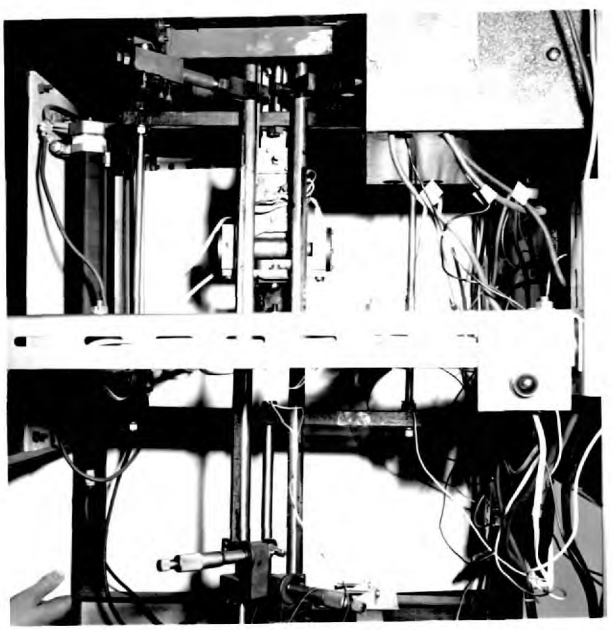


Fig. 72 Operator's view of probe micrometers.



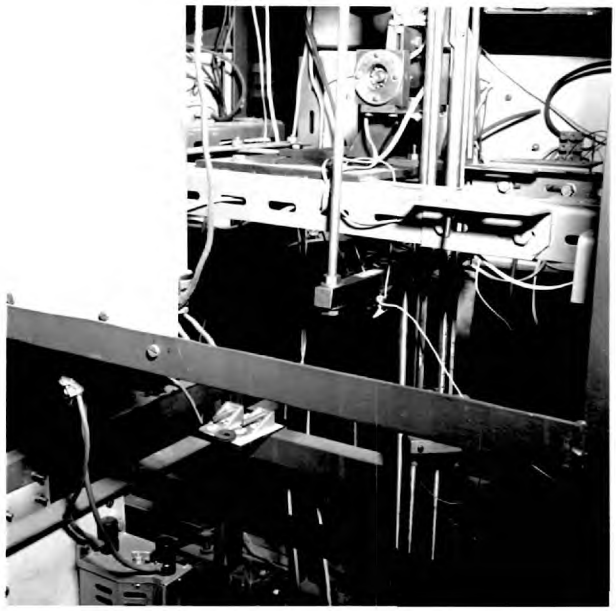
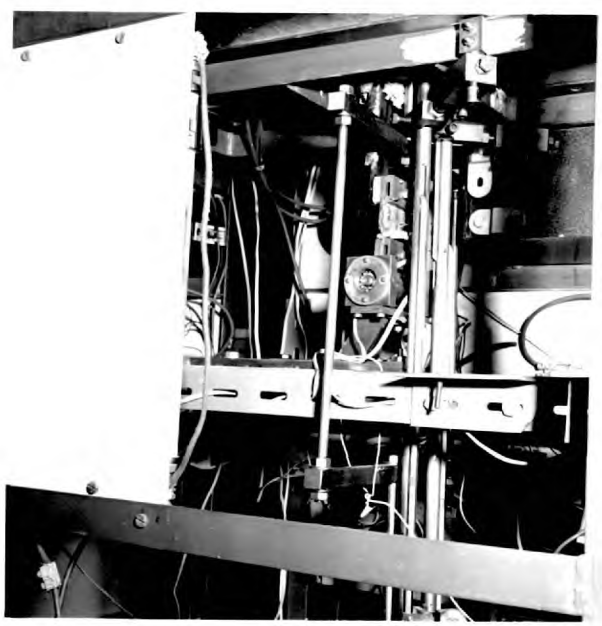


Fig. 73 Channel support assembly



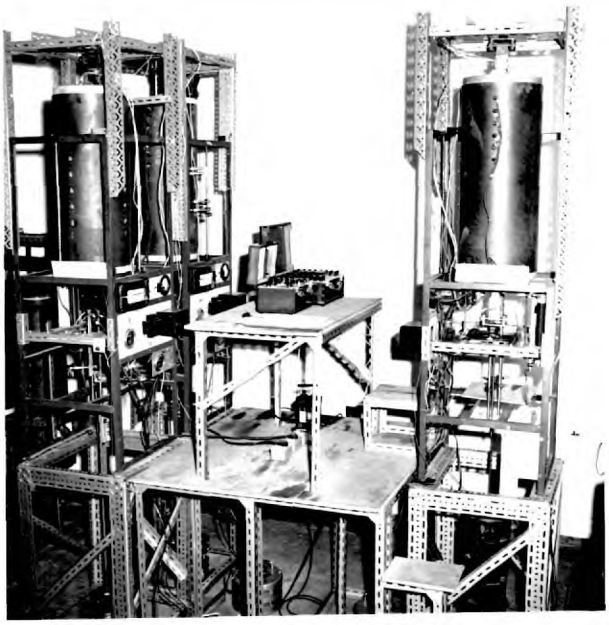


Fig. 74 Overall view of the apparatus.

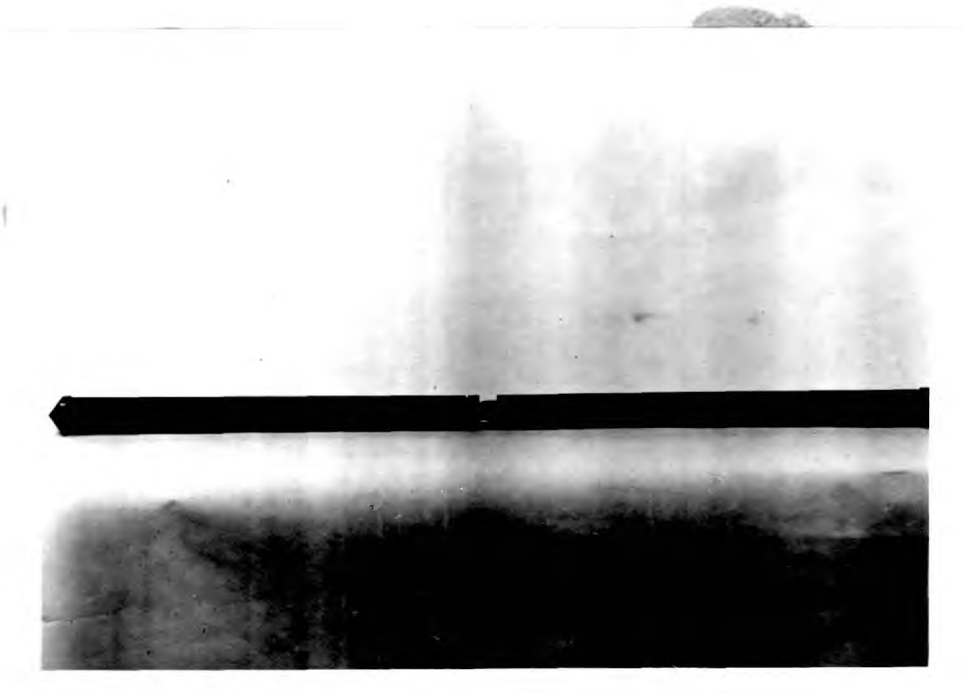


Fig. 75 Force calibrating device .

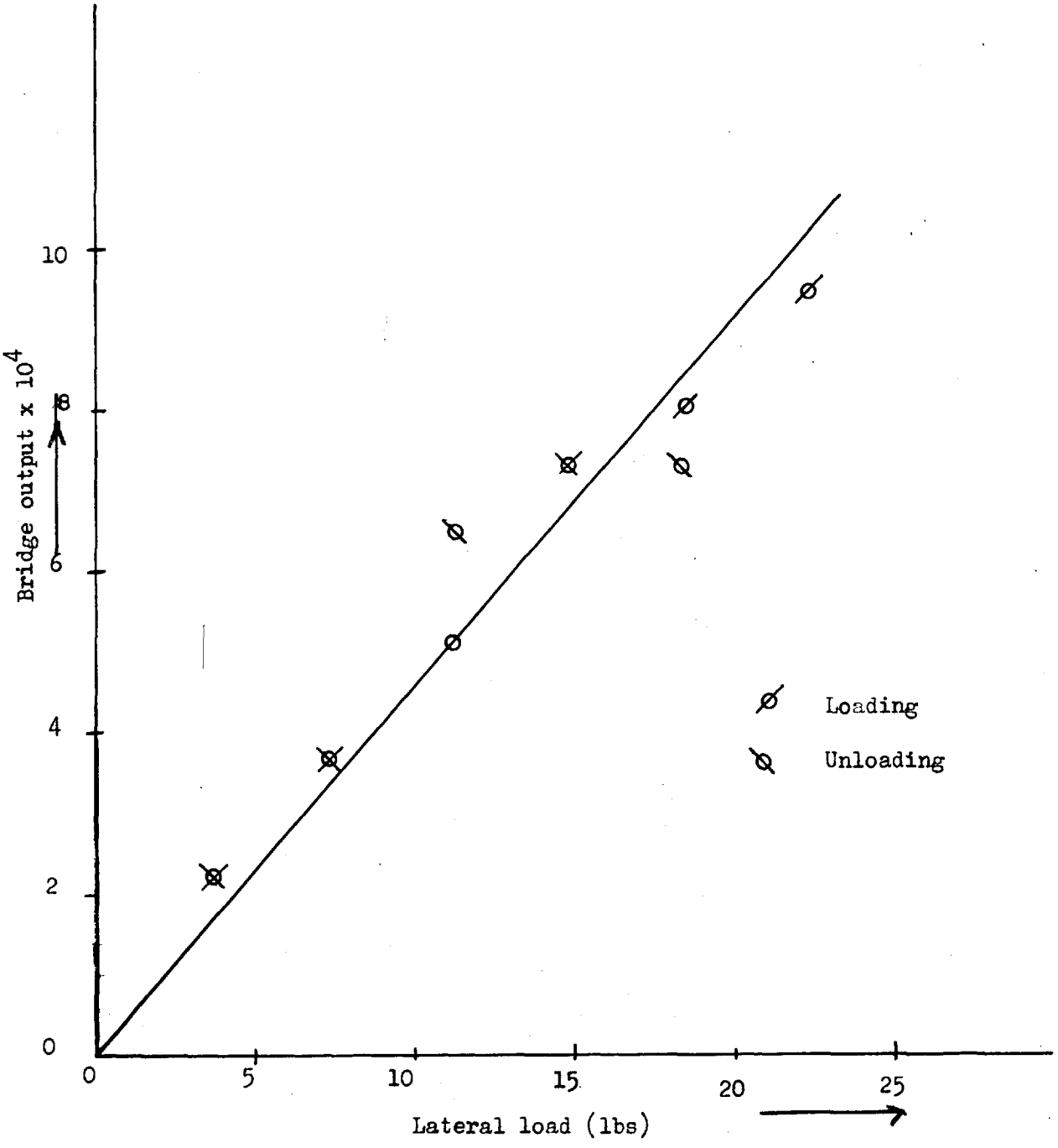


Fig. 76 Hot calibration of force measuring system.

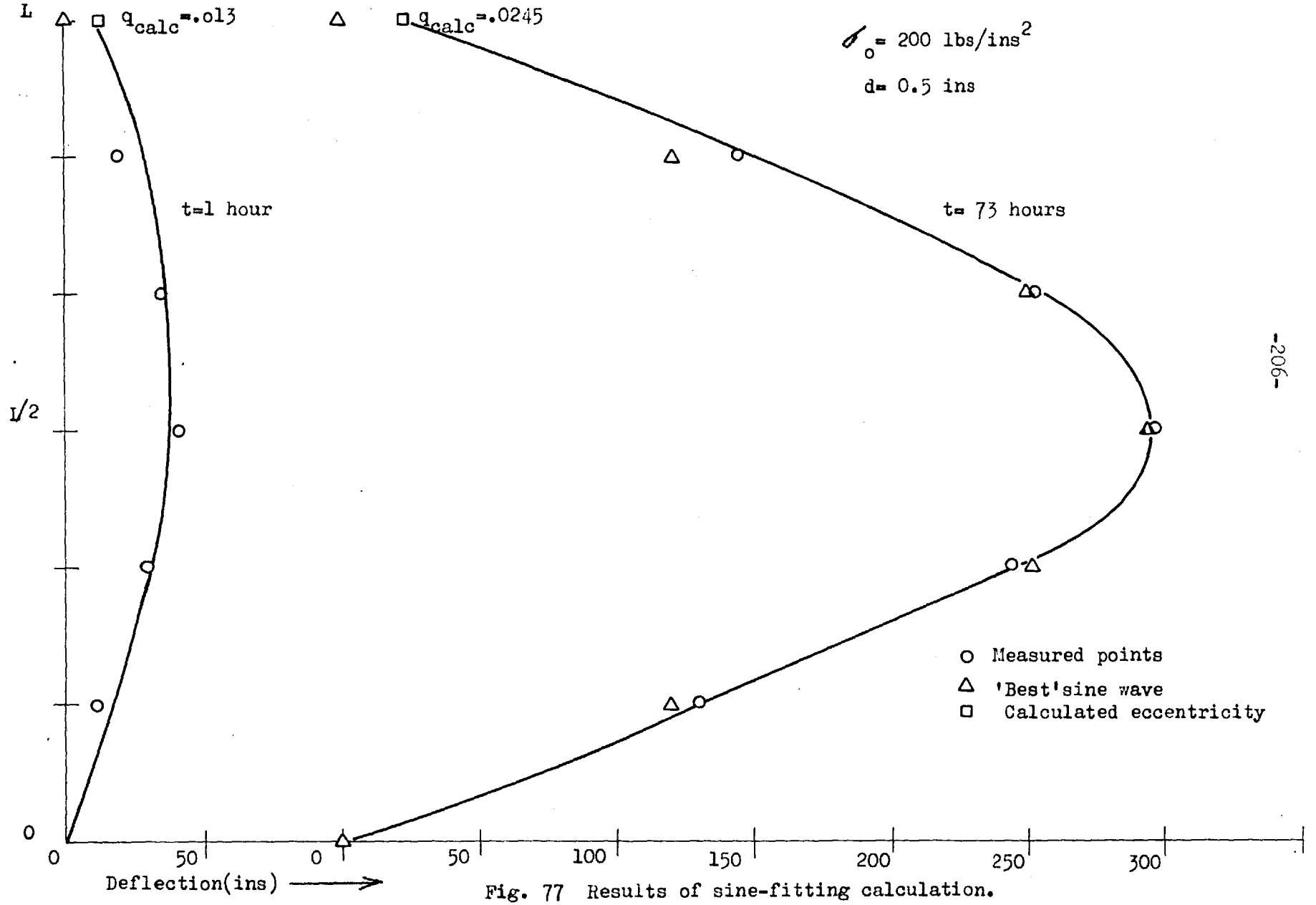


Fig. 77 Results of sine-fitting calculation.

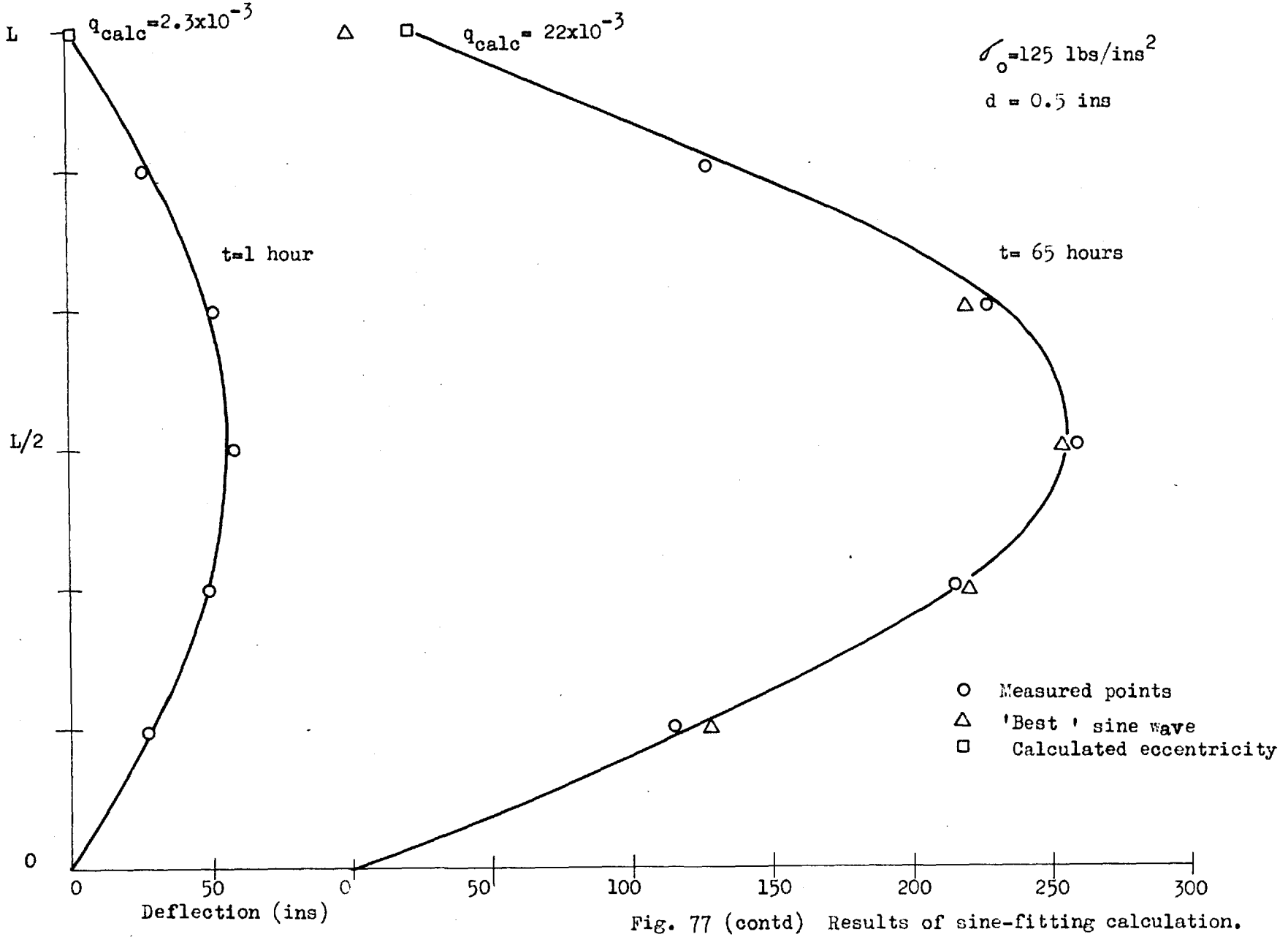


Fig. 77 (contd) Results of sine-fitting calculation.

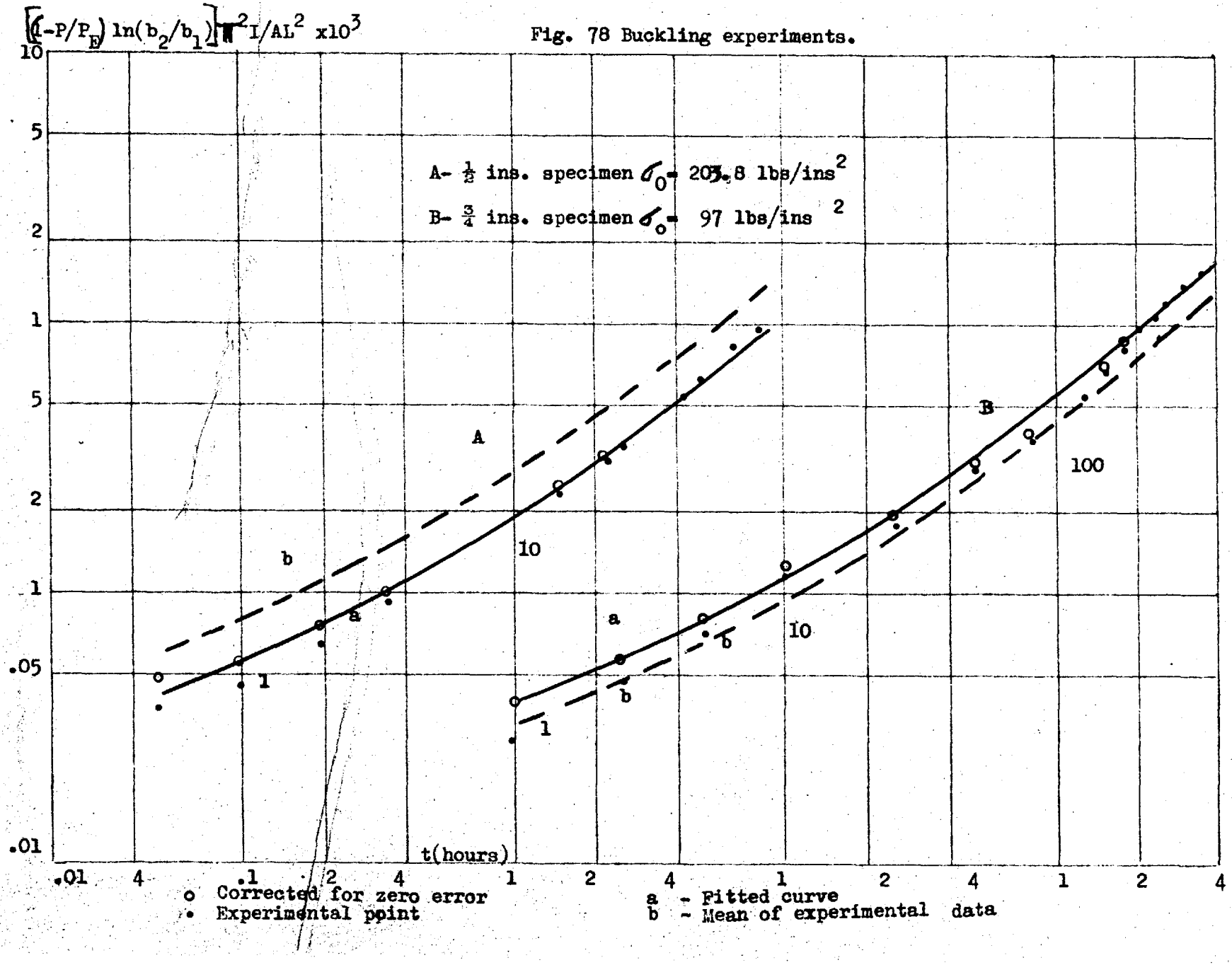


Fig. 78 Buckling experiments.

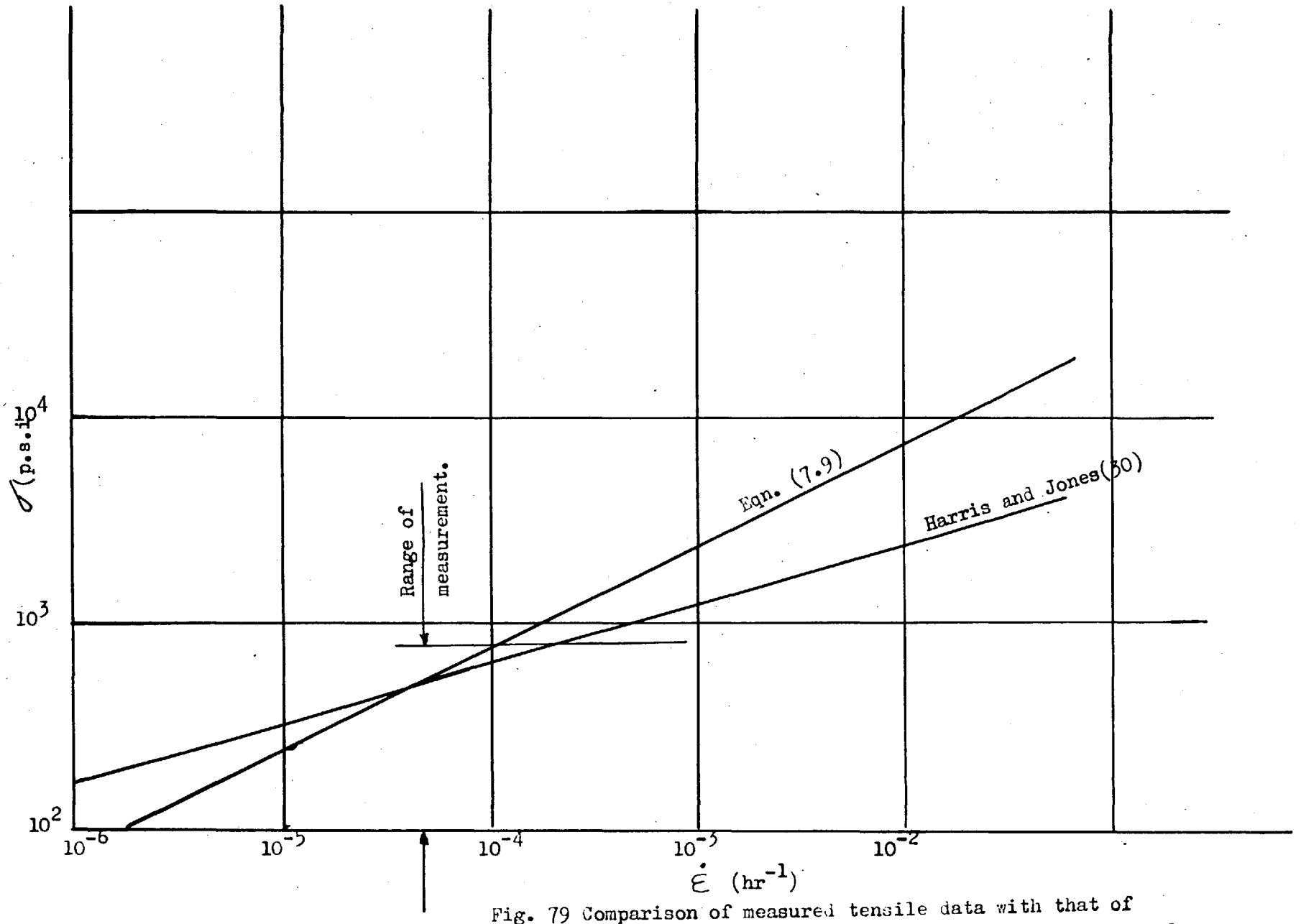
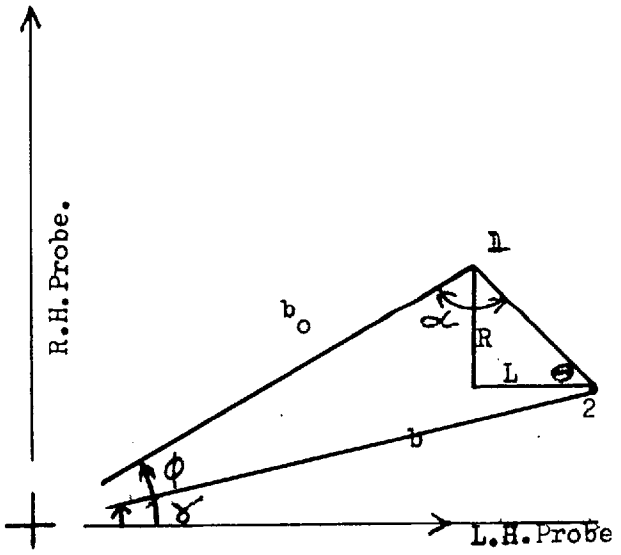


Fig. 79 Comparison of measured tensile data with that of Harris and Jones(30) - secondary creep only.



1 Position after application of the load.

2 Position at some time later.

Fig. 80 Quantities used in the calculation of b .

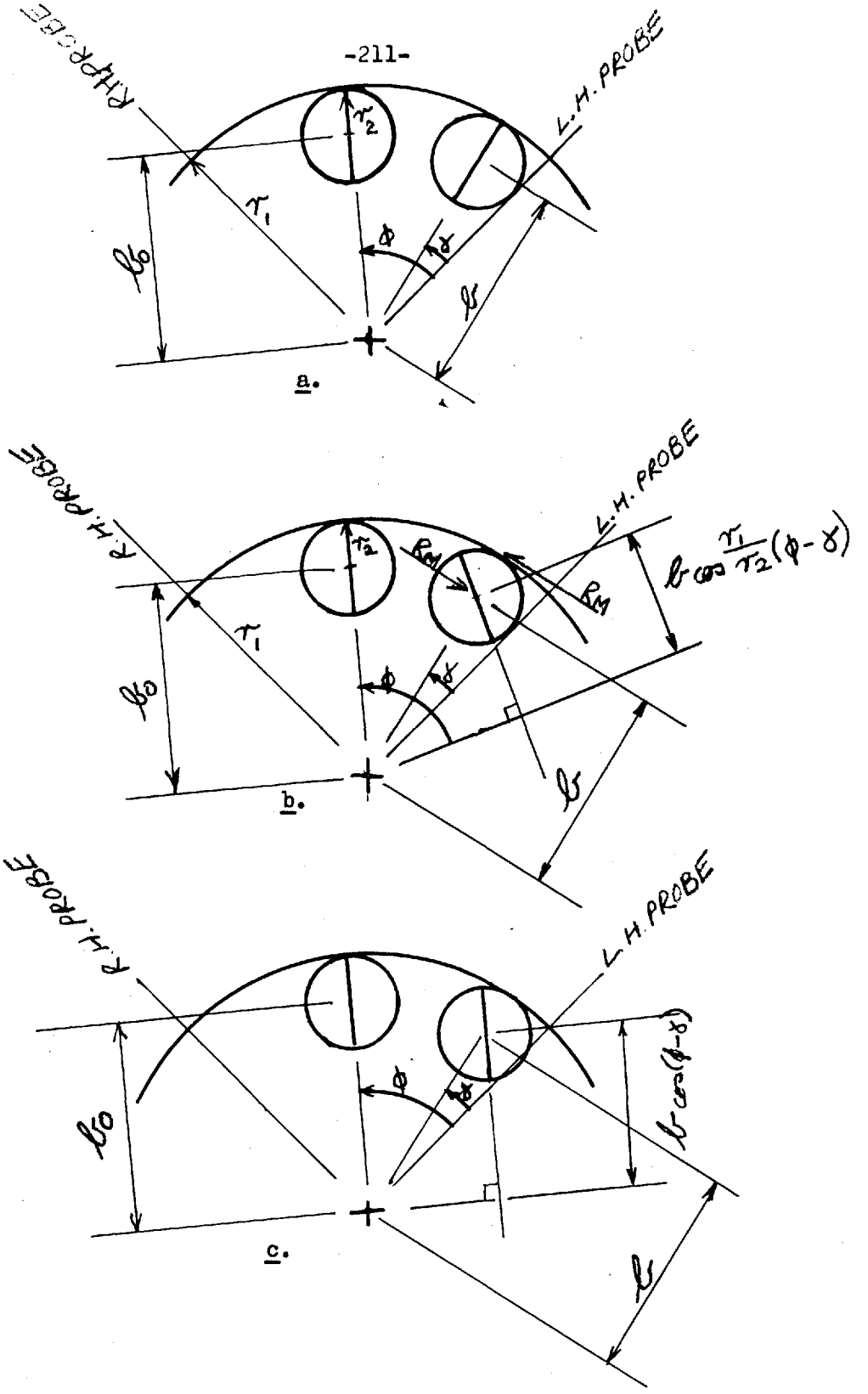
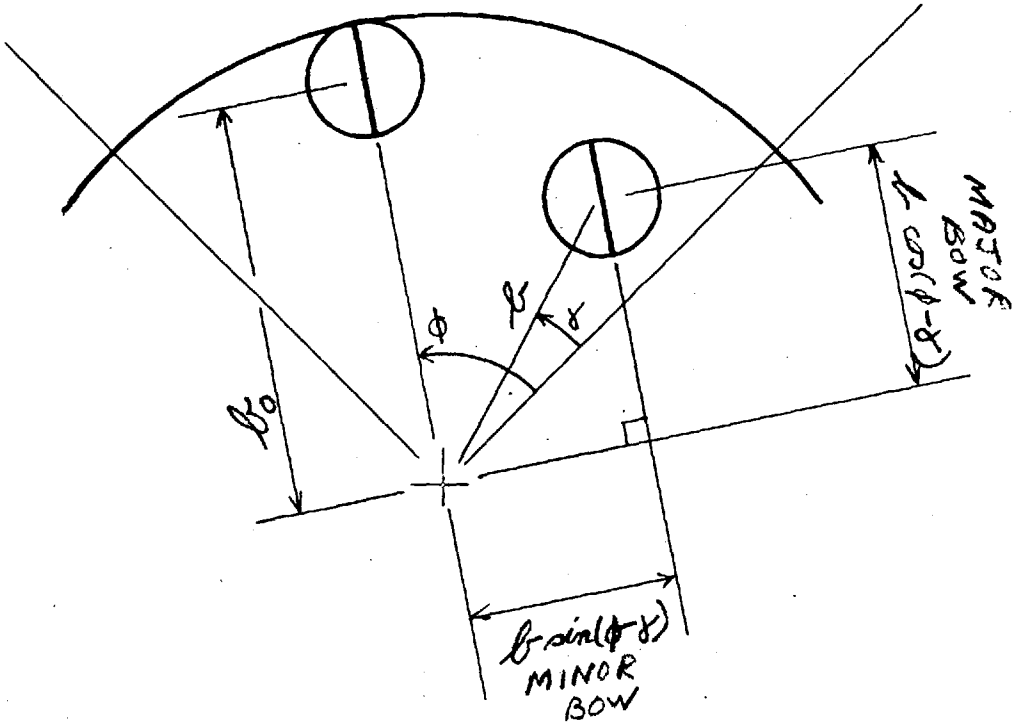


Fig. 81 Three possible interpretations of the rotation of the vector $\underset{\sim}{b}$.



From the figure, maximum clearance for major bow (with a given minor bow) is $\sqrt{1-b^2\sin^2(\phi-\gamma)}$.

For a minor bow, with a given major bow, the maximum clearance is $\sqrt{1-b^2\cos^2(\phi-\gamma)}$.

Fig. 82 Defining major and minor bows.

SMALL-DEFLECTION CREEP BUCKLING OF MAGNESIUM ALLOY (MAGNOX AL80) AT 295°C

By N. H. Freed* and F. Seyna†

The results of creep buckling experiments at 295°C on magnesium alloy specimens of two different diameters were compared with deflection rates predicted from a simple theory proposed by Alexander (1). Agreement was found to be adequate for design purposes, and within the scatter of the material data. The effect of eccentricity was evaluated and it was shown to have a negligible effect on bowing rates.

INTRODUCTION

SOME KNOWLEDGE of the expected creep deformation rates of columns operating at elevated temperatures is necessary in the fields of nuclear and aircraft engineering.

In practice, and particularly in the design of 'Magnox' nuclear power stations, designers are concerned with establishing deformation rates arising from known manufacturing tolerances in situations where the deformation will perforce be small and the cross-sections complex. Alexander (1)‡ showed that by making an approximation to the stress distribution a simple closed-form solution to the steady-state creep problem could be obtained; this was extended in a later paper (2) to include all phases of creep.

An experimental verification of this theory was attempted by Webster and Alexander (3); this showed that although the buckling results were consistent with the theory, effective comparison with measured tensile data was not possible owing to limitations of the latter.

It was therefore felt that the method warranted further study, and the present paper describes some experiments designed to provide more conclusive information. Buckling tests were performed using the apparatus described in reference (3), and these results are compared with predictions from tensile tests using redesigned extensometers. The theory is further evaluated by correlation of the buckling results for specimens of two different diameters, and a theoretical estimate of the effect of measured eccentricities on the data is given.

The MS. of this paper was first received at the Institution on 2nd February 1965 and in its revised form, as accepted by the Council for publication, on 9th April 1965.

* *Research Officer, Atomic Energy Board, Pelindaba, Transvaal, South Africa; presently Department of Mechanical Engineering, Imperial College of Science and Technology, London. Student of the Institution.*

† *Nuclear Research Institute, Warsaw.*

‡ *References are given in Appendix 3.*

Notation

A	Cross-sectional area.
B	$\dfrac{P/P_E}{(\ln 2)(1-P/P_E)}$.
C_1, C_2, C_3	Creep constants.
D	$\dfrac{1}{\pi^2(\ln 2)(1-P/P_E)}$.
E	Young's modulus.
$\dot{E}$	Creep rate modulus.
$\dot{\epsilon}$	Total strain rate.
I	Second moment of area.
K	Rate of change of curvature.
M	Bending moment.
m	Integer locating position in space mesh.
N	Number of space mesh intervals.
n_1, n_2, n_3	Creep constants.
P	Load.
P_E	Euler buckling load.
s	Dimensionless independent space variable.
δs	Finite difference space mesh size.
t	Time in hours.
u	Dimensionless deflection.
v	'Solution time', see equation (27).
δv	Solution time increment.
v^*	Standard value of v.
X	Horizontal force.
x	Distance from origin or neutral axis.
$z, \dot{z}$	Deflection and rate of change of deflection.
z_1, z_2	Initial and current deflection.
δz	Increment in deflection.
δ	Eccentricity.
$\epsilon, \dot{\epsilon}$	Creep strain, creep strain rate.
$\dot{\epsilon}', \dot{\epsilon}''$	First and second derivative with respect to x of $\dot{\epsilon}$.
ϵ^*	Arbitrary standard value of strain.
σ	Stress.

τ Integration variable.
0 Subscript referring to neutral axis.

THEORY

In the following section, the original equations of Alexander (1) are rederived to be compatible with the more usual assumption of a linear total strain distribution.

For the purposes of the analysis we make the simplifying assumption that the creep strain rate $\dot{\epsilon}$ is a function of current stress, temperature and time only*. The total strain rate $\dot{e}$ is assumed to be given by

$$\dot{e} = \frac{\dot{\sigma}}{E} + \dot{\epsilon} \quad . \quad . \quad . \quad . \quad . \quad (1)$$

From the condition that plane sections remain plane we have the additional relation

$$\dot{e} = \dot{\epsilon}_0 + \dot{K}x \quad . \quad . \quad . \quad . \quad (2)$$

The first approximation to be made is that the stress distribution, which is in practice non-linear, can be represented by the familiar linear relationship

$$\sigma = \frac{Mx}{I} + \sigma_0 \quad . \quad . \quad . \quad . \quad (3)$$

and it also follows that

$$\dot{\sigma} = \frac{\dot{M}x}{I} \quad . \quad . \quad . \quad . \quad . \quad (4)$$

The accuracy of this approximation can be assessed by comparison with the analytical solution for a rectangular column deforming by secondary creep only. This calculation is given in Appendix 1, where it is shown that agreement with the analytical solution is within 3 per cent. Similarly, good agreement was obtained by Alexander (1) from calculations on a cylindrical shell. Equating equations (1) and (2) and substituting from equation (4) we have

$$\frac{\dot{M}x}{EI} + \dot{\epsilon} = \dot{\epsilon}_0 + \dot{K}x \quad . \quad . \quad . \quad (5)$$

from which

$$\dot{K} = \frac{\dot{M}}{EI} + \frac{\dot{\epsilon} - \dot{\epsilon}_0}{x} \quad . \quad . \quad . \quad . \quad (6)$$

Now $\dot{\epsilon} = \dot{\epsilon}(\sigma, t) = \dot{\epsilon}(x, t)$

$$= \dot{\epsilon}(0, t) + \dot{\epsilon}'(0, t)x + \dot{\epsilon}''(0, t)x^2/2 + \cdots \quad (7)$$

For consistency with equation (6) we neglect terms of the second order and higher: this will be a reasonable approximation in general. Substituting this result in equation (6)

$$\dot{K} = \frac{\dot{M}}{EI} + \dot{\epsilon}'(0, t) \quad . \quad . \quad . \quad . \quad (8)$$

Now $$\dot{\epsilon}'(x, t) = \frac{\partial \dot{\epsilon}}{\partial x} = \frac{\partial \dot{\epsilon}}{\partial \sigma}\frac{\partial \sigma}{\partial x}$$

Substituting from equation (3)

$$\dot{\epsilon}'(0, t) = \left(\frac{\partial \dot{\epsilon}}{\partial \sigma}\right)_0 \frac{M}{I} \quad . \quad . \quad . \quad (9)$$

* *This approximation was found by Johnson et al. (4) to give reasonably good predictions for eccentrically loaded columns.*

The second assumption is that $(\partial\dot{\epsilon}/\partial\sigma)_0$ can be evaluated from constant stress isochronous stress–strain rate data, evaluated at the mean stress. Alexander (1) called this quantity $1/\dot{E}$, where $\dot{E}$ is the 'creep rate modulus'. Rewriting equation (8) we find

$$\dot{K} = \frac{\dot{M}}{EI} + \frac{M}{\dot{E}I} \quad . \quad . \quad . \quad . \quad (10)$$

This equation† can be used for problems in which there is a finite stress on the geometrically neutral axis.

Using equation (10), assuming a sinusoidal shape and small deflections, we arrive at the same equation as Webster and Alexander (3), namely

$$\left(1 - \frac{P}{P_E}\right)\frac{\pi^2 I}{PL^2} \ln\left(\frac{z_2}{z_1}\right) = \int_0^t \frac{d\tau}{\dot{E}(\tau)} \quad . \quad (11)$$

The assumed creep law, based on the work of Graham and Walles (5) (6) is

$$\epsilon = C_1\sigma^{n_1}t^{1/3} + C_2\sigma^{n_2}t + C_3\sigma^{n_3}t^3 \quad . \quad (12)$$

Now

$$1/\dot{E} = \left(\frac{\partial \dot{\epsilon}}{\partial \sigma}\right)_0 = \frac{n_1}{3}C_1{\sigma_0}^{n_1-1}t^{-2/3} + n_2C_2{\sigma_0}^{n_2-1} + 3n_3C_3{\sigma_0}^{n_3-1}t^2 \quad (13)$$

Substituting in equation (11) and integrating, we have

$$\left(1 - \frac{P}{P_E}\right)\frac{\pi^2 I}{PL^2} \ln\left(\frac{z_2}{z_1}\right) = n_1C_1{\sigma_0}^{n_1-1}t^{1/3} + n_2C_2{\sigma_0}^{n_2-1}t + n_3C_3{\sigma_0}^{n_3-1}t^3 \quad (14)$$

Therefore

$$\left(1 - \frac{P}{P_E}\right)\frac{\pi^2 I}{AL^2} \ln\left(\frac{z_2}{z_1}\right) = n_1C_1{\sigma_0}^{n_1}t^{1/3} + n_2C_2{\sigma_0}^{n_2}t + n_3C_3{\sigma_0}^{n_3}t^3 \quad (15)$$

It will be noted that the form of equations (12) and (15) is similar, and it is possible to use the Graham–Walles (5) (6) method of graphical analysis to correlate the data and determine the material constants.

DESCRIPTION OF EXPERIMENTS

Creep buckling

The techniques and apparatus were identical to those described in reference (3), using 18-in long magnox AL80 specimens, of $\frac{1}{2}$ in and $\frac{3}{4}$ in diameter; all specimens were selected from the middle of the extrusion. The tests were performed with the material in the 'as-extruded' condition, the specimens being machined in each case from bars twice the final diameter. A temperature distribution of 295±1°C was maintained along the length of the specimen by means of a three-zone furnace, and increments in deflections were measured to ±0·0005 in using micrometer probes and an electrical contact system. As described in (3), the specimens were given an initial bow of

† *This is to be compared with equation (7) of reference (3) in the derivation of which elastic strains were neglected.*

Table 1. *Test stresses and P/P_E ratios*

a Buckling experiments

Diameter, in	Mean stress, lb/in²	P/P_E
0·5	52·2	0·0256
	66·9	0·0327
	77·2	0·0378
	129·2	0·063
	131·3	0·064
	203·8	0·096
	324·3	0·159
	359·4	0·176
	413·2	0·202
	461·1	0·226
0·75	97·5	0·0219
	152·9	0·0344
	202·9	0·0455
	258·8	0·0582
	322·2	0·0725
	407·3	0·0916
	509	0·114
	612·6	0·138

b Tensile tests

Original diameter, in	Stress, lb/in²
0·5	152·2
	300·7
	393·6
	601·1
	797·1
0·75	99·5
	202·7
	401·8
	505
	704
	787

0·020–0·030 in, and a 24-hour soaking at test temperature before application of load.

The tests were continued until a bow of 0·3 in was attained. The test stresses and P/P_E ratios are given in Table 1.

Tensile creep

The magnox specimens, 0·187 in diameter × 1 in gauge length, were machined with 0·030 in ridges at each end of the gauge length to accommodate the extensometers*; this provided an easily and accurately reproducible gauge length which could be manufactured to a surface finish of 25 μ on an automatic lathe. Specimens were machined from both the $\frac{3}{4}$ in and $\frac{1}{2}$ in bars. The testing was performed in $\frac{3}{4}$-ton Denison machines, fitted with three-zone furnaces and saturable reactor controllers; the test temperature of 295±1°C was monitored by three thermocouples along the length of the specimen. Extension was measured autographically by differential transformers with a nominal stability of ±5 μ.

* *This design is based on that developed at the National Gas Turbine Establishment, Pyestock, Hants.*

The experiments were continued for a maximum of 1000 hours or until approximately 1 per cent strain was reached. Details of test stresses are given in Table 1.

MEASUREMENT OF YOUNG'S MODULUS

The technique described in (3) (which measured initial elastic deflections) for the measurement of E at the test temperature was not found to be reliable, owing to the considerable effect of specimen—and loading system—rotation; it was also considered that the elastic deflections were too small to be measured accurately.

Accordingly a method was devised using the tensile creep extensometers and replacing the standard recording equipment with a fast (0·5 second) potentiometric recorder. Incremental loading was used, and the record showed that it was easily possible to differentiate between the instantaneous elastic strain and the subsequent creep strain; this was possible even at the highest stress level reached—2000 lb/in².

Twenty tests were performed at 295°C on specimens machined from both bar sizes. There was no difference between the bars, and a result of $4{\cdot}1 \pm 0{\cdot}2 \times 10^6$ lb/in² was obtained. This was significantly different from the value quoted in (3) for the same nominal temperature, namely $3{\cdot}2 \times 10^6$ lb/in².

ECCENTRICITY

It was thought necessary to evaluate possible errors arising from eccentricity, as the method of alignment of the loading system was somewhat subjective. This was done at room temperature using a modified Southwell plot (7)†. Reproducible results were only obtainable when the loading system and specimen were carefully maintained in the same position, but this is not possible during an actual buckling experiment. Rotation in the 'cup and cone' end fittings occurs owing to out-of-plane bending moments arising from eccentricity and small third dimensional effects in the initial shape. It did not therefore seem worth while to attempt to adjust the eccentricity on the basis of the measurements, as a rotation of the specimen of ±60° produced variations in eccentricity of ±0·030 in about a mean of 0·030 in. It was difficult to reconcile the large values of eccentricity with known manufacturing tolerances and expected errors in centring. No satisfactory explanation for their magnitude could be found. The tests were performed with the specimen initially in the position of 0·030 in eccentricity.

ANALYSIS OF RESULTS

Tensile and buckling data

The similarity between equations (12) and (15) enables Graham–Walles techniques to be used to determine the

† *As described in reference (7) an expression can be derived relating load and elastic increments of deflection, for an eccentrically loaded column having an initial curvature. From a plot of deflection versus deflection/load the eccentricity and critical load can be ascertained. The equations were modified in this case to take account of the pre-loading due to the weight of the loading system.*

constants in these equations. The method provides in addition a convenient way of comparing the buckling and tensile data.

The equations are rewritten in the form

$$\frac{\epsilon}{\epsilon^*} = \left(\frac{t}{t_{1/3}}\right)^{1/3} + \left(\frac{t}{t_1}\right) + \left(\frac{t}{t_3}\right)^3$$

where $t_{1/3}$, t_1 and t_3 are the time in which each term contributes the standard strain ϵ^*, chosen arbitrarily as 10^{-3}, or in the buckling data a standard value of

$$\left(1-\frac{P}{P_E}\right)\frac{\pi^2 I}{AL^2}\ln\left(\frac{z_2}{z_1}\right)^*$$

The values of $t_{1/3}$, t_1 and t_3 corresponding to each stress are found by plotting log strain or

$$\log\left[\left(1-\frac{P}{P_E}\right)\frac{\pi^2 I}{AL^2}\ln\left(\frac{z_2}{z_1}\right)\right]$$

against log time and then fitting a standard curve. Typical buckling curves are shown in Fig. 1. As the initial portion of the curve is extremely sensitive to error, it is permissible to apply a correction to improve the fit in some cases. This correction is random and invariably small in comparison with experimental accuracy: a correction is illustrated in Fig. 1.

The values of $t_{1/3}$ and t_1 thus obtained are cross-plotted against stress as shown in Figs 2–5. The straight lines fitted to Figs 2 and 3 are the best least squares fit with the Graham–Walles standard slopes for $-\frac{1}{4}$ for $t_{1/3}$ and $-\frac{1}{2}$ for the t_1 lines. No tertiary creep was observed in the experiments. The lines fitting the tensile creep data of Figs 4 and 5 have been omitted for clarity but the accuracy of the fit can be gauged by reference to Table 2. According to equations (12) and (15), the data shown in Figs 2 and 4, 3 and 5 should be directly comparable when the buckling data are adjusted for the constants n_1 and n_2 in equation (15). This has been done and the lines drawn in Figs 4 and 5 represent uniaxial creep data as predicted from the buckling experiments.

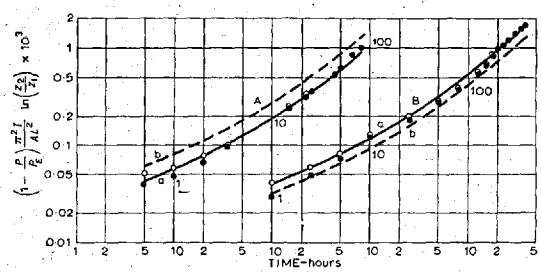
From the tensile data given in these figures, it was found that the creep equation for magnox at 295°C is

$$\epsilon = 1{\cdot}03\times10^{-7}\sigma^{4/3}t^{1/3} + 1{\cdot}66\times10^{-10}\sigma^2 t \quad (16)$$

The predictions from the buckling experiments (the lines shown in Figs 4 and 5) give

$$\epsilon = 0{\cdot}416\times10^{-7}\sigma^{4/3}t^{1/3} + 1{\cdot}51\times10^{-10}\sigma^2 t$$

* *The actual parameter used was* $\frac{\pi^2 I}{AL'^2}\left[\ln\left(\frac{z_2}{z_1}\right)\right]\left(0{\cdot}936-\frac{P}{P'_E}\right)$; *this incorporates a correction for the end fittings. Where* L' *and* P'_E *refer to the actual length excluding the fittings.*



A ½-in specimen 203·8 lb/in² mean stress.
B ¾-in specimen 97 lb/in² mean stress.
a Actual experimental curve.
b Predicted from mean experimental data.
○ Corrected for zero error.
● Experimental point.

Fig. 1. *Buckling experiments:* $\log\left[\left(1-\frac{P}{P_E}\right)\frac{\pi^2 I}{AL^2}\ln\left(\frac{z_2}{z_1}\right)\right]$ *versus log time*

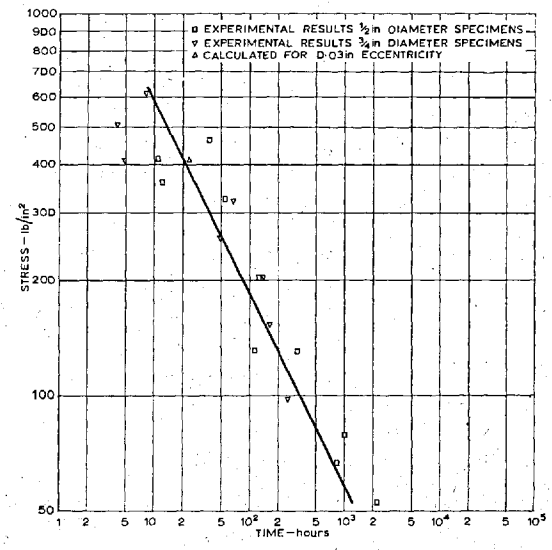


Fig. 2. *Buckling experiments: log stress versus* $\log t_1$ *for* $\left(1-\frac{P}{P_E}\right)\frac{\pi^2 I}{AL^2}\ln\left(\frac{z_2}{z_1}\right) = 0{\cdot}001$

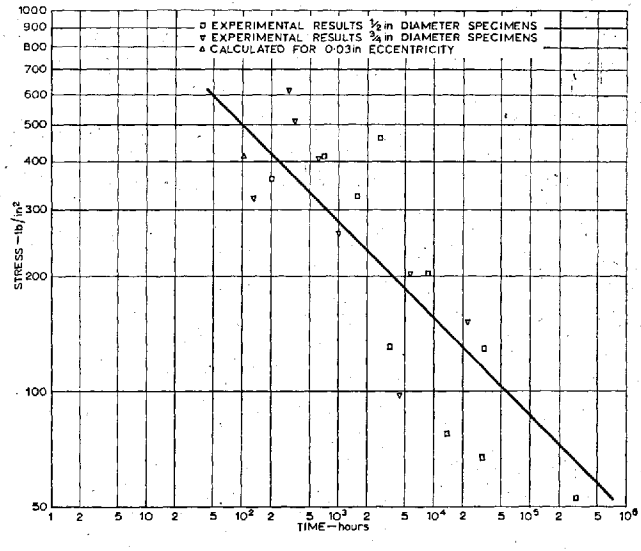
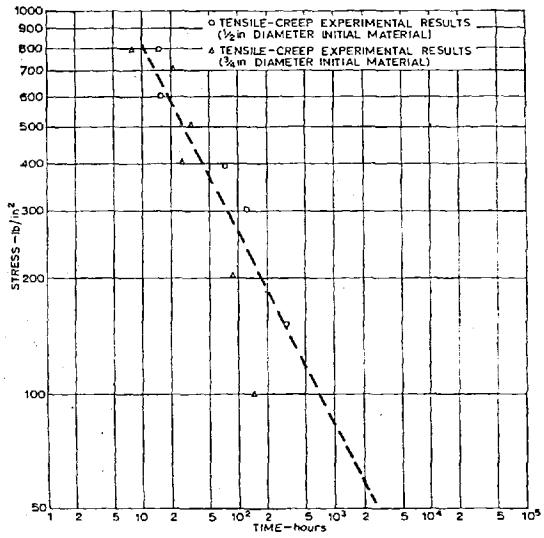
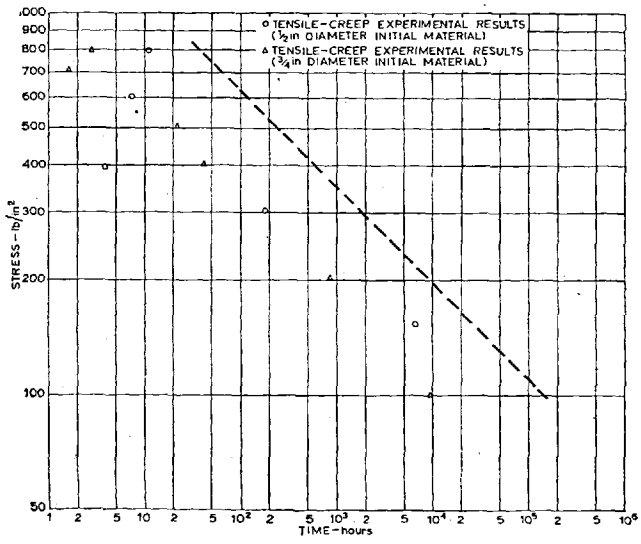


Fig. 3. *Buckling experiments: log stress versus* $\log t_{1/3}$ *for* $\left(1-\frac{P}{P_E}\right)\frac{\pi^2 I}{AL^2}\ln\left(\frac{z_2}{z_1}\right) = 0{\cdot}001$



The line drawn is predicted from the buckling data.

Fig. 4. *Log stress versus* log t_1 *for* $\epsilon^* = 0{\cdot}001$



The line drawn is predicted from the buckling data.

Fig. 5. *Log stress versus* log $t_{1/3}$ *for* $\epsilon^* = 0{\cdot}001$

Table 2. *Standard deviations (in cycles of log time) about the best straight line*

Buckling	Primary	(Fig. 3)	0·73
	Secondary	(Fig. 2)	0·3
Tensile	Primary	(Fig. 5)	0·44
	Secondary	(Fig. 4)	0·28

Effect of eccentricity

An eccentricity of 0·030 in was assumed and the theoretical sensitivity of the buckling data to this type of experimental error was investigated. The method is described fully in Appendix 2. The resulting time–deflection curve was analysed as before and the result is included in Figs 2 and 3. An interesting feature of this analysis was that the increments in deflection remained symmetric, although the actual shape was of course highly asymmetric.

For six of the experiments, the increments in deflection for each of the five measuring points were fully analysed. From the theoretical evidence quoted above, the increments would have remained symmetric even in the presence of fairly large eccentricities. It was found in fact that the increments were not symmetric, and it is believed that this was due to a considerable monotonic variation in eccentricity during the experiments due to specimen rotation. The measurements were consistent with a total change of 0·020–0·030 in in eccentricity in each test.

A third harmonic was found in only one of the experiments analysed, with amplitude of $\frac{1}{5}$th of the fundamental; this was present in the initial shape but disappeared as the asymmetric mode became more predominant.

DISCUSSION

The comparison between actual material uniaxial creep properties and that predicted from the buckling experiments is shown in Figs 4 and 5. For the secondary creep region, Fig. 4, the predicted line almost coincides with the best fit through the data. In the case of the primary data, however, the two lines are displaced by slightly more than one cycle of log time. The combined effect of these disparities was assessed by comparing a hypothetical mean buckling experiment with one predicted from the tensile data, as would be the case in practice. It was found that the error decreased from 0·8 cycles of log time in the initial stage to 0·1 cycles towards the end. As this latter is the most important from design considerations, the agreement was believed to be satisfactory.

Figs 2 and 3 show that when correlated on the basis of equation (15) the behaviour of the $\frac{1}{2}$-in and $\frac{3}{4}$-in columns is substantially the same.

Metallographic examination of the material revealed the grain size to be 0·005–0·007 in for the $\frac{1}{2}$-in material and 0·005–0·006 in for the $\frac{3}{4}$-in material. This did not cause any difference in the creep properties as shown in Figs 4 and 5. The grain size was found to remain constant during the tests, and uniform across the cross-section.

The results compared in Figs 4 and 5 are subject to the interchangeability of tensile and compressive creep; there is evidence in the literature (**8**) which shows that this is not invariably true and therefore the disparity in the primary phase may be attributable to this cause.

Creep buckling experiments are notoriously prone to scatter (**9**) even under the most carefully controlled conditions, and it is of interest to compare the total scatter in the buckling experiments with that which is inherent in the material. The scatter in the tensile data (Table 2) is of the same order as that quoted by Walles and Graham (**10**) in analysing data on the Nimonic alloys, and it is believed that in this case the figures given in Table 2 are

representative of actual material scatter, although no replicate data is available.

The remaining scatter in the buckling experiments, after excluding that assumed to be due to the material alone, is appreciable in the primary data only. The analysis of Appendix 2 showed that a constant eccentricity of 0·03 in produced an apparent deviation of 0·25 cycles of log time in the primary data (Fig. 3): this is relatively small in comparison with the total scatter. The deviation produced by eccentricity in the secondary phase (Fig. 2) is almost negligible. The six experiments which were fully analysed all showed increasing eccentricities. Equation (22) in Appendix 2 shows that this leads to larger values of z, which in turn gives smaller values of $t_{1/3}$ and t_1; this would account for the sign of the disparity shown in Fig. 5. As in the case of constant eccentricity, the effect on the secondary data would be smaller.

It is believed that variations in eccentricity during testing could only be avoided by constraining the column to buckle in one plane only, a technique which is used by the majority of workers in this field. It is then reasonable to adjust the eccentricity before each test.

CONCLUSIONS

The creep rate modulus theory, as described in the preceding paragraphs, is particularly simple in application to conventional buckling problems once the uniaxial properties have been established. The accuracy to be expected is believed to be adequate for most design purposes.

When applied to more complex loading systems (11) in three dimensions, the theory leads to linear partial differential equations which are readily solved in a non-iterative fashion, and well adapted to automatic computation.

ACKNOWLEDGEMENTS

The experimental work described in this paper was performed by F. Seyna in part fulfilment of the requirements for the Diploma of Imperial College. The whole project forms part of work to be submitted for the degree of Ph.D. in the University of London.

The authors would like to acknowledge the interest and helpful comments of Professor J. M. Alexander.

They are also indebted to Mr A. Graham and Mr K. F. A. Walles of the National Gas Turbine Establishment for enabling them to learn the curve fitting techniques and supplying the standard curves: also for advice on the design of the extensometers.

APPENDIX 1

If elastic deformation is neglected, and the creep rates assumed to be constant, an analytical relation between bending moment and curvature rate can be derived. This is shown below for the simple case of a rectangular cross-section, and comparison is made with the results of using the approximate equation (3).

The stress–strain rate relation under these conditions is

$$\dot{\epsilon} = C_2\sigma^{n_2} \quad . \quad . \quad . \quad . \quad . \quad (17)$$

From the requirement that plane sections remain plane

$$\dot{\epsilon} = \dot{\epsilon}_0 + \dot{K}x$$

and substituting from equation (17)*

$$\sigma^{n_2} = \sigma_0{}^{n_2} + \frac{\dot{K}x}{C_2}$$

Hence

$$\sigma = \left(\sigma_0{}^{n_2} + \frac{\dot{K}x}{C_2}\right)^{1/n_2} \quad . \quad . \quad . \quad . \quad (18)$$

The bending moment M

$$= \int_A \sigma x \, \mathrm{d}A \quad . \quad . \quad . \quad . \quad . \quad . \quad (19)$$

For the case of a rectangular section, $2a \times b$, and $n_2 = 2$ for magnox, integration of equation (19) gives

$$M = \frac{bC_2{}^2}{\dot{K}^2}\left[\frac{2}{5}\left\{\left(\sigma_0{}^2 + \frac{\dot{K}a}{C_2}\right)^{5/2} - \left(\sigma_0{}^2 - \frac{\dot{K}a}{C_2}\right)^{5/2}\right\} - \frac{2}{3}\sigma_0{}^2\left\{\left(\sigma_0{}^2 + \frac{\dot{K}a}{C_2}\right)^{3/2} - \left(\sigma_0{}^2 - \frac{\dot{K}a}{C_2}\right)^{3/2}\right\}\right]$$

From equation (16) $C_2 = 1{\cdot}66 \times 10^{-10}$, and assuming $a = b = 1$ in, $\dot{K} = 10^{-6}$ and $\sigma_0 = 10^2$ lb/in^2, we find

$$M = 20{\cdot}62 \text{ lb in}$$

Considering now the approximation (3), neglect of elastic strains reduces equation (10) to

$$\dot{K} = \frac{M}{\dot{E}I}$$

from which

$$M = \dot{K}\dot{E}I \quad . \quad . \quad . \quad . \quad . \quad (20)$$

From equation (13), substituting for C_2 and n_2, we find

$$\frac{1}{\dot{E}} = 3{\cdot}32 \times 10^{-10}\sigma_0$$

Substituting this in equation (20) we find under the above conditions

$$M = 20{\cdot}08 \text{ lb in}$$

Thus the approximate theory is in very close agreement with the analytical solution. It should be remarked, however, that the omission of elastic strains is not in general justified for column buckling calculations.

APPENDIX 2

EFFECT OF ECCENTRICITY ON CREEP BUCKLING (Fig. 6)

Assuming $L \gg \delta$, small deflections and neglecting the weight of the column, we have

$$X = \frac{P\delta}{L} \quad . \quad . \quad . \quad . \quad . \quad . \quad (21)$$

From equation (10)

$$\dot{K} = \frac{M}{\dot{E}I} + \frac{\dot{M}}{EI} = \frac{\partial^3 z}{\partial x^2\,\partial t} = -\frac{P}{\dot{E}I}z + \frac{Xx}{\dot{E}I} - \frac{P\dot{z}}{EI}$$

Substituting from equation (21) and rearranging

$$\frac{\dot{E}I}{P}\frac{\partial^3 z}{\partial x^2\,\partial t} + z + \frac{\dot{z}\dot{E}}{E} = \frac{\delta x}{L} \quad . \quad . \quad . \quad (22)$$

Defining the dimensionless variable $s = x/L$, and dividing by δ

$$\frac{\dot{E}I}{\delta PL^2}\frac{\partial^3 z}{\partial s^2\,\partial t} + \frac{z}{\delta} + \frac{\dot{z}}{\delta}\frac{\dot{E}}{E} = s$$

* *In the derivation it is assumed that the axis of zero strain rate remains outside the cross-section.*

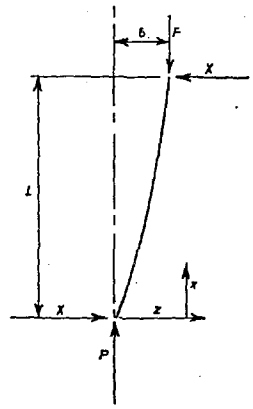


Fig. 6. *Eccentrically loaded column*

With a new dependent variable $u = z/\delta$ we have

$$\frac{\dot{E}I}{PL^2}\frac{\partial^3 u}{\partial s^2\,\partial t}+u+\frac{u\dot{E}}{E}=s \quad . \quad . \quad . \quad . \quad (23)$$

We now define a new 'solution time' variable v such that

$$\frac{\partial v}{\partial t}=\frac{PL^2}{(\ln 2)\pi^2\dot{E}I(1-P/P_E)} \quad . \quad . \quad . \quad (24)$$

and note that

$$\frac{\partial}{\partial t}=\frac{\partial v}{\partial t}\frac{\partial}{\partial v} \quad . \quad . \quad . \quad . \quad . \quad . \quad (25)$$

Substituting equations (25) and (24) in equation (23)

$$\frac{1}{\pi^2(\ln 2)(1-P/P_E)}\frac{\partial^3 u}{\partial s^2\,\partial v}+u+\frac{\partial u}{\partial v}\frac{P/P_E}{(1-P/P_E)(\ln 2)}=s \quad (26)$$

The reason for the substitution of equation (24) is that it is now possible to obtain a general solution (as shown by equation (26)) valid for any column geometry and creep properties for a particular Euler loading ratio. In certain circumstances (11) it is possible to define the 'solution time' in such a way that it is valid for all Euler loading ratios, making the solution completely general.

Putting $D=\dfrac{1}{\pi^2(\ln 2)(1-P/P_E)}$ and $B=\dfrac{P/P_E}{(\ln 2)(1-P/P_E)}$ and substituting in equation (26)

$$D\frac{\partial^3 u}{\partial s^2\,\partial v}+B\frac{\partial u}{\partial v}=s-u$$

Writing the above equation in terms of finite differences, putting $s=m\delta s$, $\delta s=1/N$, where $m=0,\ 1,\ldots N$, and replacing the derivative by its finite difference equivalent

$$N^2D\left[\frac{\partial u}{\partial v_{m-1}}-2\frac{\partial u}{\partial v_m}+\frac{\partial u}{\partial v_{m+1}}\right]+B\frac{\partial u}{\partial v_m}=m\,\delta s-u$$

$$\frac{\partial u}{\partial v_{m+1}}+\frac{\partial u}{\partial v_{m-1}}+\left(\frac{B}{DN^2}-2\right)\frac{\partial u}{\partial v_m}=\frac{m}{DN^3}-\frac{u}{DN^2}$$

and the boundary conditions $\left(\dfrac{\partial u}{\partial v}\right)_0=\left(\dfrac{\partial u}{\partial v}\right)_N=0.$

A solution by matrix inversion and matrix-vector multiplication, transforms the equations into a set of initial value problems for which the Runge–Kutta technique is well suited. Using $N=10$ and $\delta v=0{\cdot}125$ a solution was obtained on the London University ATLAS computer. Mesh size investigations showed that more subdivisions were not necessary in this case, as high accuracy was not required.

The solution obtained is in terms of the variable v, and to relate this to real time we substitute equation (13) in equation (24) and integrate, obtaining

$$v=\frac{AL^2}{(\ln 2)\pi^2 I(1-P/P_E)}(n_1C_1\sigma_0{}^{n_1}t^{1/3}+n_2C_2\sigma_0{}^{n_2}t) \quad (27)$$

The constants have been chosen so that v corresponds directly to doubling times* for a column deforming by secondary creep only. The similarity between equation (15) and (27) enables the v–t curve to be constructed as follows: the values of $t_{1/3}$ and t_1 corresponding to the chosen stress level are read off from the buckling cross plots Figs 2 and 3.

Writing equation (27) as $Cv=n_1C_1\sigma_0{}^{n_1}t^{1/3}+n_2C_2\sigma_0{}^{n_2}t$ and noting that Figs 2 and 3 are constructed for the standard value of 10^{-3}, it follows that the v–t relationship can be readily constructed using a Graham–Walles standard curve drawn for the values of $t_{1/3}$ and t_1 noted and $v^*=10^{-3}/C$.

The values of real time corresponding to that for which the solution is tabulated are now available, and the resulting deflection time curves were analysed like the experimental data.

In analysing the experimental data the quantity $\log(z_2/z_1)$ was calculated from

$$\log\frac{z_2}{z_1}=\log\left[\frac{z_{1(\text{nominal})}+\delta z}{z_{1(\text{nominal})}}\right]$$

The same procedure was used in analysing the eccentricity data, to ensure that the errors due to eccentricity were weighted in the same way as when they appeared in the experimental data. This showed that the errors were minimized in this method of presentation, and also that an eccentricity opposite in sign to that shown in Fig. 6 would give a result identical to that in Figs 2 and 3. This implied that eccentricity had no discernible effect on the rate of bowing, and it was also evident that no assymmetry was present in the bowing rates. This is to be expected for small eccentricities. The deviations shown in Figs 2 and 3 are therefore largely due to errors in curve-fitting.

* *The doubling time is the time for the current central deflection to double. It is independent of the current deflection if the creep rates are constant.*

APPENDIX 3

REFERENCES

(1) ALEXANDER, J. M. 'Approximate theory for thermal and irradiation creep buckling of a uranium fuel road and its magnesium can', *J. mech. Engng Sci.* 1959 **1** (No. 3), 211.

(2) ALEXANDER, J. M. and WEBSTER, G. A. 'The creep buckling of composite members', *J. mech. Engng Sci.* 1960 **2** (No. 4), 342.

(3) WEBSTER, G. A. and ALEXANDER, J. M. 'An investigation of small-deflection creep buckling', *Proc. Instn mech. Engrs, Lond.* 1963–64 **178** (Pt 3A), 2–1 (*Joint International Conference on Creep, New York, London*).

(4) JOHNSON, A. E., MATHUR, V. D. and HENDERSON, J. 'The creep deflection of magnesium alloy struts', *Aircraft Engineering* 1956 **28**, 419.

(5) GRAHAM, A. 'The phenomenological method in rheology', *Research* 1953 **6**, 92.

(6) GRAHAM, A. and WALLES, K. F. A. 'Regularities in creep and hot fatigue data', *Aeronautical Research Council* 1958 CP 379, 380 (H.M. Stationery Office).

(7) TIMOSHENKO, S. P. and GERE, J. M. *Theory of elastic stability* 1961 (McGraw-Hill, New York).

(8) SALAMASSY, O. K., MACDONALD, R. J., CARLSON, R. L. and MANNING, G. K. 'An investigation of the interchange of tensile creep for compressive creep', W.A.D.C. TR56-26 1956, and Pt 2, 1957.

(9) SCHLECHTE, F. R. 'Theoretical analysis of creep collapse of columns', N.A.S.A. 1959 TND 95.

(10) WALLES, K. F. A. and GRAHAM, A. 'On the extrapolation and scatter of creep data', National Gas Turbine Establishment 1961, Report No. R.247.

(11) FREED, N. H. 'An investigation of creep buckling with lateral restraint' (to be published).

```
JOB
LSC44DX1, FREED ASYMMETRICAL TEST 11
COMPUTING 55000 INSTRUCTIONS
OUTPUT
0 LINE PRINTER 700 LINES
1 FIVE HOLE PUNCH 1 BLOCKS
STORE 36 BLOCKS
COMPILER EMA
MAIN→5600
AUXILIARY(0,5120)
DUMPS 0

TITLE
FREED LSC44EX1 ASYMMETRICAL TEST 13
CHAPTER 0
A→5041
B→72
C→5
F→73
G→73
H→73
W→73
Y→73
π→40
SELECT OUTPUT 0
M'=72
N=73
N'=73
H=.0625
Y=N-2
L'=N-2
P'=M'-2
O=L'L'
Z=ψLOG(2)
READ(W)
READ(D)
READ(X)
READ(YN)
E=6160.57DDDD

K'=0
W=W/E
Z=Z-WZ
B=W/Z
Z=ππZ
A=1/Z

I=1(1)71
READ(YI)
REPEAT
J=ψMAX(Y0,30,40)
R'=40
→96
83)R'=0
I=1(1)71
YI=YI/π'
REPEAT

54)Y(N-1)=0
B'=75
D'=0
W=M'M'
W=1/W
A=M'M'A
F'=B/A

I'=0
30)INTSTEP(40)

60)K'=K'+1
I'=I'+1
→20,R'=80
20)NEWLINE
NEWLINE
PRINT(X)2,4
CAPTION
DOUBLING TIMES

PRINT(π10)0,4
+0≥≠ →(π12)0,4

π1=1-M'YN+J
π1=M'M'Y(J-1)+
π2=3M'YN-3J-2

π2=M'M'YJπ2
π3=1-3M'YN+3J
π3=M'M'Y(J+1)π3

4=M'YN-J
π4=M'M'π4Y(J+2)
PRINT(π1+π2+π3+π4)0,4
****
CAPTION
FORCE EQUALS
Z=YN-YNYN
Z=1/Z
PRINT(Z+AZWY'F(J-1)+AZEWFJ+AZWπ7F(J+1)+AZWπ8F(J+2))0,4

NEWLINE
K=ψMAX(Y0,30,40)
→57,1>YK
SELECT OUTPUT 1
NEWLINE
O'=0
I=1(1)N
PRINT(YI)0,6
O'=O'+1
→58,O'≠5
NEWLINE
O'=0
58)REPE→
→)1
57)→92,0.99995>YK
H=0.5
92)CAPTION
DEFLECTION
N'=0
I=1(1)N
PRINT(YI)0,6
N'=O'+1

→45,O'=6
→46
45)NEWLINE
O'=0
46)REPEAT
O'=0
NEWLINE
I=1(1)N
PRINT(FI)0,6
O'=O'+1
→47,O'=6
→48
47)NEWLINE
O'=0
48)REPEAT
I'=0

→71,R'=80
70)→86,4>K'
H=1
86)P=J-1
I=J+2
S=ψINTPT(0.5M'+.01)
→95,J≥S
K=ψMAX(Y0,H,L')
π1=ψMOD(YK-Y(J+1))
→97,π1>0.00015
H=0.5
97)→96,YK>Y(J+1)
→76
95)K=ψMAX(Y0,0,P)
π1=ψMOD(YK-YJ)
→98,π1>0.00015
H=0.5
98)→96,YZK>Y(J-1)
→76

96)A0=K-1
A1=K
A2=K+1
B0=Y(K-1)
C1=YK
+*2=Y(K+1)

50)π4=A0-A1
π5=A0-A2
π6=A1-A2
π7=A1+A2

π8=A0+A2
π9=A0+A1
π10=π4π5
π10=1/π10
π11=π4π6

*π11=1/π11
π12=π5π6
π12=1/π12
A3=π7C0π10-π8C1π11+π9C2π12

π16=2C0π10-2C1π11+2C2π12
A3=A3/π16
T=3
JUMPDOWN75


A4=A3-.003
T=4
JUMPDOWN 75
T=5
A5=A3+.003
JUMPDOWN 75
NEWLINE
I=0(1)5
PRINT(AI)0,6
REPEAT
NEWLINE
PRINT(CI)0,8
≃π25=A3-A4
π26=C3-C4
π25=π25/π26
π26=A5-A3
π27=C5-C3

π26=π26/π27
π25=π25π26
→51,0>π25

→81,A1>A3
→80,C3>C1
A2=A3
C2=C3
→50

80)A0=A1
C0=B1
A1=A3
C1=C3
→50
81)→*82,C1>B3
A2=A1
C2=C1
A1=A3
B1=C3
→50

82)A0=A3
C0=C3
→50
51)π'=C340
→90,R'≠80
NEWLINE
CAPTION
MAX. DEFLN
PRINT(π')0,4
CAPTION
AT X=
PRINT(A3)0,4
→91
90)C=D
D=G
F=π'
→85,π'>1
I=1(1)N
*************
WI=YI
REPEAT
→76


85)π4=π'-2D+C
π5=2HH+HX
π4=π4/π5
π=**D-C-2HXπ4+3HHπ4
π5=π5/H
π6=B-π4XX+4HXπ4-4π4HH-π5X+2Hπ5
π7=ψSQRT(π5π5-4π4π6+4π4)
π8=-0.5π5/π4+0.5π7/π4
X=X-H
H=π8-X
H=1(1)N
YI=WI
REPEAT
R'=80
→76

76)→30,56>K'
71)END
40)J=ψINTPT(M'YN)

F=M'AYN
F=1/F

U'=YN-J/M'
π1=2W-3YN/M'+3JW+YNYN-2XNJ/M'+JJW
π2=6W+6YN/M'-6JW
U'=M'M'U'π1/π2
V'=1/M'+YN-J/M'
π1=2W-3YN/M'+3JW+YNYN-2YNJ/M'+JJW

π2=2JW-2YN/M'
V'=M'M'V'π1/π2
W'=YNYN-2YNJ/M'+JJW-2YN/M'+2JW
π1=1/M'+YN-J/M'
π2=2YN/M'-2JW-2W
W'=M'M'W'π1/π2
X'=YNYN-2YNJ/M'+JJW-YN/M'+JW
π1=1/M'+YN-J/M'
π2=12*W-6YN/M'+6JW
X'=M'M'X'π1/π2
Y'=4W-12YN/M'+12JW+6YNYN-12YNJ/M'+6JJW
π1=6WW+6WYN/M'-6JWW
Y'=Y'/π1
E*=6YNYN-12XNJ/M'+6JJW-8YN/M'+8JW-2W
π1=JW-YN/M'
π2=2W
π1=π1π2
E*=E/π1
π6=12YNYN-24YNJ/M'+12JJW-12YN/M'+12JW-2W
π1=YNYN-2YNJ/M'+JJW+YN/M'-JW
π2=YNYN-2YNJ/M'+JJW-3YN/M'+3JW+2W
π1=π1π2
π6=π6/π1
π7=6YNYN-12YNJ/L'+6JJW-4YN/M'+4JW-4W
π1=2WYN/M'-2JWW-2WW
π7=π7/π1
π8=6YNYN-12YNJ/M'+6JJW-2W
π*1=12WW-6WYN/M'+6JWW
π8=π8/π1


H'=M'A-M'AYN
H'=1/H'
T=J+1
I=1(1)J
BI=IF-YI/A
REPEAT
I=T(1)L'
BI=M'H'-IH'-YI/A
REPEAT
H=J+1
Z'=M'-M'YN
Z'=1/Z'
Z=M'YN
Z=1/Z
J'=J-3
T=J-2
P=J-1
L=0(1)P'
R=L-1
S=L+1
Q=L-2
O=L-≥
Q'=L+2
S'=L+3
K=0(1)P'
AM=Q+K-L

→1,K=L
→2,K=R
→2,K=S
→4
1)AM=F'-2
→4
2)AM=1
4)→5,L≥J
→6,K=T

→7,K=P
→8,K=J
→9,K=I
→0
6)AM=AM-LZWY'-ZWY'
→10

7)AM=AM-LZWE-ZWE
→10
8)
  =AM-LZWπ7-ZWπ7
→10
9)AM=AM-LZWπ8-ZWπ8
→10
5)→11,K=T
→12,K=P
→13,K=J
→14,K=I
→10

11)AM=AM+Z'WY'+Z'LWY'-Z'M'VX'
→10
12)AM=AM+Z'WE+Z'LWE-Z'M'WE
→10

13)AM=AM+Z'Wπ7+Z'LWπ7-Z'L'Wπ7
→10
14)AM=AM+Z'Wπ8+Z'LWπ8-Z'M'Wπ8
10)REPEAT
REPEAT

ψ7(D')B1,L'
ψ7(B')A0,M
D'=ψ28(B',L',1)
ψ6(D')F1,L'

π10=U'F(J-1)+V'FJ+W'F(J+1)+X'F(J+2)

53)S=J
K=N
I=31(1)39
πI=0
REPEAT
P=S-1
Q=S+1
R=S+2

I=P(1)S
F=I/M'-YK
F=IFF/M'
π31=π31+F

F=I/M'-YK
F=IIW**π*FF
π33=π33+F
π39=π39+YI

F=I/M'-YK
F=IIIWFF/M'
π36=π36+F
F=IYI/M'=H/M'
37=π37+F
REPEAT

I=Q(1)R
F=I/M'-YK
F=IFF/M'
π32=π32+F

F=I/M'-YK
F=FFYKI/L'
π34=π34+F
F=I/M'-YK
Z=IIW-IYK/M'
π35=π35+FFZ
π38=π38+YI
REPEAT

B0=π31+π32
B1=π33+π34
B2=π35
B3=B1
B4=π36+YKYKπ32
B5=YKπ35

B6=π32
B7=π34
B8=π35

ψ7(A')B0,9
A1=π39+π38-4
A2=π38-2
A3=A2
A2=π37+YKπ38-2YK
ψ7(B')A1,3

B'=ψ28(A',3,1)
ψ6(B')A0,3
π12=2A0YK+2A1YKYK

→61,0>π12
π1=1-M'YN+J
π1=M'M'Y(J-1)π1
π2=3M'YN-3J-2

π2=M'M'YJπ2
π3=1-3M'YN+3J
π3=M'M'Y(J+1)π3

π4=M'YN-J
π4=M'M'π4Y(J+2)

π12=π1+π2+π3+π4
→61,0>π12
π12=-0.1

≃61)FN=-π10/π12
Z'=BYN-BYNYN
Z'=1/Z'
Z=1-YN
Z=1/Z
F(N-1)=AZ'WY'F(J-1)+AZ'WEFJ+AZ'Wπ7F(J+1)+AZ'Wπ8F(J+2)+ZY(N-1)FN
F(N-1)=F(M-1)+Z'-Y(N-1)/B
END AUXSEQ

75)π20=AT-K+2
π21=AT-K+1
π23=AT-K-1
π24=AT-K-2

CT=π21π22π23π24Y(K-2)/24-π20π22π23π24Y(K-1)/6+π20π21π23π24Y***K*/4-π20
CT=CT+π20π21π22π23Y(K+2)/24
RETURN
```

FREED N.H. Ph.D. 1965